

# Université Pierre et Marie Curie

Ecole doctorale 398 : Géosciences, Ressources naturelles et Environnement  
ISTeP

## Style structural, cinématique des déformations et circulations de fluides en contexte de collision: le cas des Massifs Cristallins Externes alpins.

Thèse présentée par  
**Alexandre Boutoux**

Pour obtenir le grade de : **Docteur de l'Université Pierre et Marie Curie**  
Discipline / Spécialité : Sciences de la Terre

<b>Jean Pierre Gratier</b>	Physicien, Univ. J. Fourier, Grenoble	Rapporteur
<b>Neil Mancktelow</b>	Professeur, ETH, Zurich	Rapporteur
<b>Laurent Jolivet</b>	Professeur, Univ. Orléans	Examinateur
<b>Didier Marquer</b>	Professeur, Univ. de Franche-Comté, Besançon	Examinateur
<b>Claudio Rosenberg</b>	Professeur, UPMC, Paris	Examinateur
<b>Yann Rolland</b>	Maître de Conférences, Univ. Nice-Sophia-Antipolis	Invité
<b>Nicolas Bellahsen</b>	Maître de Conférences, UPMC, Paris	Co-directeur
<b>Anne Verlaguet</b>	Maître de Conférences, UPMC, Paris	Co-directrice
<b>Olivier Lacombe</b>	Professeur, UPMC, Paris	Directeur



Je voudrais commencer par remercier mes trois encadrants de thèse, Nicolas Bellahsen, Anne Verlaguet et Olivier Lacombe. Vous m'avez pris sous votre aile depuis le Master et vous ne m'avez jamais lâché depuis. Merci d'avoir été présents à tout moment, que ce soit pour m'encourager à avancer ou, de temps à autre, me pousser un peu ; merci de m'avoir recadré dès je partais un peu dans tous les sens mais de m'avoir toujours laissé libre d'aller où je voulais. Et surtout merci d'avoir été là dans les moments plus difficiles. Vous avez toujours été prévenants , sans jamais être envahissants. Encore une fois, je m'estime particulièrement chanceux de cet encadrement.

Merci aux membres du Jury de m'avoir fait l'honneur d'évaluer ce travail. Merci à Jean-Pierre Gratier de nous avoir accompagnés dans les Alpes, pour voir ensemble le terrain qui fut celui de sa thèse et qui maintenant est le mien également. Merci à Neil Mancktelow d'avoir accepté d'évaluer mon travail, pour la plus grande partie rédigé en français. Merci aussi bien sûr à Laurent Jolivet, Didier Marquer, Claudio Rosenberg et Yann Rolland d'avoir accepté de relire ce travail.

Je voudrais aussi remercier les membres du CRPG, à Nancy de m'avoir chaleureusement reçu en ce frileux mois de décembre 2013. Merci à Raphaël Pik, à Martin Stab et à Camille Soulié pour leur accueil chaleureux. Merci aux membres du laboratoire Géoazure de Nice de m'avoir accueilli pour ces quelques semaines de septembre et particulièrement à Yann Rolland, pour

Merci à l'ISTeP de m'avoir accueilli pendant 5 ans maintenant et particulièrement à tous les thésards pour les moments de détente, salvateurs au cours de ces années de travail.

Merci aux copains parisiens d'en haut comme d'en dessous. Merci à Tristan, à Étienne, à Charlène, à Lexa, à Jacynthe, à Philippe, à Toto, à Bastien, à Quentin, à Thomas, à Taï, à Laure, pour les étoiles, pour les bouquins, pour la musique, pour les doigts écrasés, pour les têtes cognées ; pour les moments de n'importe quoi, qui se traduisent souvent par des doigts écrasés, des têtes cognées et du remblais plein les yeux. Merci de m'avoir rappelé que le monde en dehors des cailloux alpins continue de tourner, et merci de l'avoir refait avec moi.

Merci infiniment aux copains de Laval, d'Angers, de Strasbourg, de Lille, de Nice, d'être encore là, tout le temps ; quand c'est drôle et qu'on a le temps d'en profiter, et puis quand c'est plus dur mais que vous restez malgré tout.

Merci à toi Marie mon amour de m'avoir soutenu, supporté et épaulé tout ce temps.

Et enfin merci à ma famille, mes deux p'tits frères, mon père, Manou et Babette et à ma mère parce que cette thèse, vous y avez bossé, vous aussi.



## Résumé

La collision continentale implique les marges continentales héritées de la phase de divergence. Ce travail de thèse a pour but de mieux documenter les processus majeurs qui ont lieu lors de la collision : le raccourcissement crustal, l'évolution thermique et les circulations de fluides. Ce mémoire repose donc sur un travail structural et microstructural et sur des études géochimiques et thermochronologiques. Les Alpes de l'Ouest constituent un orogène très étudié et qui offre des affleurements jusqu'à la transition cassant/ductile du prisme collisionnel oligo-miocène. Il est ainsi un objet tout à fait approprié pour aborder cette thématique.

La première partie de ce travail apporte de nouvelles données thermo-chronologiques U-Th-Sm/He sur zircon (ZHe) et RSCM (Raman Spectroscopy on Carbonaceous Material, Tmax) sur les massifs des Aiguilles Rouges. Ces données sont intégrées à l'histoire thermique de ces massifs et utilisées pour contraindre l'évolution structurale de la marge dauphinoise proximale lors de son inversion. Un pic de température long de 10 Ma et une exhumation rapide par les rampes frontales vers 16-18 Ma sont ainsi documentés.

La seconde partie de ce travail consiste en la mise au point d'une nouvelle méthode de restauration des coupes qui ont subi de fortes déformations ductiles. La déformation finie des bassins de Bourg d'Oisans est utilisée afin de contraindre les taux de raccourcissement. Le travail de terrain a de plus permis de définir le cadre structural et microstructural de l'étude des circulations de fluides à l'interface entre socle et couverture dans ces mêmes bassins du massif de l'Oisans. Les données géochimiques (isotopie, microthermométrie des inclusions fluides, éléments traces) montrent que l'essentiel des fluides et de la matière des veines à quartz/calcite de la couverture proviennent de la roche encaissante. Toutefois, des fluides (en faible quantité) dérivés du socle ont percolé à la base de la couverture dès l'initiation du raccourcissement collisionnel. Tous ces résultats permettent de proposer un modèle conceptuel d'évolution des circulations de fluides à l'échelle des massifs cristallins externes alpins.

Dans une dernière partie, la modélisation thermomécanique de l'inversion de bassins hérités montre que la profondeur d'enfouissement tectonique joue un rôle primordial dans le style d'inversion des bassins. Ainsi, l'enfouissement provoque la non-réactivation des failles normales héritées tout en favorisant le pincement des bassins.

L'ensemble des résultats sont intégrés dans un modèle d'inversion collisionnelle de la marge européenne ; ce modèle est discuté en abordant notamment les questions de structure thermique du prisme, d'évolution des conditions P-T pendant l'histoire alpine et d'exhumation.

## **Abstract**

During continental collision, continental margins inherited from rifting phase are shortened. This work aims at better documenting and understanding major processes that occur during collision, such as crustal shortening, thermal evolution and fluid circulations. The work is based on structural and microstructural analyses as well as on thermochronological and geochemical studies. The Western Alps are a suitable target for this purpose, since they have been the subject of numerous studies. In addition, the External Crystalline Massifs (ECM) provide access to crustal levels deformed at the brittle/ductile transition within the oligo-miocene collisional wedge.

In the first part of the work, we provide new U-Th-Sm/He on zircon (ZHe) thermochronological data and new RSCM (Raman Spectroscopy on Carbonaceous Material) data for the Aiguilles Rouges. These data are integrated into the thermal histories of these massifs and used to constrain the structural evolution of the proximal Dauphinois margin during its collisional inversion. We especially document a 10 Ma long thermal peak and a fast exhumation due to crustal frontal ramps activation at about 16-18 Ma.

The second part of the work consists of the development of a new methodology to balance cross-sections where rocks were ductilely deformed. Finite deformation of the metasedimentary cover of the Bourg d'Oisans basins (located south of the Mont Blanc and the Aiguilles Rouges massifs) is used to constrain shortening. Fieldwork allowed us to define the structural and microstructural setting for the study of fluid circulations close to the basement/cover interface in the very same basins. Geochemical analyses (stable isotopes, microthermometry of fluid inclusions and trace elements) on cover veins highlight that most of fluids and vein filling material are derived from host-rocks. Yet, small amount of basement-derived fluids percolated into the cover as soon as the onset of collisional shortening. All those results are gathered into a conceptual model of evolution of fluid circulation through time and progressive deformation at the scale of the entire ECM.

In the last part, thermomechanical modeling of inversion of inherited extensional basins show that tectonic burial is a major parameter controlling basin inversion style. Basin burial leads to inherited normal fault reactivation inhibition and basin pinching.

Finally, all those new results are integrated into a scenario of the inversion of the European margin during Alpine collision. This model is discussed through questioning of collisional wedge thermal structure, P-T recorded condition evolution and exhumation.

<b>I. Introduction</b>	3
I.1. Thématique de l'étude.	3
I.2. Problématiques.	4
I.3. Choix du laboratoire naturel : l'Arc alpin.	8
<b>II. Contexte géologique.</b>	9
II.1. Géodynamique.	9
II.2. Structuration et déformation de la marge européenne.	11
II.2.1. Structuration liasique de la marge européenne.	11
II.2.2. Conditions P-T enregistrées dans les MCE.	13
II.2.3. Déformation du socle et de la couverture des MCE.	14
II.3. Les massifs Grandes Rousses et Nord-Ouest Oisans.	18
II.3.1 Structuration des Grandes Rousses et du Nord-Ouest Oisans.	19
II.3.2. Déformation du socle des bassins de l'Oisans.	21
II.3.3. Déformation de la couverture des bassins de Bourg d'Oisans et de Mizoën.	22
II.3.4. Schistosités des bassins de l'Oisans.	23
II.3.5. Circulations de fluides de la zone du Nord Oisans.	25
II.4. Les massifs du Mont Blanc et des Aiguilles Rouges.	25
II.4.1. Le massif des Aiguilles Rouges.	27
II.4.2. Le massif du Mont-Blanc.	27
II.4.3. Circulations de fluides.	31
<b>III. Evolution structurale, massifs des Aiguilles Rouges et du Mont-Blanc.</b>	34
III.1. Cadre et intérêt de l'étude.	34
III.2. Article.	36
III.3. Évolution structurale de la marge lors de la collision.	59
III.4. Quels variations le long de l'arc pour cette évolution structurale ?	60
<b>IV. Étude de la géométrie et de la cinématique d'inversion des bassins de l'Oisans au cours de la collision alpine.</b>	61
IV.1. Cadre et intérêt de l'étude : analyse microstructurale et nouvelle méthode de restauration.	61
IV.2. Article.	62
IV.3. Limite à la restauration des bassins de l'Oisans.	80
IV.4. Problème de la conservation du volume au cours de la déformation.	80
<b>V. Circulations de fluides pendant la collision alpine.</b>	81
V.1. Cadre et intérêt de l'étude.	81
V.2. Article.	83
V.3. Bilan : l'ouverture des systèmes géochimiques avec la déformation progressive.	103

<b>V.4. Question soulevées.</b>	104
<b>VI : Étude thermo-mécanique de l'inversion collisionnelle des bassins hérités de la marge européenne.</b>	105
<b>VI.1. Cadre et intérêt de l'étude.</b>	105
<b>VI.2. Article.</b>	106
<b>VI.3. Influence de l'enfouissement tectonique.</b>	128
<b>VI.4. Limites du modèle : raccourcissement symétrique, complexité de la marge et vitesse d'enfouissement.</b>	128
<b>VII. Discussion.</b>	130
<b>VII.1. Évolution P-T lors de l'enfouissement.</b>	130
<i>VII.1.1. Augmentation prograde de la température.</i>	130
<i>VII.1.2. Augmentation prograde de la pression.</i>	132
<b>VII.2. Pic de métamorphisme.</b>	132
<i>VII.2.1. Un long pic de température.</i>	132
<i>VII.2.2. Pic de pression.</i>	133
<b>VII.3. Exhumation versus refroidissement.</b>	134
<b>VII.4. Scenario d'inversion de la marge alpine.</b>	135
<i>VII.4.1. Etat pré-collisionnel.</i>	135
<i>VII.4.2. Enfouissement de la marge.</i>	137
<i>VII.4.3. Pic de température, pic de pression raccourcissement du socle des MCE.</i>	138
<i>VII.4.4. Raccourcissement de la couverture des bassins des MCE.</i>	140
<i>VII.4.5. Exhumation des MCE et fin de raccourcissement de la couverture des bassins.</i>	142
<b>VIII. Conclusions.</b>	144
<b>IX. Perspectives de recherche.</b>	146
<b>IX.1. Étude structurale et microstructurale et datations géochronologique de la couverture du Mont-Blanc.</b>	146
<b>IX.2. Étude de la structure thermique des nappes de Morcles, du Mont-Joly et des nappes de l'Ultra-Dauphinois.</b>	146
<b>X. Références</b>	148
<b>XI. Appendice.</b>	156

# I. Introduction

## I.1. Thématique de l'étude.

Les chaînes de collision résultent de la fermeture d'un océan et de l'affrontement de deux plaques continentales en convergence. Ces chaînes de montagne qui en résultent sont constituées d'un prisme collisionnel en partie exhumé (surtout dans les chaînes tertiaires ou anciennes) et formé à la suite de la subduction de l'océan. Pendant la collision, les anciennes marges continentales sont raccourcies. Ces zones ont donc vécu une histoire complexe, puisqu'elles sont structurées lors du rifting de l'océan subduit avant d'être inversées lors de leur intégration au prisme collisionnel. Les chaînes de collision formées à la suite d'une histoire tectonique longue et polyphasée sont marquées par des géométries très variables, elles-mêmes dépendantes de plusieurs paramètres tels que la rhéologie des marges impliquées (e.g. Mouthereau et Petit, 2003 ; Mouthereau et al., 2013), leur géométrie initiale (e.g. Butler, 1989, 2006 ; Munoz, 1992 ; Roure et Colletta, 1996) et les vitesses de convergences des plaques.

Puisque la rhéologie n'est pas directement documentable sur le terrain, on l'étudie à partir de différents proxys témoignant de l'évolution structurale et thermique du prisme, les interactions entre ces deux évolutions étant justement contrôlées par la rhéologie. L'étude structurale des déformations couplée à celle des conditions PT enregistrées et de leur timing permet d'accéder à la cinématique et ainsi au style tectonique du raccorçissement. Or le style tectonique est fortement dépendant de la thermicité précollisionnelle de la croûte et un moyen d'y accéder passe par l'analyse des taux de raccorçissement enregistrés par les zones externes des orogènes lors de la collision (Mouthereau et al., 2013). Ainsi les observables permettant d'accéder à la cinématique et au style structural sont les estimations des quantités et des taux de raccorçissement enregistrés par les différentes unités de l'orogène, les données géochronologiques et thermo-chronologiques et les données thermo-barométriques. Enfin, l'étude des systèmes de circulations de fluides et de leur évolution nous permet de contraindre, dans l'espace et dans le temps, les interactions fluides-roches témoins et acteurs de l'évolution de la rhéologie du prisme.

## I.2. Problématique.

Ce mémoire se propose d'aborder quelques questions ayant trait à l'évolution thermique, structurale et cinématique d'une marge reprise en collision :

### **Quel est le style tectonique de la déformation d'une marge en cours de collision ?**

Mouthereau et al. (2013) ont montré que le style tectonique marquant un orogène peut être relié à l'héritage thermique des marges impliquées dans la convergence (Fig.1). Ainsi, les marges «thermiquement jeunes» sont marquées par des déformations de style dit « thick-skinned » (e.g., Alpes, Zagros, Fig. 1). L'inversion de ces marges est alors caractérisée par l'implication d'une grande épaisseur de croûte dans le raccourcissement, ce qui se traduit par la réactivation potentielle de nombreux accidents structurant la marge et hérités de la phase extensive (Lacombe et Mouthereau, 2002 ; Mouthereau et Petit, 2003). Dans le cas d'une croûte « vieille », la lithosphère a eu le temps de se rééquilibrer thermiquement car la phase de rifting structurant la marge a eu lieu plusieurs centaines de Ma avant la collision. L'inversion de la marge est alors marquée par des déformations de style « thin-skinned » n'impliquant qu'une très faible section de son épaisseur, en général sa couverture uniquement (e.g., orogènes Sevier, Brooks Ranges, Fig. 1). Ces variations géométriques de l'accommodation du raccourcissement collisionnel, à travers l'état thermique de la croûte, reflètent donc la rhéologie de la croûte en cours d'inversion.

**Quelles méthodes peuvent être raisonnablement utilisées pour caractériser le style structural et quantifier la déformation ?** Un moyen d'accéder au style structural enregistré passe par la construction de coupes équilibrées et donc nécessairement par l'étude des quantités et des taux de raccourcissement des différentes unités de l'orogène (Chamberlin 1910 ; Dahlstrom, 1969). Dans les zones les plus externes des orogènes, les roches sont déformées avec un comportement essentiellement cassant à l'exception de l'effet de la pression-dissolution. On peut alors considérer que le raccourcissement unidirectionnel des couches se fait à aire et longueur constantes dans un plan parallèle à la direction de transport (e.g. Affolter et al., 2008 ; Beaumont et al., 2000 ; Mouthereau et Lacombe, 2006). Cependant cette caractéristique n'est plus valable pour les roches déformées dans les zones internes des orogènes. En effet, avec l'augmentation des conditions de pression et de température, les roches ont un comportement visco-plastique lors de leur déformation. Dans ces conditions, les transferts de matières devenant plus efficaces, seule l'hypothèse de la conservation de l'aire des couches dans un même plan parallèle à la direction de transport reste valable (Epard et

Groschong, 1993 ; Groshong et Epard, 1994 ; Bellahsen et al., 2012 ; Moretti et Callot, 2012 ; Butler, 2013).

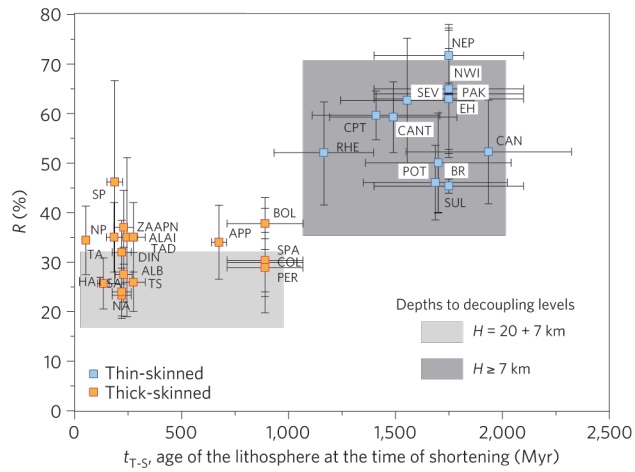


Figure 1. Taux de raccourcissement enregistré dans les zones externes des orogènes en fonction de l'âge thermique des lithosphères indiquées. Mouthereau et al. (2013). ALAI, Chaîne des Alai; ALB, Alborz; APN, Apennins; APP, Appalaches; BOL, Chaine sub Andine bolivienne; BR, Brooks Ranges; CAN, Rocheuses Canadiennes; CANT, Cantabrie; COL, Chaine sub andine Colombienne; CPT, Carpathes; DIN, Dinarides; EH, Chaine d'avant pays Est Himalayenne; HAT, Haut Atlas; NA, Alps du Nord; NEP, Chaîne d'avant pays Nepalaise; NP, Chaine d'avant pays Nord des Pyrénées ; NWI, chaine d'avant pays NW Himalayenne; PAK, Hymalaya Pakistanais; PER, Chaine d'avans pays Peruvienne; POT, Palteau du Potwar ; RHE, Chaine d'avant-pays Rheno-hercynienne; SA, Alpes du Sud; SEV, Chaines d'avant pays Sevier ; SP, Chaine d'avant pays Sud des Pyrénées; SPA, Sierras Pampeanas; SUL, Sulaiman; TA, Taiwan; TAD, chaine d'avant pays Tadjik; TS, Tien-Shan; ZA, Zagros

**Quelles sont les échelles des transferts de matière ?** La réorganisation de la matière peut se faire soit par diffusion (transport des éléments à travers un fluide stagnant par équilibrage des gradients de potentiel chimique) soit par advection (transports des éléments par un fluide circulant) (Oliver, 1996 ; Oliver et Bons, 2001). Les échelles temporelles et spatiales de ces processus dépendent de nombreux paramètres dont les conditions PT et la présence/absence d'accidents permettant de chenaliser les fluides. Puisque la restauration des coupes déformées

dans le domaine ductile se fait classiquement à volume constant, il est nécessaire de vérifier l'hypothèse de la conservation de la matière dans le plan des coupes et donc les échelles spatiales et temporelle des transferts de matière.

**Quel est l'impact de la géométrie initiale de la marge ?** La définition du style structural des déformations permet d'approcher au premier ordre la rhéologie de la croûte. L'analyse et l'interprétation de ces déformations à l'échelle locale permettent de mieux comprendre l'impact d'autres paramètres sur le développement d'un orogène. Ainsi, la construction de coupes séries et équilibrées le long de l'orogène permet d'estimer les variations les plus importantes de la géométrie initiale de la marge et ainsi d'estimer l'impact de celles-ci sur la collision (e.g. ; [Beaumont et al., 2000](#) ; [Bellahsen et al., 2014](#)). Ainsi, la réactivation (ou non) des structures extensives héritées de la phase de rifting de la marge peut fortement contrôler la géométrie des déformations compressives lors de la collision (e.g. [Butler, 1989, 2006](#), [Roure et Colletta, 1996](#)).

**Quel est le chemin P-T des unités du prisme ?** L'étude du comportement rhéologique d'une marge en cours d'inversion passe aussi par la caractérisation des conditions de pression et de température enregistrées au cours de l'évolution du prisme collisionnel. Ces estimations PT sont obtenues à partir d'études thermo-barométriques réalisées sur les phases cristallines contemporaines de la déformation des roches et à partir d'études thermo-chronologiques et thermométriques. On reconstitue ainsi la structure thermique du prisme orogénique et son évolution au cours de l'enfouissement qui contraignent fortement sa rhéologie.

**Quelle est la cinématique des unités du prisme ?** Les données thermo-chronologiques et thermo-barométriques sont ensuite confrontées aux coupes équilibrées au travers du prisme orogénique de façon à reconstituer la cinématique d'évolution du prisme. Il est en effet nécessaire de caler temporellement l'ensemble de ces informations dans le but de caractériser la cinématique des unités du prisme. Cette analyse de la cinématique passe par la datation des déformations des unités et de leur exhumation. Dans les zones les plus externes des orogènes et pour des unités peu érodées, ces datations peuvent reposer sur l'analyse stratigraphique des couches syn-tectoniques. Dans les zones plus internes du prisme, fortement enfouies au cours de la formation du prisme collisionnel, la datation des déformations repose sur l'étude géochronologique datant directement les phases cristallines syn-tectoniques. Les outils thermo-chronologiques permettent eux de dater l'évolution thermique de ces mêmes unités du

prisme au cours de l'exhumation. La comparaison des données obtenues fournit alors, sous certaines conditions, une indication des vitesses de refroidissement des unités du prisme, et à travers elles, de l'activité des accidents structurant le prisme, qu'ils soient accessibles ou non.

**Le refroidissement des unités du prisme collisionnel est-il synchrone de leur exhumation ?** Le refroidissement des unités n'implique pas nécessairement leur exhumation et inversement. Ainsi, le rééquilibrage thermique de la croûte n'est pas forcément contemporain des déformations et ainsi la baisse de température des unités peut être postérieure aux déformations (e.g. [Challandes et al., 2008](#)). De même, la topographie contrôle en partie les vitesses d'exhumation et ainsi considérer des déformations sans prendre en compte la variation du relief conduit à la sous-estimation de l'exhumation si celle-ci est initiée avant la relaxation thermique ([Elhers et Farley, 2003](#) ; [Braun et al., 2013](#)). Cette question est bien sûr aussi valable pour l'enfouissement, car celui-ci ne s'accompagne pas nécessairement du réchauffement immédiat des unités. Cette relaxation thermique sera alors dépendante de la conductivité thermique des unités enfouies (e.g. [Challandes et al., 2008](#)).

**Quels sont les systèmes de circulations de fluides et les interactions fluides-roches au sein du prisme ?** Certaines réactions métamorphiques réalisées au cours de l'enfouissement, de la déformation ou de l'exhumation des structures nécessitent l'apport de fluides. En effet, les fluides sont le vecteur des transferts de matière, que ce soit à l'échelle locale par diffusion ou à plus grande échelle par advection de la matière ([Oliver and Bons, 2001](#)). Ces transferts peuvent permettre l'accommodation d'une partie de la déformation des roches (e.g. [Fischer et al., 1995](#)) et la formation de nouvelles phases hydratées ([Cartwright et Buick, 2000](#); [Marquer et Burkhard, 1992](#); [Oliveret Bons, 2001](#)). La formation de ces phases peut elle aussi avoir un fort impact sur la rhéologie de la croûte. Ainsi, la formation des phengites dans les contacts tectoniques dans le faciès schistes verts nécessite l'apport de fluides (e.g. [Gueydan et al., 2003](#) ; [Schneider et al., 2013](#) ; [Bellanger et al., 2014](#)). Les accidents tectoniques étant reconnus pour chenaliser les circulations de fluides au sein de la croûte (e.g. [McCaig et al., 2000](#) ; [Rolland et al., 2003](#) ; [Beaudoin et al., 2011](#)), ils seront le lieu privilégié de formation des phengites, connues pour leur caractère adoucissant (e.g. [Shea and Kronenberg, 1993](#) ; [Gueydan et al., 2003](#)). Cette chenalisation des fluides étant synchrone de l'activité des zones de cisaillement ([Oliot et al., 2010, 2012](#)), l'étude du timing des circulation permet de mieux estimer celui des zones de cisaillement. L'étude des circulations de fluides permet donc de

mieux estimer la géométrie et le timing des déformations, de caractériser les interactions fluides-roches et finalement d'estimer la rhéologie du prisme collisionnel et son évolution.

### I.3. Choix du laboratoire naturel : l'Arc alpin.

Pour répondre à ces questions, les Alpes de l'Ouest, extrémité Ouest de la chaîne des Alpes ([Fig. 2](#)) constituent un domaine d'étude particulièrement intéressant. Cette chaîne est étudiée depuis de nombreuses années et de très nombreuses données sont disponibles à la fois sur la géométrie, les conditions PT et la chronologie des déformations. Les Alpes sont une chaîne de subduction/collision formée à la suite de la fermeture de l'océan Ligure ([Lemoine et al., 1986](#)). La subduction océanique a ensuite été suivie de la subduction continentale de la marge distale européenne sous la marge apulienne avant que les deux marges n'entrent en collision aux environs de 35 Ma ([Duchêne et al., 1997](#) ; [Sinclair, 1997](#) ; [Ford et Lickorish, 2004](#)). Le prisme collisionnel, initié aux alentours de 35 Ma, intègre les unités internes alpines auxquelles s'ajoutent les unités de la marge proximale européenne qui forment l'ensemble des zones externes de l'arc alpin. Ces unités de la marge proximale ont été partiellement enfouies, raccourcies et exhumées tout au long du fonctionnement du prisme. Ainsi, les unités les plus internes des zones externes alpines, les Massifs Cristallins Externes (MCE), enfouis jusqu'à la transition cassant/ductile, permettent l'étude de la partie relativement profonde du prisme collisionnel. Plus à l'Ouest, l'avant-pays alpin permet quant à lui l'étude détaillée des parties superficielles du prisme. Enfin, la chaîne est fortement arquée et marquée par d'importantes variations le long de l'arc des taux et des quantités de raccourcissement, mais aussi des conditions PT de la déformation ([Bellahsen et al., 2014](#)).

## II. Contexte géologique.

### II.1. Géodynamique.

L'orogène alpin qui s'étend depuis l'Ouest de la Méditerranée jusqu'à l'Himalaya résulte de la fermeture de l'océan Téthys. Les Alpes occidentales (Fig. 3) résultent plus particulièrement de la fermeture de l'océan Liguro-Piémontais (Lemoine et al., 1986). Elles sont divisées en deux principales unités : les Alpes internes et externes, séparées par l'accident d'échelle crustale du Front Pennique (Fig. 3). Cette structure sépare ainsi les unités de la croûte européenne ayant enregistré la subduction océanique puis continentale sous la plaque Apulie (unités internes) (Fig. 2, 3), et les unités n'ayant subi que la collision continentale (unités externes) (Fig. 2, 3).

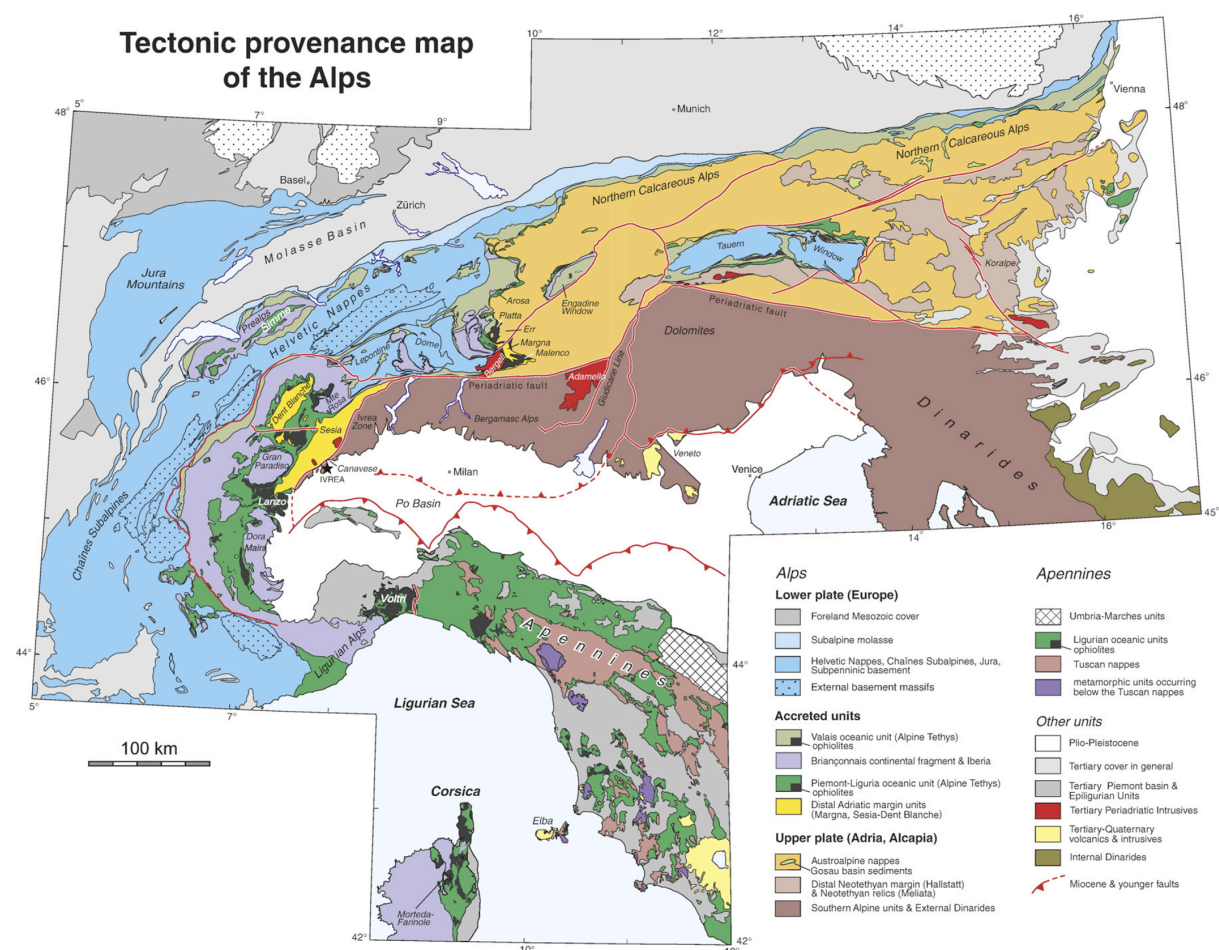


Figure 2. Carte tectonique des Alpes (Handy et al., 2010)

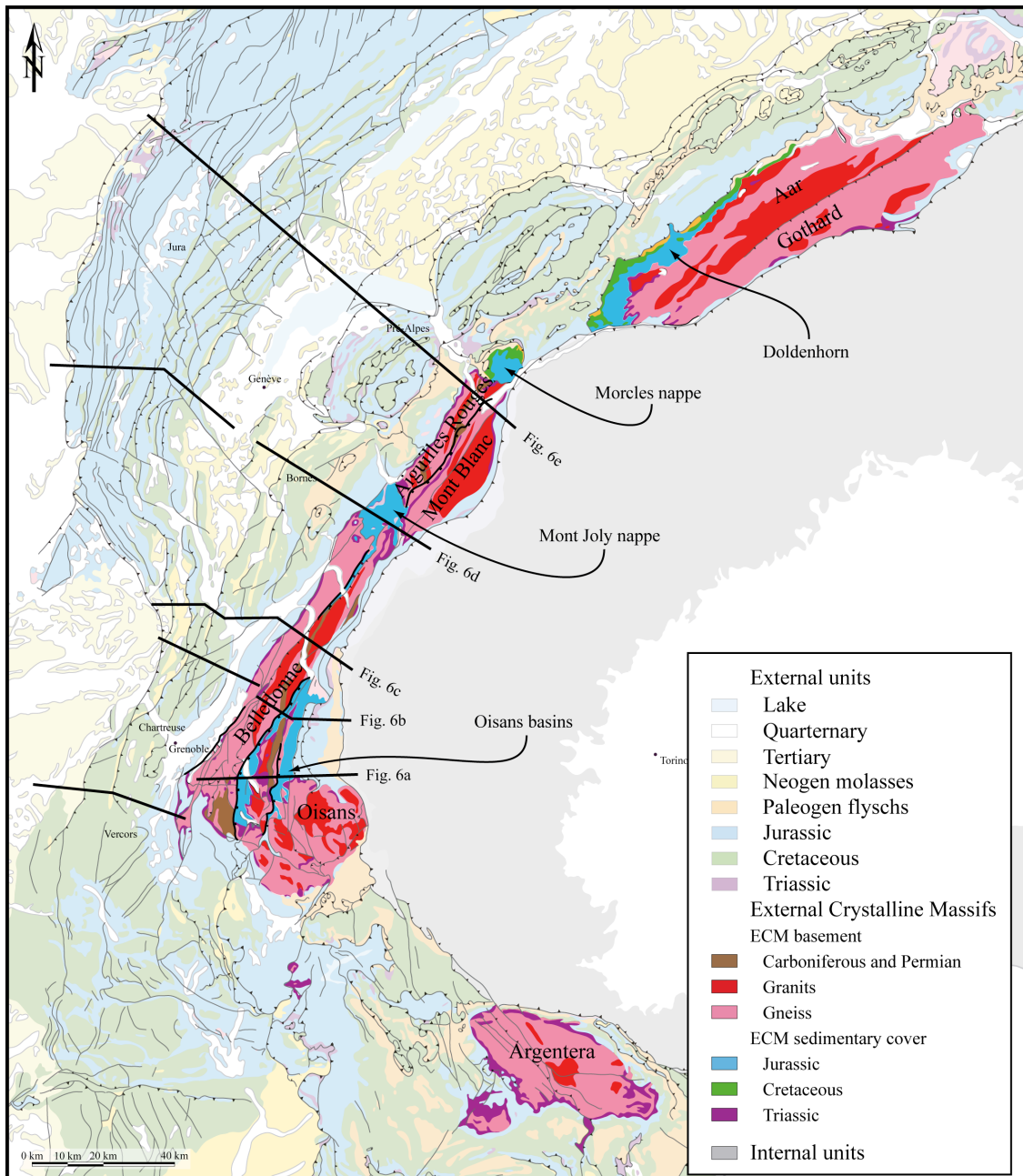


Figure 3. Carte géologique des zones externes de l'Arc Alpin. Les massifs en rouge, les massifs Cristallins Externes (MCE), constituent le socle de la marge proximale européenne. La couverture sédimentaire des MCE est en couleur vive. Les traits marquent les positions des coupes en Fig. 6. (d'après la carte géologique de France 1/1 000 000e).

Au cours la subduction continentale, certaines unités de croûte de la plaque européenne furent enfouies jusqu'à 100 km (e.g. unité de Dora Maira, Italie, [Fig. 2](#), [Chopin, 1986](#) ; [Agard et al., 2001](#)). Suite à cette phase de subduction océanique puis continentale, la collision s'initie vers

35 Ma avec l'épaississement crustal dans les zones externes (e.g., Burkhard et Sommaruga, 1998 ; Dumont et al., 2012 ; Rolland et al., 2008 ; Simon-Labréteau et al., 2009 ; Sanchez et al., 2011), la fin du remplissage du bassin de flysch et la transition flysch-molasse (Sinclair, 1997 ; Ford et al., 2006), et la création de reliefs importants (Oligocène, Jourdan et al., 2012).

## II.2. Structuration et déformation de la marge européenne.

### II.2.1. Structuration liasique de la marge européenne.

Au cours du Lias, un épisode de rifting amincit la lithosphère jusqu'à l'ouverture océanique de l'Océan Téthys/Ligure. La marge européenne est subdivisée en 3 domaines (Fig. 4, Lemoine et al., 1986 ; De Wever et Caby 1981 ; De Wever et al., 1985 ; Lemoine et Graciansky, 1988) : la zone Piémontaise, partie la plus amincie et plus distale de la marge, la zone Briançonnaise qui est marquée par un amincissement moins fort de la croûte et enfin la zone Dauphinoise qui englobe les parties les plus proximales de la marge (Fig. 4).

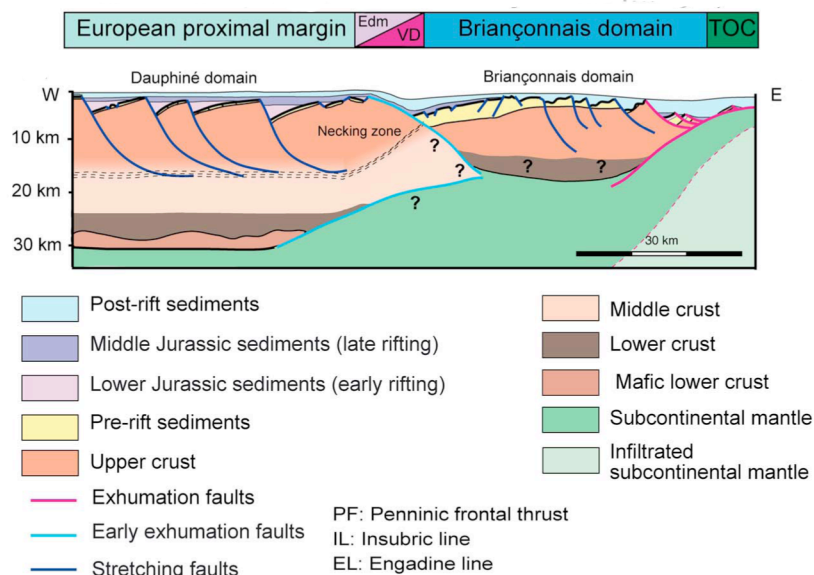


Figure 4. Coupe schématique de la marge européenne. TOC est la transition océan-continent, le domaine Piémontais. Mohn et al., 2012.

La zone Dauphinoise constitue la partie proximale et donc la moins amincie de la marge Européenne (Fig. 4). A l'Ouest du Front Pennique, on remarque de nombreux bassins extensifs et blocs basculés, orientés Nord-Sud à NNE-SSW (e.g. les bassins de l'Oisans, Fig.

3). Le remplissage syn-tectonique de ces bassins s'étale du Rhétien jusqu'au Dogger (Fig. 5). La transition entre subsidence tectonique et subsidence thermique qui marque la fin du rifting s'étale entre le Toarcien et Callovien supérieur le long de l'arc alpin (Barféty et Gidon, 1983 ; Tricart et Lemoine, 1986 ; Lemoine et al., 1986).

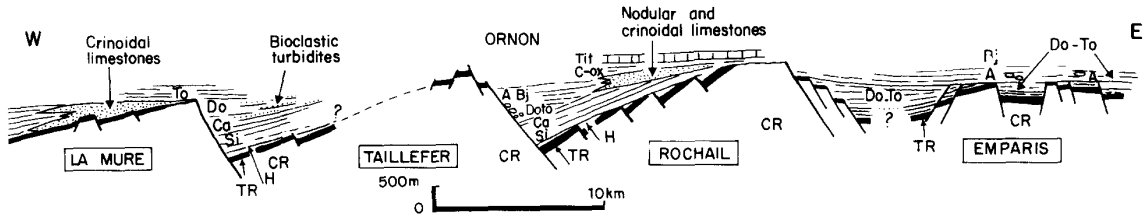


Figure 5. Coupe palinspastique simplifiée de la marge européenne à la latitude du massif de l'Oisans lors du Dogger. Cr : Socle cristallin ; Tr : Trias germanique ; H : Hettangien ; Si : Sinémurien ; Ca : Carixien ; Do : Domérien ; To : Toarcien ; A : Aalénien ; Bj : Bajocien ; C-Ox : Callovo-Oxfordien ; Tit : Tithonien. Lemoine et al., 1986

L'ouverture de ces bassins est contrôlée par des failles normales d'échelle crustale permettant un remplissage sédimentaire allant de plusieurs km au pied des failles (Fig. 5) à quelques dizaines de mètres au niveau de la crête des blocs basculés (Fig. 5). La plupart de ces failles sont considérées comme n'ayant pas, ou très peu, été réactivées lors de l'inversion des bassins (e.g., Bellahsen et al., 2012). En effet, le rejet de ces failles est encore actuellement de plusieurs km (ex : 3 km au niveau de la faille du Col d'Ornon, Tricart et Lemoine, 1986 ; Lemoine et al., 1989) et les dépôt-centres des couches syn-tectoniques sont toujours situés au pied de ces failles.

Sur la partie Nord de l'arc Alpin, la marge européenne subit un nouvel épisode extensif au cours du Crétacé inférieur (peut être initié au Jurassique, Manatchal et al. 2006) permettant l'ouverture du domaine valaisan avant sa fermeture au cours du Crétacé supérieur (Stampli, 1993). Cet épisode permet l'individualisation de la zone briançonnaise qui constitue dès lors une portion moins amincie de la marge européenne entre l'océan Ligure et la zone dauphinoise. La taille, la nature et le calendrier d'ouverture du domaine valaisan reste cependant problématique (e.g. Ceriani et al., 2001 ; Fügenshuh et al., 1999, Mohn et al., 2010).

De façon à décrire précisément les déformations affectant les MCE lors de l'intégration de la marge proximale au prisme collisionnel, on distinguera le socle de la marge qui regroupe l'ensemble des roches antérieures à l'ouverture de l'océan Téthys et donc aux dépôts mésozoïques, de la couverture qui englobe l'ensemble des roches mésozoïques et cénozoïques

contemporaines et postérieures à l'ouverture de l'océan Téthys. Le socle est constitué de roches essentiellement cristallines, métamorphiques, formées durant l'orogénèse hercynienne et de quelques roches sédimentaires datées du permo-carbonifère, déposées lors de l'effondrement de la chaîne hercynienne (Fig. 5). La couverture est constituée des dépôts sédimentaires marins, datés du Mésozoïque, syn- à postérieurs au rifting téthysien (Fig. 5) puis du rifting valaisan. Les dépôts cénozoïques, constitués de flyschs et de molasses essentiellement, témoignent de la subduction continentale puis de la progression de la collision (Sinclair, 1997 ; Ford et Lickorish, 2004). On note le cas particulier du Trias inférieur qui constitue le tégument et reste attaché au socle hercynien lors de la déformation. Au niveau des MCE, le Trias dit germanique est peu épais (quelques mètres à dizaines de mètres) et constitué de dépôts de grès, dolomies et de quelques lentilles de gypse.

#### *II.2.2. Conditions P-T enregistrées dans les MCE.*

A partir de 35 Ma, la partie proximale de la marge européenne est partiellement enfouie sous les unités internes et va être intégrée au prisme collisionnel. Du fait de cet enfouissement, on observe un gradient métamorphique de moyenne pression et moyenne température (MP-MT) dans les zones externes. Les roches de la zone externe ont ainsi été marquées au maximum par un métamorphisme de faciès schistes verts au niveau des MCE (e.g. Rolland et al., 2003 ; Fourcade et al., 1989 ; Jullien et Goffé, 1993). Les bassins hérités de la marge proximale eurasienne furent donc enfouis entre 10 et 20 km au maximum dans des conditions de pression et de température correspondant à la transition de comportement cassant/ductile des roches de la croûte (e.g. Rolland et al., 2003 ; 2009 ; Bellahsen et al., 2012 ; Goncalves et al., 2012). Dans le massif de l'Argentera (Fig. 3), le pic de métamorphisme, daté entre 34 et 32 Ma, est estimé dans le socle entre 350 et 375°C, et de 3,5 à 7 kbar (Corsini et al., 2004 ; Sanchez et al., 2011). L'estimation de la température de la couverture du massif laisse supposer un enfouissement compris entre 8 et 10 km avec un gradient géothermique compris entre 25 et 30°C.Ma<sup>-1</sup> (Labaume et al., 2008). Cette estimation de l'enfouissement est compatible avec l'estimation inférieure de pression de Corsini et al. (2004). Plus au Nord, dans le massif de l'Oisans (Fig. 3), les températures maximales enregistrées dans le socle et la couverture des bassins hérités sont estimées à 350°C +/-15°C et datées entre 31 et 25 Ma (e.g. Bernard, 1978 ; Jullien et Goffé, 1993 ; Crouzet et al., 2001 ; Bellanger et al., 2015). De même que pour le massif de l'Argentera, les estimations de pression sont bien moins contraintes que celles de la température, entre 2 et 5 kbar (Bernard,

1978 ; Jullien et Goffé, 1993), rendant incertaine la profondeur de l'enfouissement collisionnel du massif. Le pic de métamorphisme enregistré par le massif du Mont-Blanc (Fig. 3) semble le mieux contraint dans les MCE, estimé à  $400^{\circ}\text{C} \pm 25^{\circ}\text{C}$  et 5 kbar  $\pm 0,05$  kbar (Rolland et al., 2003). Enfin, le massif de l'Aar (Fig. 3) est marqué par un pic estimé à  $450^{\circ}\text{C} \pm 25^{\circ}\text{C}$  et entre 6 kbar  $\pm 1$  kbar (Fourcade et al., 1989 ; Challandes et al., 2008 ; Goncalves et al., 2012). On observe donc une augmentation des conditions P-T du pic de métamorphisme enregistré dans les MCE du Sud vers le Nord de l'Arc alpin. De même, il semble que les taux de raccourcissement des zones externes augmentent depuis le Sud vers le Nord (Fig. 6, Sinclair, 1997 ; Bellahsen et al., 2014).

#### *II.2.3. Déformation du socle et de la couverture des MCE.*

Les accidents structurant la chaîne d'avant-pays sont enracinés sous les MCE, eux-mêmes déformés avec un style purement « thick-skin » (Fig. 6). Au premier ordre, la direction de raccourcissement sur tout le pourtour de l'Arc est perpendiculaire à la chaîne (Choukroune et al., 1986 ; Platt et al., 1989 ; Lickorish et al., 2002 ; Rausenbaum et Lister, 2005).

Avec leur intégration au prisme collisionnel après leur enfouissement sous les unités internes, les bassins hérités sont progressivement inversés, accommodant ainsi le raccourcissement de la marge européenne (Fig. 6, e.g. Burkhard, 1988 ; Burkhard et Sommaruga, 1998 ; Bellahsen et al., 2012 ; 2014). Le socle est donc déformé et impliqué dans le raccourcissement et la couverture n'est pas décollée au-dessus du socle des Massifs Cristallins Externes (Fig. 6d, e). Même si la couverture et le socle des bassins hérités restent couplés lors du raccourcissement des MCE, la déformation s'exprime différemment dans les deux ensembles (e.g., Burkhard, 1988 ; Escher et al., 1993 ; 1997 ; Bellahsen et al., 2012). Ainsi, le socle est plissé avec une grande longueur d'onde (de plusieurs centaines de mètres à plusieurs kilomètres) du fait du jeu de bandes de cisaillement (Fig. 6) et la couverture est plissée disharmoniquement au-dessus des déformations du socle (Fig. 6). Il apparaît que ces déformations de la croûte se sont produites au cours, ou proche, du pic de métamorphisme des MCE (Bellanger et al., 2015). Toutefois, les timing entre pic de pression, de température et déformation sont encore mal contraints.

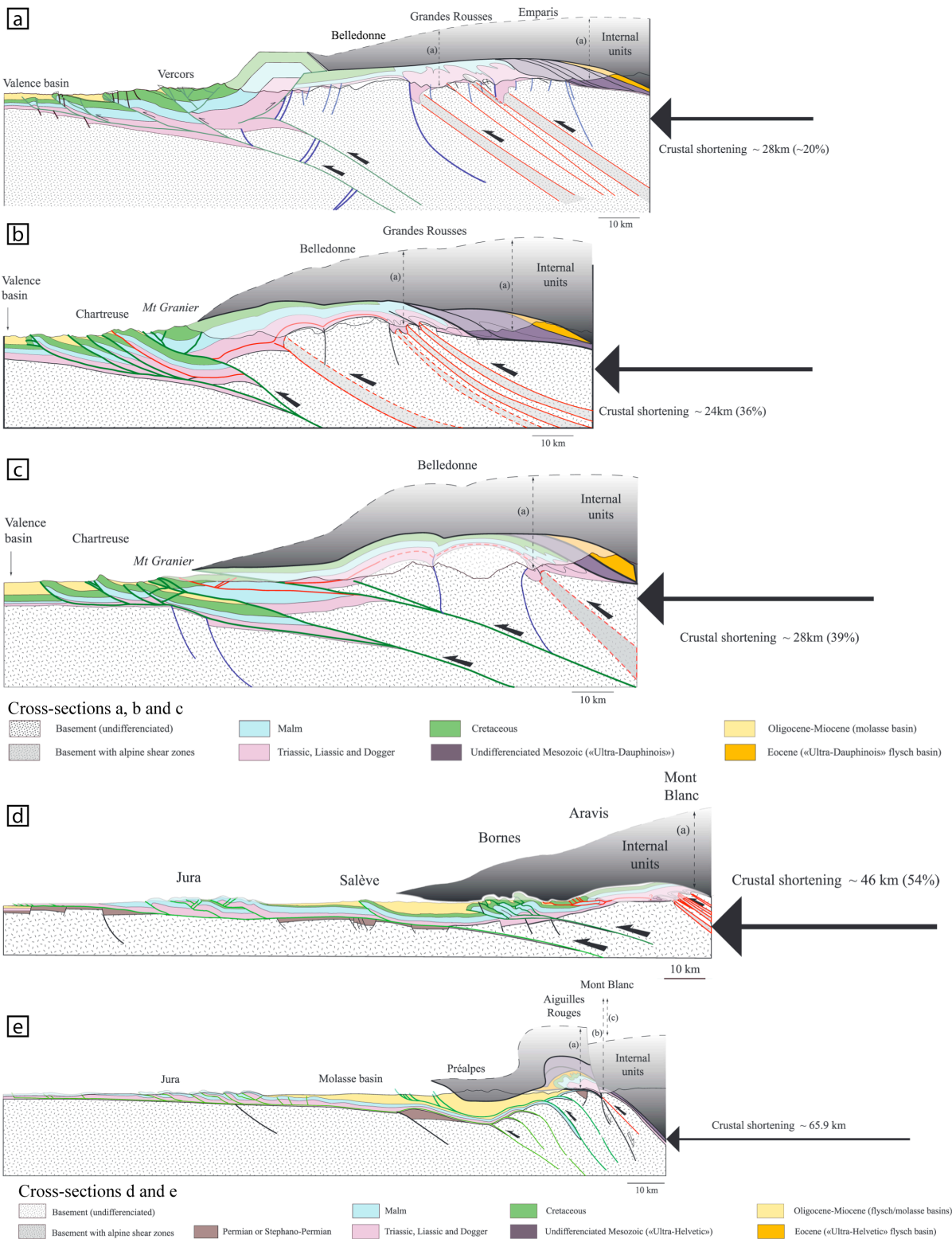


Figure 6. Coupes des zones externes de l'Arc Alpin. Les coupes sont équilibrées sur la base de la conservation de la longueur des couches dans les chaînes subalpines. Modifiée d'après Bellahsen et al., 2014.

Le massif de l'Argentera, située au Sud de l'Arc (Fig. 3), est marqué par des bandes de cisaillement dextres et inverses compatibles avec un raccourcissement N/S à NNE/SSO (Fig. 7, Corsini et al., 2004 ; Sanchez et al., 2011). L'activité de ces bandes est datées entre 29 et 20 Ma, soit après le pic de métamorphisme et pendant l'exhumation du massif (Sanchez et al., 2011).

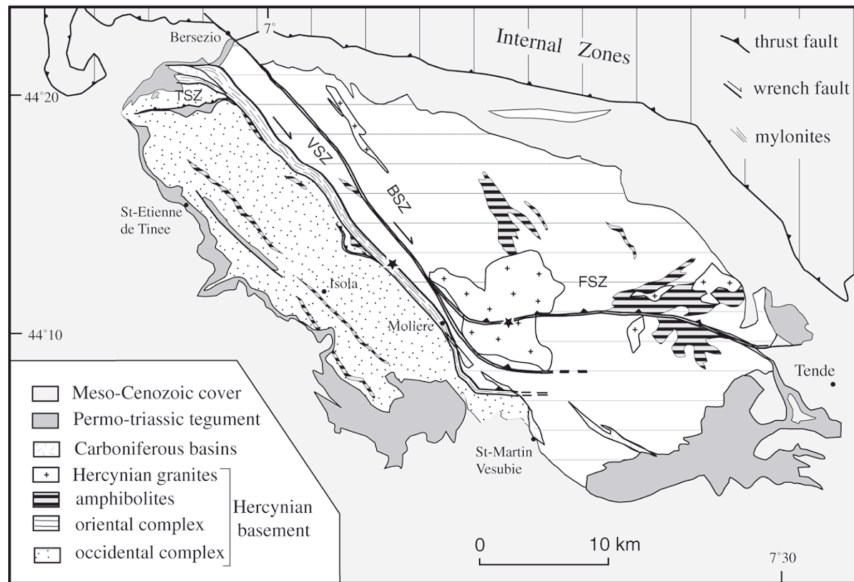


Figure 7. Carte structurale du massif de l'Argentera montrant les principales structures (Corsini et al., 2004).

Dans le massif de l'Oisans (Fig. 7), le raccourcissement Est-Ouest est accommodé par des bandes de cisaillement essentiellement inverses (Fig. 6a), datées entre 34 et 25 Ma (Bellanger et al., 2015) et décrochantes, datées entre 34 et 27 Ma (Simon-Labréteau et al., 2009). La déformation du massif de l'Oisans semble donc contemporaine du pic de métamorphisme (Bellanger et al., 2015). Dans le massif du Mont-Blanc (Fig. 3, 6), les cisaillements du socle sont inverses et décrochants dextres (Rolland et al., 2003), datés entre 29,5 et 6 Ma (Leloup et al., 2005 ; Rolland et al., 2008 ; Cenki-Tok et al., 2013). Le principal cisaillement (Fig. 6d, e) structurant le massif sur toute sa longueur, la Mont Blanc Shear Zone, épais de plusieurs kilomètres (Leloup et al., 2005), est initié à 23 Ma (Rolland et al., 2008). De la même façon que dans le massif de l'Oisans, les déformations du massif du Mont Blanc sont contemporaines du pic de métamorphisme. Enfin, le massif de l'Aar-Gothard (Fig. 3) est caractérisé par deux principales générations de cisaillements, actives respectivement entre 23 et 17 Ma et entre 14 et 12 Ma (Challandes et al., 2008 ; Rolland et al., 2009). Ainsi, l'ensemble de ces bandes de cisaillement est à peu près synchrone le long des MCE (Rolland et al., 2008 ; Simon-Labréteau et al., 2009 ; Cenki-Tok et al., 2013 ; Bellanger et al., 2014).

Peu de bandes de cisaillement du socle sont propagées dans la couverture (Fig. 6). Au niveau de la Mont-Blanc Shear Zone et des cisaillements majeurs du massif de l'Aar, on observe des lentilles de téguments au niveau du socle cisaillé indiquant une forte déformation de l'interface socle/couverture. Le reste des bandes de cisaillement des MCE est restreint au socle que ce soit dans l'Oisans (Bellahsen et al., 2012), dans le Mont-Blanc (Escher et al., 1993 ; 1997) ou dans l'Aar (Burkhard, 1998) (Fig. 6). Dans ces cas-là, la couverture se déforme de manière diffuse et disharmonique au dessus du socle.

Dans l'ensemble, on constate une augmentation de l'intensité des déformations depuis le Sud vers le Nord de l'Arc alpin (Fig. 6). Cela se traduit par une augmentation des taux de raccourcissement des MCE qui passent de 14 - 16% de raccourcissement à la latitude de l'Oisans à 29% au niveau des massifs des Aiguilles Rouges et du Mont Blanc et à 40% à la latitude du massif de l'Aar (Bellahsen et al., 2014). On note que cette évolution Nord-Sud des taux de raccourcissement se retrouve dans les chaînes d'avant-pays (i.e., chaines subalpines du Vercors, de la Chartreuse, des Bauges, des Bornes, Fig. 6) (Philippe et al., 1998 ; Affolter et al., 2008). Il apparaît donc que le raccourcissement de la zone externe augmente vers le Nord (Bellahsen et al., 2014).

Dumont et al. (2008, 2011) distinguent 4 phases principales de raccourcissement de la couverture (Fig. 8) : d'abord un raccourcissement NE-SW, datant de l'Éocène (ante-Priabonien) (D1), suivi d'un raccourcissement Nord-Sud lors de l'Oligocène inférieur (D2), et enfin deux étapes successives de raccourcissement Est-Ouest datées respectivement de l'Oligocène (D3) et du Miocène (D4) (Fig. 8). Cependant, la majorité du raccourcissement Oligo-miocène de la couverture se fait perpendiculairement à la chaîne ainsi que le montrent les grands plis de la couverture des MCE (Fig. 6, e.g. Dumont et al., 2008 ; Bellahsen et al., 2012).

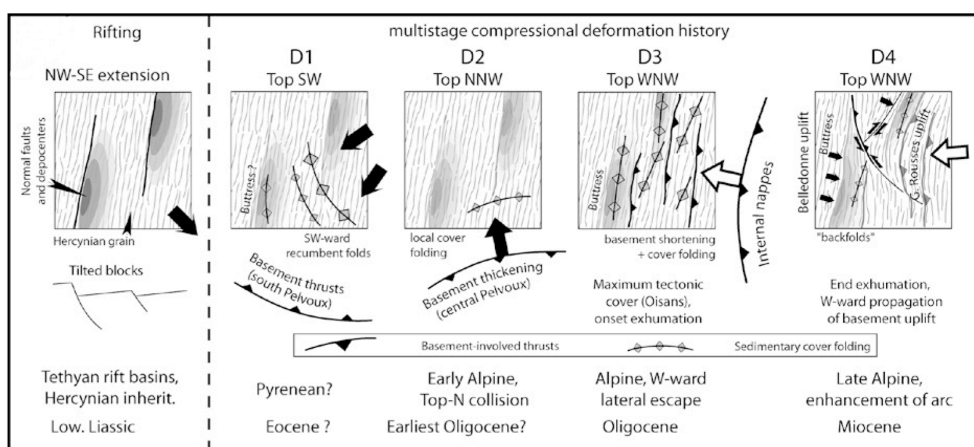


Figure 8. Schéma de la déformation de la couverture des Massifs Cristallin Externes au niveau du massif des Ecrins. (Dumont et al., 2008).

Au premier ordre, la couverture des MCE reste attachée à son socle et est affectée par de grands plis syn-schisteux disharmoniques sur les déformations du socle (e.g. [Bellahsen et al., 2012](#), [Fig. 6](#)). Ces plis sont ainsi caractérisés par une longueur d'onde systématiquement inférieure à celle des plis du socle (de quelques dizaines à quelques centaines de mètres) (e.g. [Gratier et al., 1973](#) ; [Gratier et Vialon, 1980](#) ; [Burkhard, 1988](#) ; [Escher et al., 1993](#)). A la latitude des MCE les plus septentrionaux (massifs du mont Blanc et de l'Aar), le plissement de la couverture s'intensifie jusqu'à ce que les plis soient déversés vers l'extérieur de la chaîne ([Fig. 6](#)). Le remplissage sédimentaire des bassins hérités est alors extrudé et structuré en nappes (i.e. nappes helvétiques et ultra-helvétiques, [Ramsay et Hubert, 1989](#) ; [Burkhard, 1988](#) ; [Escher et al., 1993](#) ; [1997](#) ; [Epard et al., 1990](#)). Cependant, ce style de déformation de la couverture des MCE est discuté par certains auteurs qui proposent son décollement précoce à l'initiation de la collision (i.e. décollement de la nappe de Morcles, [Leloup et al., 2005](#)).

### II.3. Les massifs Grandes Rousses et Nord-Ouest Oisans.

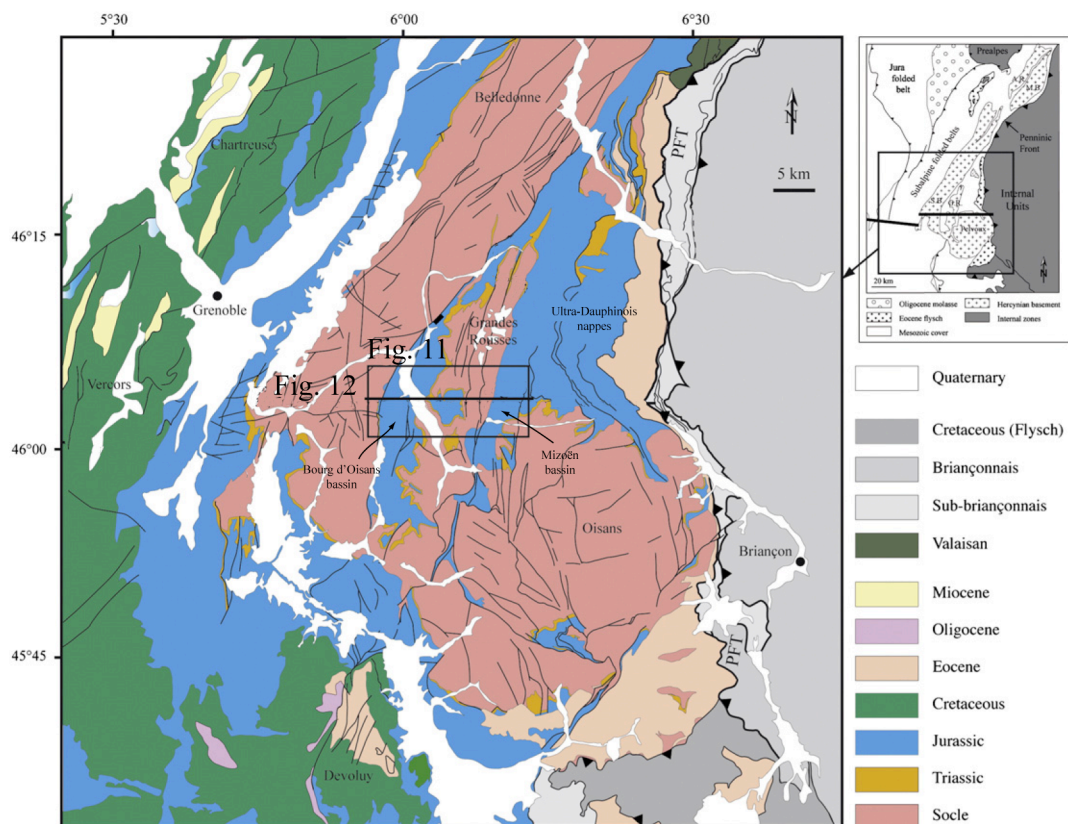


Figure 9. Carte géologique des massifs de l'Oisans, des Grandes Rousses et de la partie Sud de Belledonne. ([Bellahsen et al., 2012](#)).

Les massifs de l’Oisans et des Grandes Rousses sont situés entre le Front Pennique et le massif de Belledonne ([Fig. 3, 9](#)). Dans ce mémoire, on s’est focalisé sur deux bassins particuliers, les bassins de Bourg d’Oisans et de Mizoën, situés au sud des Grandes Rousses et au Nord-ouest du massif de l’Oisans, respectivement ([Fig. 9](#)).

### *II.3.1. Structuration des Grandes Rousses et du Nord-Ouest Oisans.*

Le bassin de Bourg d’Oisans est limité à l’Est par la crête de bloc basculé des Grandes Rousses et à l’Ouest par la faille normale du Col d’Ornon ([Fig. 10](#)). Cette faille Nord/Sud d’échelle crustale a un rejet de l’ordre de 3 km et contrôle les dépôts syn-rift dans le bassin ([Lemoine et al., 1989](#)). Les sédiments syn-rift sont datés de l’Hettangien jusqu’au Bajocien ([Barfety et al., 1972](#)). Ces sédiments disposés en éventail ([Fig. 5, 11](#)) sont essentiellement constitués de marnes et de calcaires marneux mais aussi des dépôts plus pélitiques, tel que l’Aalénien ([Barféty et al., 1972](#)). La disposition actuelle de ces sédiments suggère fortement le non-décollement de la couverture au-dessus du socle ([Tricart et Lemoine, 1986, Bellahsen et al., 2012, Fig. 11](#)).

Le bassin de Mizoën est situé entre la crête du bloc basculé des Grandes Rousses et le petit bassin de la Grave ([Fig. 10](#)). Il est limité à l’Ouest par la faille normale Nord-Sud de Mizoën. La couverture sédimentaire syn-rift est datée du Domérien au Bathonien, ce qui suggère une ouverture de ce bassin légèrement diachrone de celle du bassin de Bourg d’Oisans. Les sédiments syn-rift sont essentiellement des marnes et des calcaires marneux avec des passages extrêmement pélitiques, comme la série aalénienne ([Barbier et al., 1973](#)). De la même façon que pour le bassin de Bourg d’Oisans, la couverture du bassin de Mizoën n’est pas significativement décollée ([Bellahsen et al., 2012, Fig. 11](#)).

Enfin, immédiatement à l’Est du bassin de Mizoën se trouve le bassin de La Grave. Il est situé entre le plateau d’Emparis et les nappes de l’Ultra-Dauphinois. Ce bassin est de très modeste envergure par rapport aux deux précédents. Il est limité à l’Ouest par la faille de la Grave qui marque un jeu de quelques centaines de mètres à peine ([Barbier et al., 1973](#)), bien moins important que les failles kilométriques de Mizoën et du Col d’Ornon.

Les bassins de l’Oisans sont recouverts des dépôts post-rift dont la séquence est visible dans la région au niveau du Grand Renaud ([Barfety et al., 1972](#)).

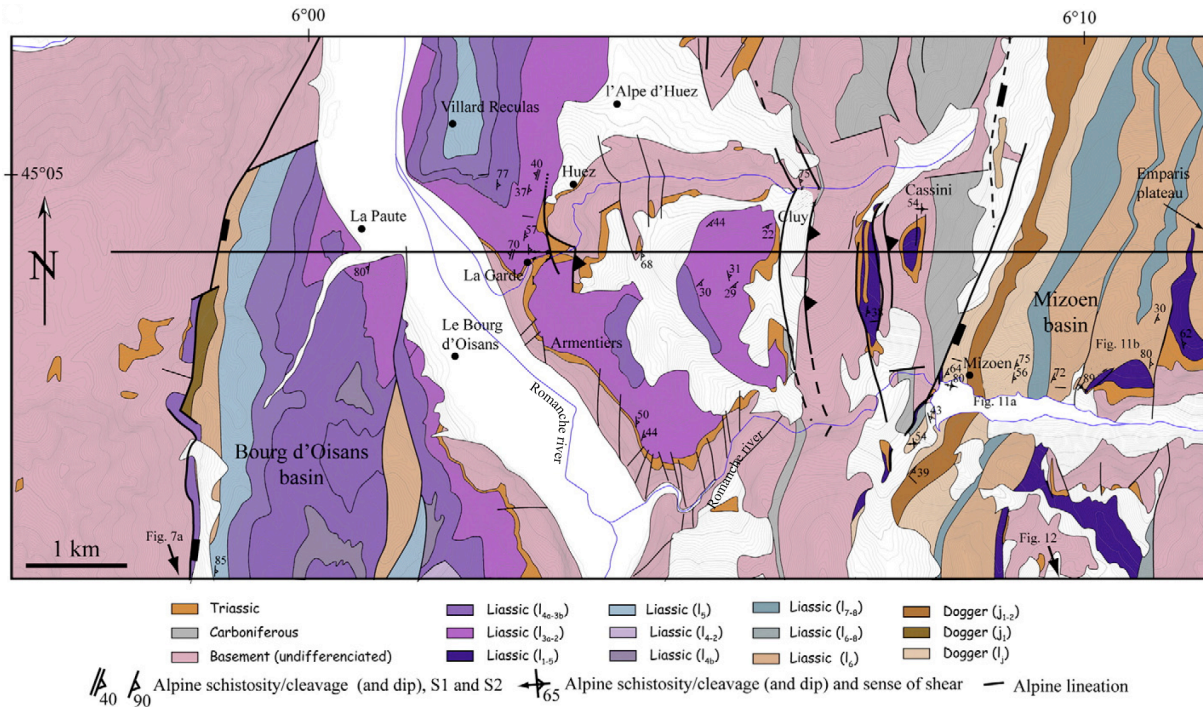


Figure 11. Carte géologique des bassins du massif de l’Oisans. Le trait de coupe correspond à la figure 12 (Bellahsen et al., 2012).

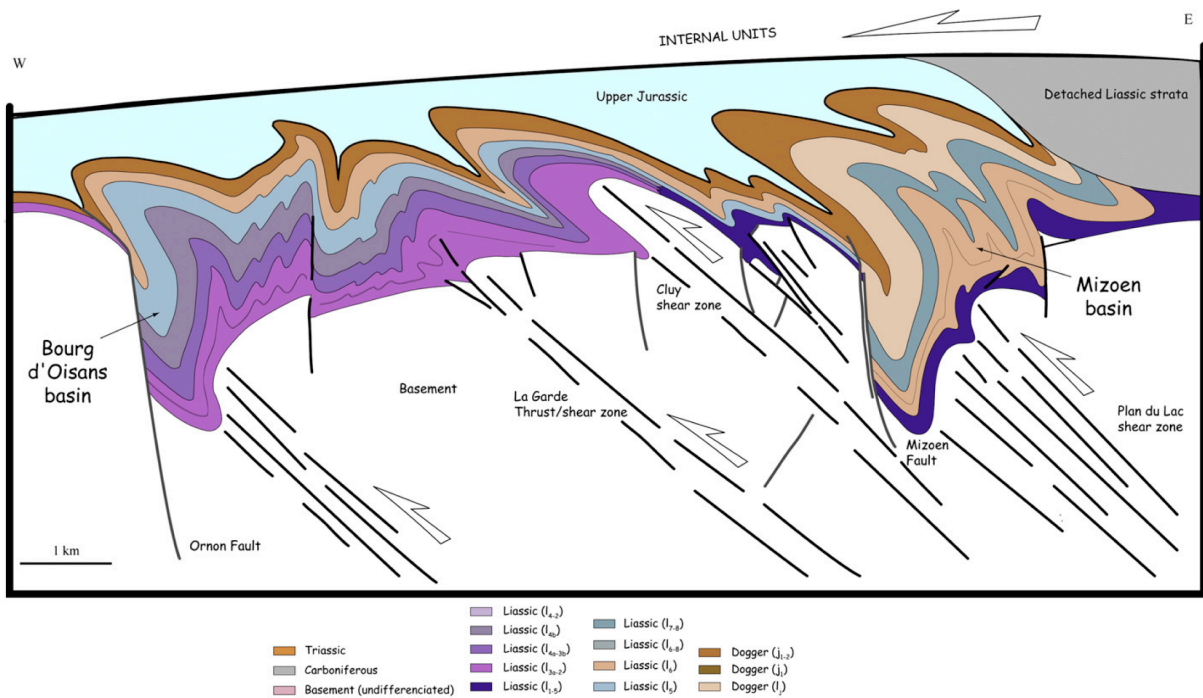


Figure 11. Coupe des bassins de l’Oisans. La couverture, non décollée du socle est plissé disharmoniquement au-dessus de celui-ci. On observe sur le terrain 3 plis de socle dans le bassin de Bourg d’Oisans, associés aux bandes de cisaillement de la Garde, de Cluy, et de la Croix de Cassini. Une autre bande de cisaillement de socle est suspectée, celle de Bourg d’Oisans. Le socle du bassin de Mizoën est déformé par la bande de cisaillement du même nom. A l’Est, les nappes de l’Ultra-Dauphinois chevauchent le bassin de Mizoën. L’emplacement de la coupe est indiqué Figure 11. (Bellahsen et al., 2012).

### *II.3.2. Déformation du socle des bassins de l’Oisans.*

Le socle du bassin de Bourg d’Oisans affleure au niveau de la vallée de la Romanche, à proximité du village de Bourg d’Oisans, au niveau de la route de l’Alpe d’Huez (Fig. 10). Il est composé de migmatites, de gneiss et d’amphibolites datées du Carbonifère au Permien (Guillot et Ménot, 1999). On rencontre également quelques granites anatectiques (ex. du granite de l’Alpetta, au Sud-est du massif des Grandes Rousses) (Barféty et al., 1984). Il existe de plus quelques bassins extensifs intracontinentaux d’âge Stéphanien à Westphalien formés lors de l’effondrement orogénique de la chaîne hercynienne (Barféty et al., 1972 ; Barbier et al., 1973, Fig. 10). A ce socle cristallin et localement détritiques s’ajoutent les dépôts de faciès peu profond, gréseux, carbonatés et localement évaporitiques du Trias. Ces sédiments sont pro parte le résultat de l’érosion de la chaîne varisque après l’orogénèse hercynienne. Le Trias inférieur est tégumentaire (Fig. 11).

Quatre plis de socle sont présents dans le socle du bassin de Bourg d’Oisans (Gratier et al., 1973 ; Gratier et Vialon, 1980 ; Tricard et Lemoine, 1986 ; Dumont et al., 2008, Fig. 11). Ces plis sont associés à des zones de cisaillement intense du socle du bassin (Bellahsen et al., 2012 ; Bellanger et al., 2014, Fig. 11). Trois sont observables sur le terrain et associés aux bandes de cisaillement de La Garde, de Cluy (Fig. 11, 12) et de Plan du Lac (Fig. 11), tandis qu’un, celui associé à la bande de cisaillement de Bourg d’Oisans, est suspecté mais pas observé dans le bassin (Bellahsen et al., 2012, Fig. 11). Ce pli, déjà dessiné par Gratier et Vialon (1980), est interprété comme les autres comme dû à un cisaillement inverse, top-vers-l’Ouest du socle. Tous ces cisaillements observables à l’affleurement montrent les mêmes caractéristiques : des pendages de 30 à 60° et ne réactivant pas la foliation hercynienne pré-existante (Bellanger et al., 2014). Le plissement du socle du bassin de Mizoën est aussi interprété comme dû au cisaillement du socle bien que celui-ci n’affleure pas (Fig. 11).

Les bandes de cisaillements du socle des deux bassins sont caractérisées par des cisaillements anastomosés, relativement peu pentés (de l’ordre de 20 à 50°) vers l’Est et par une schistosité alpine plus pentée (entre 60 et 80°) très pénétrative (Fig. 12). Sur le terrain, cette schistosité alpine semble se surimposer à la schistosité hercynienne (Bellahsen et al., 2012). L’épaisseur de ces bandes est variable, de quelques mètres/dizaines de mètre dans le cas de la bande de cisaillement de La Garde jusqu’à 1 km pour la bande du Col de Cluy (Fig. 12).

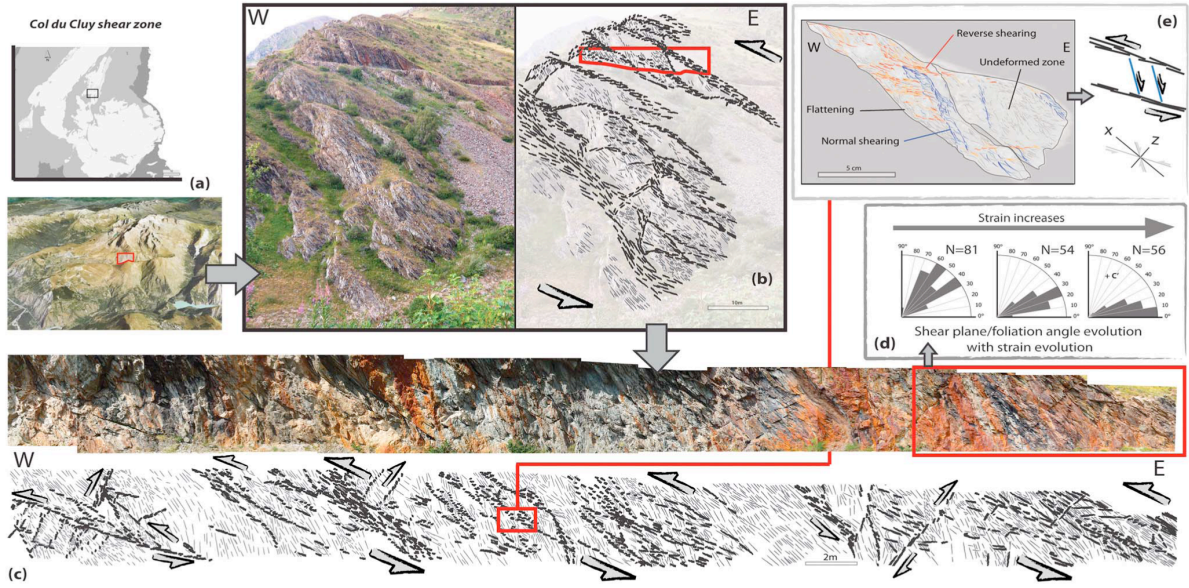


Figure 12. Observation et analyse structurale de la bande de cisaillement du Col de Cluy, Bassin de Bourg d’Oisans (a) localisation de la bande de cisaillement au Sud du massif des Grandes Rousses. (b) Photo et interprétation de la bande de cisaillement. Les plans noirs sont anastomosés et pendent majoritairement à 35° (Bellanger et al., 2014).

La composition minéralogique de ces bandes de cisaillement dépend fortement de celle des protolites déformés. Ainsi, dans le bassin de Bourg d’Oisans, la bande de cisaillement du Col de Cluy (Fig. 11, 12) se développe dans des roches acides, rhyolites et trachytes (orthophyres) et des dépôts du Carbonifère, alors que la bande de cisaillement de Huez se développe dans des micaschistes et des gneiss amphibolitiques (Barbier et al., 1972 ; Barfety et al., 1973). Cependant leur assemblage d’équilibre est caractéristique du faciès métamorphique schistes verts : chlorite + epidote + phengite (+ talc) (Bellanger et al., 2014). L’analyse microstructurale de ces bandes montre qu’elles se sont développées dans les conditions de la zone de transition de comportement cassant/ductile des roches du socle. Quelques veines métamorphiques sont associées au cisaillement du socle ; elles sont remplies d’un assemblage de Quartz + Albite + Chlorite (Poty et al., 1974, Bellanger et al., 2014).

### *II.3.3. Déformation de la couverture des bassins de Bourg d’Oisans et de Mizoën.*

De grands plis d’axe Nord/Sud d’échelle hectométrique à kilométrique sont visibles dans la couverture du bassin de Bourg d’Oisans et de Mizoën (Gratier et al., 1973, Gratier et Vialon, 1980, Fig. 11). Ces plis sont majoritairement déversés vers l’Ouest et syn-schisteux, c’est-à-dire qu’ils prennent pour plan axial une des schistosités observables dans le bassin.

Quelques plis d'axe Est/Ouest, résultant d'une phase de compression Nord/Sud ont été décrits dans ces bassins (Vialon, 1974 ; Dumont et al., 2008, Fig. 13B). Néanmoins, il semble s'agir de structures anecdotiques au vu du raccourcissement principal (Depardon, 1979 ; Gratier et Vialon, 1980). La majeure partie des structures de la couverture des bassins de l'Oisans semblent donc compatibles avec un raccourcissement Est-Ouest. Si dans leur ensemble les couvertures des bassins de Bourg d'Oisans et de Mizoën ne montrent pas de signe de décollement significatif de leur socle (Bellahsen et al., 2012), il existe cependant des décollements locaux (Gillcrist et al., 1987 ; Grand, 1988). Ces structures permettent l'accommodation du raccourcissement disharmonique des couvertures par rapport à leur socle.

La partie Est du bassin de Mizoën, au niveau du plateau d'Emparis, est constituée de fins dépôts mésozoïques autochtones (Barbier et al., 1973), chevauchés par un empilement de nappes allochtones dites de l'Ultra-Dauphinois (Barbier 1963, Fig. 11). Ces nappes sont décollées au dessus d'un chevauchement majeur, le chevauchement de Roselend (Cerniani et al., 2001) dont l'enracinement reste problématique.

#### *II.3.4. Schistosités des bassins de l'Oisans.*

On présente ici les différentes schistosités (et les phases de déformation associées le cas échéant) décrites pour ces mêmes bassins par les auteurs précédents (i.e. Gratier et Vialon, 1980 ; Dumont et al., 2008 ; Bellahsen et al., 2012, Fig. 13).

Gratier et Vialon (1980) décrivent deux schistosités résultant du plissement de la couverture du bassin de Bourg d'Oisans (Fig. 13). S<sub>1</sub><sub>Gratier et Vialon, 1980</sub> est décrite en position de plan axial des principaux plissements de la couverture du bassin de bourg d'Oisans et S<sub>2</sub><sub>Gratier et Vialon, 1980</sub> est une schistosité de crénulation résultant des derniers incrément de la déformation. Dumont et al. (2008) décrivent 4 schistosités différentes (Fig. 13). S<sub>1</sub><sub>Dumont et al., 2008</sub> est Nord-Sud à NW-SE et faiblement pentée vers l'Est et associé au plissement précoce de la couverture ; S<sub>2</sub><sub>Dumont et al., 2008</sub> est Est-Ouest et résulte d'une phase de compression Nord-Sud. S<sub>3</sub><sub>Dumont et al., 2008</sub> est orientée Nord-Sud, plus fortement pentée que S<sub>1</sub> et est associée au plissement du socle et à la déformation principale de la couverture. Enfin S<sub>4</sub><sub>Dumont et al., 2008</sub> est une schistosité Nord-Sud, verticale résultant des derniers incrément de la déformation.

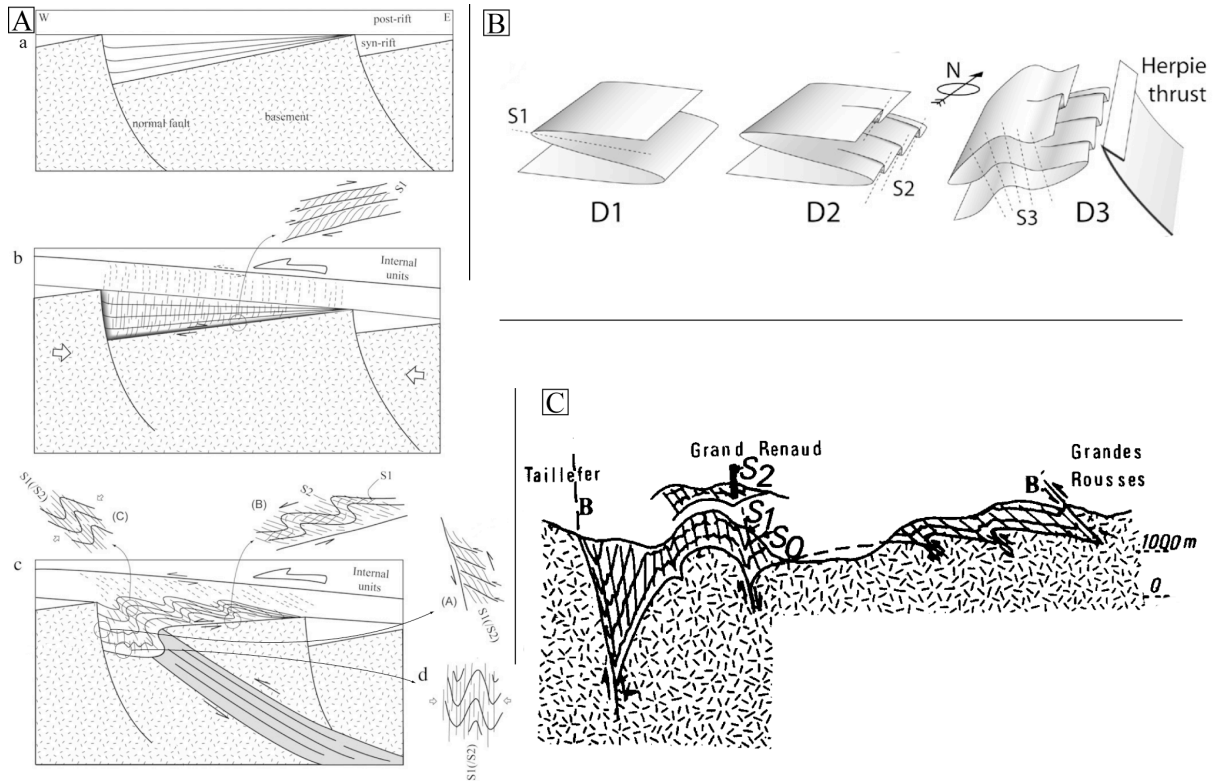


Figure 13. Différentes phases de schistosité reconnues dans les Bassins de l’Oisans suivant plusieurs auteurs. A. S1 marque le cisaillement de la couverture lors de l’initiation du raccorciissement et S2 est la schistosité de plan axial des plis majeurs des bassins. [Bellahsen et al., 2012](#). B. S1 est une schistosité approximativement N-S, très peu pentée et associée à la déformation précoce des MCE S2 est une schistosité de plan axial des plis Nord-Sud, S3 se développe de manière synchrone à la déformation du socle. [Dumont et al., 2008](#). C. S1 est la schistosité de plan axial des plis majeurs des bassins. S2 est une schistosité de crénulation. [Gratier et Vialon, 1980](#).

[Bellahsen et al., 2012](#) décrivent deux phases de schistosité principales dans les deux bassins de Bourg d’Oisans et de Mizoën (Fig. 13). S1<sub>Bellahsen et al., 2012</sub> résulte du cisaillement de l’interface socle/couverture et pend vers l’Ouest au fond du bassin et vers l’Est au niveau de la faille normale du Col d’Ornon. S2<sub>Bellahsen et al., 2012</sub> résulte du cisaillement de l’ensemble de la couverture par les nappes internes et est plan axial des grands plis de la couverture, et pend la plupart du temps fortement vers l’Est. La phase de schistosité principale visible dans les bassins de l’Oisans est donc S2<sub>Bellahsen et al., 2012</sub> qui correspond à S3<sub>Dumont et al., 2008</sub> et à S1<sub>Gratier et Vialon, 1980</sub>. Dans la suite de cette étude, on se référera à la chronologie de [Bellahsen et al. \(2012\)](#) pour la dénomination des schistosités des bassins de Bourg d’Oisans et de Mizoën.

Le socle des bassins de l’Oisans n’est affecté que par une seule phase de déformation en serrage Est-Ouest ([Dumont et al., 2008](#) ; [Bellahsen et al., 2012](#) ; [Bellanger et al., 2015](#)). Or un des scénarios cinématiques de l’inversion des bassins de l’Oisans propose que la

couverture soit affectée de grands plissements antérieurs aux déformations du socle (Dumont et al., 2008) ce qui suppose le décollement non négligeable de celle-ci. L'étude détaillée des microstructures, particulièrement au niveau de l'interface entre socle et couverture, de même que la restauration de la couverture de ces bassins pourrait permettre de mieux comprendre leur cinématique d'inversion.

#### *II.3.5. Circulations de fluides de la zone du Nord Oisans*

L'étude du remplissage des veines métamorphiques de la couverture décollée à l'Est des bassins de l'Oisans (Fig. 11) montre que les circulations de fluides se font à l'échelle des unités lithologiques (Henry et al., 1996). Ainsi, les signatures géochimiques des veines sont similaires à celle de la roche encaissante. L'étude isotopique de ces signatures montre de plus que cet équilibre entre veine et roche se fait dans les conditions du faciès métamorphique schistes verts (Henry et al., 1996). Il ne semble donc pas exister dans cette couverture, décollée de son socle, de circulations de fluides à grande échelle. Cependant aucune isotopique n'a été mené dans la couverture autochtone des bassins de l'Oisans. Les études microthermométriques font ressortir de faibles percolations de fluides à la base de la couverture des bassins de l'Oisans et diminuant avec le temps, telles que le suggèrent les températures et les salinités élevées à proximité du socle (Gratier et al., 1973 ; Bernard, 1978 ; Gratier et Vialon, 1980 ; Nienzgui, 1993).

De la même façon que cela a été montré dans les massifs du Mont Blanc ou de l'Aar (i.e. Rolland et al., 2003, 2009 ; Challandes et al., 2008 ; Goncalves et al., 2012), il est probable que des circulations de fluides aient été chenalés dans les bandes de cisaillement du socle des bassins de l'Oisans. Or ces bandes ne sont pas propagées dans la couverture (e.g. Dumont et al., 2008 ; Bellahsen et al., 2012). On peut donc s'interroger sur l'accommodation des circulations de fluides profond au niveau de l'interface entre socle et couverture.

### **II.4. Les massifs du Mont-Blanc et des Aiguilles Rouges.**

Le massif des Aiguilles Rouges (Fig. 3) est situé entre une unité de couverture partiellement décollée, à l'Est des Préalpes, et le synclinal de Chamonix (Fig. 14). Ce massif est constitué de gneiss hercyniens qui forment l'encaissant d'un granite tardi-hercynien, daté par méthode U/Pb à 300 Ma (+/-1,5 Ma) (Bussy et al., 1996 ; Bussy et al., 2000). Le massif

est décrit comme un empilement d'écailles de socle dont seule la plus haute affleure. Ces écailles sont structurées par des grands chevauchements crustaux (Burkhard et Sommaruga, 1998). La définition de la couverture sédimentaire de ce massif reste encore à ce jour problématique. En effet, quelques « patchs » de séries sédimentaires mésozoïques très fortement condensées et autochtones sont visibles sur le massif (Fig. 14). Le massif des Aiguilles Rouges est ainsi défini comme une crête de bloc basculé de la marge proximale européenne (Lemoine et al., 1986), limité à l'Est par la faille normale de Chamonix.

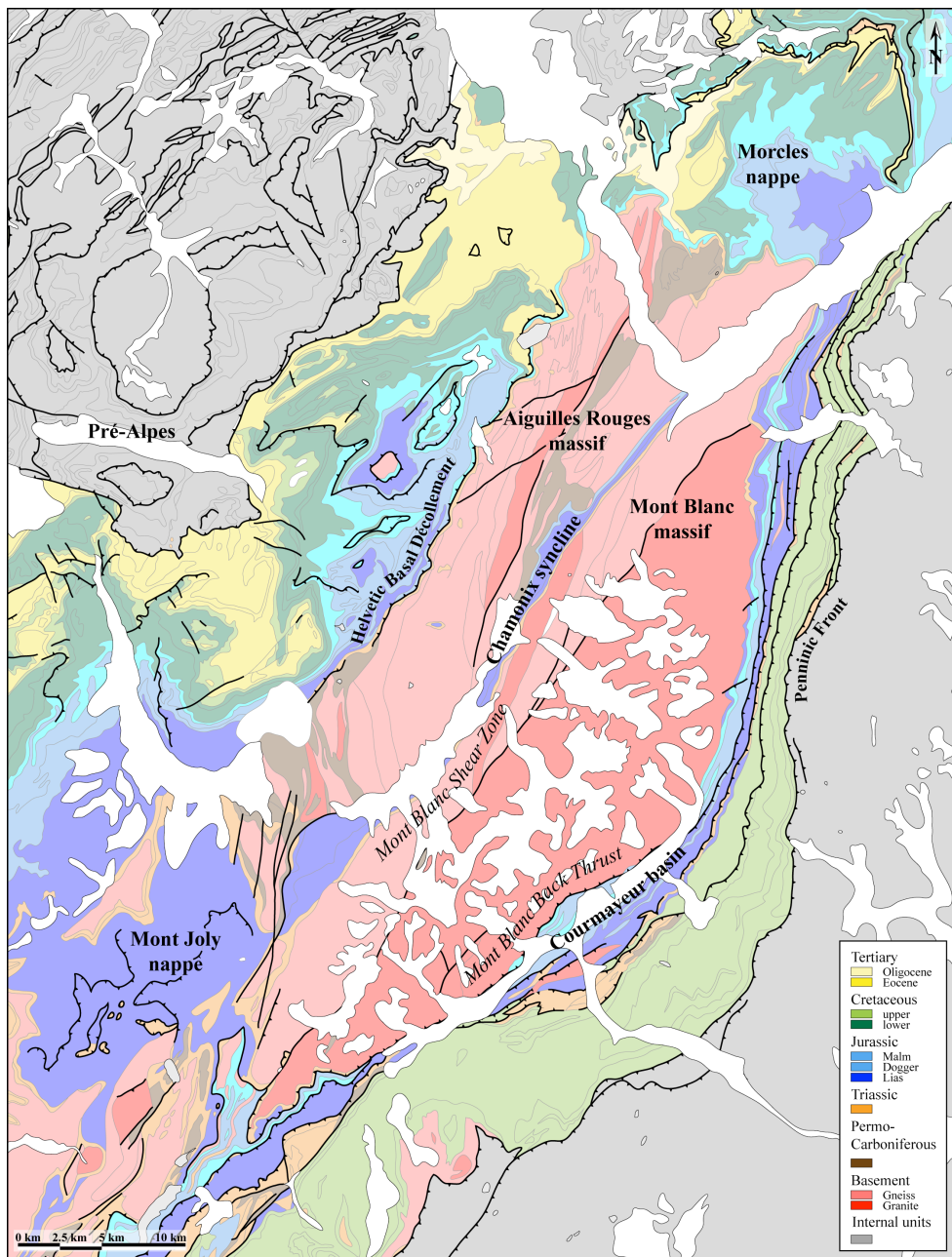


Figure 14. Carte géologique des massifs des Aiguilles Rouges et de leur couverture.

#### *II.4.1. Le massif des Aiguilles Rouges.*

Structuralement au-dessus (au NW) de cette couverture autochtone du massif, on trouve une série sédimentaire épaisse de plusieurs km et constituée de sédiments mésozoïques et des flyschs éo-oligocènes. Les deux séries, fines et épaisses, de sédiments mésozoïques ne sont actuellement distantes que de quelques centaines de mètres (Fig. 14). Il existe trois hypothèses expliquant cette variation très rapide d'épaisseur de la série : (1) la couverture épaisse des Aiguilles Rouges est en place et cette variation s'explique par l'approfondissement très rapide du socle du massif sous la couverture. Il est aussi possible qu'une faille normale, alors à pendage Ouest et délimitant le massif des Aiguilles Rouges comme un horst, permettent l'accommodation de cette variation d'épaisseur ; (2) une autre possibilité est de restaurer cette couverture épaisse du massif des Aiguilles Rouges dans le bassin de Chamonix. Il s'agirait alors d'un équivalent des nappes de Morcles et du Mont Joly (si l'on suit les interprétations d'[Escher et al., 1993, 1997](#) et [Epard, 1990](#) qui restaurent ces deux nappes dans le même bassin de Chamonix). La cinématique de mise en place de la couverture épaisse des Aiguilles Rouges serait alors différente de celle des nappes puisqu'on n'observe pas de série inverse soulignant le déversement des nappes vers le Nord-Ouest. (3) la dernière possibilité consiste à restaurer la couverture à l'Est du massif du Mont-Blanc ([Leloup et al., 2005](#)).

#### *II.5.2. Le massif du Mont-Blanc.*

Le massif du Mont-Blanc est situé à l'intersection des frontières française, italienne et suisse. Il comporte les plus hauts sommets de l'arc alpin ce qui s'explique surtout par sa structure en « pop-up » ([Leloup et al., 2005](#), Fig. 15).

Les roches encaissantes du massif granitique sont constituées de para et orthogneiss, parfois migmatitiques, datés à 435 +/- 3 Ma par la méthode U/Pb sur zircon ([Bussy and von Raumer, 1994](#)). Ce socle paléozoïque est intrudé par le granite tardi-hercynien du Mont-Blanc à 305 +/- 2 Ma ([Bussy et al., 1989](#) ; [von Raumer et al., 1993](#)). Ce granite, qui est un batholite calco-alcalin qui s'étend sur 35 km du nord au Sud et sur 10 km de large, présente plusieurs faciès magmatiques caractérisés par la taille des grains ([Bussy, 1990](#), [Bonin et al., 1993](#), [Bussy et von Raumer, 1994](#)). Ainsi, l'intrusion devient de plus en plus porphyrique depuis sa bordure Nord-Ouest vers son centre alors qu'il présente une texture très fine sur sa bordure Sud-Est ([Rolland et al., 2003](#)).

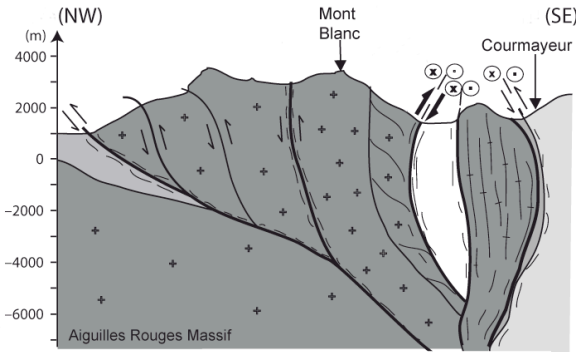


Figure 15. Coupe schématique montrant la structure en « pop-up » du massif du Mont Blanc. ([Cenki-Tok et al., 2013](#)).

Les contacts Nord-Ouest et Sud-Est de l'intrusion du Mont-Blanc qui permettent la structuration en « pop-up » sont alpins. L'essentiel du raccourcissement alpin semble avoir été accommodé par le contact Nord-Ouest du granite (Fig. 15). Il s'agit d'une épaisse zone de cisaillement faiblement inclinée (environ 30 à 35°), la Mont Blanc Shear Zone (MBSZ, Fig. 15). Cette zone de cisaillement dont l'épaisseur varie en diminuant du Sud vers le Nord du massif (Leloup et al., 2005) a été datée à 23 Ma (Rolland et al., 2008). Sur sa partie Sud-Est, le Mont Blanc Back-Thrust (MBBT) permet au massif de chevaucher les séries sédimentaires du bassin de Courmayer (e.g. Guermani et Pennacchioni, 1998, Fig. 14). Il s'agit d'une zone de cisaillement épaisse de 50 m, de pendage 50 à 65°SW (Leloup et al., 2005).

Entre ces deux zones de déformation, la déformation enregistrée par le massif est très pénétrative. Le raccourcissement alpin visible à l'affleurement au cœur du granite est caractérisé par des bandes de cisaillement alpines très raides, orientées NE-SW et N-S, et marquées par des linéations sub-verticales. Ces bandes disposées en éventail sont peu épaisses, de 1 à 50 m, et séparées par des zones de moindre déformation allant de 100 à 500m (Rolland et al., 2003, 2008, Fig. 16). La majorité de ces bandes de cisaillement sont transpressives, avec une composante dextre (bandes NE-SW) ou sénestre (bandes N-S) résultant de la compression NW-SE (Rossi et al., 2005, Fig. 16). Si la composition minéralogique du granite est à peu près uniforme, on constate des variations au sein des bandes de cisaillements. Ainsi, dans la partie Nord-Ouest l'assemblage dominant des bandes de cisaillement est epidote + quartz + muscovite ; dans la partie centrale : epidote + quartz + muscovite + phlogopite + chlorite + quartz ; dans la partie Sud-Est, les phengites sont largement dominantes (Fig. 16). Ces variations de la composition des bandes de cisaillement

formées à partir d'un même protolite proviennent du degré d'interaction fluide-roche au sein de cisaillement (Rolland et al., 2003 ; Rossi et al., 2005)

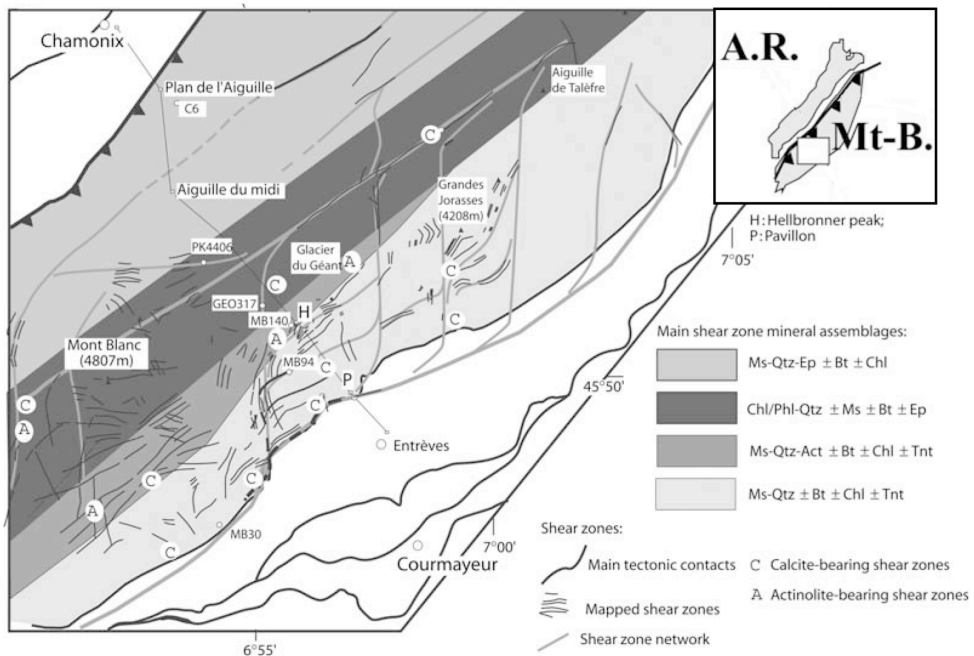


Figure 16. Carte des cisaillements et de leur composition minéralogique du massif du Mont Blanc. (Rolland et al., 2008)

Les nappes Helvétiques et Ultra-Helvétiques, localisées en Suisse, forment un ensemble de nappes empilées en une large antiforme et qui s'étale sur plus de 200 km du Sud/Ouest au Nord/Est entre les massifs du Mont Blanc/Aiguilles Rouges à l'Ouest et les massifs de l'Aar-Gothard/ Gastern (Fig. 3, 17). Ces nappes sont constituées de sédiments mésozoïques et tertiaires et sont marquées par de très fortes variations d'épaisseur de leurs couches et par un plissement disharmoniques déversé vers le Nord-Ouest (Fig. 17). Elles sont charriées depuis le Sud/Est vers le Nord/Ouest, vers les zones externes de l'Arc alpin, sur les massifs des Aiguilles Rouges à l'Ouest et sur le massif du Gastern à l'Est (Ramsay, 1981, 1983; Burkhard, 1988, Fig. 17). La base de l'empilement est formée des nappes de Morcles au Sud/Ouest et de Doldenhorn au Nord/Est (Badoux et al., 1971, Fig. 17, 18). Celles-ci sont recouvertes par les nappes de l'Ardon et de Wildhorn, que l'on divise habituellement en Diablerets, du Mont Gond et Sublage (Fig. 17, 18). Les chevauchements basaux des nappes structuralement les plus hautes, du Mont Gond et de Sublage, montrent des déplacements de l'ordre de 10 à 15 km. Le chevauchement basal de la nappe des Diablerets semble lui avoir accommodé entre 50 et 70 km de raccourcissement (Kirschner et al., 1999). De ce fait ces

nappes sont restaurées à l'Est de la nappe de Morcles (Burkhard et Sommaruga, 1998 ; Leloup et al., 2005). Le flanc inverse de la nappe de Morcles montre un très fort cisaillement (Ramsay, 1981, 1983) et est parfois interprété comme un chevauchement (Leloup et al., 2005).

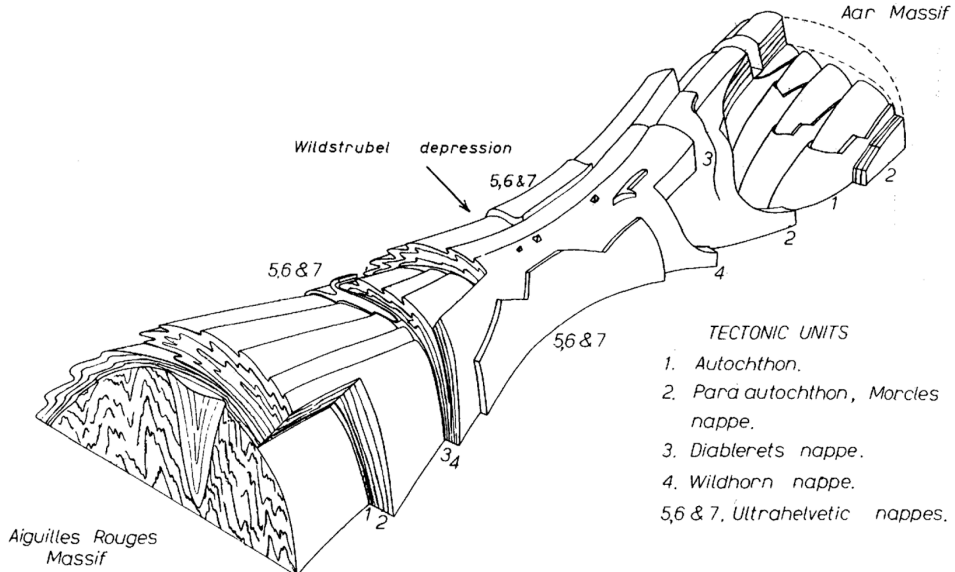


Figure 17. Relations géométriques des nappes helvétiques charriées sur le massif des Aiguilles Rouges, au Sud Ouest, enracinées sur le massif de l'Aar. Ramsay et al., 1981.

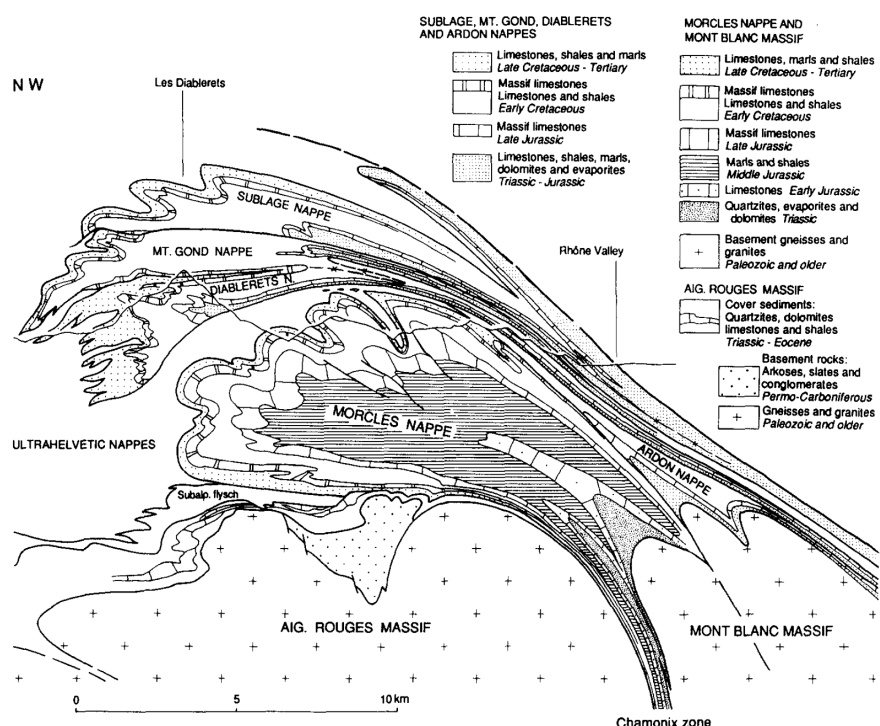


Figure 18. Coupe des nappes de Morcles de l'Ardon et de Wildhorn (regroupant les nappes des Diablerets, du Mont Gond et de Sublage). Escher et al., 1993.

Si la structure actuelle de la nappe de Morcles est bien définie et adoptée (Fig. 18), sa restauration fait encore débat. Certains auteurs proposent qu'elle soit très faiblement charriée vers les zones externes et restaurée comme couverture du massif du Mont Blanc, au sein du bassin de Chamonix (Escher et al., 1993, 1997 ; Burkhard et Sommaruga, 1998, Fig. 18). D'autres proposent que la nappe soit charriée vers les zones externes par dessus le massif du Mont Blanc avant que ce dernier ne soit raccourci puis exhumé (Leloup et al., 2005, Fig. 19). La structure thermique de ces nappes recoupe les plis, indiquant ainsi leur déformation lors de l'acquisition du pic thermique (Burkhard et Goy-Eggenberger, 2001). La nappe du Mont Joly (Fig. 14) qui se trouve dans une position structurale similaire à celle de Morcles est interprétée comme l'équivalent Sud de la nappe de Morcles (Epard, 1990).

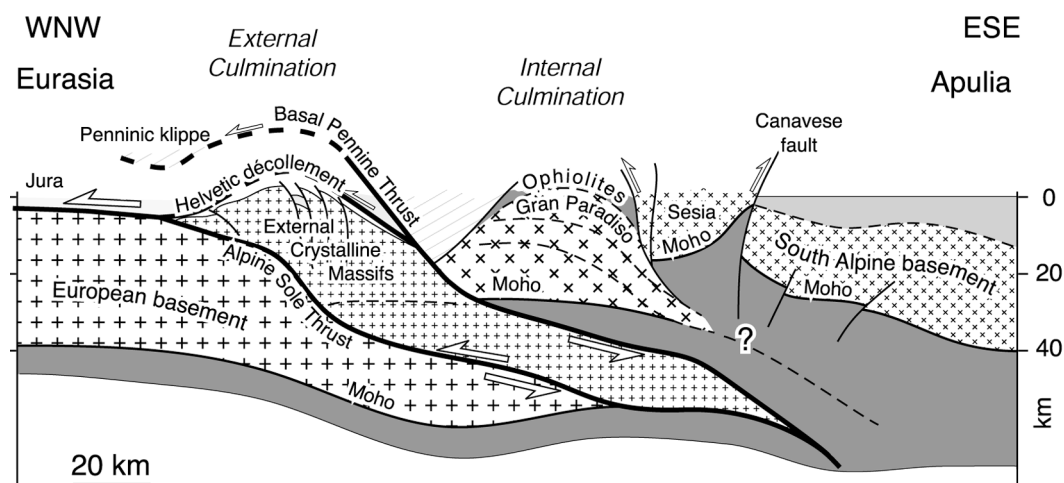


Figure 19. Coupe schématique de l'Arc alpin à la latitude du Mont Blanc et proposant le décollement des nappes helvétiques (Helvetic décollement) avant que les Massifs Cristallins Externes se soulèvent. Dans ce cas, la nappe de Morcles est restaurée à l'Est du massif du Mont Blanc (Leloup et al., 2005).

#### *II.4.3. Circulations de fluides.*

Dans le socle du Mont Blanc, l'épisode majeur de circulations de fluides se fait entre 10 et 16 Ma de manière synchrone du fonctionnement des bandes de cisaillement structurant le massif (Rossi et al., 2014). Ces bandes ont permis la chenalisation des fluides et sont ainsi le lieu d'importantes interactions entre fluides et roches conduisant par exemple au fractionnement local des Terre Rares (REE) (Rolland et al., 2003, Fig. 20).

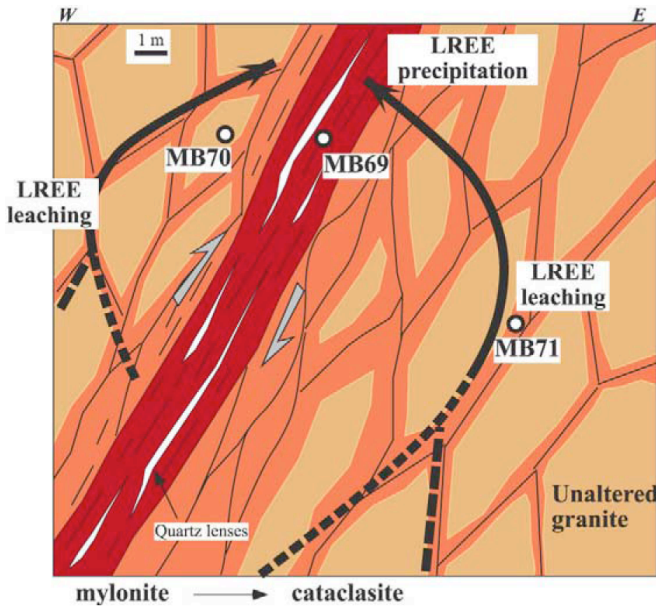


Figure 21. Interactions entre fluides chenalés par les bandes de cisaillement du massif du socle du Mont Blanc et roches encaissantes. La série des éléments Terres Rares de la roche faiblement déformée est fractionnée (appauvrissement local des Terres Rares légères) du fait de la circulation des fluides d'origine exotique. Ces mêmes éléments précipitent au niveau des zones plus intensément cisaillées. [Rolland et al., 2003](#).

Les bandes de cisaillement délimitent des zones nettement moins déformées large de quelques centaines de mètres ([Rolland et al., 2003](#)). L'étude des veines métamorphiques de ces zones peu déformées montre que la majorité de la matière remplissant les veines est d'origine locale. Celles-ci témoignent donc de circulations à petite échelle ([Fabre et al., 2002](#), [Rossi et al., 2014](#)). Ces veines sont remplies d'un assemblage de quartz + chlorite + calcite ([Poty et al., 1974](#), [Fabre et al., 2002](#), [Rolland et al., 2003](#)). A proximité des bandes de cisaillement les veines, bien que témoignant de la même façon de circulation à petite échelle, montrent néanmoins des indices ( $^{13}\text{C}$ ) de circulation de fluides exotiques, profonds ou bien en provenance des sédiments à l'aplomb du massif ([Rossi et al., 2014](#)). De ce fait, il semble que des fluides aient pu circuler sur l'ensemble de l'épaisseur de la croûte, chenalés par les bandes de cisaillements et percolant en faible quantité dans les fentes ouvertes lors du fonctionnement de ces cisaillements ([Rolland et al., 2003](#), [Oliot et al., 2010, 2012, 2014](#) ; [Rossi et al., 2014](#)).

Dans la nappe de Morcles, qui constitue la couverture probable du massif, les circulations de fluides sont très locales sur l'ensemble de la nappe ([Kirschner et al., 1995](#),

1999). Seule une partie du flanc inverse, très cisaillée (Ramsay et al., 1983) est marquée par des circulations à plus grande échelle (Kirschner et al., 1999). Il en est de même dans les nappes de Wilthorn (Fig. 18) et de ses sous-unités (les nappes charriées sur la nappe de Morcles, Fig. 18) : seuls les décollements basaux des nappes sont marqués par des indices de circulation à grande échelle (Crespo-Blanc et al., 1995 ; Kirschner et al., 1999). Ces circulations de fluides sont datées jusqu'à 30 Ma au niveau des chevauchements des Diablerets et de Whithorn et jusqu'à 15 Ma dans le flanc inverse de la nappe de Morcles (Crespo-Blanc et al., 1995 ; Kirschner et al., 2003).

### **III. Evolution structurale, massifs des Aiguilles Rouges et du Mont-Blanc.**

#### **Sequence of shortening of the Aiguilles Rouges/Mont Blanc massifs from low-temperature (U-Th-Sm/He) thermochronology.**

Alexandre Boutoux, Nicolas Bellahsen, Ugo Nanni, Raphael Pik, Anne Verlaguet, Yann Rolland, Olivier Lacombe, Alberto Vitale-Brovarone.

Article à soumettre à la revue Earth and Planetary Science Letters

#### **III.1. Cadre et intérêt de l'étude.**

La cinématique du raccourcissement collisionnel des zones externes a été étudiée par de nombreux auteurs et sous des aspects très variés, que ce soit à travers la datation de l'exhumation des MCE, l'étude du remplissage des bassins d'avant-pays ou la construction de coupes équilibrées des zones externes (e.g. Seward et Manktelow, 1994 ; Sinclair, 1997 ; Burkhard et Sommaruga, 1998 ; Ceriani et al., 2001 ; Ford et Lickorish, 2004 ; Affolter et al., 2008 ; Bellahsen et al., 2014). Du fait du tracé du profil sismique ECORS-CROP notamment, nombre de ces études se sont concentrées sur les unités traversées par le transect (i.e. les massifs du Jura, le bassin molassique suisse, la zone entre Mont Blanc et Belledonne). Pourtant, sur ce transect, si les données géochronologiques et thermochronologiques commencent à être nombreuses au niveau du massif du Mont Blanc, elles sont relativement peu nombreuses dans le massif des Aiguilles Rouges. Ainsi, la déformation collisionnelle de la marge européenne à cette latitude n'est que très peu contrainte au niveau de ce massif dont on ne connaît pas les conditions du pic de métamorphisme alpin et dont l'exhumation n'est que très peu contrainte.

Le premier objectif de cet article est donc de fournir de nouvelles données permettant de mieux contraindre la déformation et l'exhumation du massif des Aiguilles Rouges. Cependant les accidents alpins structurant le massif n'affleurant pas ou très peu, il n'est pas possible de réaliser une étude géochronologique, permettant de contraindre les conditions P-T-t des déformations. Seuls quelques cisaillements alpins, situés sur la partie sommitale du massif, ont été datés par Egli, (2013). Quelques études thermochronologiques de basse température (AFT et AHe) permettant de contraindre la fin de l'exhumation ont été conduites mais les données sont réparties essentiellement au nord du massif (Soom, 1994 ; Rahn 1994 ; Seward et Manktelow, 1994 ; Leloup et al., 2005 ; Valla et al., 2011). Au niveau du Mont Blanc, les

données géo- et thermochronologiques sont nombreuses et réparties sur l'ensemble du massif. Le tunnel du Mont Blanc à permis le prélèvement et l'analyse de nombreux échantillons répartis sur sont tracé et à son aplomb ([Leloup et al., 2005](#) ; [Glotzbach et al., 2008](#) ; [2011](#) ; [Rolland et al., 2008](#)). Ainsi dans le but d'étudier les chemins température-temps des massifs des Aiguilles Rouges et du Mont Blanc, nous avons choisi de localiser les zones d'échantillonnage sur le massif des Aiguilles Rouges, notamment sur un axe prolongeant celui du tunnel du Mont Blanc.

Le deuxième objectif de ce travail est de fournir de nouvelles contraintes sur le pic de température du massif des Aiguilles Rouges. Pour ce faire, de nombreux échantillons ont été collectés et analysés par méthode RSCM (Raman Spectroscopy of Carbonaceous Material) dans la couverture sédimentaire sur tout le pourtour du massif. ([Fig. 14](#)). Le prélèvement d'échantillons dans la couverture autochtone au Nord, au Sud et à l'Est du massif des Aiguilles Rouges nous permettra donc d'apporter une valeur pour la température maximale atteinte par le massif. La question de la restauration de la couverture à l'Ouest du massif reste débattue. Ainsi, par comparaison avec les données obtenues sur le pourtour du massif, on pourra discuter du caractère allochtone ou non de cette unité de couverture.

Le troisième objectif est de construire des chemins T-t pour les deux massifs des Aiguilles Rouges et du Mont Blanc, à partir de ces nouvelles données et de celles de la littérature. Le seul chemin complet dans la zone d'étude est celui de la nappe de Morcles ([Kirschner et al., 1995](#)). Du fait de la position actuelle de la nappe, charriée sur le massif des Aiguilles Rouges, ce chemin T-t nous permettra de discuter l'exhumation du massif. Enfin, la comparaison des chemins T-t de la nappe de Morcles et de ceux des Aiguilles Rouges et du Mont Blanc nous permettra de discuter la restauration de cette nappe.

### **III.2. Article**

# **Sequence of shortening of the Aiguilles Rouges/Mont Blanc massifs from low-temperature (U-Th-Sm/He) thermochronology and RSCM thermometry**

A. Boutoux<sup>1,2</sup>, N. Bellahsen<sup>1,2</sup>, U. Nanni<sup>1,2</sup>, R. Pik<sup>3</sup>, A. Verlaguet<sup>1,2</sup>, Y. Rolland<sup>4</sup>, O. Lacombe<sup>1,2</sup>, A. Vitale Brovarone<sup>5</sup>

<sup>1</sup> Sorbonne Universités, UPMC Univ. Paris 06, UMR 7193, ISTEPI, F-75005 Paris, France.

<sup>2</sup> CNRS, UMR 7193, ISTEPI, F-75005 Paris, France.

<sup>3</sup> CRPG, Université de Lorraine, CNRS, 7358, F-54501 Vandoeuvre-Lès-Nancy, France.

<sup>4</sup> Géoazur, Université de Nice Sophia-Antipolis, CNRS, UMR 7329, Valbonne, France.

<sup>5</sup> IMPMC, CNRS UMR 7590, Sorbonne Université, MNHN, UPMC UMR 206, 75005, Paris, France

## **Abstract**

In the Western Alps, the External Crystalline Massifs (ECM) are key places to investigate the kinematics and thermicity of collisional crustal wedges. In this contribution, from new (U-Th-Sm)/He data on zircon and new Raman Spectroscopy on Carbonaceous Material (RSCM) data on samples from the Aiguilles Rouges massif and its cover, coupled to HeFTy thermal modeling, we constrain the thermal evolution and exhumation of the massif. The maximal temperature was about 316°C (+/-25°C), which is significantly higher than previously estimated, and thus close to the maximal temperature reached in the Mont Blanc massif (400°C +/- 25°C). Moreover, (U-Th-Sm)/He data, combined to literature data, points toward a coeval cooling and exhumation of both massifs. These results allow refining both the thermal structure evolution and the structural evolution of the external Western Alps. In this scenario, which highlights a forward propagation of the shortening, the Mont Blanc massif was shortened at thermal peak during Oligocene times (30-23 Ma). It is noteworthy that the thermal peak lasted 10-15 Myrs in the Mont Blanc massif, and probably 5-10 Myrs in the Aiguilles Rouges massif. At 23 Ma, the Mont Blanc Shear Zone activated and the massif started to exhume slowly. At 16 Ma, the exhumation rate increased coevally with the activation of both a crustal ramp below the Aiguilles Rouges massif and the Mont Blanc Back Thrust, as well as a still active shortening on the Mont Blanc Shear Zone: the zone of underplating below the wedge thus widened at this time. Finally, at 11 Ma, the Jura fold-and-thrust-belt formed at the wedge front. One of the major results in this contribution is the significant shortening that the ECM experienced at their thermal peak (around 10 Myrs at 300-400°C), before the onset of their exhumation.

## **I. Introduction**

Crustal and lithospheric rheologies drive the interactions between the structural and thermal evolutions of collisional wedges. Thus, building realistic models of crustal wedge evolution require a detailed knowledge of its thermicity evolution through space and time. Thermochronologic, thermo-barometric and geochronologic data are key constraints for such analysis. In the western Alps (Fig. 1), a wealth of data is available to discuss shortening and cooling sequences. The Alpine collisional orogenic wedge results from the convergence of European and Apulian plates. During the collision, the proximal part of the European margin and its inherited structures were partially buried under the internal Alpine units. In the external zone, below the Penninic Frontal Thrust (Fig. 1), the External Crystalline Massifs (ECM) are basement units exposing Alpine Oligo-Miocene brittle-ductile transition of the European crust (Fig. 1).

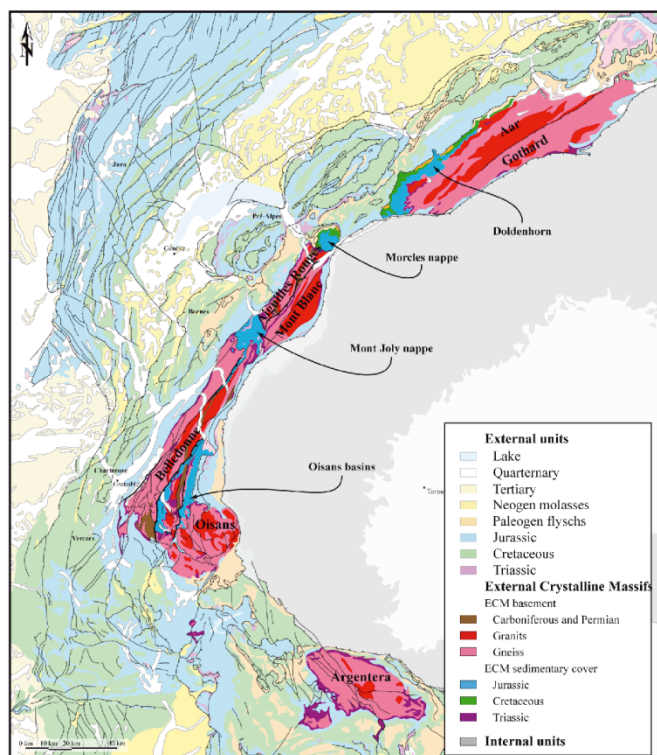


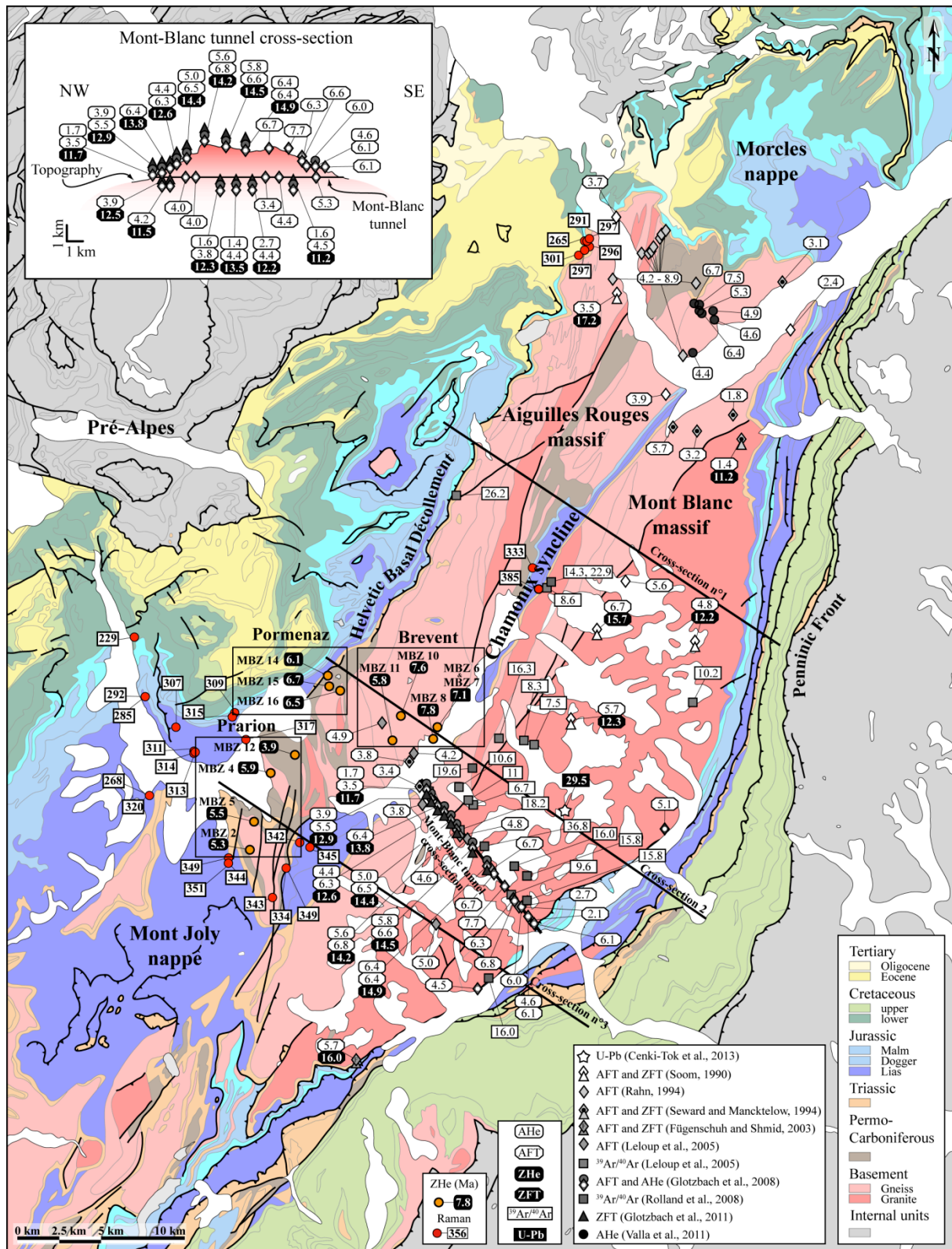
**Figure 1** Geological map of the Alpine western arc External units, highlighting the basement of the European proximal margin (the External Crystalline Massifs) and the sedimentary cover of its inherited basins (the Oisans basins, the Mont-Joly and Mordelles nappes and the Doldenhorn nappe).

The geometry of the Alpine collisional wedge can be partly constrained thanks to the ECORS profile (South of the Mont Blanc massif, e.g., [Mugnier et al., 1990](#); [Nicholas et al., 1990](#) [Guellec et al., 1990](#)). Moreover, the amount of thermochronological (e.g., [Glotzbach et al., 2008, 2011](#)), geochronological ([Leloup et al., 2005](#); [Rolland et al., 2008](#), [Cenki-Tok et al., 2013](#)), and thermo-barometric data (e.g., [Rolland et al., 2003](#)) now provides a good understanding of the pressure and temperature peaks and cooling history at the orogen-scale. However, the sequence of both shortening and exhumation of several units is still debated. For some authors, in the ECM, Tethyan inherited syn-rift basins were inverted with “thick-skinned” shortening style (e.g., the Oisans basin, [Bellahsen et al., 2012, 2014](#); [Boutoux et al., 2014](#); the Morcles nappe, [Escher et al., 1993](#); [Burkhard and Sommaruga, 1998](#)). For others, the ECM cover was shortened and displaced in a “thin-skinned” style before staking of basement units ([Leloup et al., 2005](#)). These two models have opposite implications in terms of lithospheric rheology and thermicity (e.g., [Mouthereau et al., 2013](#)).

Due to the lack of high-resolution constraints on the thermo-barometric evolution, the thermal structure of the Alpine collisional wedge is poorly constrained, especially in Western Alps. Recently, [Bellanger et al. \(2014\)](#) showed that the Oligocene temperature peak in the external southwestern Alps (Oisans massif) was quite constant over a distance of half the collisional wedge. In the external northwestern Alps, the lack of data in the Aiguilles Rouges massif does not allow deciphering the Oligo-Miocene thermal structure. In this contribution, we provide new Raman Spectroscopy on Carbonaceous Material (RSCM) thermometric data and Low-Temperature thermochronological data (U-Th-Sm/He on zircon, ZHe) on samples from both the Aiguilles Rouges and the Mont Blanc massifs. We here constrain both the thermal and structural evolution of these massifs in an attempt at shedding light on, and at better understanding, the thermo-tectonic behavior of the crust during continental collision in external zones of Alpine-type orogens,

## II. Geological setting

The Mont Blanc and the Aiguilles Rouges massifs (Figs. 1, 2) are part of the External Crystalline Massifs (ECM). These massifs are made of pre- to Variscan crystalline rocks, including granites dated at 300 Ma +/- 3Ma ([Bussy and Raumer, 1994](#)) and 306 +/- 1.5 Ma ([Bussy et al., 1996](#); [Bussy et al., 2000](#)) that were deformed during the Alpine collision.



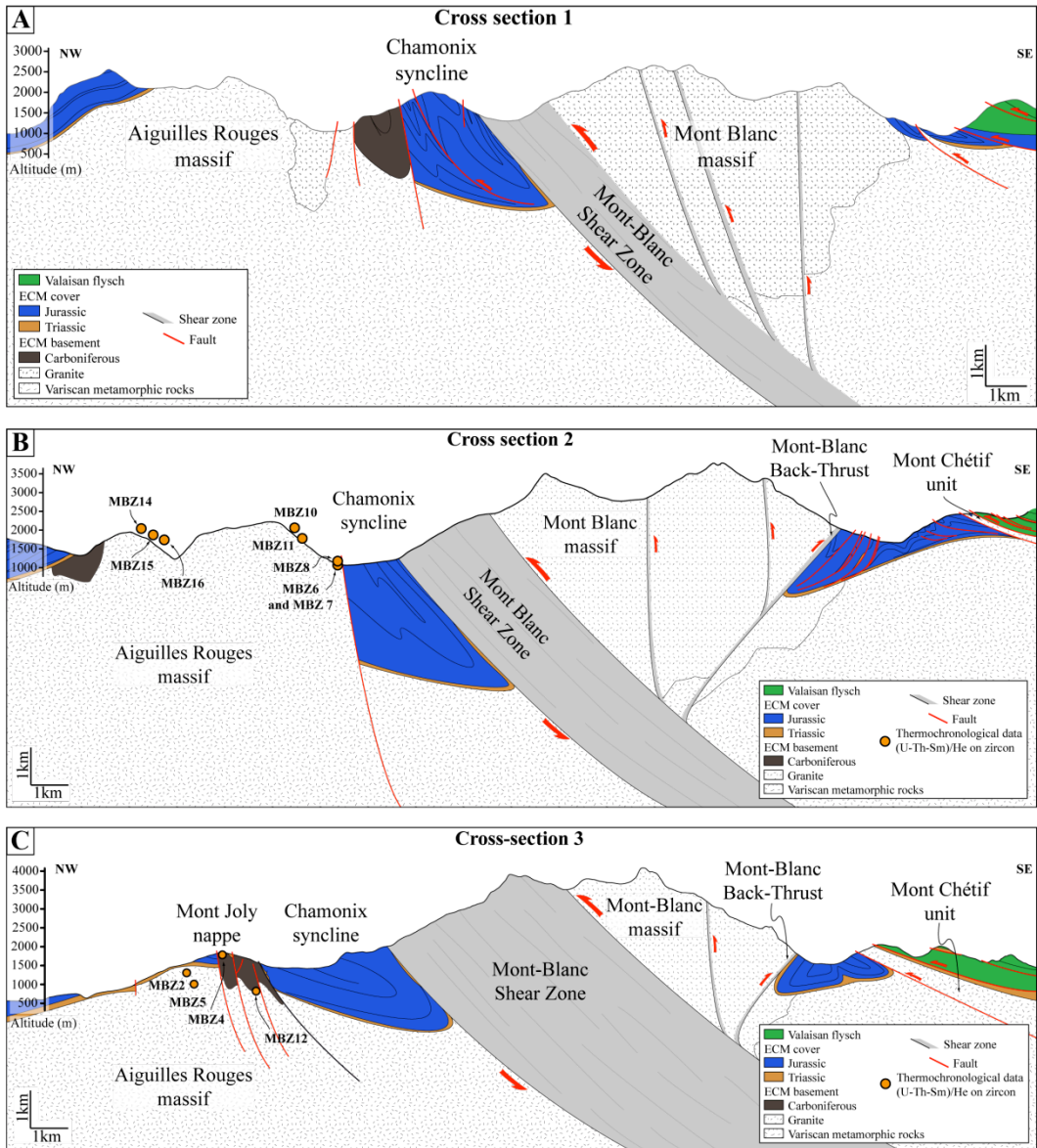


**Figure 3** Cross-sections of the Aiguilles Rouges and Mont-Blanc massifs. Locations are in Fig. 2. Orange dots are thermochronological samples (ZHe).

The Mont Blanc massif forms a pop-up structure, bordered by two main tectonic accidents: the Mont-Blanc Shear Zone (MBSZ) on its northwestern part and the Mont-Blanc Back-Thrust (MBBT) on its southeastern part (Leloup et al., 2005; Rolland et al., 2008) (Fig. 3). The inner part of the massif is structured by narrow (1-50m), steep, and transpressional shear zones separating lower strain domains (100-500m). They are arranged in a fan-like geometry and oriented N-S to NE-SW (Rolland et al., 2003; 2008; Cenki-Tok et al., 2013). The oldest shear zones are dated at 29.5 Ma (Fig. 2; U-Pb dating, Cenki-Tok et al., 2013) while the more recent ones are dated from 18.2 Ma to 6.7 Ma (Fig. 2; Ar/Ar dating, Leloup et al., 2005, Rolland et al., 2008). MBSZ initiation is dated at 29.9 Ma (Fig. 2; Ar/Ar dating, Rolland et

al., 2008). Exhumation is recorded in the Mont-Blanc massif by low temperature thermochronological data: ZFT ages are between 11.2 Ma and 16 Ma (Fig. 2; Glotzbach et al., 2011); AFT ages are between 1.8 Ma and 6.8 Ma (Fig. 2; Soom, 1990; Seward and Manktelow, 1994; Fügenschuh and Schmid, 2003; Leloup et al., 2005; Glotzbach et al., 2008); AHe ages range between 1.4 Ma and 6.4 Ma (Fig. 2; Glotzbach et al., 2008). In the Aiguilles Rouges massif, only a few low temperature thermochronological data are available: one ZFT age is at 17.2 Ma (Soom, 1990); AFT ages range between 3.1 Ma and 8.9 Ma (Fig. 2; Seward and Manktelow, 1994; Rahn, 1994; Leloup et al., 2005); AHe age are between 4.4 Ma and 6.7 Ma (Fig. 2. Valla et al., 2011).

The Morcles nappe is interpreted as the cover of the Mont Blanc massif (Escher et al., 1993) and is composed of Triassic to Cretaceous metasediments (Fig. 2). This nappe is a large recumbent anticline, which reverse limb is highly sheared (Ramsay, 1983) over the Aiguilles Rouges massif. For most authors, the reverse limb shear zone thus roots in the Chamonix syncline (Escher et al., 1993; Bauville et al., 2013), interpreted as an inverted inherited synrift basin (Burkhard and Sommaruga, 1998; Steck et al., 1999; Boutoux et al., 2014). Alternatively, the Morcles nappe may root East of the Mont Blanc massif (Leloup et al., 2005). Further South, the Mont-Joly nappe (Fig. 2) is interpreted as a southern equivalent of the Morcles nappe, rooting in the Chamonix inherited basin (Epard, 1990; Bellahsen et al., 2014).

The present-day North Alpine Foreland Basin (NAFB, Fig1; Sinclair, 1997; Ford et al., 2006) developed during Oligo-Miocene times. This molassic basin was deformed by thrusts probably linked to basement ramps below the Aiguilles Rouges massif (Burkhard and Sommaruga, 1998). The youngest thrusts also initiated below this massif and propagated below the NAFB in the Triassic evaporites and activated the Jura fold-and-thrust-belt. The Jura décollement and the NAFB were subsequently deformed by later high-angle basement thrusts related to inversion of Permo-Carboniferous basins (e.g., Lacombe and Mouthereau, 2002).

Because of the lack of thermochronological data in the Aiguilles Rouges massifs, the sequence of shortening is still debated. Leloup et al. (2005) proposed that the Aiguilles Rouges massif was exhumed first and that the Mont Blanc massif was emplaced lately out-of-sequence. However, Burkhard and Sommaruga (1998) suggested that the initiation of the basement thrusts occurred in-sequence. One goal of this contribution is to document the thermal evolution of both the Aiguilles Rouges and Mont Blanc massifs in order to better constrain the shortening and exhumation sequence during the Alpine collision.

### III. Methodology

Sampling for Raman Spectroscopy of Carbonaceous Material (RSCM) thermometry was performed in the metasedimentary cover of the [Aiguilles Rouges](#) massif in several areas distributed around the massif (Fig. 2, 3). The metasedimentary cover shows lithologies that are rich in carbonaceous material (CM), which permits the use of RSCM thermometry to estimate the maximal temperature attained by these rocks, indicated by the degree of graphitization of the CM.

Indeed, under the effect of heating, burial and subsequent metamorphism, the structure of organic matter trapped in these sediments gradually evolves towards graphite-like stable structures ([Wopenka and Pasteris, 1993](#); [Yui et al., 1996](#)). This graphitization of CM is an irreversible process and therefore records the maximum temperature (Tmax) experienced by the rocks during a P-T loop ([Beyssac et al., 2002a, 2002b](#)). The RSCM is based on the quantitative determination of the degree of graphitization of CM, measured from Raman Spectra (RS), which is a reliable indicator of metamorphic peak temperature. In a spectral window from 700 to 2000 cm<sup>-1</sup>, the RS can be divided into a graphite band (G) and defect bands (D1, D2, D3, D4). The proportion of these bands reflects the degree of graphitization. It can be quantified using the R2 parameter, defined as the relative area of the main defect bands (R2= D1/(G+D1+D2)) ([Beyssac et al., 2002b](#)). These authors proposed an empirical thermometer, which links R2 to Tmax for a temperature range of 330 to 640°C with an intrinsic calibration error of 50°C. At lower temperature (200-350°C), the D3 and D4 bands are well developed. In this case, Tmax can be estimated using the RA1 parameter (RA1=(D1+D4)/(G+D1+D2+D3+D4)), with an intrinsic calibration error of 25°C ([Lahfid et al., 2010](#)). This second determination still needs to be tested in various geological contexts to be considered as a reliable quantitative method ([Lahfid et al., 2010](#)). With samples presenting a similar lithology, the within-sample and relative uncertainties are in the 10-15°C range.

RS were obtained using a Renishaw InVIA Reflex microspectrometer (IMPMC, UPMC, France). Before each session, the spectrometer was calibrated with a silicon standard. We used 514 nm Laser Physics argon in circular polarization and measurements were done on polished thin sections, following the analytical procedures described in [Beyssac et al. \(2002b; 2003\)](#) and [Lahfid et al. \(2010\)](#). 377 spectra were obtained on 28 samples (10 to 15 spectra per thin section) in extended scanning mode (700-2000 cm<sup>-1</sup>). RS were post-processed using the software PeakFit, following the fitting procedures of both [Beyssac et al. \(2002b; 2003\)](#) and [Lahfid et al. \(2010\)](#). As our samples obviously experienced a Tmax in the overlap range of

both thermometers, Tmax was determined for each sample from the mean peak ratio (R2 or RA1) calculated from the 10 to 15 RS obtained for this sample, with the procedure giving the best fit.

ZHe samples consist of granites and gneisses collected in the southern part of the Aiguilles Rouges massif along three different sampling profiles: Brevent, Pormenaz and Prarion (Fig. 2, 3). The Brevent and the Pormenaz samples are aligned on the same NW-SE cross-section as the Mont Blanc tunnel one (Fig. 2) (e.g., [Glotzbach et al., 2008, 2010 and references therein](#)), between 1000 and 2200 m (Fig. 3). The Prarion samples are located on the southern part of the Aiguilles Rouges massif (Fig. 2) between 800 and 1800 m (Fig. 3).

Helium extraction and analyses were performed at the Laboratoire des Gaz Rares (CRPG, Nancy, France). Zircon crystals were hand-picked under binocular lens taking into account morphology size and purity. Two or three single-grain replicates per sample were loaded into Pt capsules, degassed by oven at about 1500 °C during 20 min and analyzed for He concentrations with a VGC603 noble gas mass spectrometer ([Pik et al., 2003, Godard et al., 2009](#)). U-Th-Sm content measurements were then carried out at the SARM (CRPG, Nancy, France). Zircon crystals and the Pt opened capsules were fused into Pt crucibles with ultra-pure LiBO<sub>2</sub> and B(OH)<sub>3</sub> for 2 hours at 990 °C. The crucible, capsules and zircon samples were digested during 12 hours before inductively couple plasma mass-spectrometer analysis ([Vacherat et al., 2014](#)). The overall precision of He ages determined with this procedure is within 5-6% (1σ). Zircons with He content less than 1.10<sup>-13</sup> moles and those where U concentration in the solution is less than 100 ppb after blank correction were not considered for this study. Zircon ages were corrected for α-ejection (F<sub>T</sub>) following [Ketcham et al. \(2011\)](#).

#### IV. Results

Results of the RSCM are presented in Table 1 and Figures 2 and 4. The calculated Tmax ranges from 229 to 385°C with an intrinsic error of 25°C to 50°C. Tmax ranges between 333°C and 385°C in the Chamonix basin, between 269 and 301°C in the North of the Aiguilles Rouge massif, between 334 and 351°C, in the Mont Joly nappe, between 229°C and 320 C SW of the Aiguilles Rouges massif (with a clear gradient from NW to SE in this area).. Across the Aiguilles Rouges cover, a slight increase (within the error interval) can be observed from NW to SE (Fig. 4); a mean temperature of 316°C +/- 25°C can be calculated and considered as reliable for the sedimentary cover of the Aiguilles Rouge massif.

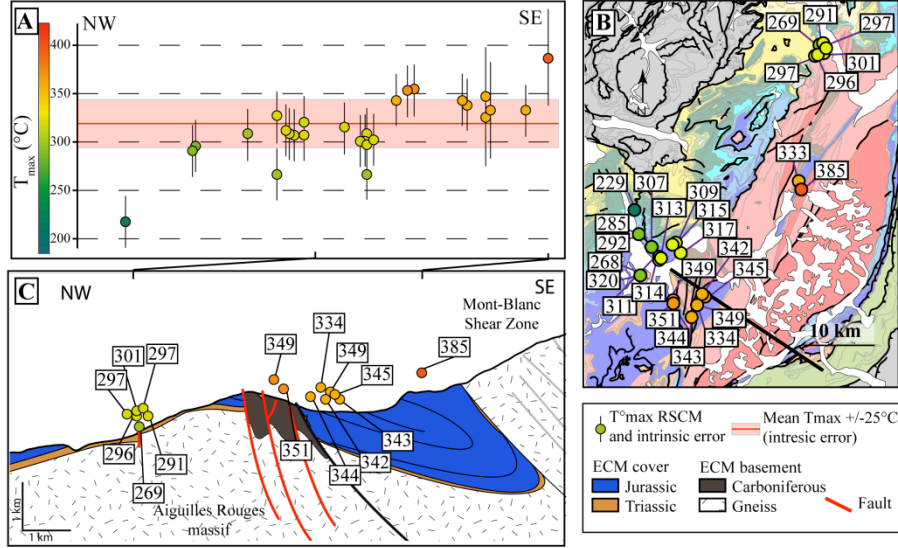


**Figure 4** Location-temperature relationship for RSCM data. (A) Temperature-distance distribution for all of our RSCM data on a NE-SW profile parallel to the cross section direction presented in Fig. 3. Recorded maximal temperature slowly decreases from East (385°C) to West (268°C). Dark line is mean RSCM value, 316°C and pink field is the +/-25°C data error (Lahfid et al., 2010). (B) RSCM data map distribution and maximal temperatures. (C) Part of cross-section n°3 presented in Fig. 3 with structural projection of part of the RSCM data and their absolute temperature. Note that RSCM data are distributed all around the Aiguilles Rouges massif. Color data are always consistent with temperature scale in (A).

Sample	Latitude	Longitude	Unit	n	RA1/R2 Ratio	T(°C)	sdv	1σ	Method
MB11-43	45°55'46.6"	6°40'34.8"	Low-mid Ju.	12	0.62	307	9	3	Lahfid et al. (2010)
ALP14-23	45°55'23.3"	6°40'56.6"	Low-mid Ju.	13	0.62	311	19	5	Lahfid et al. (2010)
ALP14-24	45°55'23.3"	6°40'56.6"	Low-mid Ju.	13	0.63	314	6	2	Lahfid et al. (2010)
ALP14-26	45°55'23.3"	6°40'56.6"	Low-mid Ju.	12	0.63	313	8	2	Lahfid et al. (2010)
ALP14-28	45°57'24.5"	6°38'49.0"	Low-mid Ju.	12	0.61	292	6	2	Lahfid et al. (2010)
ALP14-29	45°57'24.5"	6°38'49.0"	Low-mid Ju.	12	0.60	285	9	3	Lahfid et al. (2010)
ALP14-33	45°59'23.8"	6°38'11.7"	Up Ju - Low Cr.	13	0.56	229	8	2	Lahfid et al. (2010)
ALP14-35	45°54'19.7"	6°38'28.0"	Mid Ju.	13	0.59	268	5	1	Lahfid et al. (2010)
ALP14-36	45°54'19.7"	6°38'28.0"	Mid Ju.	14	0.63	320	5	1	Lahfid et al. (2010)
MB14-2	45°55'45.1"	6°42'08.8"	Low-mid Ju.	14	0.63	317	7	2	Lahfid et al. (2010)
MB14-3	45°55'45.1"	6°43'08.9"	Low-mid Ju.	15	0.64	326	18	5	Lahfid et al. (2010)
MB14-4a	45°56'40.0"	6°42'46.9"	Mid Ju.	14	0.62	310	9	2	Lahfid et al. (2010)
MB14-7	45°56'41.2"	6°42'25.0"	Mid Ju.	13	0.63	315	22	6	Lahfid et al. (2010)
ALP14-18	46°00'17.7"	6°56'42.8"	Up Ju.	13	0.64	333	16	4	Lahfid et al. (2010)
ALP14-21	45°59'54.9"	6°56'47.9"	Low Ju.	12	0.58	385	11	3	Beyssac et al. (2002b)
ALP14-02	45°51'50.0"	6°44'33.5"	Tr.	12	0.65	349	8	2	Lahfid et al. (2010)
ALP14-05	45°51'50.0"	6°44'33.5"	Tr.	13	0.64	334	19	5	Lahfid et al. (2010)
ALP14-06	45°52'12.3"	6°42'08.0"	Low Ju.	13	0.66	349	14	4	Lahfid et al. (2010)
ALP14-07	45°52'12.3"	6°42'08.0"	Low Ju.	12	0.66	351	9	2	Lahfid et al. (2010)
ALP14-07b	45°52'12.3"	6°42'08.0"	Low Ju.	13	0.65	344	9	2	Lahfid et al. (2010)
MB14-21	45°52'19.4"	6°46'03.9"	Low Ju.	15	0.67	342	3	1	Beyssac et al. (2002b)
MB14-23	45°52'36.1"	6°45'54.1"	Low Ju.	10	0.67	345	4	1	Beyssac et al. (2002b)
MB14-47	45°50'48.9"	6°44'02.2"	Up Car.	10	0.67	343	4	1	Beyssac et al. (2002b)
ALP14-08	46°10'47.6"	6°59'44.5"	Up Ju.	13	0.61	294	6	2	Lahfid et al. (2010)
ALP14-10	46°10'93.6"	6°59'50.8"	Up Ju.	15	0.62	299	10	3	Lahfid et al. (2010)
ALP14-11	46°11'09.8"	6°59'59.4"	Up Ju.	16	0.59	269	7	2	Lahfid et al. (2010)
ALP14-12	46°11'09.5"	7'00'02.9"	Up Ju.	12	0.62	302	16	5	Lahfid et al. (2010)
ALP14-14	46°11'09.5"	7'00'10.9"	Up Ju.	16	0.62	299	6	2	Lahfid et al. (2010)
ALP14-15	46°11'09.4"	7'00'10.8"	Up Ju.	12	0.61	298	10	3	Lahfid et al. (2010)

**Table 1** Results of T°max using RSCM methods. The choice between the RA1 ratio of Lahfid et al. (2010) or the R2 ratio of Beyssac et al. (2002b) depends on the best fit with Raman spectrum. Spectrums were post-processed using the software PeakFit following the methods described in Lahfid et al. (2010) and Beyssac et al. (2002b). (n) is the number of spectra used to calculate the mean ratio (RA1 or R2) and the standard deviation (sdv). The 1σ corresponds to the standard error. The absolute error on temperature is ±50°C for the Beyssac et al. (2002) method and ±25°C for the Lahfid et al. (2010) method.

ZHe analyses are presented in Table 2, and associated ages are plotted on Figures 2, 3 and 4. Brevent samples seem to be younger with increasing elevation, although the low-elevation samples are largely distributed (from 6 to 8.5 Ma, Fig. 5). Moreover, Brevent sample profile low-elevation data are not exactly consistent with Prarion ones (respectively 4-5.5 Ma and 6-8.5 Ma, Fig. 5). Prarion samples rather reveal ages increasing with elevation, with a trend about  $700\text{m.Ma}^{-1}$  (Fig. 5). Pormenaz samples are distributed at high altitudes only, between 1700 and 2000m, thus the trend cannot be easily deciphered (Fig. 5). However, the age/elevation relationships are consistent with those for Prarion for similar elevation.

The three sample profiles (Brevent, Prarion and Pormenaz) show small ranges for eU distribution: from less than 200 ppm to about 1200 ppm for Brevent samples, from 200 to 800 ppm for the Prarion ones, and from 300 to 1150 ppm for Pormenaz samples (Fig. 6).

Except for one sample from Pormenaz and one from Prarion, every sample yields a ZHe age older than the AFT ages given by samples located on the same area (Fig. 6; Leloup et al., 2005; Seward and Manktelow, 1994). The AHe samples from the North of the Aiguilles Rouges massif show an age distribution from 4.5 Ma to 7.5 Ma (Valla et al., 2011), overlapping our ZHe distribution ages (Fig. 6).

Sample	Alliote	Poids (mg)	Radius ( $\mu\text{m}$ )	$^{3}\text{He}$ mes. ( $\times 10^{-9}\text{mol/g}$ )	$^{238}\text{U}$ calc. (ppm)	$^{235}\text{U}$ calc. (ppm)	$^{232}\text{Th}$ calc. (ppm)	$^{147}\text{Sm}$ calc. (ppm)	eU (ppm)	Ft	Th/U	Measured age (Ma)	Corrected age Mean (Ma)	Corrected age (Ma)
MBZ6	a	0.009	63.5	12.8	386.87	2.80	70.58	2.16	403.81	0.82	0.18	5.9	7.1	6.9
	c	0.013	70.0	30.3	956.57	6.94	193.32	5.71	1002.97	0.84	0.20	5.69	6.7	
MBZ7	a	0.005	54.4	27.0	765.567	5.55	207.71	14.65	815.42	0.79	0.27	6.19	7.7	
	c	0.010	63.8	8.9	250.42	1.82	15.84	0	254.23	0.82	0.06	6.59	7.9	7.8
Brevent	b	0.008	61.7	5.1	173.24	1.26	9.56	3.02	175.53	0.82	0.05	5.4	6.6	
	c	0.011	66.3	7.2	262.41	1.90	9.43	8.49	264.67	0.83	0.03	5.0	6.1	
	d	0.071	113.8	4.2	80.85	0.59	89.99	6.42	124.44	0.89	1.11	7.6	8.8	7.1
	e	0.030	89.3	14.7	486.57	3.55	59.68	5.06	506.90	0.87	0.12	5.4	6.2	
	f	0.033	94.5	6.1	150.72	1.09	19.76	2.77	155.46	0.88	0.13	7.3	8.3	
	b	0.024	86.6	15.3	406.40	2.95	56.71	1.68	420.01	0.87	0.14	6.8	7.8	
MBZ9	c	0.022	85.0	5.9	185.36	1.34	32.81	0	193.23	0.87	0.18	5.7	6.6	7.2
	a	0.002	38.2	60.8	1685.72	12.23	222.28	34.57	1739.07	0.71	0.13	6.5	9.1	
MBZ10	a	0.011	67.8	19.8	642.01	4.66	274.94	0	707.99	0.83	0.43	5.2	6.2	7.6
	c	0.008	60.2	25.2	952.60	6.91	162.63	0	991.63	0.81	0.17	4.7	5.8	5.8
Prarion	a	0.050	112.8	18.5	719.37	5.22	15.53	2.14	723.10	0.90	0.02	4.7	5.3	5.3
	b	0.029	99.9	34.6	320.55	2.32	279.63	7.41	387.66	0.88	0.87	16.6	18.8	
	a	0.025	90.1	6.1	223.94	1.62	25.00	0.18	229.94	0.87	0.11	4.9	5.6	
	b	0.021	89.2	10.3	346.55	2.51	39.05	5.22	355.93	0.87	0.11	5.4	6.2	5.9
MBZ5	a	0.022	85.2	17.8	737.82	5.35	241.18	15.48	795.70	0.86	0.33	4.1	4.8	
	b	0.031	99.1	5.6	182.50	1.32	18.94	4.54	187.05	0.88	0.10	5.6	6.3	5.5
MBZ12	a	0.067	124.9	9.9	456.81	3.31	236.43	5.23	513.56	0.91	0.52	3.6	3.9	3.9
	b	0.025	87.4	9.8	277.98	2.02	217.33	11.98	330.14	0.87	0.78	5.5	6.4	6.5
Pormenaz	a	0.028	94.2	9.0	242.95	1.76	179.00	16.33	285.91	0.88	0.74	5.9	6.7	
	b	0.044	115.3	13.5	1089.89	7.90	182.84	13.25	1133.77	0.90	0.17	2.2	2.5	
MBZ14	a	0.069	123.4	14.5	376.48	2.73	290.87	15.04	446.29	0.90	0.77	6.0	6.7	6.7
	b	0.031	103.5	2.1	693.78	5.03	349.11	18.57	1067.17	0.89	0.49	5.7	6.4	6.1
MBZ15	a	0.053	110.7	3.3	955.61	6.93	464.82	60.17	777.57	0.89	0.50	5.1	5.8	
	b	0.031	103.5	2.1	693.78	5.03	349.11	18.57	1067.17	0.89	0.50	5.1	5.8	
MBZ16	a	0.053	110.7	3.3	955.61	6.93	464.82	60.17	777.57	0.89	0.49	5.7	6.4	
	b	0.031	103.5	2.1	693.78	5.03	349.11	18.57	1067.17	0.89	0.50	5.1	5.8	

**Table 2** ZHe ages obtained for three profiles on the Southern Aiguilles Rouges massif. See Fig. 2 for location. Th, U and Sm concentrations in ppm were estimated based on the determined crystal volume and element content in the sample.

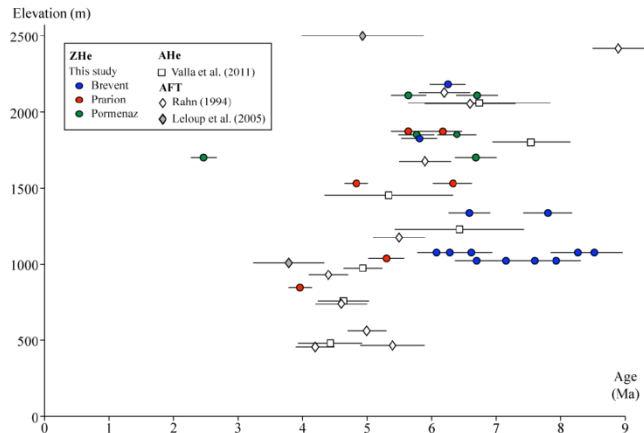


**Figure 5** Age/elevation distribution of the thermochronological data (ZHe) from this study compared to AFT (Rahn, 1994; Leloup et al., 2005) and AHe (Valla et al., 2011) age/elevations distribution data from the central and northern Aiguilles Rouges massif (see Fig. 2 for sample localization).

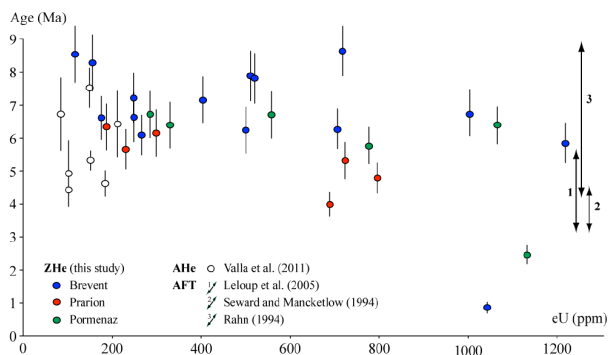


**Figure 6** Age/eU distribution of the thermochronological data (ZHe) from this study compared to the AHe ages/eU (Valla et al., 2011) and AFT age (Seward and Mactelow, 1994; Rahn, 1994; Leloup et al., 2005) distribution from the central and northern Aiguilles Rouges massif (see Fig. 2 for sample localization).

Our ZHe data were combined with thermochronological data available in the literature and close to our sampling zones in order to determine Time-temperature (Tt) paths, using the program HeFTy v.1.8.0 (Ketcham, 2005) and based on the kinetic model of Guenthner et al. (2013) and He diffusion characteristic from Ketcham et al. (2011). Each sample and replicate was put into the HeFTy inverse modeling procedure consisting of randomly testing 300,000 Tt paths for each model. The Tt paths were statistically evaluated and categorized by their value of goodness of fit (GOF), calculated separately for the age data using the equation of Ketcham (2005). ‘Acceptable’ results (in light grey in Fig. 7) correspond to a 0.05 GOF value

whereas ‘good’ results (in dark grey in Fig. 7) correspond to 0.5. For more details refer to Ketcham (2005). The maximum temperature, which corresponds to the closing temperature of ZHe system, lies between 175 and 195 °C (Reiner et al., 2002).

All thermal modeling results are presented in Fig. 7.

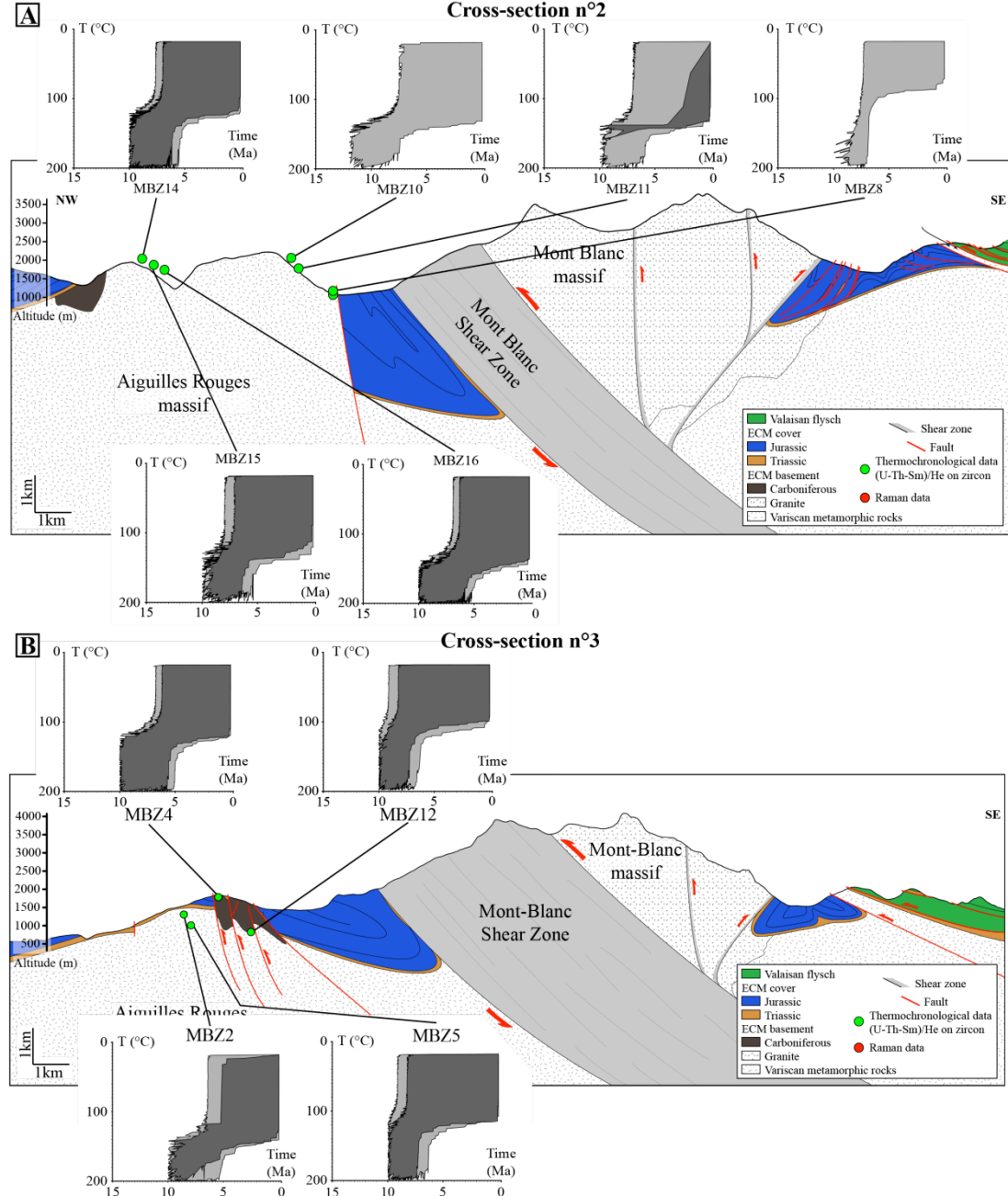


**Figure 7** Cross section n°2 (A) and n°3 (B) from Fig. 3 with results of the thermal history modeling (see Fig. 2 for cross section and sample localizations). Statistically good ( $GOF > 0.5$ ) and acceptable ( $GOF > 0.05$ ) Tt paths are respectively shown in dark and light grey. Initial Tt constraint is the same for all the samples: unrealistic maximal 10 Ma age and maximal 200 °C closing ZHe temperature system (Reiners et al., 2002; Tagami et al., 2003; Stockli, 2005).

## V. Discussion

### V.1. Aiguilles Rouges temperature peak and thermal structure at the initiation of continental collision

All around the Aiguilles Rouges massif, the RSCM temperature is around 316°C +/- 25°C (Fig. 4). These metasediments most likely represent the Aiguilles Rouges massif cover, mainly for two reasons. First, it is obvious in the north of the massif (in Switzerland) where the cover is not detached from the basement. Thus, even though there is a décollement in the southern part (Leloup et al., 2005), we can safely consider that the displacement may have remained limited for along-strike structural consistency considerations. Second, the metasediments of the Mont Joly and Morcles nappes (SW and N of the Mont Blanc massif, respectively) represent the cover of the Mont Blanc basement, based on structural considerations (e.g., Escher et al., 1993; Burkhard and Sommaruga et al., 1998; Boutoux et al., 2014). This is also suggested by the similarities between the thermal histories of the Mont-Blanc massif and the Morcles nappe (see below). Thus, if the nappes around the Mont Blanc massif represent the cover of the Mont Blanc basement, similarly the cover of the Aiguilles Rouges massif is most likely only slightly detached from its basement.

The three structural units, the Morcles nappe, the Aiguilles Rouges and Mont-Blanc massifs show a thermal peak spread in time (Fig. 8). Rocks were submitted to their maximal temperature during respectively 12, 8 and 14 Myrs (Fig. 8, Kirschner et al., 1995; Rolland et al., 2008; Cenki-Tok et al., 2013). A similar thermal peak duration is observed in the Oisans massif (Bellanger et al., 2015), which is deformed with the same pattern (shearing of the basement and disharmonic folding of the cover above it). We conclude that this pattern of deformation is likely typical for both basement and cover rocks in all the ECMs.

### V.2. Thermal history

Our new ZHe and RSCM data, together with thermochronological data available from the literature, allow to reconstruct a temperature-time (Tt) path for the Aiguilles Rouges and Mont Blanc massifs (Fig. 8). The burial initiation of the two massifs is estimated to 31 and 33 Ma from the deposition of the Val d'Illiez and the Tavayennaz flyschs, respectively (Burkhard and Sommaruga, 1998; and references therein). Between 32 Ma and 26 Ma, the

two massifs reached their maximal temperatures, 400 °C for the Mont-Blanc massif (Rolland et al., 2003; Cenki-Tok et al., 2013) and 316°C for the Aiguilles Rouges massif (this study).

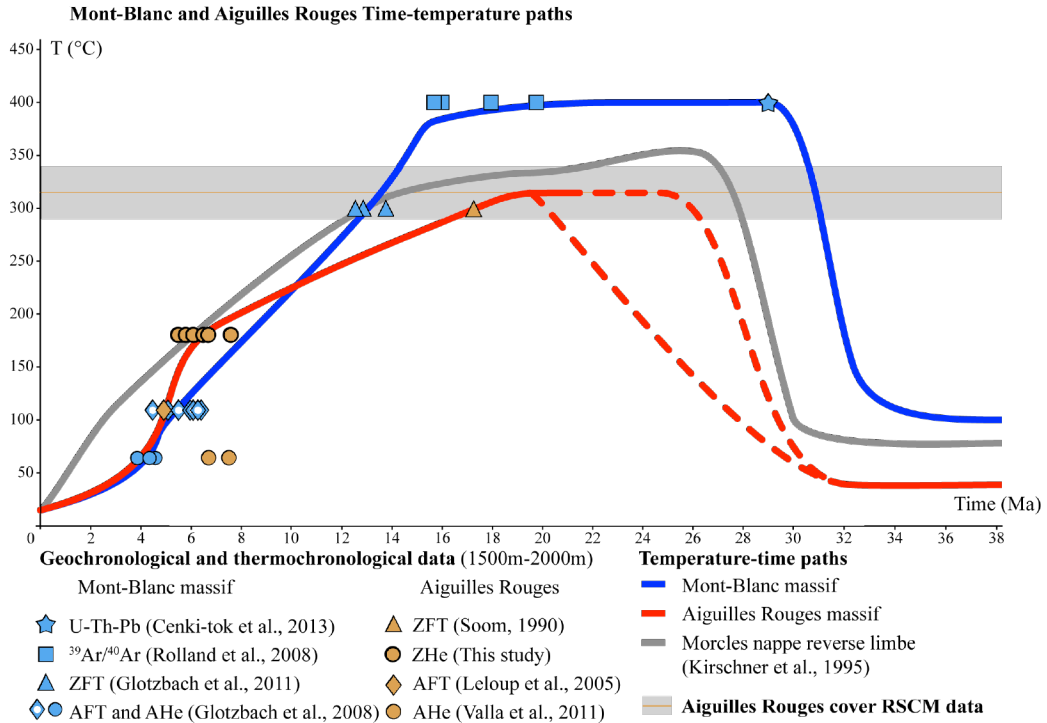


**Figure 8** Temperature-time paths for the Mont-Blanc massif (blue path), the Aiguilles Rouge massif (red path) and the Morcles nappe reverse limb (grey path, Kirschner et al., 1995). Mean Tt paths are estimated from thermochronological and geochronological data for samples collected in the same elevation range, between 1500 and 2500 m except for Soom (1990) ZFT data. See Fig. 2 for sample location. Closure temperatures are : ZFT 300-180 °C (Gleadow and Brooks, 1979; Hurford, 1986; Yamada et al., 1995; Brandon et al., 1998; Tagami et al., 1998; Rahn et al., 2004; Garver et al., 2005; Bernet, 2009); ZHe: 175-195 °C (Reiners et al., 2002; Tagami et al., 2003; Stockli, 2005); AFT: 95-160 °C (Gallagher et al., 1998); AHe: 50-110 °C (Farley, 2000; Shuster & Farley, 2009). Mont Blanc and Aiguilles Rouges massifs burial initiation is estimated from the deposition of Tavayennaz and Val d'Illez formations (Burkard and Sommaruga, 1998). Aiguilles Rouges maximal burial temperature is determined from new Raman data at about 315 °C but without any temporal constraint. Mont Blanc massif began to be isothermally shortened at 29.5 Ma until 16 Ma at the P-T peak conditions (Rolland et al., 2003; 2008; Cenki-Tok et al., 2013). The massif is then exhumed at a constant rate, according to ZFT, AFT and AHe data (Glötzbach et al., 2008, 2011). The initiation of Aiguilles Rouges Massif exhumation, recorded by the crossing of ZFT closure temperature (Soom, 1990), is linked to the activation of basement thrusts, which are connected to the Subalpine Molasse thrust activation (Burkhard and Sommaruga, 1998). Further, at 12 Ma, the infra-Aiguilles Rouges basements thrusts are activated, in connection to the Jura basal thrust. According to ZHe, AFT and AHe data, exhumation rates strongly increased around 6 Ma before slowing down at about 4 Ma until present day.

The first deformations occurred in the Mont Blanc massif at 29.5 Ma (Fig. 8; [Cenki-Tok et al., 2014](#)). At 23 Ma, the MBSZ is activated (Rolland et al., 2008), and may be associated to a very slow cooling of the Mont Blanc massif until 16 Ma (Fig. 8). After 16 Ma, as suggested by ZFT data, cooling rate increased (Fig. 8, [Glotbach et al., 2011](#)). According to our Mont Blanc Tt path, the middle to late Miocene exhumation rate is rather constant, around  $26^{\circ}\text{C}.\text{Ma}^{-1}$  (except around 6 Ma).

The age of the Aiguilles Rouges thermal peak ( $316^{\circ}\text{C}$ ) is unclear. Considering that the cooling rate between the thermal peak and the ZFT age is equal to the cooling rate defined between the ZHe and ZFT ages (around  $10^{\circ}\text{C}.\text{Ma}^{-1}$ ), the exhumation should have started at about 16-18 Ma (Fig. 8). This age is consistent with the Aiguilles Rouges basement thrust initiation, dated at about 16-18 Ma from tectono-stratigraphic observations in the NAFB ([Burkhard and Sommaruga, 1998](#)).

The Aiguilles Rouges thermal peak ( $316^{\circ}\text{C}$ ) being slighter hotter than the  $300^{\circ}\text{C}$  isotherm, which crossing is dated by the ZFT method (Fig. 8; [Soom, 1990](#)), the ZFT data provide the age of the initiation of the exhumation, i.e. around 17 Ma. The cooling rate was constant (around  $10^{\circ}\text{C}.\text{Ma}^{-1}$ ) until 6-7 Ma (Fig. 8); afterwards, our data and HeFTy thermal modeling (Fig. 7, 8) show that the Aiguilles Rouge massif cooled faster (around  $56^{\circ}\text{C}.\text{Ma}^{-1}$ ) before slowing down at 4 Ma (Fig. 8). AHe data ([Valla et al., 2011](#)) located on the northern part of the massif (Fig. 2) are younger than AFT data and thus difficult to integrate to this scenario. Yet those data could suggest earlier exhumation of northern AR.

The Aiguilles Rouges thermal peak duration is only constrained by the deposition of the last sediments above the massif (30 Ma, Val d'Illiez formation, [Burkhard and Sommaruga, 1998 and references therein](#)) and the beginning of its exhumation estimated above at 16-18 Ma. Thus, two end-member Tt path geometry can be proposed for the Aiguilles Rouges massif between 30 Ma and 16 Ma (dotted red lines in Fig. 8). (1) The massif was slowly buried, reached its maximal temperature at about 20 Ma and began its exhumation soon after. (2) If we consider that the Aiguilles Rouges massif was heated at a similar rate as the Mont Blanc massif rate (Fig. 8), then its maximum temperature might have been reached at about 26 Ma. The thermal histories of the Mont Blanc and Aiguilles Rouges massifs and the Morcles nappe (Fig. 8; [Kirschner et al. 1995](#)) may thus be very similar. In details, the early thermal history of the Morcles nappe is similar to the Mont Blanc one (Fig. 8), while it is rather close to the Aiguilles Rouges one after 15 Ma. This may provide an age for the extrusion of the Morcles nappe, which corresponds to the initiation of the MBBT (16 Ma, Rolland et al., 2008).

### V.3. Shortening sequence

On the basis of the T-t constraints for the Aiguilles Rouges massif exhumation (Fig. 2), we propose a structural sequence for the Alpine collisional shortening and exhumation in the external zone (Fig. 9).

Following the continental subduction and exhumation of internal units, the initiation of the collisional phase was characterized by underthrusting of the ECM below the internal units at Rupelian to Chattian times (Fig. 9A), constrained by the deposition of the Taveyannaz and Val d'Illiez units ([Burkhard and Sommaruga, 1998, and references therein](#)). During this burial, the innermost Helvetic nappes (Diableret and Wildhorn nappes, “ultra-helvetic”) were detached from their basement and stacked on the future Morcles nappes (Fig. 9B). First crustal deformations occurred in the Mont Blanc massif around 30 Ma (as witnessed by the crystallization of syn-tectonic allanites in anastomosed shear zones, U-Pb-Th dating in [Cenki-Tok et al., 2013](#); Fig. 9C), coevally with first deformations in the Morcles nappe (Kirchner et al., 2003; Fig. 9C). The MBSZ initiated around 23 Ma, as constrained by Ar/Ar geochronology on syn-tectonic phengites ([Rolland et al., 2008](#); Fig. 9D). This structure may have slightly exhumed the massif from 23 to 16 Ma. Then after 16 Ma, both the Mont Blanc and Aiguilles Rouge massifs were exhuming owing to crustal ramps (Mont Blanc Shear Zone and Aiguilles Rouges thrusts, respectively, Fig. 9D), but the exhumation rate was higher for the Mont Blanc due to combined reverse motions along the MBSZ and the crustal thrust ramps.

At 16-18 Ma, the Subalpine Molasse thrust was activated and connected to the crustal ramps (Fig. 9D; [Burkhard and Sommaruga, 1998](#)). At that time, the MBBT was also activated. This corresponds to (and explains) the increase of cooling rate (Fig. 8) in the Mont Blanc massif, as well as to the extrusion of the Morcles nappe (Fig. 9D). Moreover, in the Aiguilles Rouges massif, few shear zones were activated at 16 Ma ( $^{39}\text{Ar}/^{40}\text{Ar}$  dating, [Egli, 2013](#)) and the last deformations occurred in the Morcles nappe and other helvetic units (Fig. 9D; [Kirschner et al., 2003](#)). These events thus resulted in a widening of the underplating area beneath the wedge, consistent with the increase of cooling (and exhumation) rate.

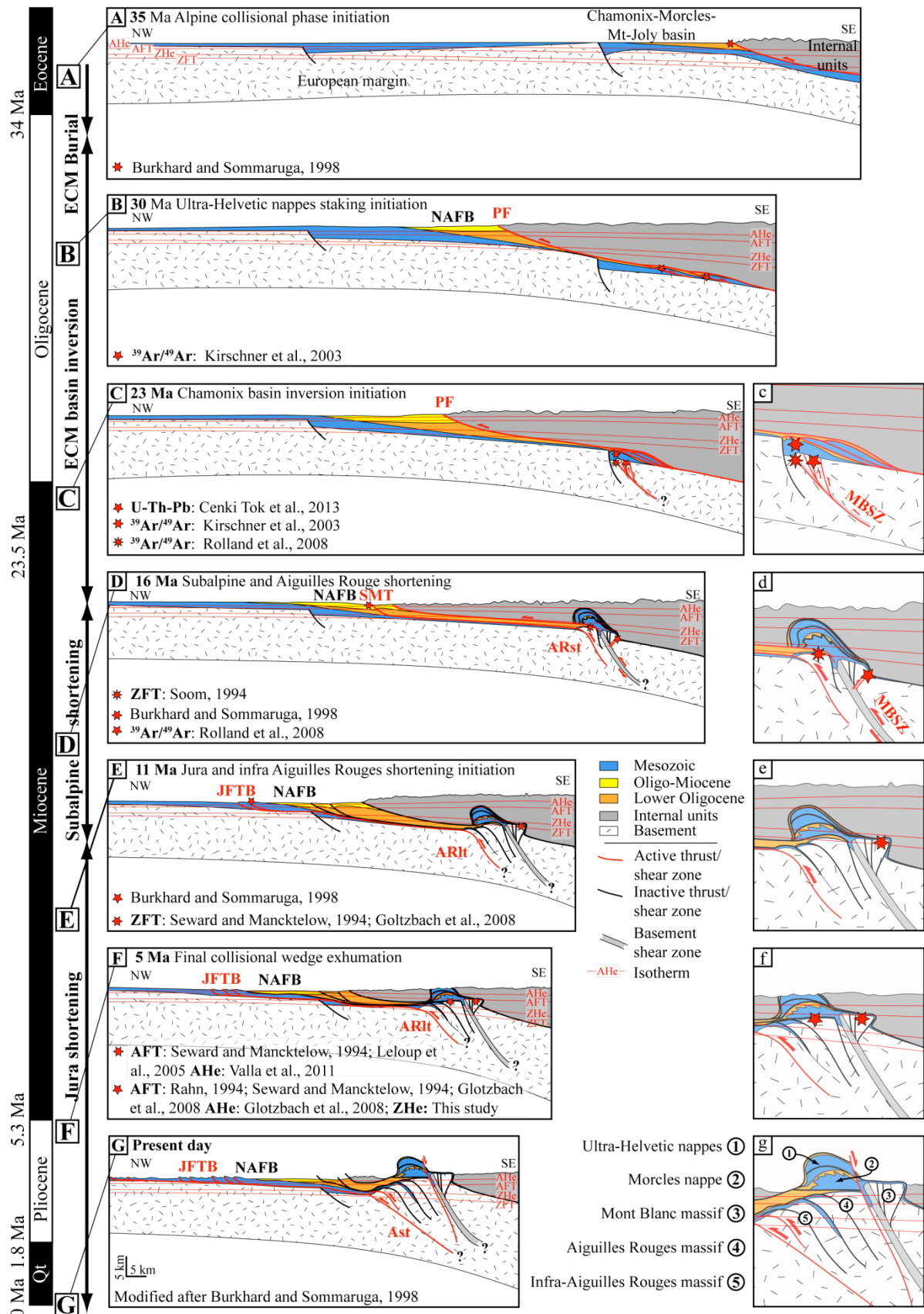
Middle to late Miocene cooling rate was higher in the Mont-Blanc massif ( $26^\circ\text{C}.\text{Ma}^{-1}$ ) than in the Aiguilles Rouges ( $10^\circ\text{C}.\text{Ma}^{-1}$ ). This difference may be linked to the activity of the MBSZ, still active until 6 Ma ([Leloup et al., 2005](#)).

At 11 Ma, the Jura fold-and-thrust-belt started to form (Bolliger et al., 1993; Steiniger et al., 1996; Kalin, 1997; Becker, 2000), linked to the initiation of basement ramps in the Infra Aiguilles Rouges massif (Fig. 9E; Burkhard and Sommaruga, 1998).

It thus comes that throughout the collisional phase, the successive activation of the main thrusts/shear zones in these massifs indicates a forward sequence. Thus, after distributed and small-scale deformations, the MBSZ initiated during late Oligocene times, followed by the Aiguilles Rouges thrusts during early Miocene times and by the Infra Aiguilles Rouges thrusts in the late Miocene. In comparison, in the Oisans massifs, the basement shear zones formed first, during Oligocene times, at their temperature peak (330°C, Bellanger et al., 2014) before the shortening localized on the frontal crustal ramps at 17 Ma (Bellahsen et al., 2014), exhuming the massif. During the first phase (shear zones activation), the temperature was nearly constant, like in the Mont Blanc massif and most probably in the Aiguilles Rouges massif (Fig. 8). Thus, such thermal evolution including a ‘plateau-like’ peak stage is most likely characteristic of collisional shortening of inverted continental margins under greenschist metamorphic facies.

**Figure 9** (Following page). Kinematic scenario of the European proximal margin burial, deformation and exhumation evolution during the collisional Alpine phase. PF: penninic Front; NAFB: North Alpine Foreland Basin; SMT: Subalpine Molasse Thrust; MBSZ: Mont-Blanc Shear Zone; ARst Aiguilles Rouges superior thrust; ARlt: Aiguilles Rouges lower thrusts; JFTB: Jura Fold and Thrust Belt. A) 35 Ma “initial stage”: end of continental subduction of the distal European margin and initiation of underthrusting of the proximal European margin below the internal (Penninic) units. (B) 30 Ma stage: initiation of the Helvetic nappes (Diablerets and Wildhorn) stacking on the future Morcles nappe (Kirschner et al., 2003). (C) 23 Ma stage: Chamonix basin inversion. The first deformations within the Morcles nappes are linked to the initiation of shortening within the Mont Blanc massif (Cenki-Tok et al., 2013). The Mont Blanc shear zone is activated during this stage (Leloup et al., 2005; Rolland et al., 2008), progressively allowing extrusion of the Mont-Blanc cover over the Aiguilles Rouge massif thus forming the Morcle nappe (e.g. Kirschner et al., 2003). (D) 16 Ma stage: Widening of the crustal deformation (1) to the West with the initiation of the Aiguilles Rouges massif deformation, suggested by both the activation of the Subalpine Molasse thrust (Burkhard and Sommaruga, 1998) and by the ZFT data (Soom, 1990); and (2) to the East with the activation of the Mont-Blanc Back-Thrust (Rolland et al., 2008), which allows the Morcles nappe overthrusting over the Aiguilles Rouges massif. (E) Westward propagation of crustal deformation as suggested by the activation of the Jura decollement connected to the deformation of the infra Aiguilles Rouges massif (Burkhard and Sommaruga, 1998). (F) Progressive exhumation of both the Aiguilles Rouges and Mont-Blanc massifs, which reached successively the ZHe, AFT and AHe closing temperature isotherms (This study; Rahn, 1994; Seward and Manktelow, 1994; Fügenschuh and Schimdt, 2003; Leloup et al., 2005; Glotzbach et al., 2008; Valla et al., 2011) (H) Present-day stage (modified after Burkhard

and Sommaruga, 1998): end of Aiguilles Rouges staking and Mont-Blanc basement extension with the activation of the Simplon transtensional fault.



## VI. Conclusions

In this contribution we present new RSCM and (U-Th-Sm)/He thermochronologic data on zircons (ZHe) from the Aiguilles and its cover. RSCM data provide the maximal temperature reached by the Aiguilles Rouges cover about 315°C, which is significantly higher than previously estimated. The temperature peak for the Mont Blanc massif, at 400°C, was about 15 Myrs long. It is most likely that the temperature peak of the Aiguilles Rouges massif was also quite long (5-10 Myrs).

Thermal modeling of our thermochronological data coupled to literature data suggest cooling rates about  $10^{\circ}\text{C}.\text{Ma}^{-1}$  and  $20^{\circ}\text{C}.\text{Ma}^{-1}$ , for the Aiguilles Rouges and the Mont Blanc, respectively, for the middle to late Miocene period. This rate strongly increased at about 6 Ma. We estimate the onset of the Aiguilles Rouges exhumation at about 17 Ma. This corresponds to the activation of the crustal ramps, connected to the Subalpine Molasse Thrust. This also corresponds to the onset of the Mont Blanc massif exhumation.

As a main result, we provide a new sequence of shortening for the European margin during the Alpine collision. This sequence highlights the shortening initiation of the Mont-Blanc and its cover at 30 Ma, after its burial during Rupelian times. The Aiguilles Rouges massif may have been buried slightly later. The Mont-Blanc exhumation probably started slowly at 23 Ma with the activation of the Mont-Blanc Shear Zone and accelerated at about 16 Ma. At this time, the Mont-Blanc Back-Thrust and a crustal ramp beneath the Aiguilles Rouges massif were activated, the latter being connected to a cover décollement and the Subalpine Molasse Thrust. These events thus characterize a widening of the underplating domain beneath the wedge during middle to late Miocene times. Finally, at 11 Ma the Jura fold-and-thrust-belt initiated linked to the activation of the infra Aiguilles Rouges crustal ramp.

Thus, as for the Oisans massif further South, and probably within the entire ECMs in the western Alps, collisional shortening propagated in a forward sequence and the ECM experienced significant shortening at their metamorphic peak, before the onset of their exhumation.

## Acknowledgements

The authors wants to thanks C. Rosenberg for discussions during fieldtrip, B. Tibari for (U-Th-Sm)/He analysis and O. Beyssac for his help on RSCM analysis. This study was founded by the “Syster” INSU program and ISTeP founds.

## References

- Bauville, A., Epard, J.-L. and Schmalholz, S.M., 2013. A simple thermo-mechanical shear model applied to the Morcles fold nappe (Western Alps): *Tectonophysics*, 583, p. 76–87, doi: 10.1016/j.tecto.2012.10.022.
- Bellahsen, N., Jolivet, L., Lacombe, O., Bellanger, M., Boutoux, A., Garcia, S., Mouthereau, F., Le Pourhiet, L. and Gumiiaux, C., 2012. Mechanisms of margin inversion in the external Western Alps: Implications for crustal rheology: *Tectonophysics*, 560-561, p. 62–83, doi: 10.1016/j.tecto.2012.06.022.
- Bellahsen, N., Mouthereau, F., Boutoux, A., Bellanger, M., Lacombe, O., Jolivet, L., Rolland, Y., 2014. Collision kinematics in the western external Alps. *Tectonics* 33, 1–34. doi:10.1002/2013TC003453
- Bellanger, M., Bellahsen, N., Jolivet, L., Baudin, T., Augier, R. and Boutoux, A., 2014. Basement shear zones development and shortening kinematics in the Ecrins Massif, Western Alps: *Tectonics*, 33, 84-111. doi: 10.1002/2013TC003294.
- Bellanger, M., Augier, R., Bellahsen, N., Jolivet, L., Monié, P., Baudin, T., Beyssac, O., 2015. Shortening of the European Dauphinois margin (Oisans Massif, Western Alps): New insights from RSCM maximum temperature estimates and  $^{40}\text{Ar}/^{39}\text{Ar}$  in situ dating. *J. Geodyn.* 83, 37–64. doi:10.1016/j.jog.2014.09.004
- Bernet M., 2009, A field-based estimate of the zircon fission-track closure temperature, *Chemical Geology*, 259 (3-4), p 181-189.
- Beyssac, O., J.-N. Rouzaud, B. Goffé, F. Brunet, and C. Chopin (2002a), Graphitization in a high-pressure, low-temperature metamorphic gradient: a Raman microspectroscopy and HRTEM study, *Contrib Mineral Petrol*, 143(1), 19–31, doi:10.1007/s00410-001-0324-7.
- Beyssac, O., B. Goffé, C. Chopin, and J. N. Rouzaud (2002b), Raman spectra of carbonaceous material in metasediments: a new geothermometer, *Journal of Metamorphic Geology*, 20(9), 859–871, doi:10.1046/j.1525-1314.2002.00408.x.
- Boutoux, A., Bellahsen, N., Lacombe, O., Verlaguet, A. and Mouthereau, F., 2014. Inversion of pre-orogenic extensional basins in the external Western Alps: Structure, microstructures and restoration: *Journal of Structural Geology*, 60, p. 13–29, doi: 10.1016/j.jsg.2013.12.014.
- Brandon MT, Roden-Tice MK, Garver JI, 1998, Late Cenozoic exhumation of the Cascadia accretionary wedge in the Olympic Mountains, northwest Washington State, *Geological Society of America Bulletin*, 110, no. 8, p. 985-1009.
- Bussy, F., and von Raumer, J. F., 1994. U–Pb geochronology of Palaeozoic magmatic events in the Mont-Blanc Crystalline Massif, Western Alps. *Schweizerische Mineralogische und Petrographische Mitteilungen*, 74, p. 514–515.
- Bussy, F., Hernandez, J., and Von Raumer, J., 2000. Bimodal magmatism as a consequence of the post-collisional readjustment of the thickened Variscan continental lithosphere (Aiguilles Rouges–Mont Blanc Massifs, Western Alps). *Geological Society of America Special Papers*, 350, p. 221-233. doi: 10.1130/0-8137-2350-7.221
- Butler, R.W.H., 1983. Balanced cross-sections and their implications for the deep structure of the North-West Alps: *Journal of Structural Geology*, 5, p. 125–137.
- Burkhard, M. and Sommaruga, A., 1998. Evolution of the western Swiss Molasse basin: structural relations with the Alps and the Jura belt: Cenozoic Foreland Basins of Western Europe, geological Society, London, Special Publication, 134, p. 279–298, doi: 10.144/GSL.SP.1998.134.013.
- Cenki-Tok, B., Darling, J.R., Rolland, Y., Dhuime, B. and Storey, C.D., 2013. Direct dating of mid-crustal shear zones with synkinematic allanite: new in situ U-Th-Pb geochronological approaches applied to the Mont Blanc massif: *Terra Nova*, 26, p. 29–37, doi: 10.1111/ter.12066.
- Egli, D. and Mancktelow, N.S., 2013. The structural history of the Mont Blanc massif with regard to models for its recent exhumation: *Swiss Journal of Geosciences*, 106, p. 469–489, doi: 10.1007/s00015-013-0153-5.

- Epard, J.-L., 1990. La nappe de Morcles au sud-ouest du Mont-Blanc. 165p. (Thesis 3e cycle) Univ. Lausane.
- Escher, A., Masson, H. and Steck, A., 1993. Nappe geometry in the western Swiss Alps: Journal of Structural Geology, 15, p. 501–509.
- Farley K. A. (2000), Helium diffusion from apatite: general behavior as illustrated by Durango apatite, Journal of Geophysical Research 105, 2903-2914
- Fügenschuh, B. and Schmid, S.M., 2003. Late stages of deformation and exhumation of an orogen constrained by fission-track data : A case study in the Western Alps: Geological Society of America Bulletin, 115, p. 1425–1440, doi: 10.1130/B25092.1.
- Gallagher K., Brown R., Johnson, C. (1998), Fission track analysis and its applications to geological problems, Annual Review of Earth & Planetary Sciences 26, 519-572
- Garver JI, Reiners PW, Walker LJ, Ramage JM, Perry SE, 2005, Implications for timing of Andean uplift from thermal resetting of radiation-damaged zircon in the Cordillera Huayhuash, Northern Peru, The Journal of Geology, 113 (2), p 117-138.
- Guellec, S., Lajat, D., Mascle, A., Roure, F., and Tardy, M., 1990. Deep seismic profiling and petroleum potential in the western Alps: Constraints with ECORS data, balanced cross-sections and hydrocarbon modeling. The Potential of Deep Seismic Profiling for Hydrocarbon Exploration. Edition Technip, Paris, p. 425-437.
- Gleadow and Brooks, 1979, Fission track dating, thermal histories and tectonics of igneous intrusions in East Greenland, Contributions to Mineralogy and Petrology, 71 (1), pp 45-60.
- Glotzbach, C., Reinecker, J., Danišík, M., Rahn, M., Frisch, W. and Spiegel, C., 2008. Neogene exhumation history of the Mont Blanc massif, western Alps: Tectonics, 27, p. n/a–n/a, doi: 10.1029/2008TC002257.
- Glotzbach, C., van der Beek, P. A. and Spiegel, C., 2011. Episodic exhumation and relief growth in the Mont Blanc massif, Western Alps from numerical modelling of thermochronology data: Earth and Planetary Science Letters, 304, p. 417–430, doi: 10.1016/j.epsl.2011.02.020.
- Godard, V., Pik, R., Lavé, J., Cattin, R., Tibari, B., de Sigoyer, J., Pubellier, M. and Zhu, J., 2009. Late Cenozoic evolution of the central Longmen Shan, eastern Tibet: Insight from (U-Th)/He thermochronometry: Tectonics, 28, p. 73–88, doi: 10.1029/2008TC002407.
- Guenther, W.R., Reiners, P.W., Ketcham, R.A., Nasdala, L., and Giester, G., 2013. Helium diffusion in natural zircon: Radiation damage, anisotropy, and the interpretation of zircon (U-Th)/He thermochronometry. American Journal of Science, 313, p. 145-198, doi: 10.2475/03.2013.01.
- Hurford, 1986, Cooling and uplift patterns in the Lepontine Alps South Central Switzerland and an age of vertical movement on the Insubric fault line, Contributions to Mineralogy and Petrology, 92 (4), pp 413-427.
- Ketcham, R.A., 2005. Forward and Inverse Modeling of Low-Temperature Thermochronometry Data: Reviews in Mineralogy and Geochemistry, 58, p. 275–314, doi: 10.2138/rmg.2005.58.11.
- Ketcham, R.A., Gautheron, C. and Tassan-Got, L., 2011. Accounting for long alpha-particle stopping distances in (U–Th–Sm)/He geochronology: Refinement of the baseline case: Geochimica et Cosmochimica Acta, 75, p. 7779–7791, doi: 10.1016/j.gca.2011.10.011.
- Kirschner, D.L., Masson, H. and Sharp, Z.D., 1999. Fluid migration through thrust faults in the Helvetic nappes (Western Swiss Alps): Contributions to Mineralogy and Petrology, 136, p. 169–183, doi: 10.1007/s004100050530.
- Kirschner, D.L., Masson, H. and Cosca, M. A., 2003. An  $^{40}\text{Ar}/^{39}\text{Ar}$ , Rb/Sr, and stable isotope study of micas in low-grade fold-and-thrust belt: an example from the Swiss Helvetic Alps: Contributions to Mineralogy and Petrology, 145, p. 460–480, doi: 10.1007/s00410-003-0461-2.
- Lahfid, A., O. Beyssac, E. Deville, F. Negro, C. Chopin, and B. Goffé, 2010. Evolution of the Raman spectrum of carbonaceous material in low-grade metasediments of the Glarus Alps (Switzerland), Terra Nova, 22(5), 354–360, doi:10.1111/j.13653121.2010.00956.x.

- Lacombe, O., Mouthereau, F., 2002. Basement-involved shortening and deep detachment tectonics in forelands of orogens: Insights from recent collision belts (Taiwan, Western Alps, Pyrenees). *Tectonics* 21, 12–1–12–22. doi:10.1029/2001TC901018
- Leloup, P.H., Arnaud, N., Sobel, E.R. and Lacassin, R., 2005. Alpine thermal and structural evolution of the highest external crystalline massif: The Mont Blanc: *Tectonics*, 24, p. n/a–n/a, doi: 10.1029/2004TC001676.
- Marquer, D. and Burkhard, M., 1992. Progressive deformation and mass-transfer processes in the upper crust: the example of basement-cover relationships in the External Crystalline Massifs, Switzerland: *Journal of Structural Geology*, 14, p. 1047–1057.
- Mouthereau, F., Watts, A.B., Burov, E., 2013. Structure of orogenic belts controlled by lithosphere age. *Nat. Geosci.* 6, 785–789. doi:10.1038/ngeo1902
- Mugnier, J. L., Guellec, S., Menard, G., Roure, F., Tardy, M., and Vialon, P., 1990. A crustal scale balanced cross-section through the external Alps deduced from the ECORS profile. *Mémoires de la Société géologique de France*, 156, p. 203–216.
- Nicolas, A., Hirn, A., Nicolich, R., & Polino, R., 1990. Lithospheric wedging in the western Alps inferred from the ECORS-CROP traverse. *Geology*, 18(7), 587–590.
- Pik, R., Marty, B., Carignan, J. and Lavé, J., 2003. Stability of the Upper Nile drainage network (Ethiopia) deduced from (U–Th)/He thermochronometry: implications for uplift and erosion of the Afar plume dome: *Earth and Planetary Science Letters*, 215, p. 73–88, doi: 10.1016/S0012-821X(03)00457-6.
- Ramsay, J.G., Casey, M. and Kligfield, R., 1983. Geology Role of shear in development of the Helvetic fold-thrust belt of Switzerland Role of shear in development of the Helvetic fold-thrust belt of Switzerland: *Geology*, 11, p. 439–442, doi: 10.1130/0091-7613(1983)11<439:ROSIDO>2.0.CO;2.
- Rahn, M. K., 1994), Incipient metamorphism of the Glarus Alps: Petrology of the Taveyanne Greywacke and fission track dating, Ph.D. thesis, 209 pp., Univ. of Basel, Basel, Switzerland.
- Rahn, Brandon M.T., Batt G.E., Garver J.I., 2004, A zero-damage model for fission-track annealing in zircon, *American Mineralogist*, 89 (4), p.473-484.
- Reiners PW, Farley KA, Hickes HJ, 2002, He diffusion and (U–Th)/He thermochronometry of zircon: initial results from Fish Canyon Tuff and Gold Butte, *Tectonophysics*, 349 (1-4), p 297–308, doi:10.1016/S0040-1951(02)00058-6.
- Rolland, Y., Cox, S.F., Boullier, A.-M., Pennacchioni, G. and Mancktelow, N.S., 2003. Rare earth and trace element mobility in mid-crustal shear zones: insights from the Mont Blanc Massif (Western Alps): *Earth and Planetary Science Letters*, 214, p. 203–219, doi: 10.1016/S0012-821X(03)00372-8.
- Rolland, Y., Rossi, M., Cox, S.F., Corsini, M., Mancktelow, N.S., Pennacchioni, G., Fornari, M. and Boullier, A., 2008.  $^{40}\text{Ar}/^{39}\text{Ar}$  dating of synkinematic white mica: insights from fluid-rock reaction in low-grade shear zones (Mont Blanc Massif) and constraints on timing of deformation in the NW external Alps: *Geological Society, London, Special Publications*, 299, p. 293–315, doi: 10.1144/SP299.18.
- Rossi, M., and Rolland Y., 2014. Stable isotope and Ar/Ar evidence of prolonged multiscale fluid flow during exhumation of orogenic crust: Example from the Mont Blanc and Aar Massifs (NW Alps) : *Tectonics*, 33, doi:10.1002/2013TC003438.
- Seward, D. and Mancktelow, N.S., 1994. Neogene kinematics of the central and western Alps : Evidence from fission-track dating: *Geology*, 22, p. 803–806, doi: 10.1130/0091-7613(1994)022<0803:NKOTCA>2.3.CO;2. Shuster D. L., Farley K. A. (2009), The influence of artificial radiation damage and thermal annealing on helium diffusion kinetics in apatite, *Geochimica et Cosmochimica Acta* 73, 183–196
- Simon-Labré, T., Y. Rolland, T. Dumont, T. Heymes, C. Authemayou, M. Corsini and M. Fornari, 2009.  $^{40}\text{Ar}/^{39}\text{Ar}$  dating of Penninic Front tectonic displacement (W Alps) during the Lower Oligocene (31–34 Ma). *Terra Nova*, 21, 127–136.

- Sinclair, H.D., 1997. Tectonostratigraphic model for underfilled peripheral foreland basins: an Alpine perspective: Geological Society of America Bulletin, 109, p. 324–346.
- Stockli D. F. (2005), Application of low-temperature thermochronometry to extensional tectonic settings, Reviews in Mineralogy and Geochemistry 58, 411-448
- Tagami T., Galbraith RF., Yamada R., Laslett GM., 1998, Revised Annealing Kinetics of Fission Tracks in Zircon and Geological Implications, Advances in Fission-Track Geochronology, Solid Earth Science Library, 10, pp.99-112.
- Tagami T., Farley K.A., Stockli D. F. (2003), Thermal sensitivities of zircon (U-Th)/He and fission-track systems, *Geochimica et Cosmochimica Acta* 67:A466
- Valla, P.G., van der Beek, P. a., Shuster, D.L., Braun, J., Herman, F., Tassan-Got, L. and Gautheron, C., 2012. Late Neogene exhumation and relief development of the Aar and Aiguilles Rouges massifs (Swiss Alps) from low-temperature thermochronology modeling and  $4\text{He}/3\text{He}$  thermochronometry: *Journal of Geophysical Research*, 117, F01004, doi: 10.1029/2011JF002043.
- Von Raumer, J., Bussy, F., and Sharp, Z. D., 1996. Lac Cornu revisited: The evolution from lower to upper crust (Aiguilles-Rouges Massif, western Alps). *Schweizerische Mineralogische und Petrographische Mitteilungen*, 76, p. 120-121.
- Wopenka, B., and J. D. Pasteris (1993), Structural characterization of kerogens to granulitefacies graphite; applicability of Raman microprobe spectroscopy, *American Mineralogist*, 78(5-6), 533–557.
- Yamada R., Tagami T., Nishimura S., Ito H., 1995, Annealing kinetics of fission tracks in zircon: an experimental study, *Chemical Geology*, 122 (1-4), pp 249-258, doi:10.1016/0009-2541(95)00006-8
- Yui, T.-F., E. Huang, and J. Xu (1996), Raman spectrum of carbonaceous material: a possible metamorphic grade indicator for low-grade metamorphic rocks, *Journal of Metamorphic Geology*, 14(2), 115–124, doi:10.1046/j.15251314.1996.05792.x.

### **III.3. Évolution structurale de la marge lors de la collision.**

Les nouvelles données thermochronologiques (ZHe) et leur inversion avec HeFTy donnent des âges d'exhumation compris entre 5,3 Ma et 7,8 Ma pour une température entre 175 et 195°C ([Reiners et al., 2002](#); [Tagami et al., 2003](#); [Stockli, 2005](#)). Les données RSCM montrent une température moyenne maximale de la couverture du massif des Aiguilles Rouges de 315°C +/- 25°C.

Le chemin T-t du massif du Mont Blanc, construit à partir des données de la littérature, montre un réchauffement rapide entre 32 et 29 Ma, un plateau thermique à 400°C conservé jusqu'à 16 Ma et un refroidissement à peu près constant entre 16 et 6 Ma. La vitesse de réchauffement du massif entre 32 et 29 Ma est semblable à celle de Morcles, suggérant la restauration de la nappe au dessus plutôt à l'Est du massif du Mont Blanc. Le réchauffement plus précoce de la nappe par rapport à celui du massif du Mont Blanc ne semble être dû qu'à une différence dans les dates d'enfouissement (i.e. entre 29 et 31 Ma dans [Kirschner et al., 1995](#) et au plus tard à 32,5 Ma dans cette étude). Notons pour une telle restauration de la nappe, que son enfouissement après 30 Ma n'est pas compatible avec la déformation du massif du Mont Blanc à 29,5 Ma au pic P-T ([Cenki-Tok et al., 2013](#)). Le chemin construit pour le massif des Aiguilles Rouges montre un refroidissement relativement plus lent que celui du Mont Blanc entre 16 et 6 Ma, semblable à celui de la nappe de Morcles. Ce résultat suggère l'extrusion de la nappe et son charriage au dessus du massif des Aiguilles Rouge autour de 16 Ma.

On a proposé une évolution structurale de l'enfouissement, de l'inversion et de l'exhumation de la marge européenne à la latitude des massifs du Mont Blanc et des Aiguilles Rouges. La compilation de nos données et de celles de la littérature (e.g. [Lateltin et Muller, 1987](#); [Sinclair, 1997](#); [Kirschner et al., 1999](#); [Cenki-Tok et al., 2013](#)) montre que l'enfouissement de la marge se fait rapidement, entre 35 et 30 Ma, et sans déformation majeure. On note l'exception du décollement et de l'empilement des nappes Ultra-Hélvétiques au dessus de la couverture du Mont Blanc.

Une fois le pic de pression et de température atteint, à 30 Ma, la croûte commence à être légèrement raccourcie au niveau du Mont Blanc. Le pic de métamorphisme semble s'étaler pour les deux massifs du mont Blanc et des Aiguilles Rouges jusqu'à 16 à 18 Ma lorsque les rampes crustales, connectées aux chaînes subalpines, sont activées. L'exhumation des massifs est alors en grande partie due à l'activité de ces rampes mais aussi, dans le cas du Mont Blanc, à celle de la Mont Blanc Shear Zone.

### **III.4. Quelles variations le long de l'arc pour cette évolution structurale ?**

Tout d'abord, les exhumations des deux massifs des Aiguilles Rouges et du mont Blanc ne sont pas étudiées avec exactement les mêmes données. Il manque ainsi des données ZHe pour le massif du Mont Blanc et il est nécessaire de densifier les données ZFT du massif des Aiguilles Rouges. Ces données pourraient nous permettre de mieux contraindre les vitesses d'exhumation et ainsi de mieux estimer la part de l'exhumation due à l'activité des rampes crustales et celle due aux cisaillements du Mont Blanc. De plus, les vitesses de réchauffement proposées pour le massif du Mont Blanc et sa couverture sont très rapides, de l'ordre de  $100^{\circ}\text{C}.\text{Ma}^{-1}$ . Cela suppose des vitesses de relaxation thermique très rapides, bien plus que celle proposée pour le massif de l'Aar par [Challandes et al. \(2008\)](#).

On peut aussi s'interroger sur l'extension du scénario cinématique proposé à tous les MCE. Ainsi, en plus des variations des vitesses de réchauffement des unités lors du chemin prograde le long de l'arc (e.g.  $40^{\circ}\text{C}.\text{Ma}^{-1}$  dans l'Aar, sur la base de modélisation thermiques, [Challandes et al., 2008](#), contre  $100^{\circ}\text{C}.\text{Ma}^{-1}$  dans le Mont Blanc), on observe des variations des âges d'activation des déformations collisionnelles. Celles ci sont initiées légèrement plus tard dans le massif de l'Aar (23 Ma, [Challandes et al., 2008](#) ; [Rolland et al., 2009](#)) que dans les massifs de l'Oisans-Pelvoux (34 à 31 Ma, [Simon-Labbrick et al., 2009](#) ; [Bellanger et al., 2015](#)). Ces variations existent aussi pour la longueur du pic thermique enregistré dans l'Oisans, moins étalé dans le temps (5 à 6 Ma, [Bellanger et al., 2015](#)) que dans le Mont Blanc (13 Ma). Enfin, les chemins T-t, similaires pour les trois unités, des Aiguilles Rouges, du Mont Blanc et de Morcles, appuient la restauration de la nappe de Morcles au-dessus du massif du Mont Blanc telle que le proposent [Burkhard et Sommaruga \(1998\)](#). Pourtant, cette restauration, réalisée avec l'hypothèse de la conservation de l'aire de la nappe dans le plan de la coupe, ne tient pas compte des déformations internes des couches ([Ramsay, 1983](#)). Ce point soulève un problème méthodologique puisqu'il n'existe pas de méthode de restauration des couches déformées dans le domaine ductile et tenant compte de la déformation interne des couches mesurée sur le terrain. C'est cette méthode que nous développons dans la partie suivante.

## **IV. Étude de la géométrie et de la cinématique d'inversion des bassins de l'Oisans au cours de la collision alpine.**

**Inversion of pre-orogenic extensional basins in the external Western Alps: Structure, microstructures and restoration.**

Alexandre Boutoux, Nicolas Bellahsen, Olivier Lacombe, Anne Verlaguet, Frédéric Moutherau.

Article publié dans la revue Journal of Structural Geology

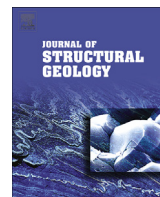
### **IV.1. Cadre et intérêt de l'étude : analyse microstructurale et nouvelle méthode de restauration.**

Un des moyens utilisés pour contraindre les déformations collisionnelles est la construction de coupes équilibrées du prisme ([Burkhard et Sommaruga, 1998](#) ; [Affolter et al., 2008](#) ; [Bellahsen et al., 2012, 2014](#)). Ces différentes coupes sont construites sur la base de l'hypothèse de (1) la conservation des longueurs des couches pour les unités déformées dans le domaine cassant (i.e. les chaînes d'avant pays) dont la longueur est supposée ne pas avoir varié au cours du raccourcissement et (2) la conservation de l'aire des unités déformées dans le domaine ductile (e.g. la couverture des MCE, [Burkhard et Sommaruga, 1998](#)). Pourtant, la restauration de la nappe de Morcles proposée par [Burkhard et Sommaruga \(1998\)](#) ne tient pas compte de la déformation interne des couches déterminée à partir des données de terrain ([Ramsay et al., 1983](#)).

Dans les MCE, la déformation du socle est localisée au niveau de bandes de cisaillement alors que la couverture est plissée dysharmoniquement au-dessus du socle (e.g., Burkhard, 1988 ; Escher et al., 1993 ; Epard, 1990 ; [Bellahsen et al., 2012](#) ; [Bellanger et al., 2014](#)). Si il est possible de calculer l'ellipsoïde de la déformation finie au sein de la couverture (e.g. [Ramsay et al., 1983](#) ; [Ramsay et Hubert, 1989](#)), la déformation localisée du socle ne le permet pas forcément. Ainsi, la mesure de la déformation finie dans les bandes de cisaillement n'est pas forcément réalisable. De ce fait, dans les MCE, le raccourcissement du socle peut être mesuré à partir de la déformation du tégument (le Trias) ([Bellahsen et al., 2012](#)). Mais dans le cas où le tégument des unités de socle n'affleure que de manière très parcellaire, le calcul des quantités de raccourcissement de socle n'est pas possible (cas de la nappe de Morcles et du Mont Blanc).

De façon à mieux contraindre les déformations de la couverture des MCE mais aussi du socle, il nous faut développer une méthode analytique de restauration des couvertures des bassins hérités qui tienne compte de la déformation interne des couches. Dans les bassins de l’Oisans (bassin de Bourg d’Oisans et de Mizoën), la couverture n’est pas décollée de son socle et le tégument triasique affleure largement ([Barféty et al., 1972](#) ; [Barbier et al., 1973](#)). La zone semble donc appropriée au développement d’une telle méthode de restauration.

#### **IV.2. Article.**



# Inversion of pre-orogenic extensional basins in the external Western Alps: Structure, microstructures and restoration



Alexandre Boutoux <sup>a,b,\*</sup>, Nicolas Bellahsen <sup>a,b</sup>, Olivier Lacombe <sup>a,b</sup>, Anne Verlaguet <sup>a,b</sup>, Frédéric Moutherieu <sup>a,b</sup>

<sup>a</sup> UPMC Univ. Paris 06, UMR 7193, ISTE, F-75005 Paris, France

<sup>b</sup> CNRS, UMR 7193, ISTE, F-75005 Paris, France

## ARTICLE INFO

### Article history:

Received 31 May 2013

Received in revised form

7 December 2013

Accepted 19 December 2013

Available online 31 December 2013

### Keywords:

Shear zones

Dysharmonic folding

Balanced cross-section

Finite strain ellipsoids

Western Alps

## ABSTRACT

During collision, continental margins are shortened along with the inversion inherited syn-rift basins. In this contribution, we explore the internal deformation of pre-orogenic basins during their inversion in the external Western Alps. New structural and microstructural data allow us to provide a new kinematic scenario for the shortening of two inherited basins in the Oisans External Crystalline Massif. Two cleavages and three vein sets are documented by field observations in the sedimentary cover metamorphosed in the greenschist facies. Their spatial and temporal development is strongly dependent on the structural style that is controlled by the initial basin geometry. In the basement, shear zones accommodate the shortening while the cover is disharmonically folded. We present a new approach for the restoration of cross-sections where ductile deformation prevailed, thus for which classical methods do not apply. Both length conservation for basement top and area conservation for the sedimentary cover, as well as fixed hinge kinematics for the cover folds, are assumed. Such restoration is discussed in the light of cover strain ellipsoid quantification based on field data analysis. We apply this approach to the Mörles nappe and propose a new restored geometry, which is further compared to the Oisans section.

© 2014 Elsevier Ltd. All rights reserved.

## 1. Introduction

Continental collision occurs when proximal continental margins get shortened during convergence. During such events, the inherited syn-rift basins are inverted, with normal fault reactivation (Letouzey et al., 1990; Roure and Colletta, 1996; Lacombe and Moutherieu, 2002; Moutherieu and Lacombe, 2006) or not (Butler, 1989; Tavarnelli, 1999; Scisciani et al., 2002; Buitier and Pfiffner, 2003; Panien et al., 2005; Butler et al., 2006). In particular, tectonic burial has been suggested to inhibit normal fault reactivation (Bellahsen et al., 2012): indeed, the P-T conditions that prevail during collisional shortening associated to the intrinsic weakness of syn-rift marly sedimentary rocks may significantly weaken the crust, down to the strength of the inherited faults. In such case, the inverted inherited basins exhibit strong internal ductile deformation (e.g., cleavage) that affects the

metasedimentary cover. The tectonic burial, as well as the inherited structure of the lithosphere (Watts et al., 1995; Moutherieu et al., 2003), also control the structural style during shortening: a rather hot lithosphere most likely deforms with a thick-skinned structural style.

One problem in such setting is the balancing of cross-sections because ductile deformation precludes any use of classical methods of restoration. The methodology of balanced cross-section was established since Chamberlin (1910) and Dahlstrom (1969) essentially in the external parts of orogens by using length or area conservation, as deformations are mainly brittle. In this case, balanced cross-sections provide key insights on the structural style and on the amount of shortening. Recently, new approaches have been proposed to balance cross-sections, not based into length conservation but only into area conservation in order to take into account the internal deformation of the layers (Epard and Groshong, 1993; Groshong and Epard, 1994; Bellahsen et al., 2012; Moretti and Callot, 2012; Butler, 2013). These recent approaches allow balancing ductile deformation but do not take into account the analysis of finite strain from field data.

In internal domains of many collisional orogens, key data on both the precise amount and the kinematics of collisional

\* Corresponding author. Université Pierre et Marie Curie, ISTE, UMR 7193 UPMC-CNRS, Case 129 T46-00, 2<sup>eme</sup> étage, 4 place Jussieu, 75252 Paris Cedex 05, France.  
Tel.: +33 1 44 27 71 81; fax: +33 1 44 27 50 85.

E-mail address: [alexandre.boutoux@upmc.fr](mailto:alexandre.boutoux@upmc.fr) (A. Boutoux).

shortening are still missing. This is mainly due to the lack of clear strain/kinematical markers as collisional shortening is superimposed onto subduction-related deformation and metamorphism and/or to significant ductile deformation. In the external Western Alps (Fig. 1), during the continental collision that started during early Oligocene times, the proximal European continental margin has been tectonically buried below the internal (Penninic) units down to the brittle–ductile transition (e.g. Crouzet et al., 2001; Simon-Labréteau et al., 2009; for the Oisans massifs: Fig. 1). In such a setting, inherited normal faults were not reactivated and the structural style is thick-skinned in the pre-orogenic extensional basins and locally thin-skinned where the crust was not previously significantly thinned (Bellahsen et al., 2012). Thus, if the shortening of the alpine external zones is now well-constrained (Guellec et al., 1990; Mugnier et al., 1990; Ford, 1996; Burkhard and Sommaruga, 1998; Deville and Sassi, 2006; Bellahsen et al., 2012), second-order variations in structure and kinematics require refinements.

This paper aims at providing new structural and microstructural data to better constrain the kinematics of inversion of pre-orogenic syn-rift basins in the Oisans External Crystalline Massif (ECM, Fig. 1). We especially show that the spatial and temporal development of cleavages and vein sets depends on the structural style that is itself controlled by the initial basin geometry. We also propose a new approach to balance cross-sections in such settings where significant ductile deformation precludes the use of the classical length conservation hypothesis. In this approach, we then assume for the North Oisans basins a constant length for the basement top and a constant area for the sedimentary cover. The sedimentary layer length variations predicted by the restoration are validated *a posteriori* with field-derived data on finite strain. This technique is also applied to the Mörclles nappe in the Aiguilles Rouges-Mont

Blanc ECM (Fig. 1). The comparison between Oisans and Aiguilles Rouges-Mont Blanc ECM further provides new insights into the variations of the accommodation of collisional shortening along the strike of the Alpine arc.

## 2. Geological setting

The Alps are the result of the closure of the Ligurian part of the Tethyan ocean (Lemoine et al., 1986). The ECM in Western Alps (Fig. 1) represent the inverted proximal European continental margin of the Ligurian ocean, where rifting occurred during Liassic and Dogger times, as attested by several N–S to NE–SW half-grabens. These basins are bounded by normal faults that controlled the deposition of marly syn-rift Liassic and Dogger series (Barfeté et al., 1979; Lemoine et al., 1981, 1986; Lemoine and Tricart, 1986; De Graciansky et al., 1989). In southeastern Oisans, from the end of Dogger to Cretaceous, a thick post-rift sedimentary cover was deposited, but most of it has subsequently been eroded (Fig. 1).

The subduction of the Ligurian ocean began during Cretaceous and ended during Eocene times, with the continental subduction of the distal parts of the European margin (Butler, 1986; Chopin, 1987). Then, the collision started at about 30–35 Ma with shortening of the proximal margin and final exhumation of the internal units (e.g., Rolland et al., 2008; Simon-Labréteau et al., 2009; Van Der Beek et al., 2010; Sanchez et al., 2011). During this Oligo-Miocene phase, the external units (the so-called Dauphinois units) were tectonically buried below the internal units with the activation of the Penninic Frontal Thrust (PFT) and coevally underwent metamorphism under greenschist facies P–T conditions. The ECM experienced peak temperatures of 280–350 °C (Crouzet et al., 2001; Simon-Labréteau et al., 2009), which suggests that they reached about 10 km depth assuming a 30 °C “normal geotherm”. During the Alpine shortening, the structural style was thick-skinned and no major decollement occurred between the cover and the basement, most likely because of the low crustal strength under collisional greenschist facies P–T conditions. Few hundred meter-thick shear zones deformed the basement while the cover was disharmonically folded over these shear zones (Bellahsen et al., 2012).

At the latitude of our study area (Figs. 1 and 2), two main inherited Jurassic half-grabens can still be recognized. The Bourg d’Oisans basin (Figs. 2 and 3) is limited to the West by the Ornon normal fault, which has a Jurassic throw of about 3000 m (Tricart and Lemoine, 1986; Lemoine et al., 1989) and was not significantly reactivated during the Alpine shortening (Fig. 3; Tricart and Lemoine, 1986). The pre-rift series consist of thin Triassic sandstones and dolomites and lower Liassic limestones and represent the cover that remained attached to the basement. The geometry of these Triassic (and lower Liassic) layers will be used in this study as a reliable proxy for the basement top geometry. The syn-rift deposits are Liassic to Dogger in age and are essentially marls and marly limestones with thicknesses varying from a few tens of meters on the crest of tilted blocks (Croix de Cassini and Emparis plateau, Fig. 2) to 2–3 km near the border normal faults (La Pautre and Mizoën, Fig. 2). The post-rift sedimentary rocks have been significantly eroded and can only be observed at one locality (Le Grand Renaud, Fig. 2): they consist of a few hundred meters of upper Jurassic and Cretaceous limestones and marls. The Mizoën basin (Figs. 2 and 3) is limited to the West by the Mizoën normal fault, whose Jurassic throw is lower than that of the Ornon fault (about 2.5 km). The pre-rift series are similar to those observed in the Bourg d’Oisans basin; the post-rift sedimentary rocks do not crop out in this basin. Syn-rift subsidence and normal fault activity started a few million years later in the Mizoën basin than in the Bourg d’Oisans one (Barbier et al., 1973).

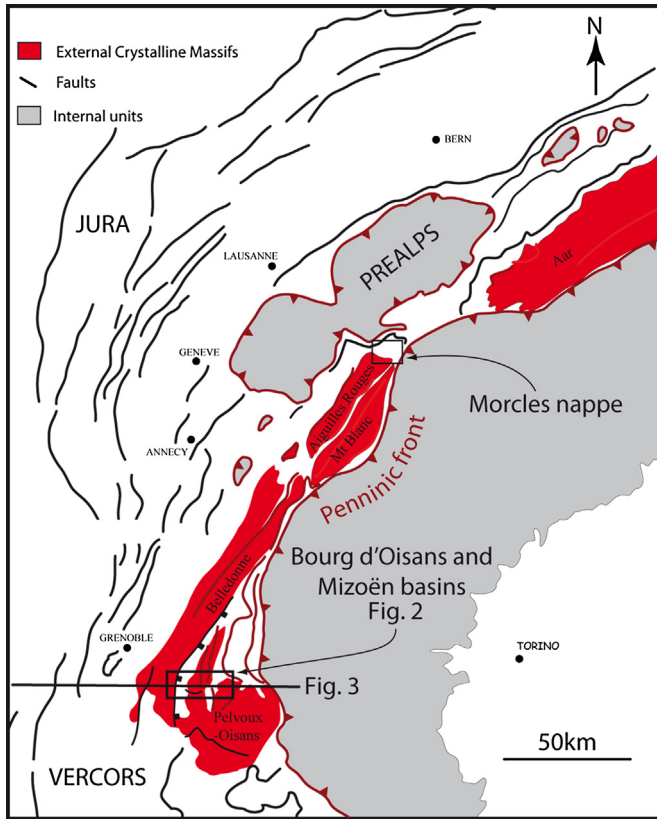


**Fig. 1.** Location of the studied area in western Alps. The frame in the northwestern Oisans massif represents the map in Fig. 2. The straight line indicates the cross-section of Fig. 3.

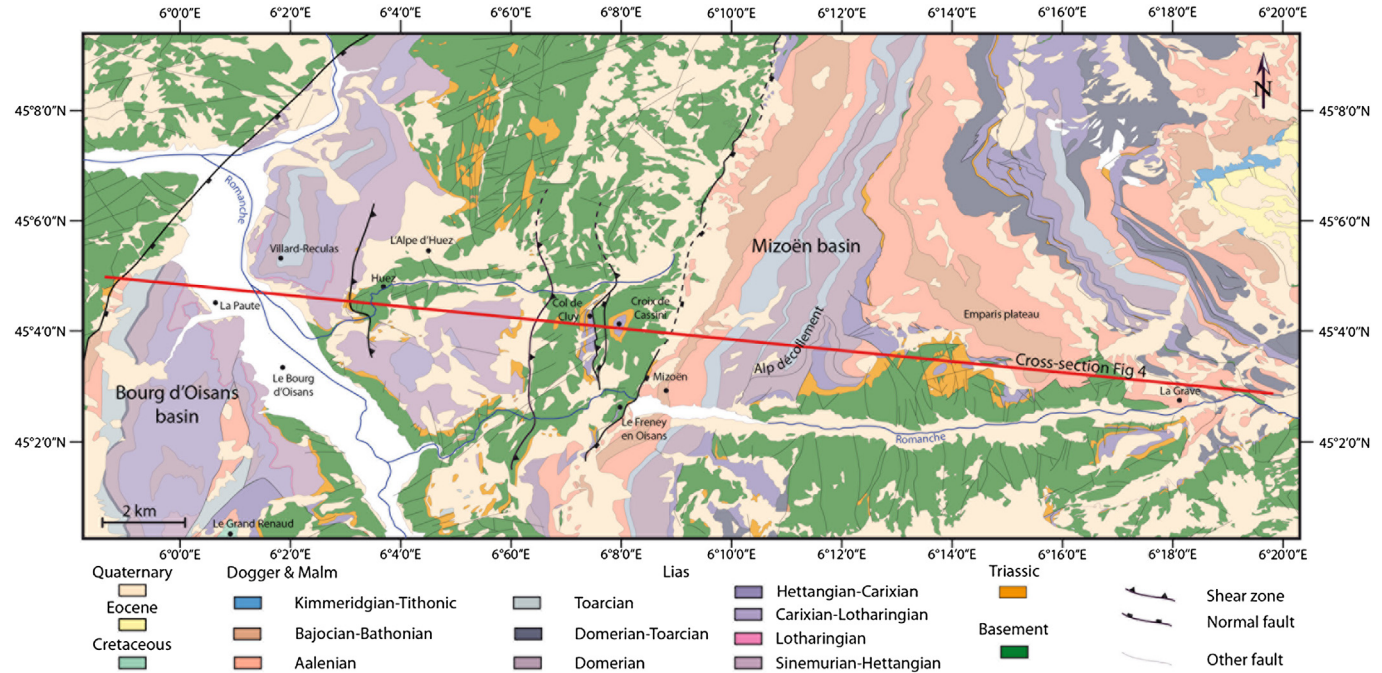


**Fig. 2.** Geological map of the Bourg d'Oisans and Mizoën basins, modified after Barfétty et al. (1972) and Barbier et al. (1973). The Ornon and Mizoën normal faults and the basement shear zones are highlighted. The red line indicates the cross-section of Fig. 3. [For interpretation of color referred in this figure legend, the reader is referred to web version of the article.]

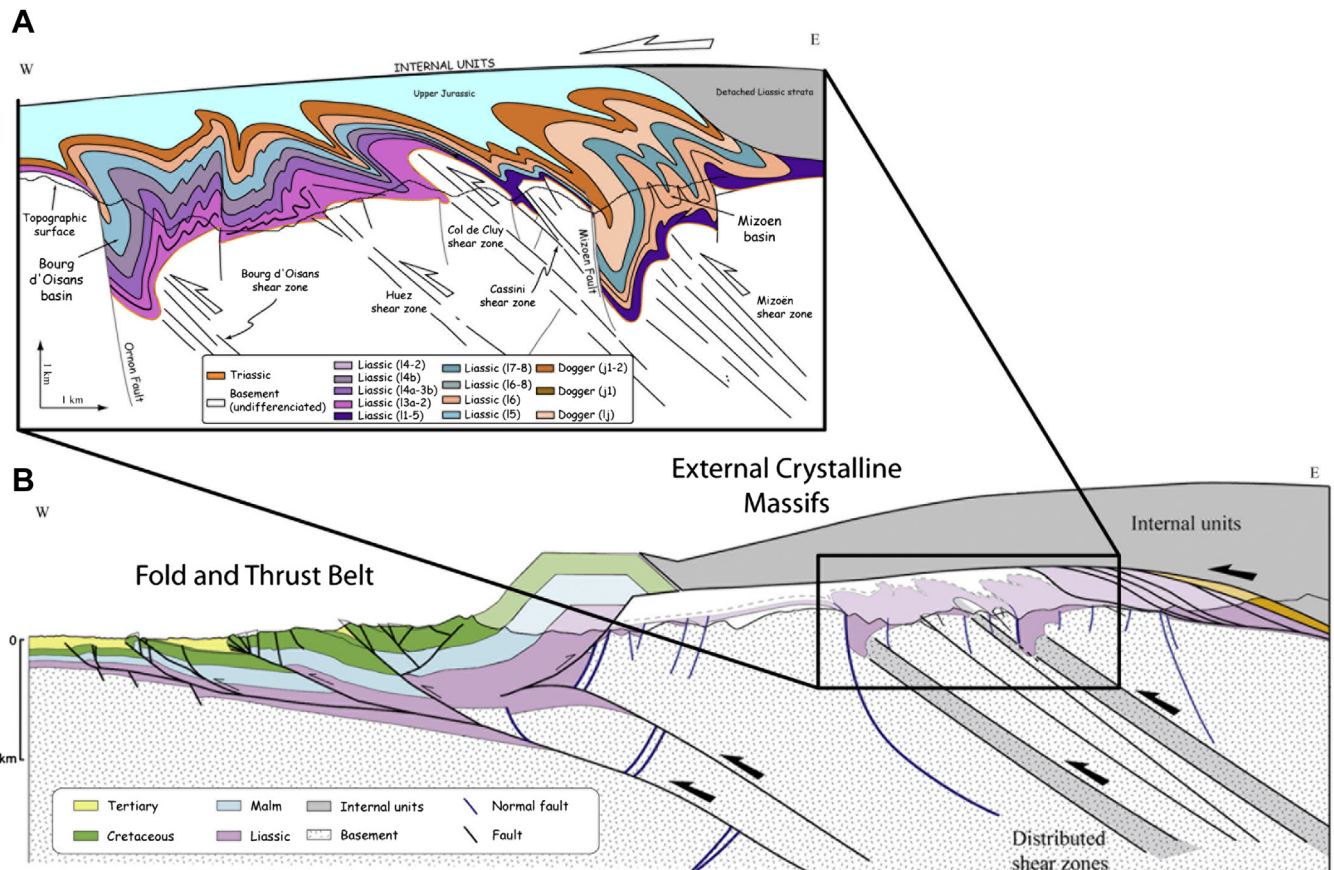


**Fig. 3.** Cross-sections after Bellahsen et al. (2012). A: Cross-section of the Mizoën and the Bourg d'Oisans basins. B: Bed-length and constant area balanced cross-section of the external zone. See location on Fig. 1.

### 3. Balanced cross-section and restoration

#### 3.1. Restoration method

In the external Western Alps, the fold-and-thrust belts can reliably be balanced using constant length assumption for the Mesozoic layers (e.g., Philippe et al., 1998; Deville and Chauvière, 2000; Affolter et al., 2008). Dahlstrom (1969) established the conservation of the layer length and area during brittle deformation. In the innermost part of the Alpine external zone (i.e., in the ECM), deformation is partly ductile and metasedimentary layers are strongly internally deformed (Gratier and Vialon, 1980; Beach, 1982). Bellahsen et al. (2012) provided a balanced cross-section of the external zone at the latitude of northern Oisans ([Figs. 1](#) and [3](#)) by restoring the initial geometry of the Triassic layer, which is widely cropping out and is the best proxy for the basement top geometry. The Jurassic layers were restored under the assumption that their total surface is conserved during shortening. Indeed, Moretti and Callot (2012) underlined the occurrence of length variation of internally deformed strata due to pressure solution during shortening. Here, in order to balance the cross-section ([Fig. 4](#)), we propose a new approach based on these recent contributions.

During shortening and burial of marly layers, internal deformation mainly occurred through pressure-solution and mass diffusion at the cm- to dm-scale (Gratier et al., 1973; Henry et al., 1996; Oliver, 1996). Furthermore, we assume that there was no material displacement outside areas bounded by both stratigraphic interfaces and fold axial surfaces, as folds develop with fixed hinges. Finally, as only few veins are parallel to the cross-section (see further down and in Gratier et al., 1973; Gratier and Vialon, 1980), there was probably no flow perpendicular to the cross-section. As the section furthermore strikes parallel to the Alpine stretching lineations (i.e., E–W, see further down), area conservation during Alpine shortening appears to be a robust assumption. Practically, the Triassic layer length is first restored assuming a pre-collision geometry given by the Jurassic normal fault throw (about 3000 m) and a low dip for Triassic layers ( $5.5^\circ$ ), as another major assumption for restoration purposes is that no significant reactivation of the inherited Jurassic normal faults occurred during collision. Then, both the whole Jurassic layers and each of their cells defined by stratigraphic limits and fold axial surfaces are restored considering constant area ([Fig. 5](#)).

The lower Triassic layers are then used as proxies to characterize the basement top shape and to quantify basement shortening. These layers show some internal deformation: field observations indicate that they were stretched (as attested by bed perpendicular veins) and sheared (as witnessed by sigmoidal cleavage). Considering constant width shear zones, the Triassic layer length, when deformed within a basement shear zone, suffered length variations: a decrease followed by an increase (Bellahsen et al., 2012). In the Bourg d’Oisans basin, considering the geometry of the observed shear zones, the cumulated length variation is a lengthening of about 500 m (with an initial length of 14.5 km). Thus, the error is less than 4% and has been neglected in the restoration.

The two basins were restored to their geometry before any tectonic burial and after the end of post-rift sediment deposition, which implies that the restoration does not need to take into account the volume variation due to porosity loss during diagenesis.

#### 3.2. Basement shear zones

In the Bourg d’Oisans basin, Alpine shortening in the basement has been accommodated by four main shear zones: the Bourg d’Oisans, La Garde, Col de Cluy, and Cassini shear zones ([Fig. 4](#)). The

Bourg d’Oisans shear zone is only inferred as no basement rocks crop out in the Bourg d’Oisans area. However, it is likely that such a basement shear zone exists as lower Liassic rocks can be observed 2 km East of the Ornon normal fault ([Fig. 2](#)) indicating basement uplift. The Cassini shear zone is only poorly exposed, although its displacement is well constrained by the geological map ([Fig. 2](#); Barféty et al., 1972). The two other shear zones can be observed and documented in the field ([Fig. 4](#)). These shear zones cut across and deform the Variscan foliation and dip at shallower angle (i.e.,  $30$ – $50^\circ$  to the East, compared to the  $70^\circ$  East-dipping Variscan foliation). The restoration of the Triassic cover–basement interface provides shortening values of 4.3 km (29%) for the Bourg d’Oisans basin.

In the Mizoën basin, basement deformation cannot be easily documented, due to the lack of exposure. However, its shortening can be estimated by the restoration of the Triassic cover–basement interface, which provides shortening values of 2.7 km (24%) for the Mizoën basin.

#### 3.3. Cover folds

Five main cover folds, located above the basement shear zones can be mapped in the Bourg d’Oisans basin ([Figs. 2](#) and [4](#)). They are disharmonic folds and/or folds slightly detached from the basement ([Fig. 4](#)). Whatever the type, folding is here always associated with internal layer deformation. The upward extension of these folds is controlled by the restoration hypothesis of constant area. The area drawn on the cross-section must fit the restored syn-rift basin geometry based on the Triassic layer length and the dip of the normal fault throw. The geometry of all the folds and their East-dipping axial surface are consistent with a top-to-the-West shearing of the cover.

The location of the Liassic depocenters close to their associated normal faults and the strong link between cover folds and basement shear zones imply that no significant décollement occurred between the cover and the basement. However, where the cover folds are tight and their axial surfaces rather steep (above the Bourg d’Oisans shear zone, [Fig. 4A](#)), short décollements occur within the lower Liassic layers (Sinemurian–Hettangian). The layers of the Bourg d’Oisans metasedimentary cover show internal deformation (thinning of the fold limbs and thickening of fold hinges, [Fig. 3](#)), which makes shortening computations very complicated. However, because there is no large décollement of the meta sedimentary cover, cover shortening has to be similar to basement shortening.

Deformations of the Mizoën basin show slight differences with deformations of the Bourg d’Oisans basin, although the cover is also strongly folded and displays East-dipping fold axial surfaces. The main difference is the activation, in the Mizoën basin, of a décollement (the Alp décollement, [Figs. 2](#) and [4A](#)) restricted to the eastern part of the basin and localized within the Sinemurian layer. Under this décollement, two small-scale folds are associated with an East-verging shear zone within the cover ([Fig. 4A](#)). At a large scale, the eastern part of the basin consists of the Emparis Plateau ([Fig. 4A](#)), where the strata are thin and overthrust by a meta sedimentary nappe, usually mapped as Ultra-Dauphinois ([Figs. 2](#) and [4](#); Ceriani et al., 2001) that probably roots further East. Because of uncertainties in this nappe rooting, the Mizoën basin is only balanced considering Triassic length preservation, layer area conservation and no reactivation of the inherited Mizoën normal fault.

The Oxfordian (upper Jurassic) shales observed at Le Grand Renaud ([Fig. 2](#)) were likely also present in the synclines although now eroded away. This weak layer may have allowed decoupling of the Dauphinois cover from the younger Mesozoic series and the internal units: the PFT has thus been drawn much less folded than

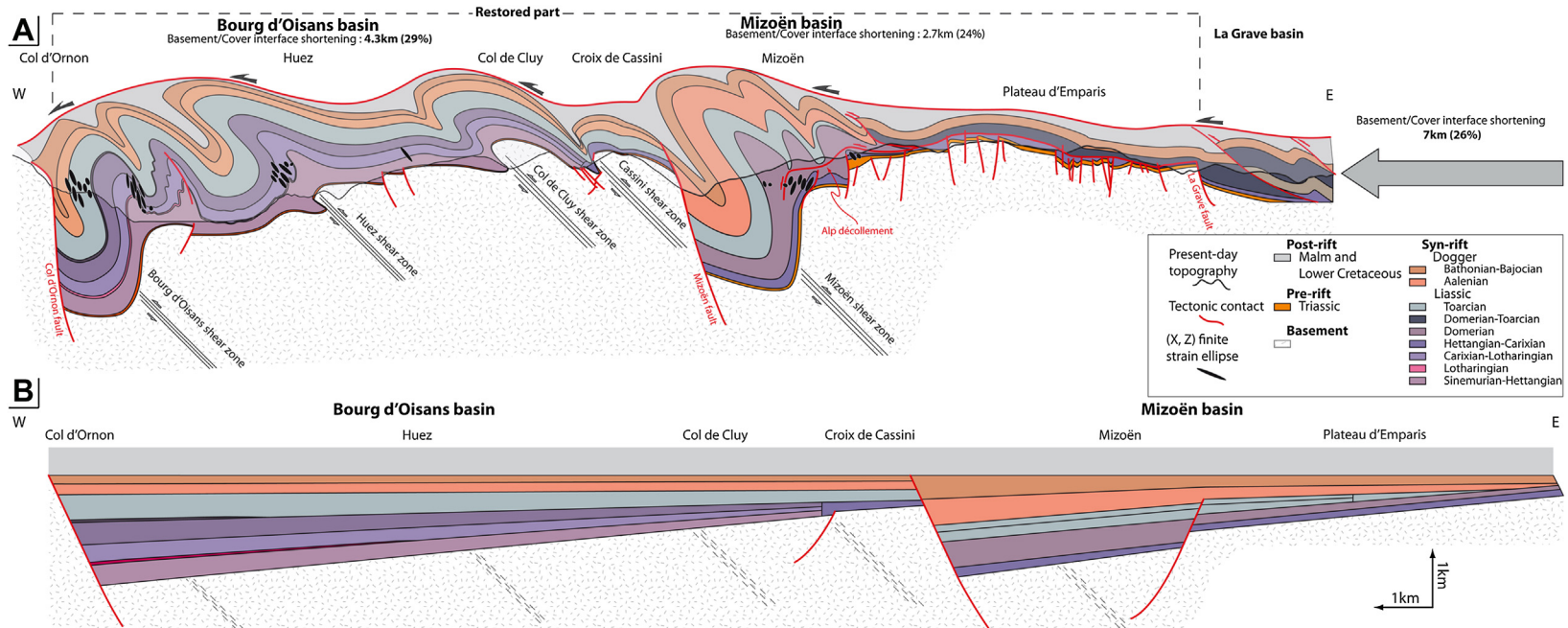


**Fig. 4.** A: New balanced cross-section of the Bourg d'Oisans and Mizoën basins after field data and geological maps (Barf  ty et al., 1972; Barbier et al., 1973). B: Restored cross-section. The Mizo  n basin was restored with area conservation of the cover. See Fig. 5 for the Bourg d'Oisans hypothesis of restoration.

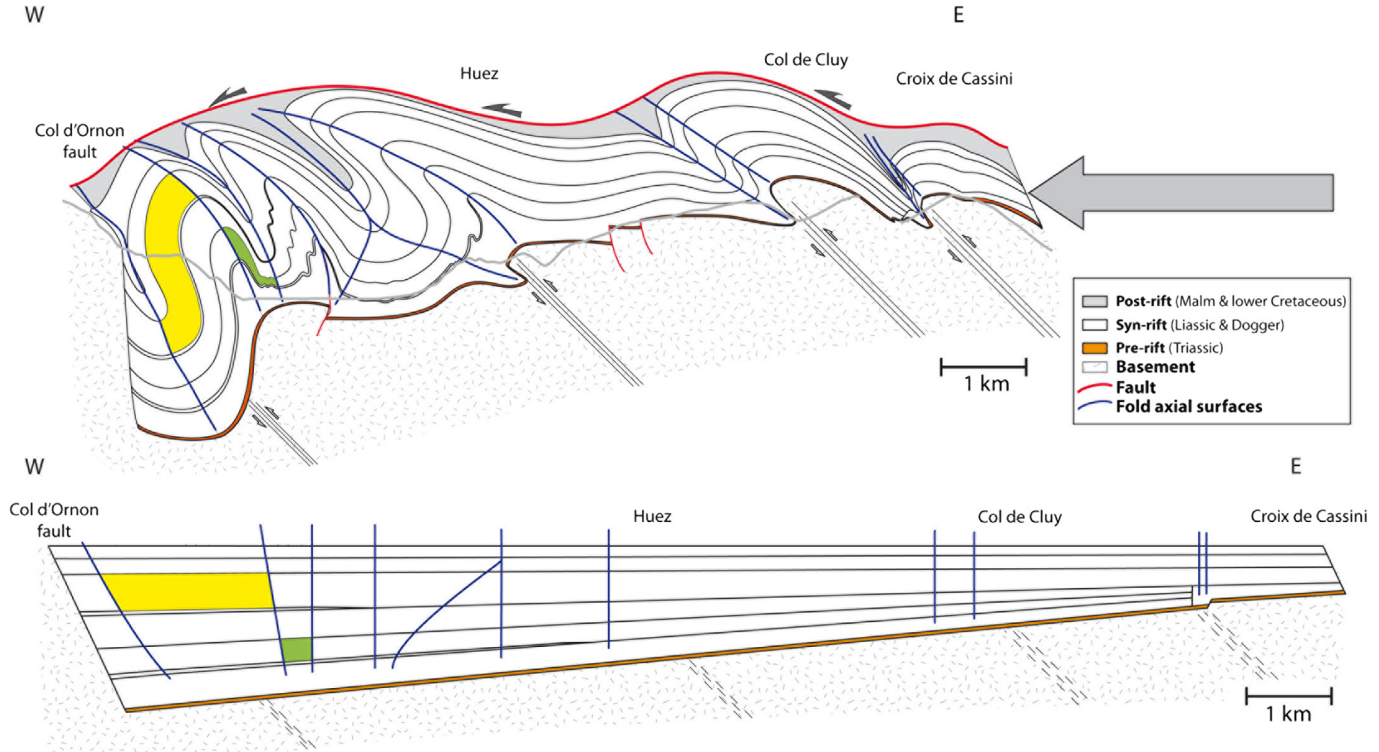


**Fig. 5.** Restoration of the Bourg d'Oisans basin. The restoration was built assuming: (1) area conservation for the entire cover (the syn-rift sediments) and for each cell defined by bedding and fold axes, (2) conservation of the Triassic basement–cover interface length, (3) no reactivation of the normal faults dipping  $65^\circ\text{E}$ , and (4) a dip of  $5.5^\circ\text{E}$  for the Triassic.

the underlying rocks (Fig. 4A). This drawing implies that basement shortening and basin inversion were coeval with the PFT activation or at least started during this thrust activity.

#### 4. Outcrop-scale and micro-scale structural analysis

##### 4.1. Cleavages and lineations

In the Bourg d'Oisans basin, two main cleavages, S1 and S2, have been documented in the field (Figs. 6 and 7). Chronological relationships can be deciphered close to the basement, for example near Huez (Fig. 2). Fig. 6 shows an East-verging fold with an axial surface parallel to the early cleavage (S1) which is oriented nearly N–S and oblique to bedding (S0). This likely witnesses a top-to-the-East shearing event of the cover. The vergence of this local shearing during early crustal shortening was probably controlled by the West-dipping top basement surfaces within the inherited tilted blocks.

S1 cleavage predates an East-dipping S2 cleavage consistent with cover folding, itself consistent with a top-to-the-West shearing. It is noteworthy that the S1 cleavage can be observed only near the basement (Fig. 7). The second S2 cleavage is observed all over the basin. It is oriented parallel to the main fold axial surfaces, i.e., N–S and sub-vertical to East-dipping (Fig. 7). Associated to this S2 cleavage, stretching lineations strike mainly E–W, with a scatter from  $060^\circ\text{E}$  to  $120^\circ\text{E}$  (Fig. 7). They are steeply East-plunging in the western part of the basin, where the cleavage is itself steep and associated to steep fold axial surfaces.

In the Mizoën basin, both cleavages can also be observed. S1 cleavage can be documented only below the Alp décollement (Fig. 8); it is a steep, West-dipping cleavage consistent with the East-verging folds affecting the lower Liassic layers above the hidden basement shear zones (Mizoën shear zone) (Figs. 4 and

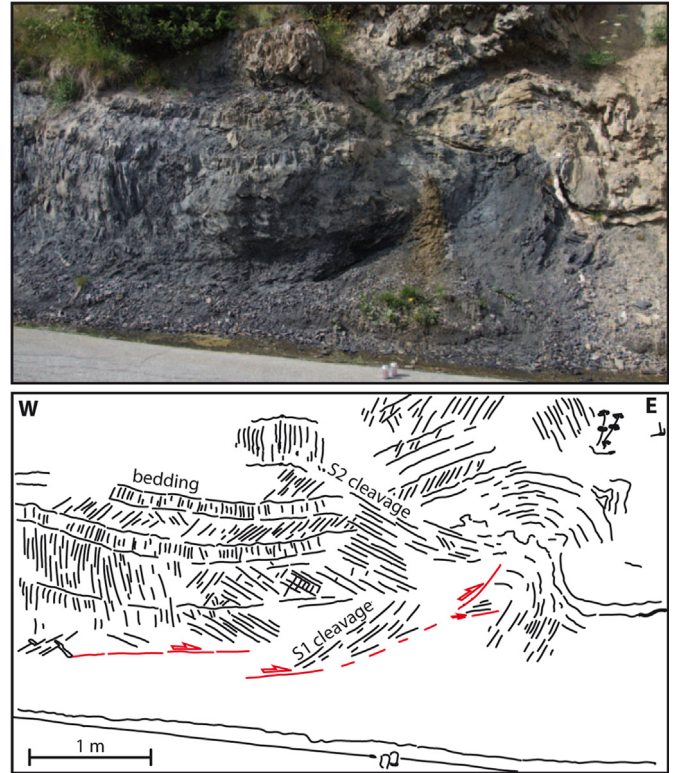


**Fig. 6.** Chronological relationship between S1 and S2 near Huez (see location on Fig. 2). Modified after Bellahsen et al. (2012). The fold axial surface is parallel to the S1 cleavage. S1 cleavage thus probably results from an East-verging shearing of the cover. The S2 cleavage postdates the S1 cleavage and is parallel to the axial surfaces of the large folds of the cover.

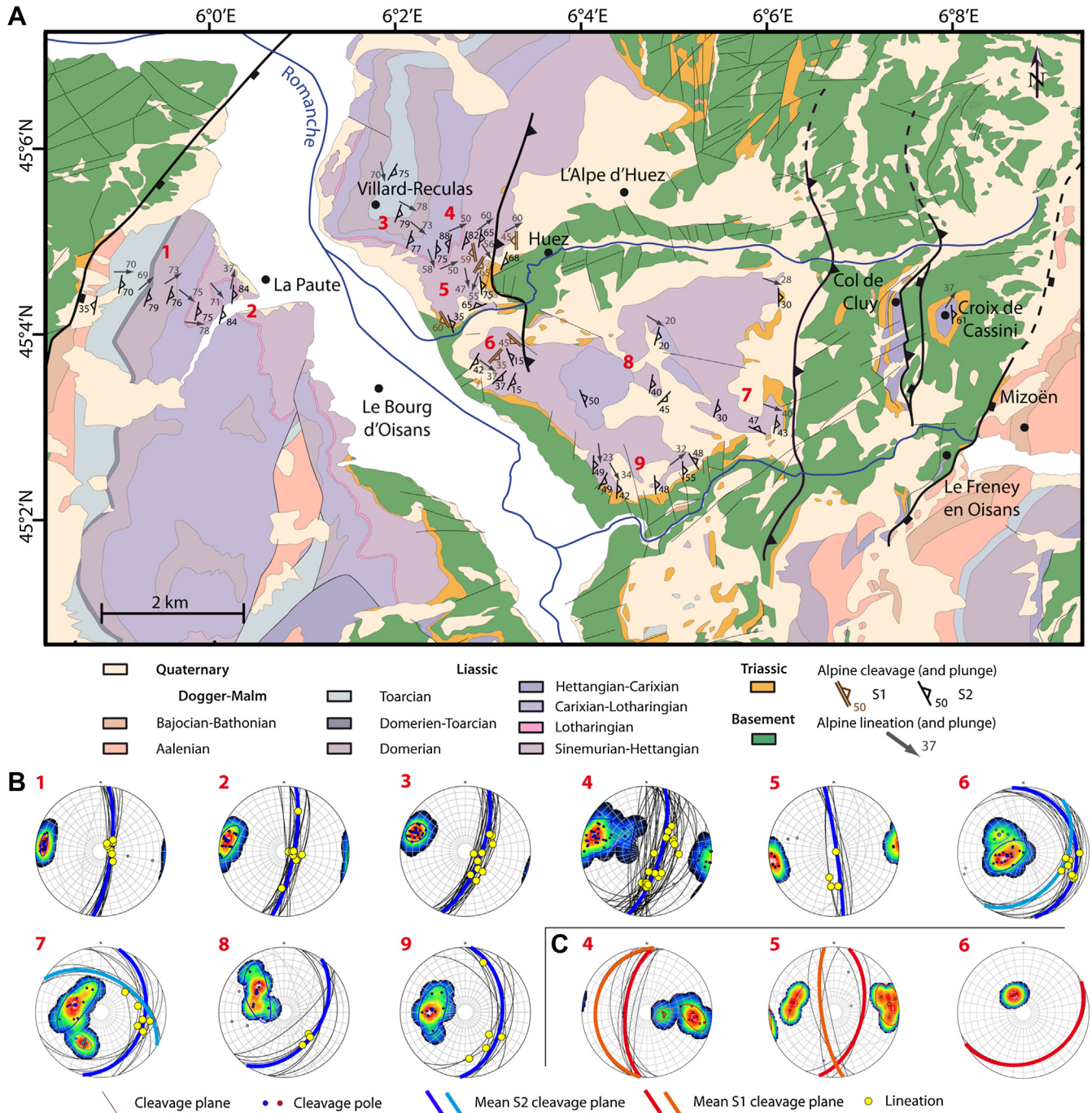


**Fig. 7.** (A) Alpine cleavages and lineation in Bourg d'Oisans basin. The geological map is modified after Barf  ty et al. (1972). Two N-S Alpine cleavages (S1 and S2) are observed in Liassic rocks. S2 is usually either vertical or steeply dipping East. (B) Alpine S2 cleavage in the sedimentary cover and lineation (L2) on it. The cleavage and the lineation are mainly dipping toward the East, the cleavage dip decreases from West to East (C). Alpine S1 cleavage can be observed close to the basement, especially West of the Huez shear zone. Because S1 is overprinted by S2 cleavage, lineations on S1 (L1) were not observed.

8). S2 cleavage is absent below the décollement. Above the décollement, however, only the N–S East-dipping S2 cleavage is observed (Fig. 8). It is parallel to the main fold axial surfaces and is thus considered as equivalent to the S2 cleavage of the Bourg d’Oisans basin. On this cleavage, the stretching lineation is trending NE–SW to E–W and is plunging Eastward (Fig. 8). It is noteworthy that toward the basement, the lineation trend becomes closer to N–S.

Small-scale folds can be observed in the field: their axial plane is parallel to the N–S S2 cleavage and their axis is parallel to the

stretching lineation on S2. Thus, they are interpreted as witnessing a strong stretching associated with the E–W shortening.

## 4.2. Cover veins

Calcite/quartz veins are found in many places in the cover. Two types of vein/cleavage chronological relationships have been recognized: veins cutting across cleavages are interpreted as postdating them; conversely, veins that are either transposed and stretched within the cleavage or folded with axial surfaces parallel

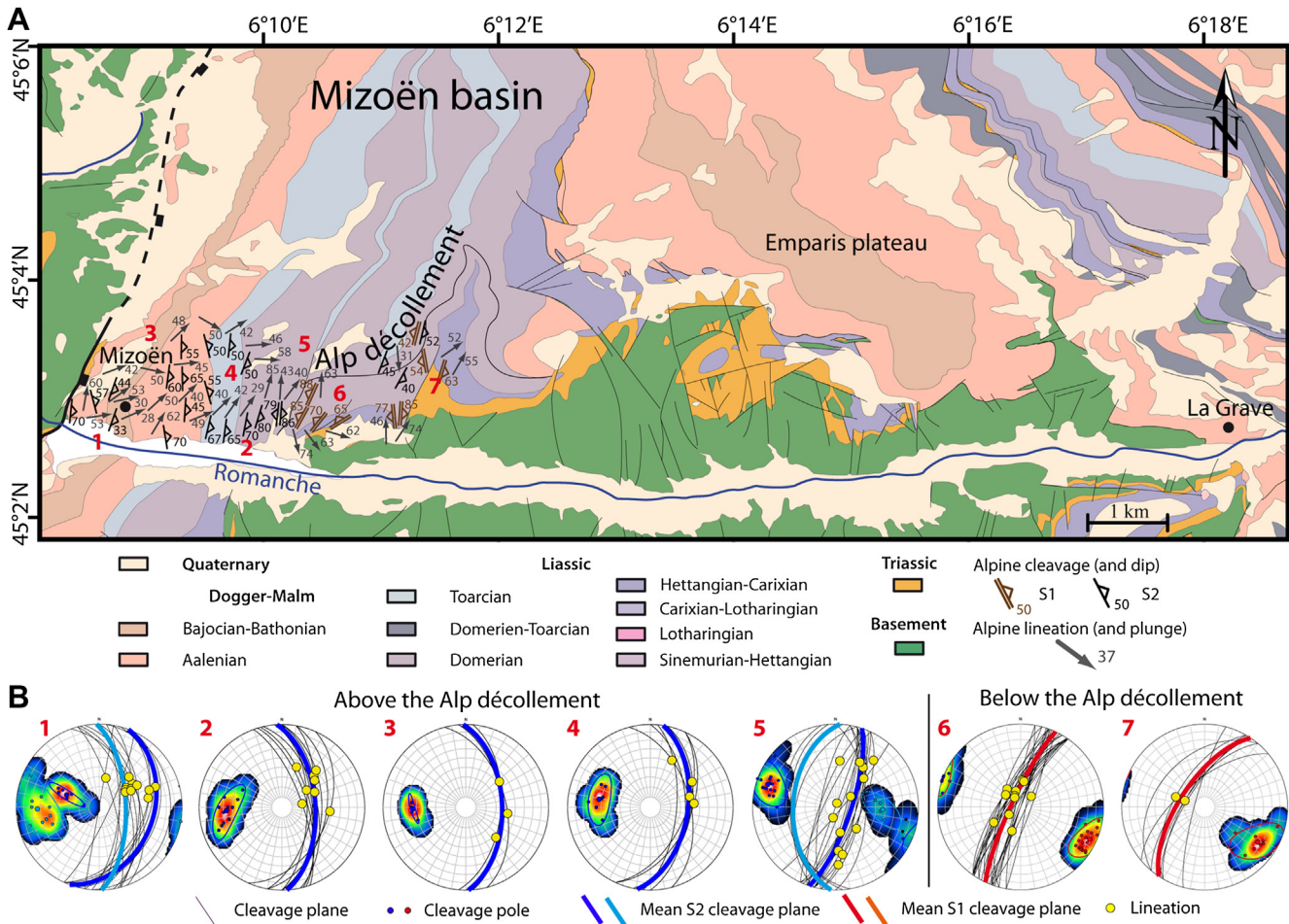


**Fig. 8.** (A) Alpine cleavages and lineation in Mizoën basin. The geological map is modified after Barbier et al. (1973). Two Alpine cleavages (S2 and S2) are documented in the Liassic rocks. S1 cleavage is restricted to the area close to the basement-cover interface, under the Alp décollement, and generally West-dipping. The S2 cleavage is observed above the Alp décollement and is East-dipping. (B) Alpine S2 cleavage and lineation (L2) on it at sites 1 to 5. The cleavage is mainly dipping toward the East; the dip decreases from West to East. The L2 lineation are East-West in the western part of the basin and tend to become NE-SW and less steep from West to East. The S1 cleavage and lineations (L1) on it are restricted to the structural unit below the Alp décollement is mainly west-dipping and very steep. They are at sites 6 and 7.

to the cleavage (ptygmatic folds) are interpreted as predating cleavage development.

In the Bourg d'Oisans basin, where two main cleavages are observed in the same sites, three sets of veins can be distinguished. V1 veins are deformed by S1 cleavage (Fig. 9D). V2 veins are deformed by S2 cleavage (Fig. 9A) and cut across both S1 cleavage and V1 veins (Fig. 9D). Finally, V3 veins cut across both S1 and S2 cleavages (Fig. 9B and D). The relative chronology of these three vein sets is summarized on Fig. 10A.

In the Mizoën basin, where only the S1 cleavage only is documented below the Alp décollement (Fig. 8), only two vein sets can be defined: V2 and V3 veins cannot be discriminated and are therefore denominated simply as "late veins". Fig. 9C and F shows early veins (V1) that are deformed (ptygmatic or transposed) by the S1 cleavage. Conversely, above the décollement where only S2 cleavage has been identified (Fig. 8), V1 and V2 cannot be discriminated: all veins transposed in S2 are thus simply labeled "early veins". The relative chronological relationships between these vein sets in the two structural units are summarized on Fig. 10B.

It is noteworthy that other problems of vein set determination may also arise locally in the Bourg d'Oisans basin, as the S1 cleavage tends to disappear far from the basement. As a consequence, in younger stratigraphic units, V1 and V2 again cannot be distinguished.

#### 4.3. Synthesis and interpretation

The relative chronology of both cleavages and vein sets is represented in 3D views in Fig. 11. This pattern can be explained by the following kinematic scenario (Fig. 11): (1) The initial geometry consists of two inherited Liassic syn-rift basins (the Bourg d'Oisans and Mizoën basins, Fig. 11A). (2) During the early stage of E-W shortening, the inherited West-dipping basement-cover interface controlled the deformation kinematics and caused East-verging shearing and development of S1 cleavage (Fig. 11B). Meanwhile, veins consistent with this top-to-the-East shearing initiated with an eastward dip. Close to the main Jurassic faults, shearing is instead top-to-the-West (Fig. 11B). (3) During ongoing shortening, V1 veins were continuously formed and progressively either deformed as ptygmatic veins or transposed by the development of the S1 cleavage (Fig. 11C). At the end of this stage, the latest veins were not deformed by S1 and may thus be recognized in the field as V2 veins. (4) Finally, S2 cleavage started to develop during the West-verging shearing and deformed these former V2 veins (Fig. 11D). The S2 cleavage is synchronous with the top-to-the-West shearing. Successive V2 veins formed during this whole stage and were either transposed or deformed as ptygmatic veins depending on their initial dip angle with respect to the cleavage S2. It is noteworthy that in the field, where the strata are overturned and S1

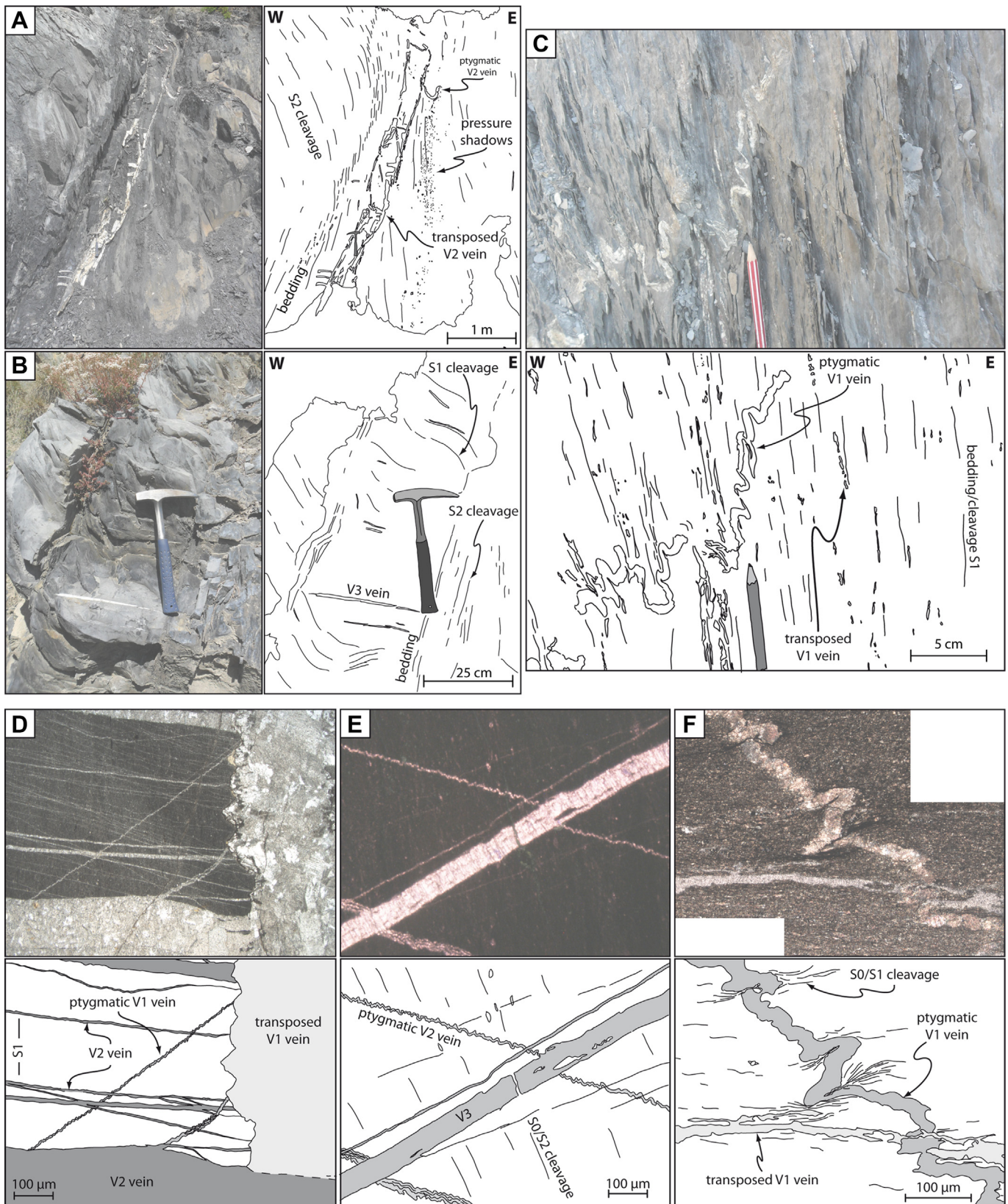


**Fig. 9.** Veins from the Bourg d'Oisans and Mizoën basins observed at the outcrop or in thin section: (A), (B), (D) and (E) Near Huez village (C) and (F) near Mizoën, under the Alp décollement (see locations on Fig. 2). (A) Transposed V2 vein and S2 cleavage. (B) Late V3 vein compatible with the S2. (C) Ptygmatic vein (V1), S1 cleavage parallel to fold axial surface and V1 vein transposed in the S1 cleavage. (D) Thin section of V1 vein transposed in the S1 cleavage, ptygmatic V1 veins with S1 cleavage parallel to their axial surface and V2 veins cross-cutting the V1 veins. (E) Thin section of ptygmatic V2 veins with S2 cleavage parallel to their axial surface and late V3 veins cross cutting the S2 cleavage and the V2 veins. (F) Thin section of transposed V1 vein in the S1 cleavage and ptygmatic V1 veins with S1 cleavage parallel to their axial surface.

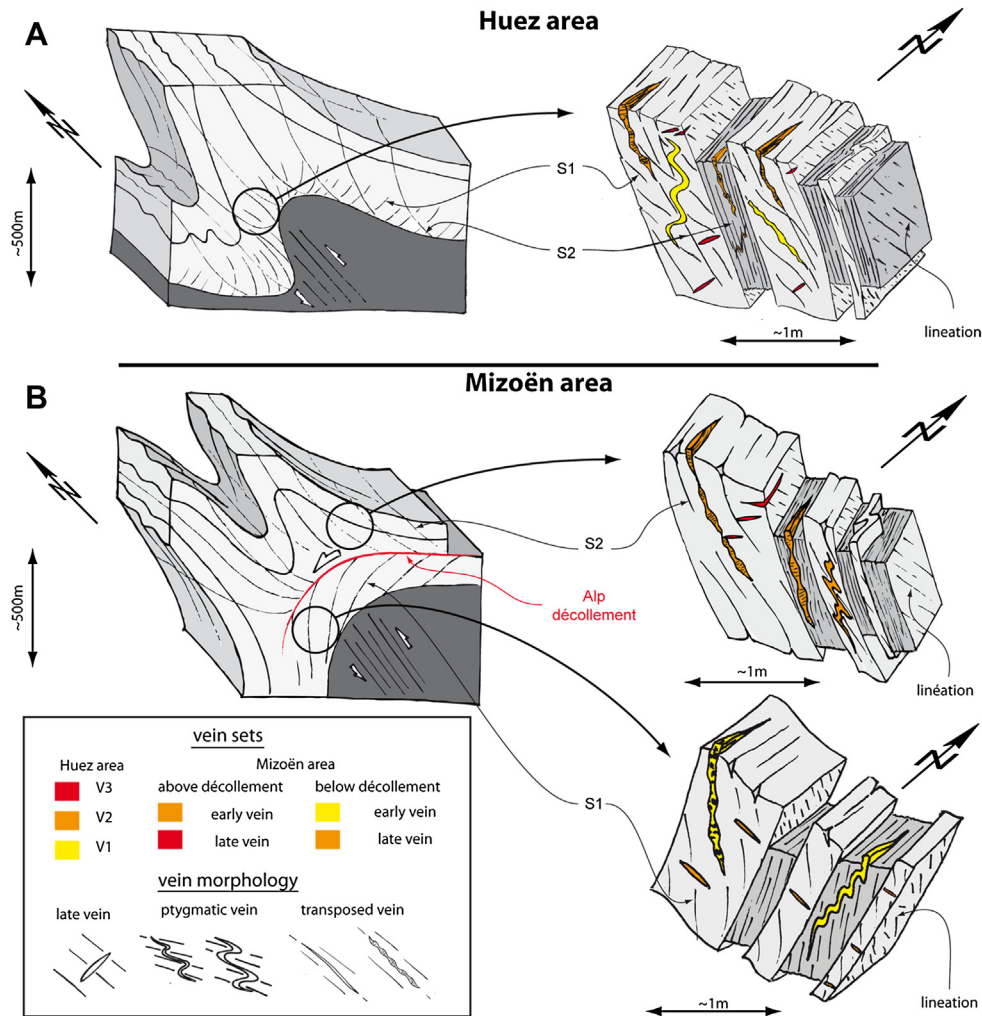


**Fig. 10.** 3D views of the geometric relationships between the two sets of cleavage and the three sets of veins from field data. In the Bourg d'Oisans area, close to the basement, the two sets of cleavage (S1 and S2) are present. V1 veins are deformed (transposed or ptygmatic) by S1; V2 veins are deformed by S2 and cutting across S1. V3 are non-deformed veins cutting across S1 and S2. In the Mizoën area, under the Alp décollement, only one cleavage associated with west-verging shearing is observed. This is considered as S1 cleavage. Veins deformed by S1 cleavage are early veins (V1) whereas veins cutting across S1 cleavage are late veins (V2/V3). Above the décollement, there is only one cleavage, East-dipping and parallel to the axial plane of overturned folds. This is considered as S2 cleavage. Veins deformed by cleavage are early veins (V1/V2) veins whereas veins cutting across S2 cleavage are late veins (V3).

and S2 sub-parallel, V1 and V2 cannot be discriminated (see Fig. 11D). The latest veins formed were not affected by S2, and even cut across S2; they may therefore be recognized as V3 veins.

#### 4.4. Analysis of the layer internal strain

##### 4.4.1. Methodology

If, at large scale, cover deformation is ductile, at small scale (mm to cm-scale) both brittle and ductile deformation can be observed. The development of cleavages is associated with pressure-solution processes (Gratier et al., 1973), along with pressure shadow development around clasts (e.g., belemnite fragments) or blasts (e.g., euhedral pyrites). Stretching and boudinage of belemnites are however brittle processes, associated with calcite, quartz and pyrophyllite recrystallization between the belemnite clasts. In order to quantify finite strain, we adopted the method proposed by Ramsay and Huber (1989), which is based on the deformation of different inherited clasts within the ductile matrix.

To estimate the X/Y ratio (noted  $R_{XY}$  in the following, X and Y being the maximum and intermediate axes of the finite strain ellipsoid, respectively), we used feeding burrows, assuming that

they were initially horizontal (parallel to the bedding surface) and randomly oriented (Fig. 12A). Because those burrows were filled during sedimentation, they have the same composition than the host rock, hence a similar viscosity. There is therefore no significant underestimate of the finite strain (Ramsay and Huber, 1989). When the layers were deformed during shortening, these burrows were passively reoriented within the cleavage plane (XY) that developed perpendicular to the local shortening. Their mean orientation in the cleavage plane thus indicates the stretching lineation.  $R_{XY}$  was determined on fold limbs where cleavage planes are sub-parallel to bedding so that the initial distribution of burrows in the bedding and the cleavage planes were roughly parallel. In order to have a representative angle distribution and mean orientation of the burrows, we measured at least 300 angles in each sample. Following Ramsay and Huber (1989), the  $R_{XY}$  histograms were compared with theoretical Gaussian envelopes (Fig. 12A) computed for theoretical  $R_{XY}^{th}$  values (ranging from 1 to 5): the best fit gave us the value for  $R_{XY}$ .

The  $R_{XZ}$  ratio of the finite strain ellipsoid can be directly estimated from the shape of the pressure shadows (Fig. 12B; Etchecopar and Malavieille, 1987; Ramsay and Huber, 1989) and we

assume that it can be extrapolated to the surrounding host rocks. Here, in order to estimate finite strain we measured only the pressure shadows around framboïdal pyrites (Fig. 12B), which are related to bacterial activity during early diagenesis and so recorded the whole tectonic history. Because the  $R_{XZ}$  values do not show important variations, we assume that the average of ten pressure shadows by sample confidently constrains the  $R_{XZ}$  ratio for a given outcrop.

To fully quantify the strain ellipsoid, we estimated volume changes during shortening. The numerous vein sets observed in the sedimentary rocks (Fig. 9) are mm- to m-scale veins and are not connected over long distances. Therefore, there is no field evidence for large-scale channels allowing large amounts of fluid flow in these rocks. From stable isotope and trace- and major-element analyses, Henry et al. (1996) concluded that there was no large-scale fluid infiltration in similar Dauphinois cover rocks close to La Grave (East of the Mizoën basin, Fig. 2), but only formation-scale fluid circulations. Both isotopic and trace element analyses evidenced an equilibrium between the mineral vein filling and their host-rock, which implies that the vein filling material has a local origin. It was transported from the surrounding host-rock to veins by pressure-solution/precipitation and small-scale diffusion processes (Oliver, 1996; Oliver and Bons, 2001). Therefore, as pressure-solution/precipitation processes cause local mass redistribution only, the volume change (i.e., mass gain or loss) at the outcrop-scale can be neglected. Rock volume change may also arise due to metamorphic dehydration reactions during burial. In these cover marls, modal calculations (from XRD and bulk rock ICP-AES analysis) show that the pelitic fraction is highly variable, from 0 to about 50 wt.%. Considering that, in the protolith, this pelitic fraction was composed of hydrated clay minerals, the estimated reaction volume ( $\Delta V$ ) is negligible ( $\pm 2\%$  maximum) and the mineral volume change due to metamorphic dehydration reactions may not exceed a few percents: a maximum of 8% can be calculated for a highly pelitic sample. Thus, it is reasonable to assume that there was no or very few volume change at the outcrop-scale (i.e., meter-scale) in the cover rocks during deformation.

With  $R_{XY}$ ,  $R_{XZ}$  ratios and the constant volume hypothesis, the absolute values of the X, Y and Z axes of the finite strain ellipsoid were computed, as long as  $R_{XY}$  and  $R_{XZ}$  were measured on the same outcrop (Fig. 12C).

#### 4.4.2. Field data

The  $R_{XY}$  and  $R_{XZ}$  ratios were measured in the field along the E–W cross-section in the Bourg d’Oisans basin: above the Bourg d’Oisans shear zone (17 ellipsoids) and above the Huez shear zone (12 ellipsoids) (Fig. 4). The ellipsoids were also reconstructed in the Mizoën basin, along a transect above the Mizoën shear zone (12 ellipsoids) (Fig. 4). Each ellipsoid was computed and then projected as an apparent (XZ) ellipse on the cross-section plane (Fig. 4).

In the cover fold above the Bourg d’Oisans shear zone, the (XZ) ellipse distribution shows few variations. The  $R_{XZ}$  ratios are mainly between 3 and 4, with two exceptions: two  $R_{XZ}$  ratios of 1.5 on the eastern side of the fold (Fig. 4). This variation does not indicate a local strain decrease but are due to a local change of lineation orientation (Fig. 7, on the western side of “La Paute” village). Above the Huez shear zone, the (XZ) ellipse shape seems to be more variable, although constant in orientation. This variability could be related to second-order folding (Fig. 4).

In the Mizoën basin, we observe a change in the (XZ) ellipse dip across the Alp décollement, which is consistent with the change in cleavage dip: above the décollement, the ellipses are East-dipping like S2, whereas below the décollement, the ellipses are West-dipping like S1. The apparent increase in the (XZ) ellipse elongation from the Alp décollement ( $X/Z = 1$ ) to the basement ( $X/Z = 3.5$ )

is due to the projection of the ellipsoids on the cross-section, because the lineation trend is N–S close to the décollement and progressively turns to E–W below it (Fig. 8).

## 5. Discussion

### 5.1. (Micro)-structural evolution

In the Bourg d’Oisans basin, an S1 cleavage developed during a transient event of top-to-the-East shearing only close to the basement–cover interface. This cleavage is overprinted by the main (S2) cleavage that affected the whole cover. In the Mizoën basin, the presence of the Alp décollement apparently spatially segregated the two cleavages: the S1 cleavage is mainly located below the décollement while the S2 one is restricted to the upper unit. This suggests that the lower unit has been less affected by the shortening and shearing phase that formed the S2 cleavage. Conversely, above the décollement, the S1 cleavage is absent because the layers were too far from the basement–cover interface to be affected by the local top-to-the-East early shearing.

Both cleavages can thus be explained by a continuum of deformation during E–W shortening that corresponds to the D3 phase in Dumont et al. (2008, 2011). Their spatial variability is strongly linked to the larger-scale deformation and, in particular, to the structural style.

### 5.2. Robustness of restorations

In order to check the robustness of the Bourg d’Oisans basin restoration, we computed the initial bottom and top length for two cells using the (XZ) finite strain ellipses. A similar approach was followed by Yakovlev (2012). Here, we reduce of  $x$  times cells bottom and top lengths of the Bourg d’Oisans cross-section, where  $x$  is the absolute extension value (X axis on strain ellipsoids) previously computed (see Fig. 13A for the location and Fig. 13B for comparison). Then, we compare those “inverted” lengths to the bottom and the top lengths of the restored cells (see Fig. 13A for the construction and the location of cells and Fig. 13B for comparison).

The computed (XZ) ellipses have similar ranges of shape (extension from 1.5 to 2.5 along X and about 0.45 along Z) (Fig. 4A). These ellipses result from the interpretation of various objects widespread within several samples for each outcrop, and thus are confidently representative of internal strain at the outcrop scale.

The comparison of bottom and top lengths of our restored cells with the lengths restored with the (X,Z) ellipses inversion (Fig. 13B) shows a good fit, except for the top of the cell 1. It suggests that the balancing of the Bourg d’Oisans cross-section is correct because the two methods of cell restoration are in agreement. Furthermore, it shows that one may reliably restore any major fold of a basin cover without using the basement–cover interface, but only by considering the cover layer surfaces and their internal finite strain.

In the western part of the La Paute fold however, the cell 1 (Fig. 13B) is geometrically balanced (the area conservation requirement is fulfilled) but the top cell length deduced from the strain ellipsoid data does not fit exactly the one given by the restoration. One solution to solve the problem would be to deepen the Col d’Ornon syncline and so the pinching of the Bourg d’Oisans basin or to move up the top of the La Paute anticline. But it would imply to strongly increase the size of the La Paute anticline limb (yellow, in the web version cells on Fig. 13) and move up its hinge. This also implies to strongly thin the limb, as the cell areas are constant. However, the limb widths are constrained by field data and geological maps. Thus, the misfit between restoration approaches cannot be easily solved. More strain ellipsoids are probably needed to precisely address this discrepancy.

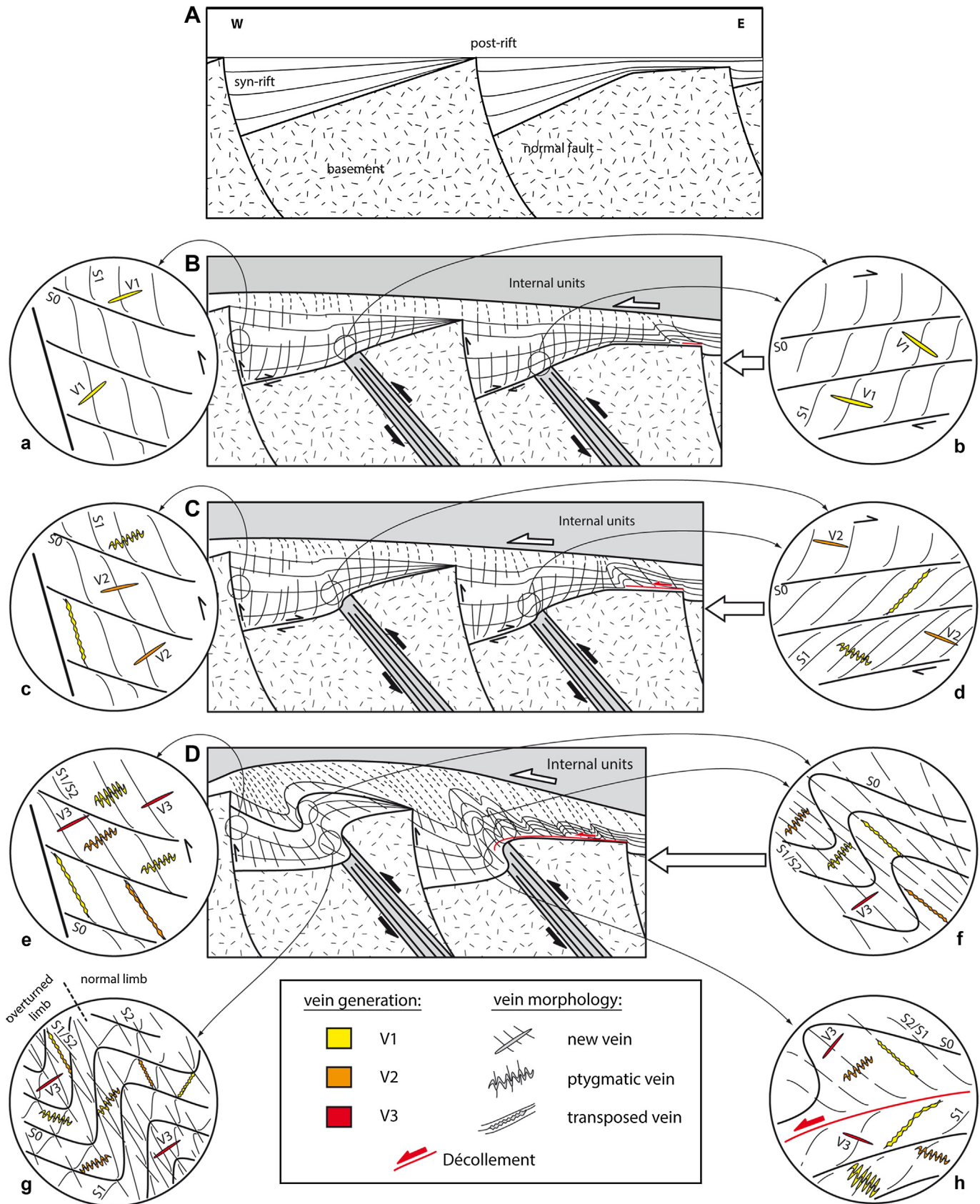


**Fig. 11.** Kinematic scenario of cleavage and vein development in the cover. A) Inherited Mesozoic setting. The basins were West-dipping and controlled by East-dipping normal faults. B) First stage of shortening. The cover and the basement began to be folded and a sub vertical cleavage (S1) and V1 veins formed: (a) near the inherited normal fault and (b) at the bottom of the basin (above the Triassic layer). C) End of the first shortening stage: (c, d) as the cover was deformed, veins were continuously formed. The veins with a small initial angle between the vein and the cleavage were progressively transposed into S1 while other ones, with a high initial angle with the cleavage, became ptygmatic. At the end of

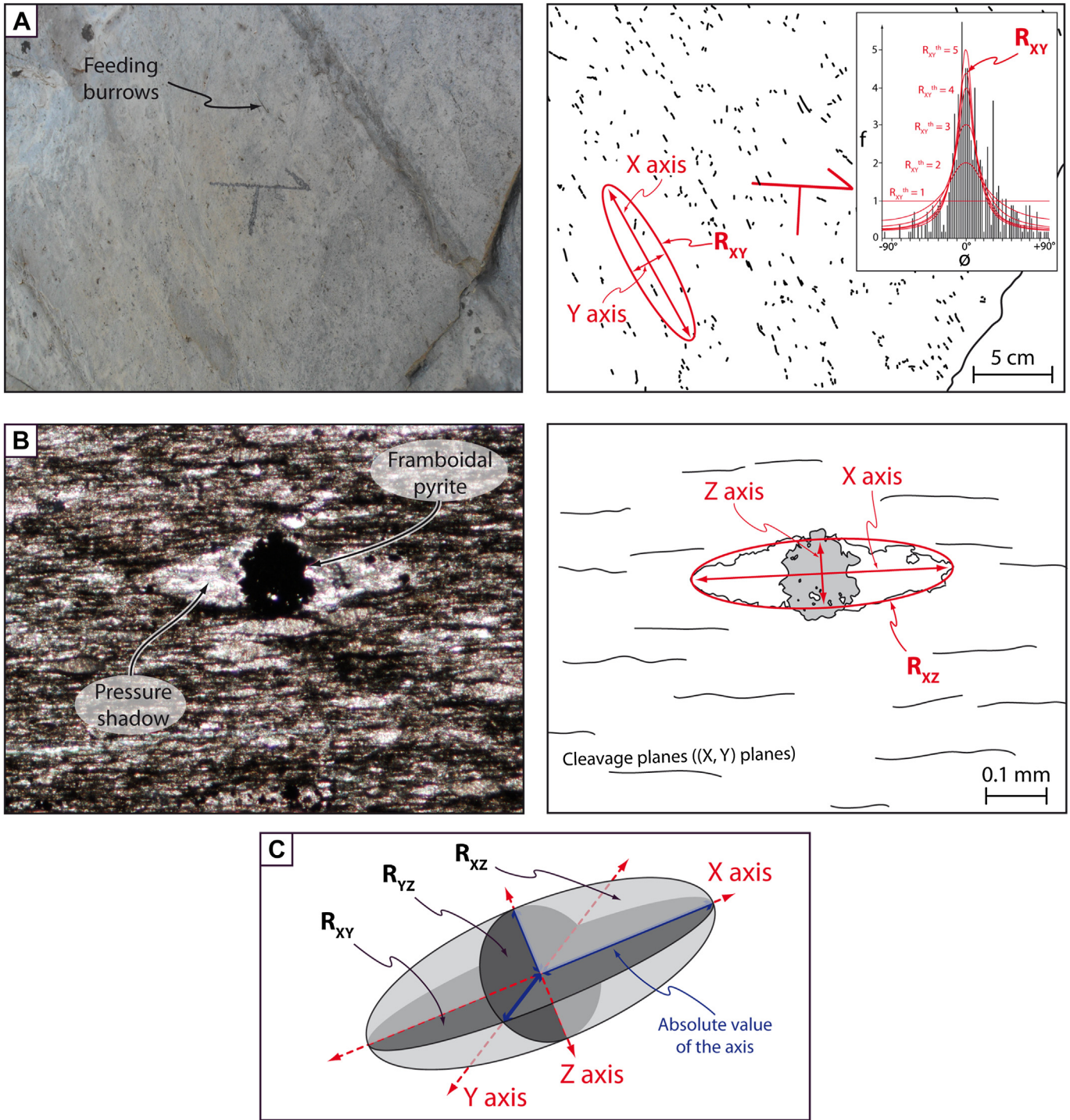


**Fig. 12.** Methodology of finite strain ellipsoid construction. (A)  $R_{XY}$  determination with passive reorientation of feeding burrows around the X axis. The angle distribution is compared to a theoretical  $R_{XY}^{th}$  plot on the graph (Ramsay and Huber, 1989). On the displayed example, 528 feeding burrows were measured and  $R_{XY} = 4.5$ . (B)  $R_{XZ}$  determination with direct estimation from frambooidal pressure shadow shape (Etchecopar and Malavieille, 1987; Ramsay and Huber, 1989). Here  $R_{XZ} = 3.8$ .

the East-verging shearing phase, V2 veins were formed, not deformed by S1 but only by S2. D) A second phase of shortening, still contemporaneous with basement shearing, strongly deformed the cover. Various configurations can be found depending on the structural location in the basin. Close to the normal faults (e) and in the basin center (f), cleavage (S1/S2) kept forming during shearing or folding (S1 and S2 cannot be distinguished). V2 veins are still forming and deformed (V1 and V2 cannot be distinguished). (g) Close to the bottom of the basins, west-verging shearing and associated S2 cleavage overprinted East-verging shearing and associated S1 cleavage. S2 was parallel to the axial surface of the folds whereas S1 was deformed. In overturned limbs, S1 and S2 were sub-parallel and cannot be distinguished. In normal limbs, S1 and S2 show a high angle and allow the distinction between V1 and V2. (h) Where the cover was detached from the basement, there was no overprinting of the cleavage and S2 was developed only above the décollement. V1 and V2, as well as V2 and V3, cannot be distinguished above and under the décollement, respectively. V3 were formed at the end of west-verging shearing phase and were not deformed by S2.

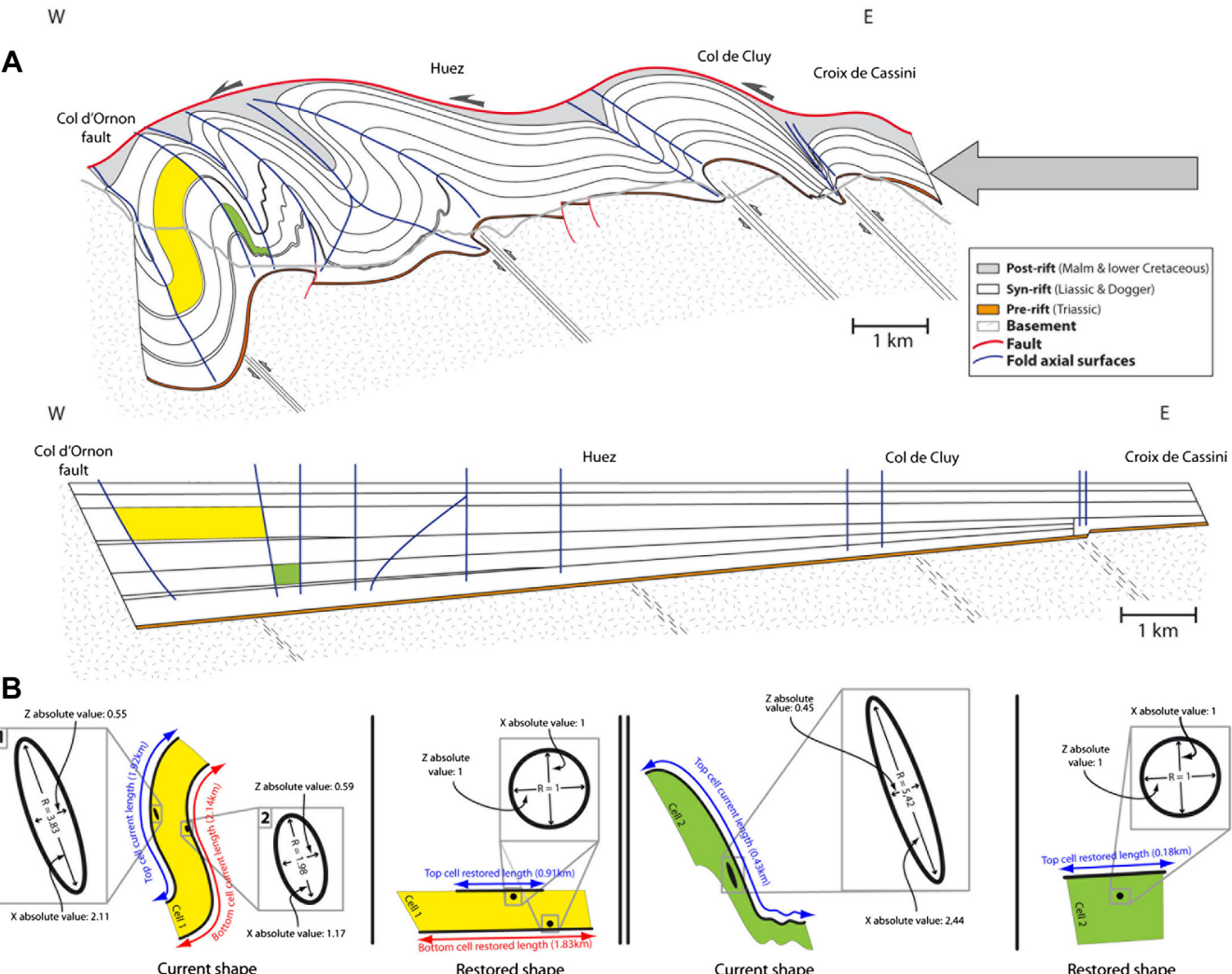


**Fig. 13.** Restoration of two cells from the Bourg d'Oisans cross-section. The cells are limited by stratigraphic boundaries and fold hinges, in the western part (cell 1) and in the eastern part (cell 2). The presented ellipses are representative of 9 ellipses for cell 1 and 8 ellipses for cell 2. The restorations are performed with constant area hypothesis (yellow and green cells) and with the (XZ) finite strain ellipses inversion method (blue double arrows). [For interpretation of color referred in this figure legend, the reader is referred to web version of the article.]

### 5.3. Structural evolution and amount of shortening in the Oisans massif

The fold wavelength in the Mizoën basin ( $\sim 1$  km) is shorter than in the Bourg d'Oisans ( $\sim 2$  km) (Fig. 3). This is likely due to the décollement in the Mizoën basin (Alp décollement; Fig. 3). The different structural styles (décollement in the Mizoën basin vs no significant décollement in the Bourg d'Oisans basin) may be linked to the amount of basement shortening in the Mizoën basin (2.7 km) which is lower than in the Bourg d'Oisans basin (4.3 km). The weakening effect of the thick syn-rift series (up to 3 km) in the Bourg d'Oisans basin may have promoted basement shortening, hence precluding significant cover décollement, whereas the wide weakly thinned crustal domain of the Emparis Plateau was less shortened and therefore likely more prone to deform in a thin-skinned style with décollement of the thin cover (Bellahsen et al., 2012). Note that this difference in amount of basement shortening and structural style, which is controlled by the geometry and subsidence of pre-orogenic extensional basins, controls the microstructural evolution and the spatial segregation of cleavages, the S2 cleavage in the cover of the Mizoën basin being restricted to

the detached part of the cover while the lower unit below the décollement only shows evidence of S1 cleavage.

### 5.4. Shortening in the External Crystalline Massifs

In Liassic times, the European crust was stretched and structured in tilted blocks. In Tertiary times, this crust was subsequently deformed in two steps. First, the distal parts were subducted and formed the so-called internal units. Later, the proximal parts were buried under the internal units and formed the external zone (Fig. 14A and B). Along the strike of the Alpine ECM, the burial conditions of the proximal part increased from South (2–3 kbar, 300 °C in the Oisans, Crouzet et al., 2001; Simon-Labréte et al., 2009) to North (5 kbar, 450 °C in the Mont Blanc, Rolland et al., 2008). The cover of the northern massifs (e.g., Mont Blanc) is highly deformed and slightly detached and translated from its basement (Morcles nappe, Figs. 1 and 14). As a consequence, its restoration is still debated even though most authors, except Leloup et al. (2005), suggest that the Morcles nappe corresponds to the former Mont Blanc cover (e.g. Escher et al., 1993; Burkhard and Sommaruga, 1998). There is also a debate in the literature concerning the

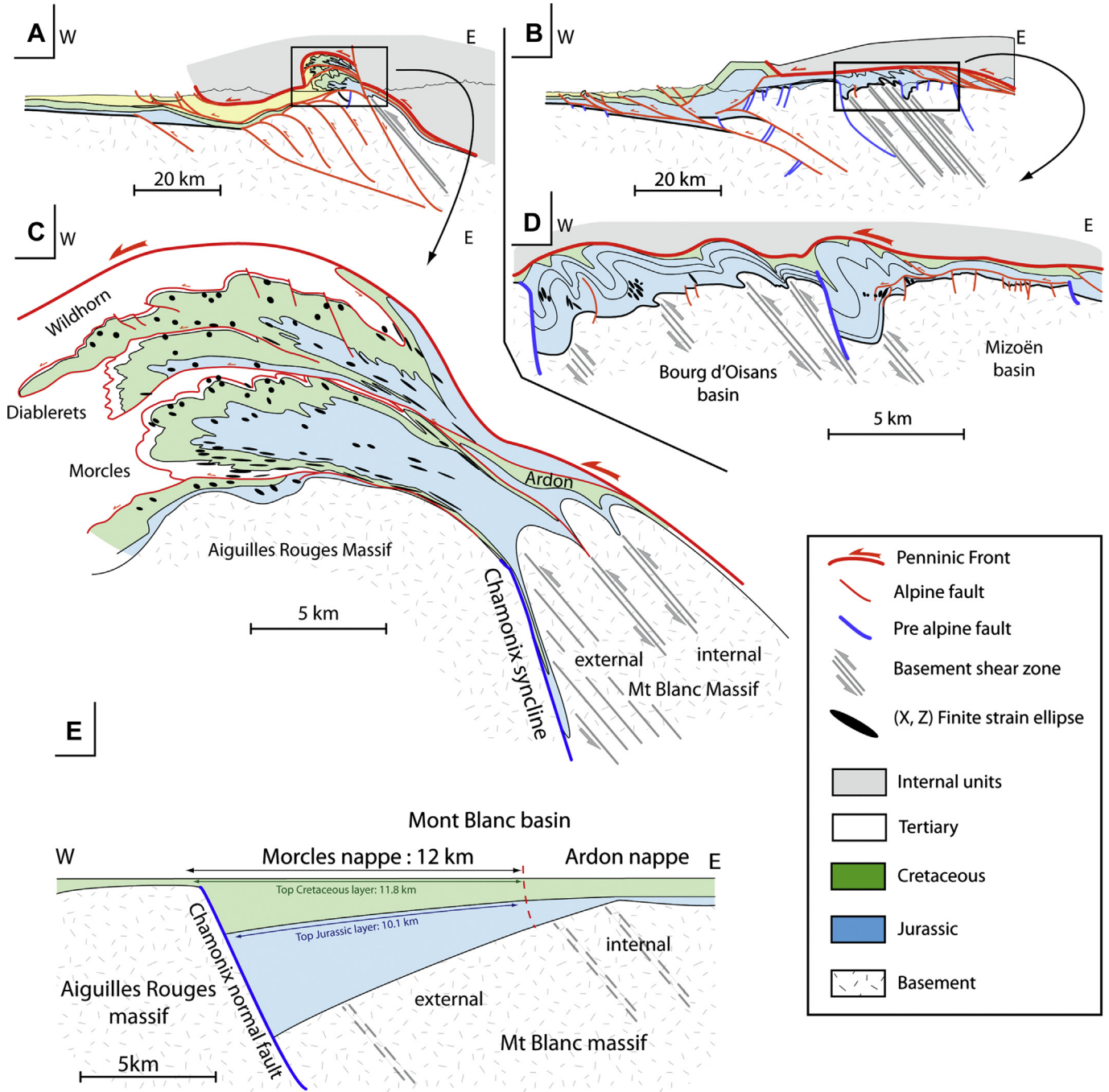


**Fig. 14.** Cross-sections of the external zone and ECM. A) External zone in the Mont Blanc area, modified after Burkhard and Sommaruga (1998). B) External zone at the North Oisans latitude, modified after Bellahsen et al. (2012). C) Cross-section of the ECM and (XZ) finite strain ellipses at the Mt Blanc latitude, modified after Ramsay et al. (1983) and Escher et al. (1993). D) Cross-section of the ECM and (XZ) finite strain ellipses at the North Oisans latitude (this study). (E) Restoration of the Morcles nappe based on cover area conservation hypothesis and (XZ) finite strain ellipse inversion.

Ardon nappe, located East of Morcles nappe : still attached to the internal Mont Blanc massif (Escher et al., 1993) or detached and carried on the Mont Blanc massif (Burkhard and Sommaruga, 1998). In the following, the Morcles and the Ardon nappes are compared to the deformed metasedimentary cover of the Oisans massifs.

We here assume that the Morcles and the Ardon nappes (Fig. 14C), now located above the Aiguilles Rouges massif, represent the former sedimentary cover of the external and internal Mont Blanc basement, respectively (Escher et al., 1993). The Morcles nappe is a recumbent fold, consisting primarily of Jurassic and Cretaceous limestones. At its base, the shear zone roots in the Mont Blanc massif

(Pfiffner, 1981; Ramsay, 1981; Escher et al., 1993). The Morcles nappe was the cover of a tilted block in which sedimentation was probably controlled by the Chamonix normal fault, although the latter does not clearly crop out in the Chamonix syncline (Burkhard and Sommaruga, 1998). The basement of the Mont Blanc massif is strongly sheared (Mont Blanc shear zone, Leloup et al., 2005; Rolland et al., 2008). This resembles our Oisans cross-section where the basement of inherited Jurassic basins is strongly sheared (Fig. 14D). The Morcles nappe and the Mont Blanc basement may thus be considered as analog to the basement-cover system observed in the Oisans massif, where the cover is disharmonically folded above

basement shear zones. However, in the Mont Blanc, both the shortening and the P–T conditions were significantly higher (Poty et al., 1974; Hoschek, 1980; Rolland et al., 2008), which makes the structural interpretation more complicated than in the Oisans even though the structural style is basically the same.

The cross-section in the northeastern Mont Blanc massif was balanced by Burkhard and Sommaruga (1998; Fig. 14A) with constant length for the Triassic layers and constant area for the overlying Mesozoic metasedimentary formations. Here, we tentatively restore the Morcles nappe using only the internal strain field characterized by the available strain ellipses (Ramsay, 1981; Ramsay and Huber, 1989): in other words, the basement–cover interface geometry and length were not taken into account. The goal is to test if such restorations can be performed for a ductilely deformed unit and with no or few constraints on the basement–cover interface geometry. We used the (XZ) ellipse data (Ramsay and Hubert, 1989) on a section (Fig. 14C) modified after Escher et al. (1993) to determine the restored length of the top of two specific layers, namely the Cretaceous and the Jurassic. The section was modified as follows: the Chamonix normal fault has been added with an initial dip of 65°. The Chamonix syncline has thus been drawn very pinched. We assume that the normal fault was not reactivated. The restoration was performed with constant area for the cover layers.

This new restoration of the Morcles nappe was performed in two successive steps. First, we inverted the (XZ) ellipse data of Ramsay and Huber (1989) to obtain the initial length of the top of Cretaceous and Jurassic layers. The ellipses are not perfectly homogeneously distributed within the nappe. Thus, we cannot assess the variability of layer internal strain for each fold (Ramsay and Huber, 1989). A second problem is that (XZ) ellipses are available neither for the Chamonix syncline nor for the eastern normal limb of the Morcles nappe (Fig. 14C). For those two places, we chose to extend the value of the easternmost ellipses towards the East. Because these ellipses are extremely long (the X/Z ratio is about 20 in the inverted limb and about 10 in the normal limb), the corresponding restored lengths are very short.

The second step of the restoration is the area conservation for the nappe layers along the cross-section plane. Because the top of the Cretaceous and the top of the Jurassic lengths (11.8 and 10.1 km, respectively) are fixed by the previous step, the area constrains the inherited normal fault displacement and so the depth of the half-graben, which is here about 6 km (Fig. 14).

Finally, from the restored geometry of the Morcles nappe fixed by the previous steps, we restored the Ardon nappe on the eastern part of the half graben. The restoration was done with constant area hypothesis for the Jurassic and Cretaceous layers and the thickness was constrained by the thickness of the restored Morcles nappe along its eastern boundary (Fig. 14E).

The restored length of the Morcles nappe is about 12 km, which represents the western part of a half-graben, the Mont Blanc basin. This basin includes the restored Ardon nappe; the total basin length is then about 15 km and the depth about 6 km (Fig. 14E). This result is quite different from the restoration by Burkhard and Sommaruga (1998), as these authors proposed a basin about 24 km long and 2 km deep. Even though the two restorations are both based on area conservation, our restoration reveals a pre-orogenic graben structure which is narrower but twice deeper than that in Burkhard and Sommaruga (1998). These authors preserved the Triassic length in order to restore the basement top: however, this layer has probably been strongly stretched above the numerous basement shear bands of the Mont Blanc shear zone (Leloup et al., 2005; Rolland et al., 2008). This may explain the difference between the two restorations. The Mont Blanc basin size that we obtain implies a very strong increase (of 43% or 6 km) of the length of the basement–cover interface during the inversion of the European margin. Moreover,

this increase is more important for the internal part (101% or 4.2 km) than for the external one (18% or 1.8 km). This is consistent with the overturned attitude of the Triassic layers below the Mont Blanc shear zone and their scarce outcrops due to their strong thinning (Mennessier et al., 1977; Antoine et al., 1978; Ayrton et al., 1987).

## 6. Conclusion

In this contribution, we present balanced cross-sections of the External Crystalline Massifs based on a new approach. Indeed, we show that microstructural studies and quantification of the strain ellipsoid in the cover can help restore areas where strong length changes affected the sedimentary layers. We show that contrasting amounts of shortening affected the different inverted pre-orogenic basins with (micro)structural consequences in terms of cleavage development. In places where the basement was strongly shortened, there is no significant décollement of the cover, whereas such a décollement initiated in places where the amount of basement shortening was lower, and led to a spatial segregation of cleavages within the cover. Such various amounts of collisional basement shortening are probably due to different pre-orogenic extensional geometries/crustal structures: in domains of thick and large syn-rift basins, the crust is weak and a high amount of shortening is recorded; in contrast, in domains with thin syn-rift basins, less crustal shortening is accommodated.

## Acknowledgments

The authors would like to thanks Y. Rolland, C. Rosenberg, L. Jolivet and M. Bellanger for discussions and X. and M.O. Gonord for their warm welcome during field trips. Reviews by J.L. Epard and F. Roure greatly improved the original version of the manuscript. This study was funded by the "Syster" INSU program, the BRGM contract L10 U 044, and ISTeP (UPMC) funds.

## References

- Affolter, T., Faure, J.L., Gratier, J.P., Colletta, B., 2008. Kinematic models of deformation at the front of the Alps: new data from map-view restoration. *Swiss J. Geosci.* 101 (2), 289–303.
- Antoine, P., Féraud, J., Poulain, P.-A., 1978. Carte géologique de la France (1/50.000), feuille du Mont Blanc (704). Bureau de Recherche géologique et minière, Orléans.
- Ayrton, S., Barféty, J.-C., Bellière, J., Gubier, Y., Jemelin, L., 1987. Carte géologique de la France (1/50.000), feuille de Chamonix (680). Bureau de Recherche géologique et minière, Orléans.
- Barbier, R., Barféty, J.C., Bocquet, A., Bordet, P., Le Fort, P., Meloux, J., Mouterde, R., Pöcher, A., Petitville, M., 1973. Carte géologique de la France (1/50.000), feuille de La Grave (798). Bureau de Recherches géologiques et minières, Orléans.
- Barféty, J.C., Bordet, P., Carme, F., Debemas, J., Meloux, M., Montjuvent, G., Mouterde, R., Sarrot-Reynaud, J., 1972. Carte géologique de la France (1/50.000), feuille de Vizille (797). Bureau de Recherches géologiques et minières, Orléans.
- Barféty, J.C., Gidon, M., Lemoine, M., Mouterde, R., 1979. Tectonique synsédimentaire liasique dans les massifs cristallins de la zone externe des Alpes occidentales françaises: la faille du col d'Ornon. *C.R. Acad. Sci. Paris* 289, 1207–1210.
- Beach, A., 1982. Strain analysis in a cover thrust zone, external French Alps. *Tectonophysics* 88 (3), 333–346. [http://dx.doi.org/10.1016/0040-1951\(82\)90245-1](http://dx.doi.org/10.1016/0040-1951(82)90245-1).
- Bellahsen, N., Jolivet, L., Lacombe, O., Bellanger, M., Boutoux, A., Garcia, S., Mouthereau, F., LePourhiet, L., Gumiaux, C., 2012. Mechanisms of margin inversion in the external Western Alps: implications for crustal rheology. *Tectonophysics* 560, 62–83. <http://dx.doi.org/10.1016/j.tecto.2012.06.022>.
- Buitner, S.J., Pfiffner, O.A., 2003. Numerical models of the inversion of half-graben basins. *Tectonics* 22 (5), 1057. <http://dx.doi.org/10.1306/06301009165>.
- Burkhard, M., Sommaruga, A., 1998. Evolution of the Western Swiss Molasse basin: structural relations with the Alps and the Jura belt. In: Masclé, A., Puigdefabregas, C., Luterbacher, H.P., Fernanzez, M. (Eds.), *Cenozoic Foreland Basins of Western Europe*, Geological Society, London Special Publication, vol. 134, pp. 279–298. <http://dx.doi.org/10.1144/GSL.SP.1998.134.01.13>.
- Butler, R.W.H., 1986. Thrust tectonics, deep structure and crustal subduction in the Alps and Himalayas. *J. Geol. Soc.* 143 (6), 857–873. <http://dx.doi.org/10.1144/gsjgs.143.6.0857>.
- Butler, R.W.H., 1989. The influence of pre-existing basin structure on thrust system evolution in the Western Alps. *Geol. Soc. Lond. Spec. Publ.* 44 (1), 105–122. <http://dx.doi.org/10.1144/GSL.SP.1989.044.01.07>.

- Butler, R.W., 2013. Area balancing as a test of models for the deep structure of mountain belts, with specific reference to the Alps. *J. Struct. Geol.* 52 (13), 2–16. <http://dx.doi.org/10.1016/j.jsg.2013.03.009>.
- Butler, R.W., Tavarnelli, E., Grasso, M., 2006. Structural inheritance in mountain belts: an Alpine–Apennine perspective. *J. Struct. Geol.* 28 (11), 1893–1908. <http://dx.doi.org/10.1016/j.jsg.2006.09.006>.
- Ceriani, S., Fügenschuh, B., Schmid, S.M., 2001. Multi-stage thrusting at the “Penninic Front” in the Western Alps between Mont Blanc and Pelvoux massifs. *Int. J. Earth Sci.* 90 (3), 685–702. <http://dx.doi.org/10.1007/s005310000188>.
- Chamberlin, R.T., 1910. The Appalachian folds of central Pennsylvania. *J. Geol.* 18 (3), 228–251.
- Chopin, C., 1987. Very-high-pressure metamorphism in the Western Alps: implications for subduction of continental crust [and Discussion]. *Philos. Trans. R. Soc. Lond. Ser. A Math. Phys. Eng. Sci.* 321 (1557), 183–197. <http://dx.doi.org/10.1088/rsta.1987.0010>.
- Crouzet, C., Ménard, G., Rochette, P., 2001. Cooling history of the Dauphinoise Zone (Western Alps, France) deduced from the thermopaleomagnetic record: geo-dynamic implications. *Tectonophysics* 340 (1), 79–93. [http://dx.doi.org/10.1016/S0040-1951\(01\)00142-1](http://dx.doi.org/10.1016/S0040-1951(01)00142-1).
- Dahlstrom, C.D.A., 1969. Balanced cross-sections. *Can. J. Earth Sci.* 6 (4), 743–757.
- De Graciansky, P.C., Dardeau, G., Lemoine, M., Tricart, P., 1989. The inverted margin of the French Alps and foreland basin inversion. *Geol. Soc. Lond. Spec. Publ.* 44 (1), 87–104. <http://dx.doi.org/10.1144/GSL.SP.1989.044.01.06>.
- Deville, É., Chauvière, A., 2000. Thrust tectonics at the front of the Western Alps: constraints provided by the processing of seismic reflection data along the Chambéry transect. *C.R. Acad. Sci. Sér. II* 331 (11), 725–732. [http://dx.doi.org/10.1016/S1251-8050\(00\)01463-4](http://dx.doi.org/10.1016/S1251-8050(00)01463-4).
- Deville, É., Sassi, W., 2006. Contrasting thermal evolution of thrust systems: an analytical and modeling approach in the front of the western Alps. *AAPG Bull.* 90 (6), 887–907. <http://dx.doi.org/10.1306/01090605046>.
- Dumont, T., Champagnac, J.D., Crouzet, C., Rochat, P., 2008. Multistage shortening in the Dauphine zone (French Alps): the record of Alpine collision and implications for pre-Alpine restoration. *Swiss J. Geosci.* 101 (1), 89–110. [http://dx.doi.org/10.1007/978-3-7643-9950-4\\_6](http://dx.doi.org/10.1007/978-3-7643-9950-4_6).
- Dumont, T., Simon-Labréte, T., Authemayou, C., Heymes, T., 2011. Lateral termination of the North-directed Alpine orogeny and onset of Westward escape in the Western Alpine arc: structural and sedimentary evidence from the external zone. *Tectonics* 30 (5). <http://dx.doi.org/10.1029/2010TC002836>.
- Epard, J.L., Groshong Jr., R.H., 1993. Excess area and depth to detachment. *AAPG Bull.* 77 (8), 1291–1302.
- Escher, A., Masson, H., Steck, A., 1993. Nappe geometry in the western Swiss Alps. *J. Struct. Geol.* 15 (3), 501–509. [http://dx.doi.org/10.1016/0191-8141\(93\)90144-Y](http://dx.doi.org/10.1016/0191-8141(93)90144-Y).
- Etchecopar, A., Malavieille, J., 1987. Computer models of pressure shadows: a method for strain measurement and shear-sense determination. *J. Struct. Geol.* 9 (5), 667–677. [http://dx.doi.org/10.1016/0191-8141\(87\)90151-9](http://dx.doi.org/10.1016/0191-8141(87)90151-9).
- Ford, M., 1996. Kinematics and geometry of early Alpine, basement-involved folds, SW Pelvoux Massif, SE France. *Eclogae Geol. Helv.* 89 (1), 269–296.
- Gratier, J.P., Vialon, P., 1980. Deformation pattern in a heterogeneous material: folded and cleaved sedimentary cover immediately overlying a crystalline basement (Oisans, French Alps). *Tectonophysics* 65 (1), 151–179. [http://dx.doi.org/10.1016/0040-1951\(80\)90228-0](http://dx.doi.org/10.1016/0040-1951(80)90228-0).
- Gratier, J.P., Lejeune, B., Vergne, J.L., 1973. Etude des déformations de la couverture et des bordures sédimentaires des massifs cristallins externes de Belledonne, des Grandes Rousses et du Pelvoux. Thesis 3e cycle Univ., Grenoble.
- Groshong Jr., R.H., Epard, J.L., 1994. The role of strain in area-constant detachment folding. *J. Struct. Geol.* 16 (5), 613–618. [http://dx.doi.org/10.1016/0191-8141\(94\)90113-9](http://dx.doi.org/10.1016/0191-8141(94)90113-9).
- Guellec, S., Lajat, D., Mascle, A., Roure, F., Tardy, M., 1990. Deep seismic profiling and petroleum potential in the western alps: constraints with ECORS data, balanced cross-sections and hydrocarbon modeling. *The Potential of Deep Seismic Profiling for Hydrocarbon Exploration*. Edition Technip, Paris, pp. 425–437.
- Henry, C., Burkhard, M., Goffe, B., 1996. Evolution of synmetamorphic veins and their wallrocks through a Western Alps transect: no evidence for large-scale fluid flow. Stable isotope, major-and trace-element systematics. *Chem. Geol.* 127 (1), 81–109. [http://dx.doi.org/10.1016/0009-2541\(95\)00106-9](http://dx.doi.org/10.1016/0009-2541(95)00106-9).
- Hoschek, G., 1980. Phase relations of a simplified marly rock system with application to the Western Hohe Tauern (Austria). *Contribut. Minera. Petrol.* 73 (1), 53–68. <http://dx.doi.org/10.1007/BF00376260>.
- Lacombe, O., Mouthereau, F., 2002. Basement-involved shortening and deep detachment tectonics in forelands of orogens: Insights from recent collision belts (Taiwan, Western Alps, Pyrenees). *Tectonics* 21 (4), 1030. <http://dx.doi.org/10.1029/2001TC901018>.
- Leloup, P.H., Arnaud, N., Sobel, E.R., Lacassin, R., 2005. Alpine thermal and structural evolution of the highest external crystalline massif: the Mont Blanc. *Tectonics* 24 (4). <http://dx.doi.org/10.1029/2004TC001676>.
- Lemoine, M., Tricart, P., 1986. Les Schistes Lustrés piémontais des Alpes Occidentales: Approche stratigraphique, structurale et sédimentologique. *Eclogae Geol. Helv.* 79 (2), 271–294.
- Lemoine, M., Gidon, M., Barféty, J.C., 1981. Les massifs cristallins externes des Alpes occidentales: d'anciens blocs basculés nés au Lias lors du rifting téthysien. *C.R. Acad. Sci. Paris* 292, 917–920.
- Lemoine, M., Bas, T., Arnaud-Vanneau, A., Arnaud, H., Dumont, T., Gidon, M., Bourbon, M., De Graciansky, P.-C., Rudkiewicz, J.-L., Megard-Galli, J., Tricart, P., 1986. The continental margin of the Mesozoic Tethys in the Western Alps. *Mar. Petrol. Geol.* 3 (3), 179–199. [http://dx.doi.org/10.1016/0264-8172\(86\)90044-9](http://dx.doi.org/10.1016/0264-8172(86)90044-9).
- Lemoine, M., Dardeau, G., Delpech, P.Y., Dumont, T., De Graciansky, P.C., Graham, R., Jolivet, L., Roberts, D., Tricart, P., 1989. Extension synrift et failles transformantes jurassiques dans les Alpes occidentales. *C.R. Acad. Sci. Sér. II Méc. Phys. Chim. Sci. Univ. Sci. Terre* 309 (17), 1711–1716.
- Letouzey, J., Werner, P., Marty, A., 1990. Fault reactivation and structural inversion. Backarc and intraplate compressive deformations. Example of the Eastern Sunda shelf (Indonesia). *Tectonophysics* 183 (1), 341–362. [http://dx.doi.org/10.1016/0040-1951\(90\)90425-8](http://dx.doi.org/10.1016/0040-1951(90)90425-8).
- Mennessier, G., Carme, F., Bellière, J., Dhelleme, R., Antoine, P., Dabrowski, H., Meloux, J., Bordet, C., 1977. Carte géologique de la France (1/50.000), feuille de Saint-Gervais-les-Bains. Bureau de Recherche géologique et minière, Orléans.
- Moretti, I., Callot, J.P., 2012. Area, length and thickness conservation: Dogma or reality? *J. Struct. Geol.* 41, 64–75. <http://dx.doi.org/10.1016/j.jsg.2012.02.014>.
- Mouthereau, F., Lacombe, O., 2006. Inversion of the Paleogene Chinese continental margin and thick-skinned deformation in the Western Foreland of Taiwan. *J. Struct. Geol.* 28 (11), 1977–1993. <http://dx.doi.org/10.1016/j.jsg.2006.08.007>.
- Mouthereau, F., Watts, A.B., Burov, E., 2003. Structure of orogenic belts controlled by lithosphere age. *Nature Geosci.* 6 (9), 785–789. <http://dx.doi.org/10.1038/ngeo1902>.
- Mugnier, J.L., Guellec, S., Menard, G., Roure, F., Tardy, M., Vialon, P., 1990. A crustal scale balanced cross-section through the external Alps deduced from the ECORS profile. *Mém. Soc. Géol. Fr.* 156, 203–216.
- Oliver, N.H.S., 1996. Review and classification of structural controls on fluid flow during regional metamorphism. *J. Metamorph. Geol.* 14, 477–492. <http://dx.doi.org/10.1046/j.1525-1314.1996.00347.x>.
- Oliver, N.H., Bons, P.D., 2001. Mechanisms of fluid flow and fluid–rock interaction in fossil metamorphic hydrothermal systems inferred from vein–wallrock patterns, geometry and microstructure. *Geofluids* 1 (2), 137–162. <http://dx.doi.org/10.1046/j.1468-8123.2001.00013.x>.
- Panien, M., Schreurs, G., Pfiffner, A., 2005. Sandbox experiments on basin inversion: testing the influence of basin orientation and basin fill. *J. Struct. Geol.* 27 (3), 433–445. <http://dx.doi.org/10.1016/j.jsg.2004.11.001>.
- Pfiffner, O.A., 1981. Fold-and-thrust tectonics in the Helvetic Nappes (E Switzerland). *Geol. Soc. Lond. Spec. Publ.* 9 (1), 319–327. <http://dx.doi.org/10.1144/GSL.SP.1981.009.01.28>.
- Philippe, Y., Deville, E., Mascle, A., 1998. Thin-skinned inversion tectonics at oblique basin margins: example of the Western Vercors and Chartreuse Subalpine massifs (SE France). *Geol. Soc. Lond. Spec. Publ.* 134 (1), 239–262. <http://dx.doi.org/10.1144/GSL.SP.1998.134.01.11>.
- Poty, B.P., Stalder, H.A., Weisbrod, A.M., 1974. Fluid inclusion studies in quartz from fissures of Western and Central Alps. *Schweiz. Mineral. Petrogr. Mitt.* 54, 717–752.
- Ramsay, J.G., 1981. Tectonics of the Helvetic nappes. *Geol. Soc. Lond. Spec. Publ.* 9 (1), 293–309. <http://dx.doi.org/10.1144/GSL.SP.1981.009.01.26>.
- Ramsay, J.G., Huber, M.I., 1989. *The Techniques of Modern Structural Geology*, vol. 2. Folds and Fractures Academic Press, London.
- Ramsay, J.G., Casey, M., Kligfield, R., 1983. Role of shear in development of the helvetic fold-thrust belt of Switzerland. *Geology* 11 (8), 439–442. [http://dx.doi.org/10.1130/0091-7613\(1983\)11<439:ROSIDO>2.0.CO;2](http://dx.doi.org/10.1130/0091-7613(1983)11<439:ROSIDO>2.0.CO;2).
- Rolland, Y., Rossi, M., Cox, S.F., Corsini, M., Mancktelow, N., Pennacchioni, G., Fornari, M., Boullier, A.M., 2008.  $^{40}\text{Ar}/^{39}\text{Ar}$  dating of synkinematic white mica: insights from fluid–rock reaction in low-grade shear zones (Mont Blanc Massif) and constraints on timing of deformation in the NW external Alps. *Geol. Soc. Lond. Spec. Publ.* 299 (1), 293–315. <http://dx.doi.org/10.1144/SP299.18>.
- Roure, F., Colletta, B., 1996. Cenozoic inversion structures in the foreland of the Pyrenees and Alps. *Mém. Mus. Natl. Nat.* 170, 173–209.
- Sanchez, G., Rolland, Y., Schneider, J., Corsini, M., Oliot, E., Goncalves, P., Verati, C., Lardeaux, J.-M., Marquer, D., 2011. Dating low-temperature deformation by  $^{40}\text{Ar}/^{39}\text{Ar}$  on white mica, insights from the Argentera-Mercantour Massif (SW Alps). *Lithos* 125 (1), 521–536. <http://dx.doi.org/10.1016/j.lithos.2011.03.009>.
- Scisciani, V., Tavarnelli, E., Calamita, F., Paltrinieri, W., 2002. Pre-thrusting normal faults within syn-orogenic basins of the outer Central Apennines, Italy: implications for Apennine tectonics. *Bol. Soc. Geol. Ital.* 121 (1), 295–304. [http://dx.doi.org/10.1016/S0191-8141\(01\)00164-X](http://dx.doi.org/10.1016/S0191-8141(01)00164-X).
- Simon-Labréte, T., Rolland, Y., Dumont, T., Heymes, T., Authemayou, C., Corsini, M., Fornari, M., 2009.  $40\text{Ar}/39\text{Ar}$  dating of Penninic Front tectonic displacement (W Alps) during the lower oligocene (31–34 Ma). *Terra Nova* 21 (2), 127–136. <http://dx.doi.org/10.1111/j.1365-3121.2009.00865.x>.
- Tavarnelli, E., 1999. Normal faults in thrust sheets: pre-orogenic extension, post-orogenic extension, or both? *J. Struct. Geol.* 21 (8), 1011–1018. [http://dx.doi.org/10.1016/S0191-8141\(99\)00034-6](http://dx.doi.org/10.1016/S0191-8141(99)00034-6).
- Tricart, P., Lemoine, M., 1986. From faulted blocks to megamullions and megaboudins: Tethyan heritage in the structure of the Western Alps. *Tectonics* 5 (1), 95–118.
- Van Der Beek, P.A., Valla, P.G., Herman, F., Braun, J., Persano, C., Dobson, K.J., Labrin, E., 2010. Inversion of thermochronological age–elevation profiles to extract independent estimates of denudation and relief history—II: application to the French Western Alps. *Earth Planet. Sci. Lett.* 296 (1), 9–22. <http://dx.doi.org/10.1016/j.epsl.2010.04.032>.
- Watts, A.B., Lamb, S.H., Fairhead, J.D., Dewey, J.F., 1995. Lithospheric flexure and bending of the Central Andes. *Earth Planet. Sci. Lett.* 134 (1), 9–21. [http://dx.doi.org/10.1016/0012-821X\(95\)00095-T](http://dx.doi.org/10.1016/0012-821X(95)00095-T).
- Yakovlev, F.L., 2012. Methods for detecting formation mechanisms and determining a final strain value for different scales of folded structures. *C.R. Acad. Geosci.* 344 (3), 125–137. <http://dx.doi.org/10.1016/j.crte.2012.02.005>.

#### **IV.3. Limite à la restauration des bassins de l’Oisans.**

Cette nouvelle méthode montre cependant ses limites, en effet, dans le cas du bassin de Mizoën, une restauration de ce type n'est pas encore envisageable. Si l'interface socle/couverture du bassin affleure très bien, notamment sur le haut de socle d'Emparis, on ne connaît pas précisément l'enracinement du décollement de la couverture. Ainsi, si on peut restaurer la forme générale du bassin, toujours sur les mêmes hypothèses de non réactivation de la faille normale bordière (la faille de Mizoën) et de conservation de la longueur de l'interface socle-couverture, on ne peut restaurer précisément cette couverture en partie décollée. Une solution à ce problème serait de multiplier les données de la déformation finie dans la couverture du bassin, au dessus du décollement de l’Alp.

#### **IV.4. Problème de la conservation du volume au cours de la déformation.**

Pour réaliser cette restauration des couches, on fait l'hypothèse de la conservation de la matière au cours de la déformation. La restauration est contrôlée à l'échelle de l'affleurement par les ellipsoïdes de la déformation finie. Ainsi, l'hypothèse de la conservation de la matière doit rester valable à cette échelle. Pour mieux contraindre les transferts de matière, nous avons étudié les veines métamorphiques des deux bassins à partir de données géochimiques et microthermométriques notamment afin de déterminer les chemins et l'échelle de migration des fluides ainsi que leur interaction avec les roches. Ce travail est présenté dans la partie suivante.

## V. Circulations de fluides pendant de la collision alpine.

### Fluid systems above basement shear zones during inversion of pre-orogenic sedimentary basins (External Crystalline Massifs, Western Alps).

Alexandre Boutoux, Anne Verlaguet, Nicolas Bellahsen, Olivier Lacombe, Benoit Villemant, Benoit Caron, Erwan Martin, Nelly Assayag, Pierre Cartigny.

Article publié dans la revue Lithos

#### V.1. Cadre et intérêt de l'étude.

Au cours de l'étude précédente, on a montré qu'il est possible de restaurer finement la couverture, décollée ou non, et déformée de façon ductile lors de la collision. Cependant, le contrôle des restaurations proposées repose notamment sur l'hypothèse de la conservation du volume des roches au cours de leur déformation. On suppose ainsi que les transferts de matière réalisés dans la couverture lors de son plissement se font à une échelle inférieure à celle de la mesure des ellipsoïdes de la déformation finie (échelle de l'affleurement). Cette hypothèse reste cependant à vérifier dans le cas des bassins de l'Oisans.

Les transferts de matière réalisés via les fluides se font soit, à petite échelle, par diffusion dans un fluide local stagnant, soit, à bien plus grande échelle, par advection de la matière dans des fluides circulant dans la croûte (e.g. [Oliver, 1996; Oliver et Bons, 2001](#)).

Les transports advectifs peuvent permettre des déplacements sur de grandes distance des éléments (e.g. [pluri kilométriques Beaudoin et al., 2011; à l'échelle de la croute, Rolland et al., 2009](#)). Ces transferts à grande échelle sont réalisés par advection doivent être chenalés pour permettre le déplacement de quantités significatives de matière. Or les circulations de fluides sont chenalés dans la croûte au niveau des cisaillements et ce dès leur initiation (e.g. [Rolland et al., 2003 Oliot et al., 2014](#)). Ainsi seules les zones fortement cisaillées, socle ou couverture, des MCE pourraient être le lieu de de transferts de matière importants. Ces transports ont notamment été étudiés au niveau des chevauchements basaux des nappes de couverture charriées au-dessus des MCE (e.g. chevauchement du Glarus, [Bukhard et al., 1992 ; Badertscher et al., 2002, Abart et al., 20 ??; Chevauchement basaux des nappes helvétiques : Kirschner et al., 1999](#)) et au niveau des bandes de cisaillement structurant le socle des MCE (e.g. Mont Blanc : [Rolland et al., 2003, 2008 ; Rossi et al., 2014 Oliot et al.,](#)

2010 ; 2012 ; 2014 ; Aar : Marquer et Burkhard, 1992 ; Rolland et al., 2009 ; Goncalves et al., 2012).

Les transports de matière par diffusion ne permettent le déplacement de la matière qu'à une échelle bien plus restreinte. Ainsi, la pression solution est un processus chimique permettant l'accommodation de la déformation mécanique en présence de fluide. Elle est réalisée lors de la mise sous contrainte différentielle des grains de la roche. Les différences de pression exercée entre les zones protégées et non protégées des grains (i.e. les zones de contacts entre les grains et les autres faces telles les pores de la roche) entraînent alors des variations de potentiels chimiques entre ces zones. Ces différences de potentiels chimiques permettent (1) la dissolution des faces des grains soumis aux contraintes maximales, (2) la diffusion des éléments dissous à travers les pores de la roche, et (3) la précipitation des éléments dissous au niveau des zones (Sorby, 1863; Weyl, 1959; Renard et al., 1997; Croizé et al., 2010). L'accommodation de la déformation est alors limitée par le processus le plus lent des trois précédemment cités. Ainsi, en l'absence de structure tectonique pouvant chenaliser les fluides, les transferts de matière au sein de la roche devraient être dus uniquement à la pression dissolution et à la percolation des fluides produits localement par les réactions de déshydratation réalisée lors de l'enfouissement (e.g., déshydratation des phyllosilicates; Cartwright et Buick, 2000; Marquer et Burkhard, 1992; Oliveret Bons, 2001). Ces types de transferts ont été étudié au niveau des nappes helvétiques. Ainsi, les zones non cisaillées ne semblent pas être sous l'influence de circulation à grande échelle des fluides (e.g. Kirschner et al., 1995). De même, dans la couverture de l'Oisans, peu plissée et non cisaillée ne montre que des circulations à petite échelle et des transferts de matière par pression-solution (Gratier et Vialon, 1980, Henry et al., 1996).

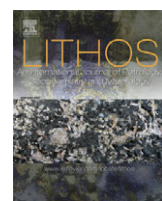
Il a été montré que les systèmes isotopiques fermés, qui caractérisent les circulations de fluides à petite échelle et donc les transport diffusifs, s'ouvrent lors de la propagation des cisaillement de socle dans la couverture. L'ouverture de ces systèmes suggèrent alors l'établissement de circulation de fluides dérivé du socle au sein des cisaillement de la couverture (Marqueur et Burkhard, 1992 ; Kirschner et al., 1999).

Dans les bassins de l'Oisans les bandes de cisaillement qui structurent le socle ne recoupent pas la couverture (e.g. Dumont et al., 2008). De ce fait on peut s'interroger sur l'état et le timing des circulations de fluides juste à l'aplomb de ces cisaillements, au niveau de l'interface entre les zones zones de circulations de fluides à petite et à grande échelle.

D'autre part, les interactions entre fluides et roches peuvent avoir de fortes implications rhéologiques. Ainsi la formation de phyllosilicates localisée du fait de circulations importantes de fluides chenalés dans des cisaillements aura tendant à adoucir les contacts tectoniques (e.g. [Gueydan et al., 2003](#)). L'étude de l'ouverture des systèmes de circulations de fluide et ses liens avec la localisation de la déformation semble ainsi importante pour mieux comprendre l'évolution rhéologique de la croûte lors de sa déformation.

Enfin, la séquence de formation des veines métamorphiques des bassins de l'Oisans montre que celles-ci sont contemporaines du raccourcissement de la couverture. L'étude des conditions P-T de la formation de ces veines pourrait nous permettre de mieux caractériser les conditions P-T de la déformation des bassins de l'Oisans, précises pour ce qui est de la température (330°C, [Bellanger et al., 2015](#)) mais beaucoup moins pour ce qui est de la pression (e.g. 2-5 kbar, [Jullien et Goffé 1993, Bellanger et al., 2015](#)).

## V.2. Article



# Fluid systems above basement shear zones during inversion of pre-orogenic sedimentary basins (External Crystalline Massifs, Western Alps)



Alexandre Boutoux <sup>a,b,\*</sup>, Anne Verlaguet <sup>a,b</sup>, Nicolas Bellahsen <sup>a,b</sup>, Olivier Lacombe <sup>a,b</sup>, Benoit Villemant <sup>a,b</sup>, Benoit Caron <sup>a,b</sup>, Erwan Martin <sup>a,b</sup>, Nelly Assayag <sup>c</sup>, Pierre Cartigny <sup>c</sup>

<sup>a</sup> Sorbonne Universités, UPMC Univ. Paris 06, UMR 7193, IStEP, F-75005 Paris, France

<sup>b</sup> CNRS, UMR 7193, IStEP, F-75005 Paris, France

<sup>c</sup> Equipe de Géochimie des Isotopes Stables de l'Institut de Physique du Globe de Paris, Sorbonne Paris Cité, Université Paris Diderot, UMR 7154 CNRS, F-75005 Paris, France

## ARTICLE INFO

### Article history:

Received 9 February 2014

Accepted 5 July 2014

Available online 21 July 2014

### Keywords:

Western Alps

Shear zone

Trace elements

Stable isotopes

Fluid circulations

Closed system

## ABSTRACT

In the inner part of the External Alps, inherited Liassic basins were buried and inverted during the Oligo-Miocene collisional phase of the Alpine orogeny. In northern Oisans, during crustal shortening, the basement was locally sheared while the cover was disharmonically folded above the main basement shear zones that did not propagate into the cover. In this contribution, we analyze the witnesses of paleo-fluid circulations associated with these crustal deformations, focusing particularly on Bourg d'Oisans and Mizoën basins (external Western Alps). On the basis of structural and microstructural observations coupled to geochemical analyses (cathodoluminescence, O and C stable isotopes, trace elements) of vein versus host-rock minerals, we show that in the cover, fluids mainly circulated over short distances (closed-system). However, trace element data also show that percolation of small amounts of basement-derived fluids occurred over several tens of meters in cover rocks right above basement shear zones. Indeed, the three successive vein sets recognized in the field display enrichments in basement-derived Ni, Co, and Cr, which indicate that fluid transfer from the basement was efficient since the beginning of basin inversion, therefore confirming the synchronous deformation of cover and basement. Fluid temperatures and pressures are estimated (microthermometry coupled to  $\delta^{18}\text{O}$  of vein minerals) to about 250–400 °C and 2–5 kbar for veins that most likely formed at or close to metamorphic peak conditions. These results coupled to literature data are finally integrated into a model of fluid circulation evolution through progressive deformation of the whole external Western Alps.

© 2014 Elsevier B.V. All rights reserved.

## 1. Introduction

In convergent settings (subduction or collision), large amounts of fluids are released in rocks by successive metamorphic dehydration reactions occurring during burial (e.g., Walther and Orville, 1982). The occurrence of fluids in rocks, in particular water, has crucial effects not only on the scale of mass transfer processes and fluid–rock interactions (e.g., John et al., 2012; Penniston-Dorland et al., 2010), but also on the deformation mechanisms and rock rheology (e.g., Bos and Spiers, 2000, 2002; Gueydan et al., 2004; and references therein). Moreover, there is a strong link between mass transfer and deformation mechanisms (Stünitz, 1998). Indeed, the scale of fluid circulation and mass transfer through rocks is mainly controlled by the size and connectivity of the deformation structures, and their evolution through time (Fisher

et al., 1995). The permeability of high-pressure rocks being low and fluid pressure close to lithostatic (Etheridge, 1983), most rocks may behave as almost closed-systems, experiencing only small-scale (mm–dm) diffusive mass transfer through the pervasive fluid produced locally by dehydration reactions (Cartwright and Buick, 2000; Fisher et al., 1995; Garofalo, 2012; Spandler et al., 2011; Verlaguet et al., 2011). In these rocks, fluid flow may be channelized in highly deformed zones (shear zones, faults), which form localized preferential pathways for large-scale (m–km) advective mass transfer; open-system fluid–rock interactions are restricted to mm–m scale halos in the surrounding rocks (Abart et al., 2002; Badertscher et al., 2002; Burkhard et al., 1992; John et al., 2012; Li et al., 2013; McCaig et al., 1995, 2000a,b).

However, it is still unclear how open systems develop in previously closed-system rocks and what are the transitional stages. Yet these stages are keys for understanding the fluid system evolution and constraining the (early) rheological evolution of the continental crust when it is subducted or underthrusted. It is therefore a major issue to characterize the fluid system(s) at that time, i.e., the fluid source, the

\* Corresponding author at: Université Pierre et Marie Curie, IStEP, UMR 7193 UPMC-CNRS, Case 129 T46-0, 2ème étage, 4 place Jussieu, 75252 Paris Cedex 05, France. Tel.: +33 1 44 27 71 81; fax: +33 1 27 50 85.

E-mail address: [Alexandre.boutoux@upmc.fr](mailto:Alexandre.boutoux@upmc.fr) (A. Boutoux).

circulation timescale and pathways, the intensity of fluid–rock interactions along pathways, as well as the evolution of the fluid system with progressive deformation, especially during the early stages.

Such a study has been performed in the External Crystalline Massifs (ECM) of the external Western Alps. During the Alpine collision phase, this proximal part of the European passive margin was buried to mid-crustal depth below the internal Alpine units at Oligo-Miocene times (Bellahsen et al., 2012; Rolland et al., 2008; Simon-Labréteau et al., 2009). The ECM experienced mainly thick-skinned deformation during collision: shortening was accommodated by hundred meter-wide shear zones in the basement, while the overlying sedimentary cover was disharmonically folded (Bellahsen et al., 2012; Bellanger et al., 2014; Boutoux et al., 2014). In the northern ECM, i.e., the Mont-Blanc and Aar-Gothard massifs (Fig. 1), the fluid system in the sedimentary cover nappes remained closed to external fluid infiltration, even in highly cleaved metasediments (e.g., Kirschner et al., 1995, 1999; Marquer and Burkhard, 1992). However, the major cover thrusts or mylonites and associated veins record the infiltration of important amounts of basement-derived fluids (Burkhard and Kerrich, 1988; Kirschner et al., 1995, 1999; Marquer and Burkhard, 1992). Indeed, the major basement shear zones propagated as thrusts into the cover, resulting in local opening of the fluid system: ascendant fluids were then channelized within the thrust zones and flowed through both basement and cover (Marquer and Burkhard, 1992; Rolland et al., 2003). Further North, in the Glarus thrust, a localized fluid flow occurred at the basal contact of the sedimentary nappes, as attested by a clear isotopic front due to northward metamorphic fluid flow (Badertscher et al., 2002).

Was the fluid evolution similar in the southern ECM (i.e., North Oisans), which underwent less burial and shortening? In the north-eastern part of the northern Oisans massif (Fig. 1), the cover is locally detached from its basement, which is consequently not involved in crustal shortening (i.e., local thin-skinned tectonic style; Bellahsen et al., 2012). There, cover rocks behaved as a closed-system during the

whole deformation process; fluid circulations were restricted to the sedimentary unit scale (Henry et al., 1996). On the contrary, the north-western part of the Oisans massif is characterized by thick-skinned deformation (Bellahsen et al., 2012). However, basement shear zones did not propagate into the cover. Each of these structures having accommodated an amount of shortening of only a few hundred meters they are most likely key features on which one can study the early fluid circulations and probably the transition from closed to open fluid system.

The questions we address in this contribution are the following: what is the scale of the fluid system and its evolution with progressive deformation? As the basement shear bands did not propagate into the cover, how is the deep fluid circulation (if any) accommodated at the basement-cover interface? Can the fluid system give information about the relative timing of basement and cover shortening during the margin inversion? In order to answer these questions, we combine the structural and microstructural analysis of basement shear zones and the overlying metasedimentary cover in the northern Oisans massif with geochemical and microthermometric investigation of the successive vein filling material and host-rocks.

## 2. Geological setting

### 2.1. The External Alps

The external zone of the Western Alps arc consists of fold-and-thrust belts (Vercors, Chartreuse, Bauges, Bornes, Aravis, Haut Griffre) and External Crystalline Massifs (ECM, Argentera, Oisans, Grandes Roussettes, Belledonne, Mont Blanc, Aiguilles Rouges, Aar, Gothard; Fig. 1). It corresponds to the proximal part of the European margin, thinned during Liassic to Dogger times, with the formation of tilted blocks (Lemoine et al., 1989) limited by normal faults oriented N–S to NE–SW in the ECM (Figs. 1, 2).

During the collisional phase of the Alpine orogeny, the ECM were buried down to mid-crustal depth below the internal (Penninic) units. The ECM burial was deeper in the North (400 °C, 5 kbar in the Mont Blanc massif; Rolland et al., 2003; Rossi et al., 2005; 450 °C, 6 kbar in the Aar massif; Challandes et al., 2008) than in the South (270–360 °C and 2–5 kbar in the Oisans massif; Bellanger, 2013; Crouzet et al., 2001; Jullien and Goffé, 1993; Poty et al., 1974).

During collision, basement shortening was accommodated by West-verging reverse shear zones (e.g., Bellahsen et al., 2012; Bellanger et al., 2014; Leloup et al., 2005; Rolland et al., 2008) or anastomosed steep shear zones (e.g., Marquer et al., 2006; Rolland et al., 2008; Oliot et al., 2010, 2014). In the northern Oisans area, the cover was mainly disharmonically folded over basement West-verging shear zones, without significant décollement between the basement and its sedimentary cover (Fig. 3). The main difference between the northern and the southern ECM is that, in the North (Mont Blanc, Aar), basement shear zones propagated into the cover, while in the South (Oisans) shear zones were restricted to the basement and did not propagate into the cover. Moreover, basement shear zones and the associated significant crustal shortening are mainly observed in inverted pre-orogenic Liassic basins (Bellahsen et al., 2012). On the contrary, where the crust was not pre-structured by Liassic extensional basins (e.g., La Grave area in the north-eastern Oisans; Figs. 2, 3), there is less field evidence of significant crustal East–West shortening in the basement, and the cover is detached from the basement, i.e., the shortening style is locally thin-skinned. A striking point in all the basins is the absence of any significant reactivation of the inherited normal faults (Bellahsen et al., 2012; Tricart and Lemoine, 1986).

### 2.2. Bourg d'Oisans and Mizoën basins

The Bourg d'Oisans and Mizoën basins are pre-orogenic Liassic–Dogger N–S extensional basins bounded by East-dipping normal faults,

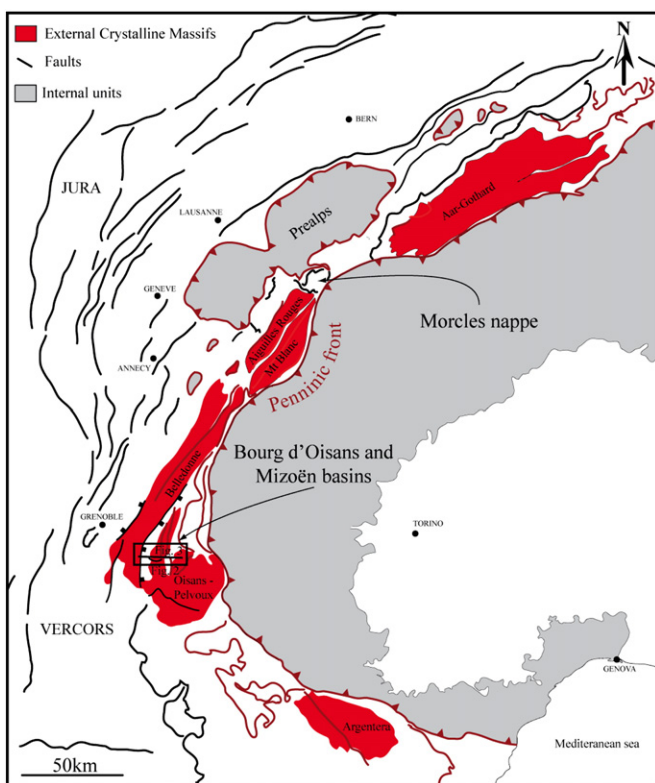


**Fig. 1.** Schematic structural map of the Western Alps showing the location of the studied area.

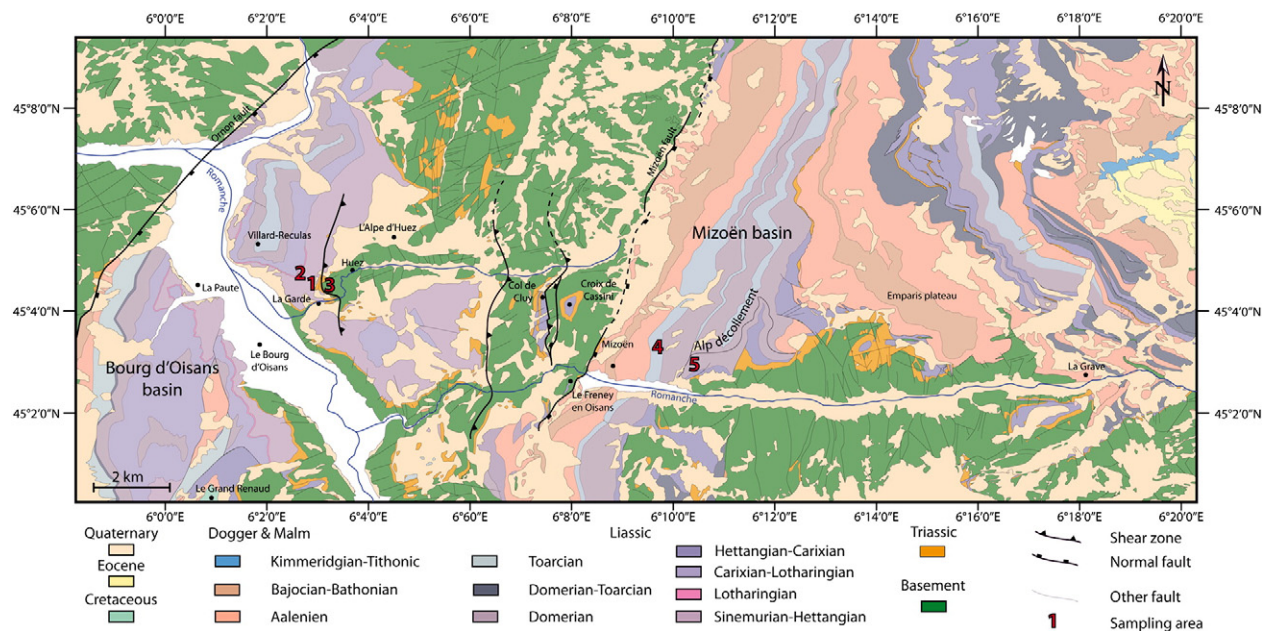


**Fig. 2.** Geological map of Bourg d'Oisans and Mizoën basins and sampling area location (inset Fig. 1). Modified after Barf  t  y et al. (1972) and Barbier et al. (1973).

the Col d'Ornon and the Mizoën faults, respectively (Figs. 2, 3). Their normal offset values were of 3 and 2.5 km, respectively (Lemoine et al., 1981). The base of the sedimentary cover is composed of a thin Triassic layer (few tens of m) of sandstones and dolomites with scarce gypsum lenses (Figs. 2, 3; Barbier et al., 1973; Barfety et al., 1972). The Bourg d'Oisans basin underwent important subsidence during Liassic (Sinemurian) to Dogger (Bajocian) times, which resulted in the deposition of thick marls or marly limestones. The Mizoën basin was also filled with marls and shales but mainly during Domerian to Bajocian subsidence (Figs. 2, 3).

### 2.3. Fluid flow in the ECM

In the northern ECM (Mont Blanc and Aar massifs), most studies so far concluded that Alpine fluids were channelized in the major basement and cover shear zones (Badertscher et al., 2002; Kirschner et al., 1999; Marquer and Burkhard, 1992; Rolland et al., 2003; Rossi et al., 2005). Indeed, at the proximity of large thrusts (i.e., within a few meters), oxygen isotopic values ( $\delta^{18}\text{O}$ ) in shear zones and associated veins are locally much lower than in the surrounding rocks within the cover nappes (e.g., Badertscher et al., 2002; Burkhard and Kerrich,

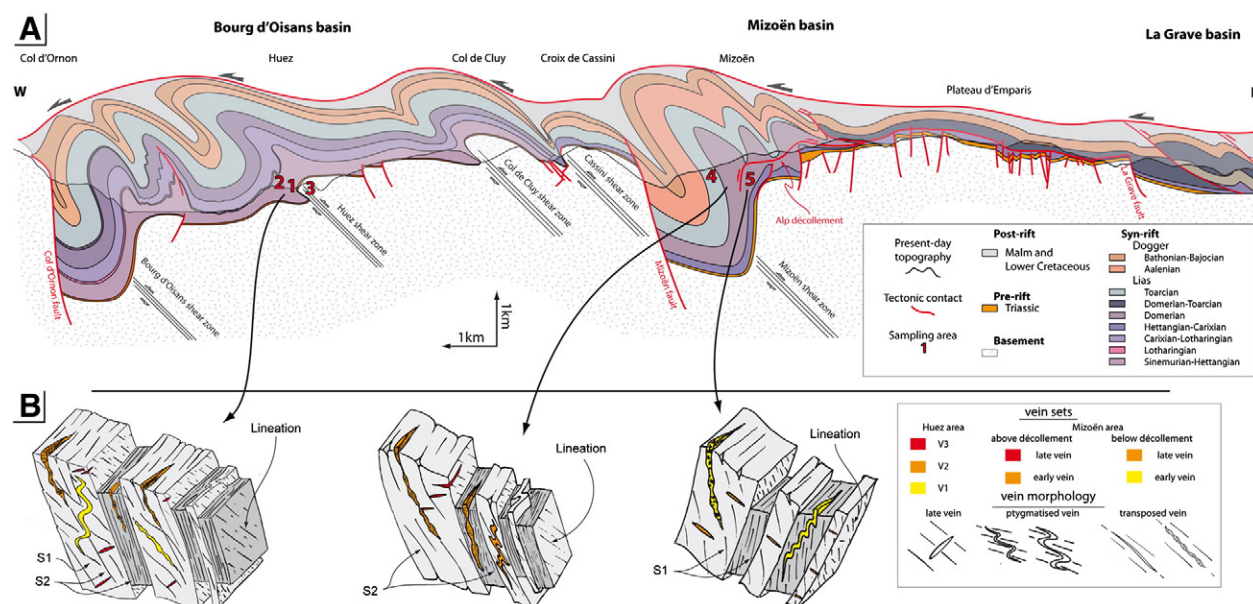


**Fig. 3.** Cross-section of Bourg d'Oisans and Mizoën basins and sketch of metamorphic vein formation. A. Cross-section of Bourg d'Oisans and Mizoën basins showing sample locations, modified after [Boutoux et al. \(2014\)](#). The basement is locally sheared while the overlying cover is disharmonically folded. B. 3D schematic representation of the vein sets relative chronology and their relationships with the cleavages.

1988; Marquer and Burkhard, 1992), which is interpreted as the result of large-scale fluid flow from deeper (basement) parts of the shear zones. However, apart from the basal thrusts of the largest nappes, similar values of oxygen isotopic compositions ( $\delta^{18}\text{O}$ ) were observed in the cover shear zones and the surrounding rocks within the nappes (Kirschner et al., 1999), suggesting that these rocks underwent little to no advection of isotopically distinct fluid.

In the southern ECM and especially in the Oisans area, few geochemical studies have been performed and none of them provided any evidence of large-scale fluid circulation. In particular, Henry et al. (1996) carried out a geochemical study of the metasedimentary rocks of La Grave (Fig. 2), where the cover is detached from its probably undeformed underlying basement (Bellahsen et al., 2012). Isotopic and trace element signatures of metamorphic vein filling material and their host-rocks show that the metasedimentary cover behaved as a chemically closed-system, locally-derived fluid circulations being restricted to the metasedimentary Jurassic units (i.e., few tens of meter scale; Henry et al., 1996).

Microthermometric studies all over the Bourg d'Oisans basin carried out on fluid inclusions trapped within vein mineral phases also suggest the absence of large-scale fluid circulation in the Oisans Jurassic cover, although high salinities recorded in some fluid inclusions in the deeper Liassic layers were interpreted as due to a local percolation of fluids from the underlying Triassic gypsum (Bernard, 1978; Gratier and Vialon, 1980; Gratier et al., 1973; Nziengui, 1993; Poty et al., 1974).

### 3. Large-scale structures and microstructures

#### 3.1. Large-scale structures

In both the Bourg d'Oisans and Mizoën basins, basement shortening was accommodated by West-verging 100–500 m wide shear zones (Bellanger et al., 2014) restricted to the basement (i.e., they did not propagate significantly into the cover) and that cut across the Variscan foliation (Fig. 3A), without any evidence for its reactivation. The two basins have slightly different styles of shortening. In the Bourg d'Oisans basin, there are five units (Dumont et al., 2008) that are separated by four West-verging shear zones named Bourg d'Oisans, Huez, Col de Cluy, and Croix de Cassini shear zones (Fig. 3A). Above these basement shear zones, the sedimentary cover is disharmonically folded. The observed meter-to-kilometer scale fold axes are N–S and synchronous with the main cleavage. The Mizoën basin is divided into two parts: the eastern part is a basement horst named the Emparis Plateau, with a thin metasedimentary cover (Figs. 2, 3A), whereas the western part is composed of a thicker disharmonically folded metasedimentary cover (Fig. 3A) underlain by the main West-verging basement shear zone (the Mizoën shear zone). Just West of the Emparis Plateau, the Mizoën metasedimentary cover is composed of two structural units separated by the Alp décollement (Fig. 3A). Note that the base of the sedimentary cover is composed of a thin Triassic layer (a few tens of meters wide) attached to the basement, i.e., not disharmonically folded.

#### 3.2. Cleavages in the sedimentary cover

Several cleavages affecting the metasedimentary cover are documented in the field (Bellahsen et al., 2012; Boutoux et al., 2014; Dumont et al., 2008, 2012). In the Bourg d'Oisans basin, one main cleavage (S2) is observed (Figs. 3, 4A–B), striking N–S and dipping eastward. This cleavage is associated with the main folds whose axial surface is East-dipping (Gratier and Vialon, 1980; Gratier et al., 1973). Close to the basement of the Bourg d'Oisans basin, a previous cleavage (S1) can also be documented (Fig. 3B), striking N–S and dipping westward. The chronological relationships between the two cleavage sets are described in Bellahsen et al. (2012) and Boutoux et al. (2014): during the initiation of the basin inversion, the base of the sedimentary cover underwent a top-to-the-East shearing that locally formed the West-

dipping S1 cleavage. This cleavage was then overprinted by the S2 main cleavage resulting from the top-to-the-West shearing of the entire basin (Fig. 3). In the Mizoën basin, the S1 cleavage is only recorded below the Alp décollement, while the S2 cleavage developed only above it (Figs. 3, 4C–D).

#### 3.3. Vein pattern and sequence

During the development of the two cleavages, metamorphic veins were continuously formed and deformed in the metasedimentary cover. Vein deformation occurred either by transposition into cleavage or by folding (i.e., ptygmatic vein; Fig. 4). In the field, three successive vein sets could be distinguished owing to their crosscutting relationships with S1 and S2 cleavages (Boutoux et al., 2014). V1 veins were deformed by both cleavages (Fig. 4C), V2 veins cut across S1 but were deformed by S2 cleavage (Fig. 4A), and V3 veins are undeformed and cut across both cleavages (Fig. 4B). V1 veins are interpreted as pre- to syn-S1 cleavage, V2 veins as pre- to syn-S2 cleavage and V3 veins as late- to post-S2 cleavage. Indeed, most V3 veins are perpendicular to S2 but undeformed, therefore compatible with the end of the ductile event forming the S2 cleavage. Therefore, most of the veins are related to the main ductile deformation event associated to the development of S1 and S2 cleavages (Boutoux et al., 2014), except the latest V3 veins that can be related to the basin exhumation.

Locally, where only one cleavage is expressed, only two vein generations can be distinguished, e.g., far from the basement in both basins, where S1 and S2 cannot be distinguished. In this case, V1 and V2 veins cannot be discriminated and are labeled as “early veins” (Fig. 4B–D). Moreover, under the Alp décollement in the Mizoën basin, where S1 only is expressed, V2 and V3 veins are undistinguishable and considered as “late veins”. The structural relationships between vein sets and cleavages are summarized in Fig. 3B.

### 4. Sampling strategy and analytical techniques

In order to investigate the scale of fluid circulation in the metasedimentary cover rocks in the Bourg d'Oisans basin and to identify potential basement-derived fluid infiltration, we collected samples in the Huez basement shear zone and in the cover right above, at different distances above the basement-cover interface (Fig. 3). Basement samples from the Huez shear zone itself were sampled on the road between La Garde and l'Alpe d'Huez, a few meters under the basement-cover contact (location 3 in Figs. 2, 3A), along with Triassic samples. Cover samples were collected in two places: (1) a few tens of meters above the basement-cover contact on the road between La Garde and l'Alpe d'Huez (called “Huez samples” thereafter; location 1 in Figs. 2, 3A) and (2) about 300 m structurally higher, on the road between Huez and Villard-Reculas (called “Villard-Reculas samples” in this study; location 2 in Figs. 2, 3A).

We also collected samples from the cover in the Mizoën basin, between the Mizoën village and the Emparis plateau, from both tectonic units separated by the Alp décollement, i.e., above (location 4 in Figs. 2, 3A) and below it (location 5 in Figs. 2, 3A), in order to investigate the possible effect of this tectonic contact on potential fluid circulations. Unfortunately, the underlying basement shear zone could not be sampled, because (1) it does not crop out around the Romanche valley (Fig. 3A) and (2) further South, in the Veneon valley, the sheared basement is accessible, but according to Barbier et al. (1973), the lithology is quite different than in the Romanche valley.

Most analyses were performed at ISTeP (Paris, France), except when specified in the following. Whole-rock analyses were performed at the SARM (Nancy, France) on six representative cover and basement samples from the Huez area (locations 1, 2, and 3 in Figs. 2, 3A). The vein and host-rock mineralogy was determined by X-ray diffraction (D2 Phaser Bruker) and EDS analyses (SDD detector PGT Sahara) associated to scanning electron microscopy (SEM Zeiss Supra 55VP). Cover vein

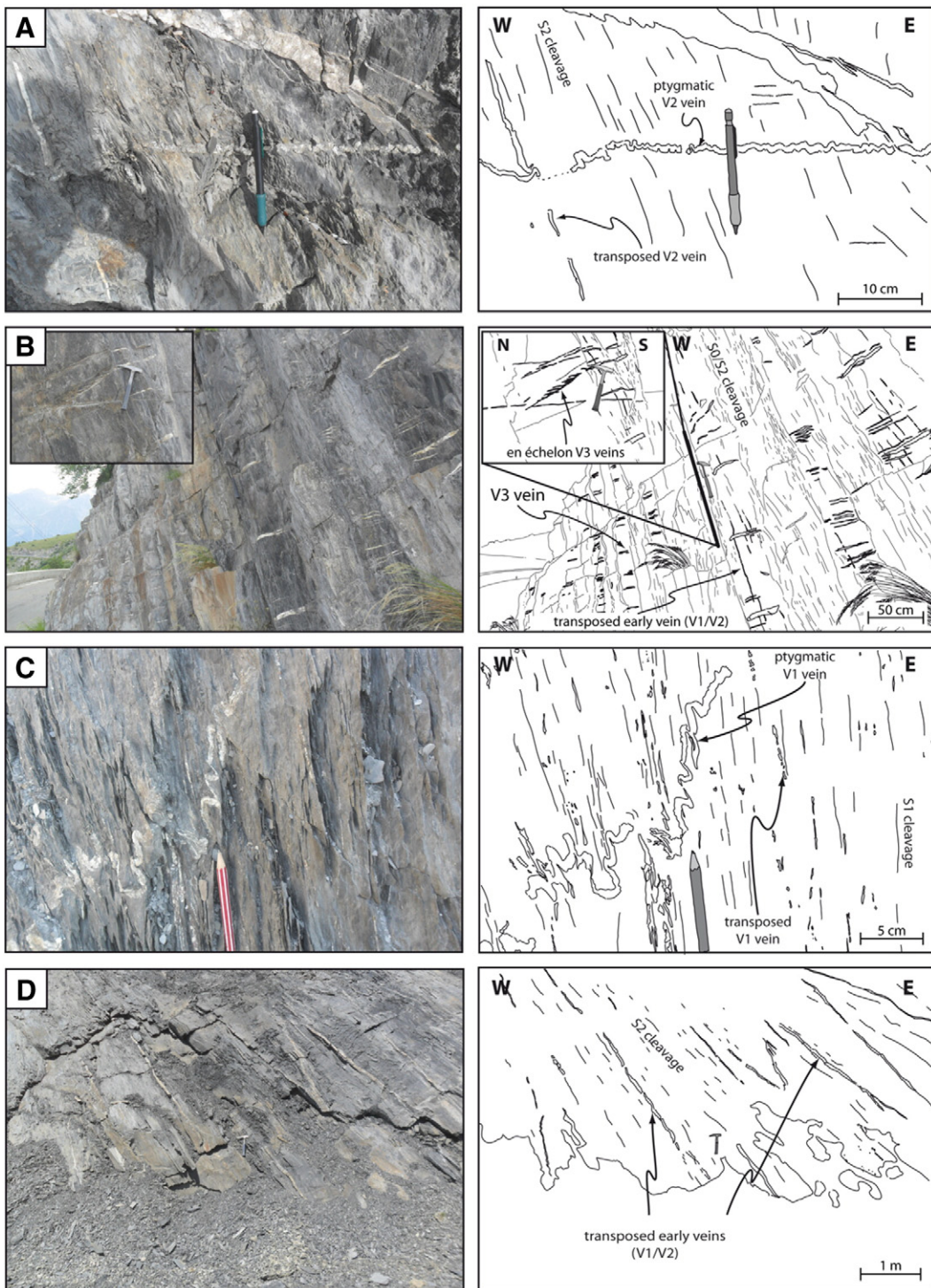


**Fig. 4.** Successive metamorphic veins and their chronological relationships with the cleavage sets in cover rocks from Bourg d’Oisans and Mizoën basins, microphotographs and schematic interpretation. A–B: Bourg d’Oisans basin (location 2 in Figs. 2, 3A). A. Transposed V2 vein into the S2 cleavage and folded (ptygmatic) V2 vein with S2 cleavage as fold axial plane. B. Late V3 veins, sometimes en-échelon, crosscutting the S2 cleavage in pelitic-rich layers. C. Mizoën basin, below the Alp décollement (location 5 in Figs. 2, 3A). V1 vein transposed into S1 cleavage and ptygmatic V1 vein with S1 cleavage as fold axial plane. D. Mizoën basin, above the Alp décollement (location 4 in Figs. 2, 3A). Early veins (V1 or V2) transposed into S2 cleavage.

microstructures were characterized under SEM and optical microscope. Cathodoluminescence (Cathodyne OPEA) on cover veins and host-rocks was used to identify successive crystallization generations. To investigate local versus external fluid infiltration in metasedimentary cover rocks, the isotopic signature ( $\delta^{13}\text{C}$ , VPDB and  $\delta^{18}\text{O}$ , SMOW) of vein calcite was compared to that of their surrounding host-rocks. The  $\delta^{18}\text{O}$  of quartz (laser fluorination at IPGP, Paris, France) and calcite in textural equilibrium in the different vein sets were combined in order to

constrain the fluid temperature during vein mineral crystallization. Trace element analyses were performed (ICP-MS, following the methodology of Salaün et al., 2010) on the different vein sets and their host-rocks, and on samples from the underlying basement (for the Huez shear zone) in order to detect any basement-derived fluid infiltration into cover rocks. Besides, microthermometric measurements were performed on primary fluid inclusions in quartz and calcite from Huez and Mizoën (locations 1 and 5 in Figs. 2, 3A, respectively) cover veins,

providing fluid salinity and isochoric evolution paths. Finally, the combination of calculated isochors and quartz–calcite equilibrium temperature provided fluid pressure estimates during the vein formation. More details about the analytical procedures can be found in Appendix A.1.

## 5. Mineralogy and textures of basement and cover rocks and veins

### 5.1. Mineralogy of basement rocks

In the Bourg d'Oisans basin, the Huez Alpine shear zone (location 3 in Figs. 2, 3A) presents a thick talc-rich zone of a few meters width. This talc-rich zone is composed of rocks with very mafic Ca-rich composition (Table 1) exhibiting the following minerals: talc, Cr-rich chlorite, Mg–Ca-amphibole, plagioclase, Ni-rich pyrite, sphene, chromite, rutile and titanomagnetite (Fig. 5). Talc, chlorite and sphene are observed to have co-crystallized in shear zones, where they clearly replace amphibole (Fig. 5A) and plagioclase. Pyrite cores included in amphibole crystals are rimmed by iron-oxide or hydroxide (Fig. 5B), which formation is associated and coeval with talc crystallization in cracks through the amphibole crystals. Zoned chromite crystals are partly dissolved and embedded in Cr-rich chlorite (Fig. 5C, D, E). These mineralogical reactions required both rock hydration (to form phyllosilicates) and progressive evolution towards more oxidizing conditions (i.e., pyrite rims).

Therefore, two successive parageneses can be identified: (1) the assemblage amphibole + plagioclase + pyrite + chromite + rutile corresponds to the Variscan paragenesis also observed by Barf  t  y et al. (1972) in the unsheared basement and is in agreement with description by Guillot and M  not (2009), and (2) the assemblage talc + chlorite + sphene + Fe-oxide/hydroxide + titanomagnetite is obviously related to basement shearing, accompanied by external fluid influx, during the Alpine collision. Indeed, this second paragenesis grew in Alpine shear zones, and the presence of chlorite is characteristic of the greenschist facies P-T conditions undergone by basement rocks during the Alpine collision.

In the talc zone, numerous quartz veins and scarce calcite veins (e.g., sample Alp10-5 in the following results) are kinematically consistent with Alpine shearing, and thus considered of Alpine age.

### 5.2. Mineralogy of cover rocks

The Triassic layers, still attached to the basement rocks, are mainly composed of sandstone, dolomite and scarce lenses of gypsum (Table 1). Above the Huez basement shear zone, fractures in the Triassic layers are mainly filled with calcite, dolomite and quartz, with local

enrichments in galena (PbS), pyrite (FeS<sub>2</sub>) and/or sphalerite (ZnS). These minerals can be locally concentrated, e.g., in the La Gardette (Cathelineau et al., 1990; Marignac et al., 1997; Poty, 1967) and Le Pontet (Feybesse et al., 2004) ancient gold mines: these sulfur minerals crystallized in a 500 meter long quartz vein affecting both the basement (granite and gneiss) and the lowermost Triassic dolomites. In La Gardette, similar sulfur minerals are also concentrated in a specific level of the Triassic dolomite, where they were interpreted as syn-sedimentary enrichments (Poty, 1967).

In both the Huez and Mizo  n basins, the metasedimentary cover is made of marls (Table 1) containing calcite, quartz, phyllosilicates (mainly pyrophyllite, chlorite, phengite and rare cookeite), iron oxides, rutile, and pyrite (Fig. 6A–B). Framboidal pyrite is observed and is interpreted as formed during early diagenesis (Wilkin et al., 1996). The pyrites are often partially to completely oxidized (Fig. 6A). Detrital albite grains and rare dolomite (Fig. 6B) and apatite crystals were also observed. The phyllosilicate paragenesis is characteristic of the Alpine greenschist facies metamorphism. The analyzed samples (Table 1) show a large compositional variability, which results in variable proportions of calcite (30–90 vol.%) versus quartz (0–20 vol.%), phyllosilicate fraction (5–40 vol.%) and organic matter (0.5–1.5 wt.%; modal composition calculations according to Verlaguet et al., 2011).

Finally, host-rocks show calcite dissolution zones (Fig. 6A), attesting material displacement by pressure-solution into the sedimentary cover.

### 5.3. Textures and mineralogy of veins

In both basins, veins are mainly filled with calcite and quartz, the quartz amount decreasing from V1 to V3, so that many V3 veins are devoid of quartz and only filled with calcite. Calcite and quartz display either fibrous crystals elongated perpendicular to the vein walls ("fibrous texture" in the classification of Oliver and Bons, 2001; Fig. 6C) or euhedral morphologies ("blocky texture" in Oliver and Bons, 2001; Fig. 6C, D, E), whatever the vein generation. Both textures can coexist in synchronous veins in the same thin section (e.g., late veins in Fig. 6C), and mixed textures are also observed.

Quartz and calcite crystals show multiple evidences of textural equilibrium: they often show mutual micro-indentations (intergrowth textures), and some calcite crystals are embedded within quartz crystals, themselves surrounded by calcite crystals of similar composition (Fig. 6F). The textural equilibrium of calcite and quartz in veins indicates their co-precipitation.

Scarce accessory micrometric phases such as dolomite, apatite, oxidized pyrite and chlorite can be recognized with SEM.

**Table 1**  
Chemical analysis (wt.%) of Bourg d'Oisans basin cover and basement rocks.

Sample	Alp10-8 <sup>a</sup>	Alp10-13 <sup>a</sup>	Alp 10-34 <sup>b</sup>	Alp10-II-15 <sup>a</sup>	Alp10-II-16 <sup>a</sup>	Alp10-3 <sup>c</sup>
Sample location	1	1	1	2	2	3
SiO <sub>2</sub>	40.38	23.02	2.17	4.88	32.45	34.84
Al <sub>2</sub> O <sub>3</sub>	14.21	6.04	0.53	2.84	8.55	0.79
Fe <sub>2</sub> O <sub>3</sub> total	3.16	2.41	2.51	1.1	3.52	4.78
MnO	0.04	0.04	0.37	0.25	0.37	0.39
MgO	3.34	4.3	19.13	1.24	3.13	26.38
CaO	15.42	30.57	30.06	47.93	24.25	12.38
Na <sub>2</sub> O	0.35	0.51	0.26	0.15	0.56	–
K <sub>2</sub> O	4.01	1.20	0.07	0.55	1.69	–
TiO <sub>2</sub>	0.57	0.31	0.03	0.12	0.41	0.02
P <sub>2</sub> O <sub>5</sub>	0.17	0.18	–	0.06	0.17	–
L.O.I.	17.83	30.04	43.79	39.49	24.13	21.08
Total	99.48	98.63	98.92	98.62	99.24	100.67
CO <sub>2</sub> total	16.85	31.76	44.77	39.78	23.34	18.38
H <sub>2</sub> O total	2.87	1.67	0.73	1.23	2.22	3.45

L.O.I., loss on ignition. Whole-rock chemical analysis (oxide weight %).

<sup>a</sup> Jurassic.

<sup>b</sup> Triassic.

<sup>c</sup> Sheared basement.

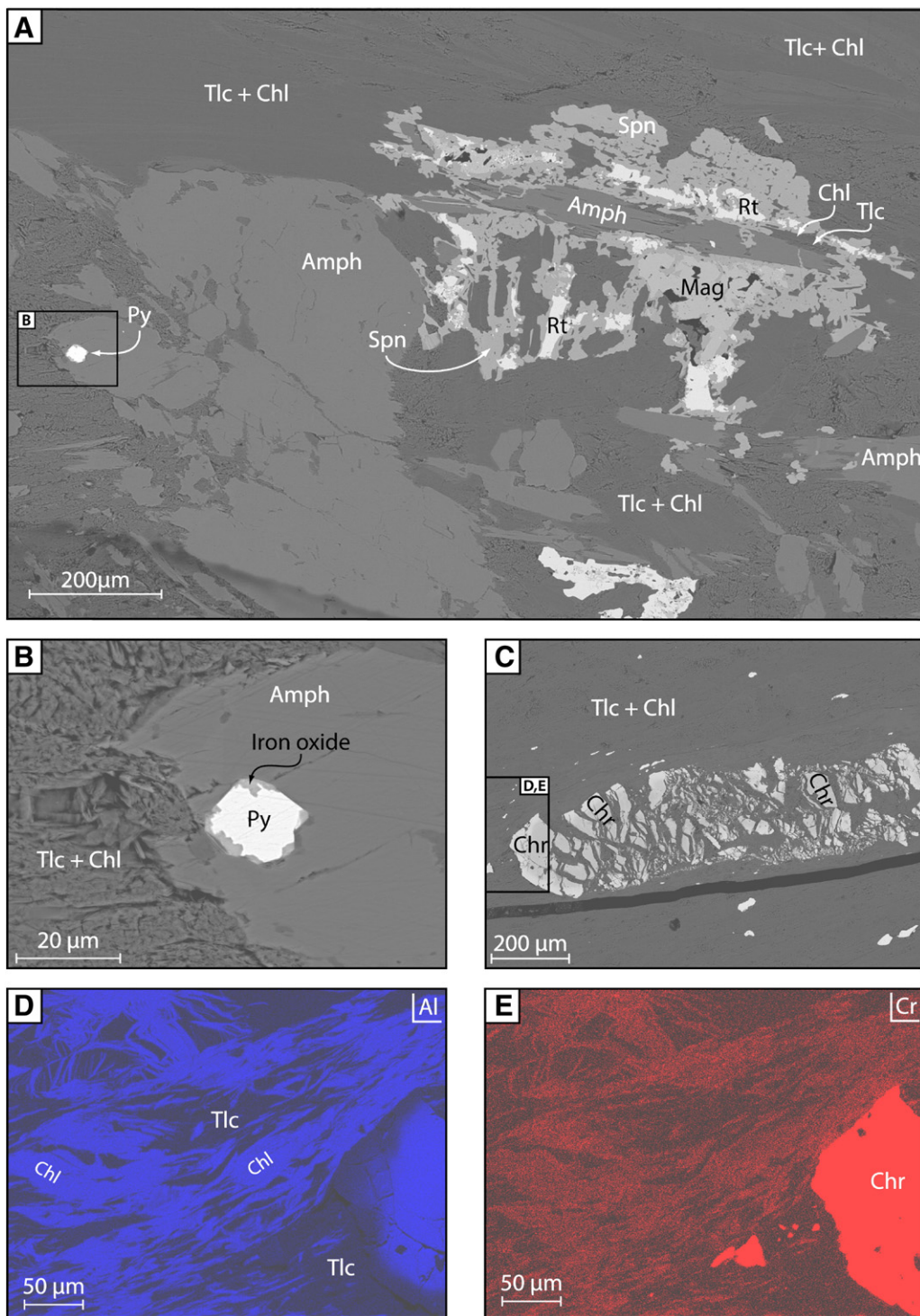


**Fig. 5.** Thin section of the Huez talc-rich basement shear zone (sampling location 3 in Figs. 2, 3A). BSE-SEM images. A. Hercynian paragenesis amphibole (Amph) + pyrite (Py) + rutile (Rt) partially replaced by the Alpine assemblage talc (Tlc) + chlorite (Chl) + spheine (Spn) + titanomagnetite (Mag). B. Ni-rich pyrite included in Hercynian amphibole is altered into iron-oxide rims by fluid ingressions into amphibole cracks during the Alpine shearing, as attested by the coeval retrogression of amphibole into talc + chlorite. C. Hercynian chromite (Chr) partially dissolved and replaced by talc + chlorite. D-E Elementary maps (EDS-SEM analysis) of AlO (D) and CrO (E), showing that the Alpine chlorite locally incorporates part of the chromium liberated by the Hercynian chromite dissolution (mineral abbreviations following Kretz, 1983).

## 6. Geochemical signatures and microthermometry of veins and host-rocks

### 6.1. Cathodoluminescence microscopy

Several samples from the three vein generations (from both the Bourg d'Oisans and Mizoën basins, locations 1–2 and 4–5 in Figs. 2–3A,

respectively) were analyzed under cathodoluminescence. Two representative V1 and V2 veins are illustrated in Fig. 6G–H. In V1, V2 and their host-rock, calcite displays the same red color, with the same intensity (Fig. 6H). Quartz in V1 vein and other phyllosilicate phases in the host-rock appear in black and lighter red, respectively (Fig. 6H), as they do not incorporate the same amount of luminescent elements. A similar red color was observed in V3 veins and their host-rocks on other samples.

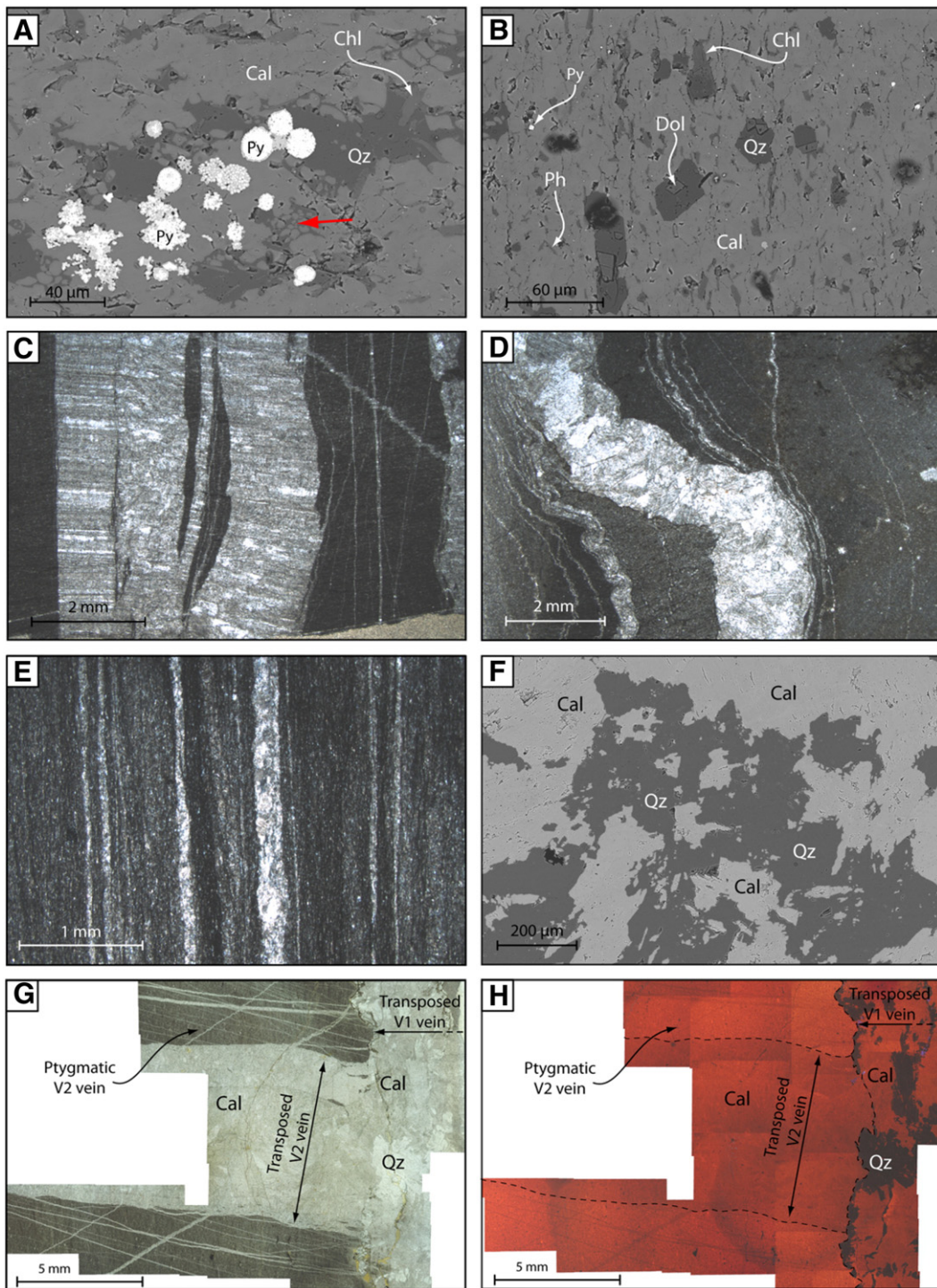


**Fig. 6.** Thin-sections of cover veins and their host-rocks. SE-SEM images (A, B), photomicrographs in natural light (C, D, E, F) and under cathodoluminescence (H). A. Calcite (Cal), quartz (Qz), chlorite (Chl), and frambooidal pyrite (Py) observed within cover host-rock thin section. Pyrite cores are partly oxidized. The arrow highlights a calcite dissolution zone within the host-rock. B. Host-rock mineralogical assemblage composed of calcite, quartz, phengite (Ph), chlorite, frambooidal pyrites and scarce dolomite (Dol). C. Late V3 veins (calcite + quartz) showing either blocky or fibrous texture, crosscutting V2 ptygmatic vein. D. Ptygmatic V1 veins with blocky textures. E. Transposed V2 veins with blocky textures. F. Calcite and quartz in textural equilibrium (micro-indentation) in V1 vein: calcite is included in quartz crystals, which are embedded in calcite crystals. G–H. Thin section of cover veins from sample Alp10-20 (location 1 in Figs. 2, 3A) observed under natural light (G) and cathodoluminescence (H). Sample showing two vein generations: V1 transposed into S1 cleavage, and numerous V2 (only the major one is underlined) transposed into S2 cleavage and crosscutting V1. V1 contains quartz + calcite + scarce apatite, while V2 is filled with calcite only. Mineral abbreviations following Kretz (1983).

These observations indicate that the nature and concentration of luminescent elements incorporated in calcite did not vary during the successive vein crystallization, and are similar to that of the host-rock calcite. In these samples, calcite appears red although pure calcite is usually orange under cathodoluminescence microscopy (Machel and Burton, 1991): this

may indicate a high concentration in red luminescent elements such as manganese or magnesium.

The absence of variation in either color or intensity of calcite within the veins precludes any evidence of successive growing phase in any vein generation.

## 6.2. $\delta^{18}\text{O}$ and $\delta^{13}\text{C}$ signatures of calcite from veins and host-rocks

$\delta^{18}\text{O}$  and  $\delta^{13}\text{C}$  signatures of calcite from cover veins and their host-rocks from both basins (sample locations 1, 2, 4, and 5 in Figs. 2, 3) along with one calcite vein from the talc-rich zone of the Huez basement shear zone (sample location 3 in Figs. 2, 3) are reported in Fig. 7A. In the Bourg d'Oisans basin, the isotopic ratios, whatever the vein generation, are very close to that of their host-rock (Fig. 7B–C).  $\delta^{18}\text{O}$  and  $\delta^{13}\text{C}$  composition ranges of most veins and host-rocks are relatively narrow: +18 to +23.5‰ and –2 to +1.5‰, respectively (Fig. 7A). These variations mainly reflect lithological variations: the most pelitic (i.e., phyllosilicate-rich) samples exhibit the lowest  $\delta^{18}\text{O}$  and  $\delta^{13}\text{C}$  signatures. In the Mizoën basin, the isotopic signatures of each vein are also very close to those of their host-rocks (Fig. 7B–C). Two groups can be identified: one group has isotopic composition within the range of Bourg d'Oisans rocks ( $\delta^{18}\text{O} = +21.5$  to +23.5‰,  $\delta^{13}\text{C} = -1$  to +1.5‰, Fig. 7A), while the second group has lower  $\delta^{18}\text{O}$  (+19.5 to +21.5‰) and  $\delta^{13}\text{C}$  (–2.5‰ to –6‰, Fig. 7A). This bimodal distribution is correlated to the rock lithology: all samples with negative  $\delta^{13}\text{C}$  (pelitic layers on Fig. 7A) belong to the Aalenian layer, which is particularly rich in phyllosilicates and organic matter, while other compositions correspond to samples collected in marls.

Cover vein and host-rock calcite presents very homogeneous isotopic signatures (Fig. 7B–C). On the contrary, the isotopic signature of the calcite vein from the Huez basement shear zone shows a strikingly different value ( $\delta^{13}\text{C} = -9.2\text{\textperthousand}$  and  $\delta^{18}\text{O} = +13.3\text{\textperthousand}$ , Fig. 7A) compared to the cover vein calcite. In the Triassic layer, the isotopic composition of the vein ( $\delta^{13}\text{C} = -5.3\text{\textperthousand}$ ,  $\delta^{18}\text{O} = +19.5\text{\textperthousand}$ ) is very different from that of its host-rock ( $\delta^{13}\text{C} = -1.5\text{\textperthousand}$ ,  $\delta^{18}\text{O} = +25.7\text{\textperthousand}$ , Fig. 7A), and intermediate between Triassic host-rock and basement vein composition (Fig. 7A).

## 6.3. $\delta^{18}\text{O}$ signatures of quartz from cover veins

The  $\delta^{18}\text{O}$  signatures of quartz crystals in textural equilibrium with calcite in cover veins from both basins (sample locations 1, 2, 4, and 5 in

Figs. 2, 3A) are relatively homogeneous for most veins ( $\delta^{18}\text{O} = +22.3$  to +26.3‰, Table 2) whatever the sampling site or vein generation.

## 6.4. Microthermometric study of fluid inclusions in veins

Microthermometric measurements were performed on about 80 fluid inclusions in either quartz or calcite crystals from V1 or early (V1/V2) cover veins from both basins (locations 1 and 5 in Figs. 2, 3). In order to characterize the fluid phase present in cover veins during mineral crystallization, we focused on primary fluid inclusions, which are interpreted as being trapped during crystal growth (Roedder, 1984; Touret and Frezzotti, 2003). Primary fluid inclusions are distributed either in trails along successive crystal growth surfaces (Fig. 8A) or in clusters (Fig. 8B) throughout the vein crystals (Roedder, 1984). In veins showing fibrous textures, we also analyzed the pseudo-secondary trails of fluid inclusions (Fig. 8C, D).

For each fluid inclusion, the salinity of the fluid was calculated from the measured melting temperature ( $T_m$ ) with the equation presented in Bodnar (1993). Measured  $T_m$  is between –1 °C and –10 °C (dispersion of  $\pm 3$  °C for each sample), which corresponds to 1.74wt.% eq. NaCl and 13.94wt.% eq. NaCl, respectively. Measured homogenization temperatures ( $T_h$ ) are between 125 °C and 198 °C (dispersion of  $\pm 12$  °C in a single sample). Then, isochoric P-T relationships were calculated for each sample from the mean measured  $T_h$  and mean calculated salinity, using the equation of Bodnar and Vityk (1994). The isochors (Fig. 9) are almost parallel, with P-T relationships of  $16.5 \text{ MPa} \cdot \text{C}^{-1}$  to  $21 \text{ MPa} \cdot \text{C}^{-1}$ , whatever the basin (Bourg d'Oisans or Mizoën).

## 6.5. Trace element analysis in veins and host-rocks

For both basement and cover rocks, trace element concentrations of 3d transition elements (Sc, V, Cr, Co, Ni, Cu and Zn) and HFSE (Zr, Hf, Nb, Ta, Mo, Sb) were normalized to mean crust composition (Taylor and McLennan, 1985; Fig. 10A, B) to allow comparison. However, basement rocks have Ca-rich basic compositions, and cover rocks are Triassic

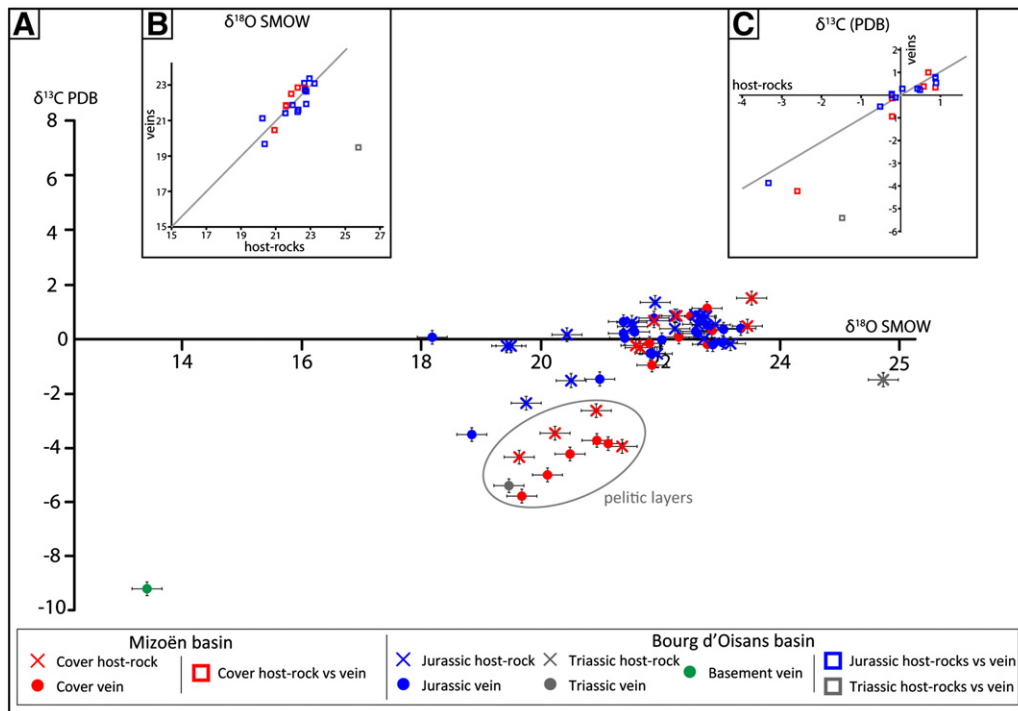


**Fig. 7.** Stable isotopic ratios ( $\delta^{18}\text{O}$  and  $\delta^{13}\text{C}$ ) of calcite from vein and host-rock samples in Bourg d'Oisans (locations 1 and 2 in Figs. 2, 3A) and Mizoën (locations 4 and 5 in Figs. 2, 3A) basins. A.  $\delta^{18}\text{O}$  versus  $\delta^{13}\text{C}$  for Jurassic and Triassic calcite. In addition, the isotopic analysis of a calcite vein from the talc-rich zone of the sheared basement shear zone is plotted (location 3 in Fig. 2, 3A). "Pelitic layers" highlights samples from the Aalenian layer, which is particularly phyllosilicate-rich (Barbier et al., 1973). B and C.  $\delta^{18}\text{O}$  (B) and  $\delta^{13}\text{C}$  (C) of vein calcite versus their respective host-rock calcite (i.e., for samples where both vein and host-rock calcite was analyzed). Solid line: linear relationship between vein and host-rock isotopic ratios.

**Table 2**

$\delta^{18}\text{O}$  of vein calcite and quartz presenting textural equilibrium (fine micro-indentation, see Fig. 6F).

Sample	Sample location	Quartz $\delta^{18}\text{O}$ (‰)	Calcite $\delta^{18}\text{O}$ (‰)	T (°C)
Alp10-13 <sup>a</sup>	1	25.2	22	251
Alp10-15	1	24.8	21.8	274
Alp10-18	1	24	21.8	358
Alp10-20 <sup>a</sup>	1	25.2	23.1	421
Alp10-21	1	25.3	23	344
Alp10-22 <sup>a</sup>	1	25.7	21.6	189
Alp10-34	1	24.6	19.5	144
Alp10-II-2	2	24.7	22.2	327
Alp10-II-6 <sup>a</sup>	2	26.3	23.5	292
Alp10-II-11	2	25.8	23.2	314
Alp10-52	4	22.3	19.7	306
Alp10-55 <sup>b</sup>	4	22.3	20.5	429
Alp10-64 <sup>b</sup>	4	23.8	21.9	402
Alp10-74	4	24.6	22.8	417
Alp11-15	5	25.7	23.9	436

$\delta^{18}\text{O}$  for quartz and calcite expressed in ‰ SMOW.  $\delta^{18}\text{O}$  on quartz corrected from standard analysis (UWG2 garnet).

Analytical precision for  $\delta^{18}\text{O}$  on calcite (0.1‰) and quartz (0.08‰) gives a propagated error on  $\Delta^{18}\text{O}_{\text{quartz-calcite}}$  ( $= \delta^{18}\text{O}_{\text{quartz}} - \delta^{18}\text{O}_{\text{calcite}}$ ) of 0.12‰.

Equilibrium quartz–calcite temperatures calculated from Sharp and Kirschner (1994); estimated uncertainty on the thermometer: from  $\pm 15$  °C to  $\pm 26$  °C in the 200–450 °C range, systematically higher than the maximum error on the equilibrium temperature calculated from the analytical precision on quartz and calcite  $\delta^{18}\text{O}$ : from  $\pm 7$  °C to  $\pm 22$  °C in the 200–450 °C range.

Veins are all V1 veins for Bourg d’Oisans samples (locations 1 and 2 on Figs. 2, 3A) or early veins (undetermined V1 or V2 veins) for Mizoën samples (locations 4 and 5 on Figs. 2, 3A).

<sup>a</sup> Duplicated samples showing a deviation from mean value  $\leq \pm 0.3\%$ ; equilibrium quartz–calcite temperature calculated from the mean  $\delta^{18}\text{O}$  value.

<sup>b</sup> Samples showing highly dispersed duplicates ( $\pm 0.6$  and 0.9‰): for both samples, the highest  $\delta^{18}\text{O}$  value gives an unrealistically high equilibrium temperature (863 °C and 3944 °C respectively), exceeding both the thermometer calibration temperature range and the maximum temperature estimated for these rocks (300–350 °C; Bellanger, 2013; Crouzet et al., 2001; Jullien and Goffé, 1993); these unrealistic  $\delta^{18}\text{O}$  values were discarded, and the equilibrium quartz–calcite temperature was calculated from the valid  $\delta^{18}\text{O}$  analysis.

dolomites and Liassic marls, thus these rocks display accordingly specific patterns relative to the mean crust composition. As the aim of this study was to trace potential basement-derived fluid infiltration in cover rocks, trace element patterns normalized to mean crust composition are discussed hereinafter in terms of relative variations of shapes rather than in terms of absolute values. The trace element patterns of sheared and unsheared basement, basement and cover rock, and cover vein versus host-rock are also compared. Trace element values can be found in Appendix Table A.2.

### 6.5.1. Basement trace element patterns

Trace elements were analyzed in samples collected both in the Huez basement shear zone (including the talc-rich area, Fig. 10D) and just outside the shear zone in less deformed rocks.

Basement trace element concentrations are presented on Fig. 10A normalized to the mean crust (Taylor and McLennan, 1985). For most elements, trace element patterns of samples from the sheared basement are similar to those of the unsheared basement with however lower absolute contents, except in Ni, Co and Cr (Fig. 10A). These lower concentrations in sheared basement samples reflect either trace element depletion in basement rocks during shearing or trace element dilution effects due to depletion or enrichment in some major elements.

Concerning the sheared basement, trace element compositions in samples from the shear zone outside of the talc-rich zone follow the same trend than the talc-rich zone samples (Fig. 10A–D), except for the Cr, Co, and Ni concentrations that are clearly higher in the talc-rich zone: Cr, Co, and Ni patterns are even inversely correlated in both zones. This suggests that the shearing of basement rocks has mainly affected the compositions in Cr, Co and Ni, probably through fluid-assisted

mobilization, while other 3d transition elements and HFSE (known as the least mobile) remained unaffected.

In the talc-rich shear zone, the calcite vein from sample Alp10-5 has a similar pattern (except in Zn and Mo) than its host-rock, with bulk depletion in all trace elements.

### 6.5.2. Cover trace element patterns

Trace element concentrations of cover rocks are presented normalized to the mean crust ones (Fig. 10B; Taylor and McLennan, 1985) whereas the vein trace element concentrations are presented normalized to their host-rocks (Fig. 10C).

Composition patterns of Triassic dolomites are slightly enriched in Zn, Mo, and Sb compared to the mean crust composition (Fig. 10B). The associated veins are enriched in Zn ± Sb and V compared to their host-rocks (Fig. 10C).

In Liassic layers above the Huez shear zone, the samples have very similar trace element patterns, whatever their distance to the contact (Fig. 10B): indeed, both Huez (a few tens of meters above the basement, location 1 in Figs. 2, 3, 10D) and Villard-Reculas (a few hundred meters from the basement, location 2 in Figs. 2, 3, 10D) samples exhibit similar concentrations in all elements (Fig. 10B), with higher concentrations in V, Zn, Mo and Sb than mean crust composition (Fig. 10B). The variability of trace element concentrations in marls may reflect their heterogeneous calcite content (30–90 vol.%, Table 1) versus pelitic fraction content.

All the veins sampled just above the Huez basement shear zone (location 1 in Figs. 2, 3A, 10D) present strong enrichments in Ni (up to 100 times) and/or Co (up to 10 times), Cr (up to 10 times), Zr and Hf (up to 100 times) compared to their respective host-rocks (Fig. 10C), for V1, V2 and V3 veins. On the contrary, veins sampled farther from the basement-cover interface (location 2 in Figs. 2, 3A, 10D) display a bulk depletion in all trace elements compared to their host-rocks, and do not present any particular trace element enrichment (Fig. 10C).

## 7. Interpretation of results and discussion

### 7.1. Scale of fluid circulation and mass transfer in the metasedimentary cover

#### 7.1.1. Isotopic reequilibration of host-rocks during burial

In samples from the metasedimentary cover of the Bourg d’Oisans and Mizoën basins, calcite shows a homogeneous isotopic composition in each lithological unit (Fig. 7A). However, the calcite isotopic signal is not that of a typical marine limestone, and plots between “normal marine limestones” and “metamarls-metapelites” isotopic values (Fig. 11) reported by Henry et al. (1996). This means that isotopic reequilibration occurred among the different minerals (quartz, calcite, phyllosilicate fraction, organic matter) during burial. Following Henry et al. (1996), we conclude that these cover rocks attained complete isotopic reequilibration under greenschist facies conditions.

As a consequence, the isotopic signature of host-rocks seems to be mainly controlled by the lithology, i.e., it depends on the calcite–quartz–organic matter–phyllosilicate fraction relative amounts. This is the reason why the Aalenian samples from Mizoën (“pelitic layers” on Fig. 7A), which are much richer in phyllosilicates, present different isotopic signatures (i.e., lower  $\delta^{18}\text{O}$  and  $\delta^{13}\text{C}$ ) than all other Liassic marls. These isotopic ratios are in agreement with those analyzed all along the ECM cover, in metapelites (Aalenian samples in Burkhard and Kerrich, 1988; Henry et al., 1996) and metamarls (Burkhard and Kerrich, 1988; Henry et al., 1996; Kirschner et al., 1995) respectively, and reported in Fig. 11. Note that rocks from the La Grave basin (East of our study area) being globally richer in pelitic fraction than our samples, their isotopic signatures are accordingly slightly lower than our Aalenian Mizoën samples (Henry et al., 1996; reported as “ultra-Dauphinois metapelites” in Fig. 11).

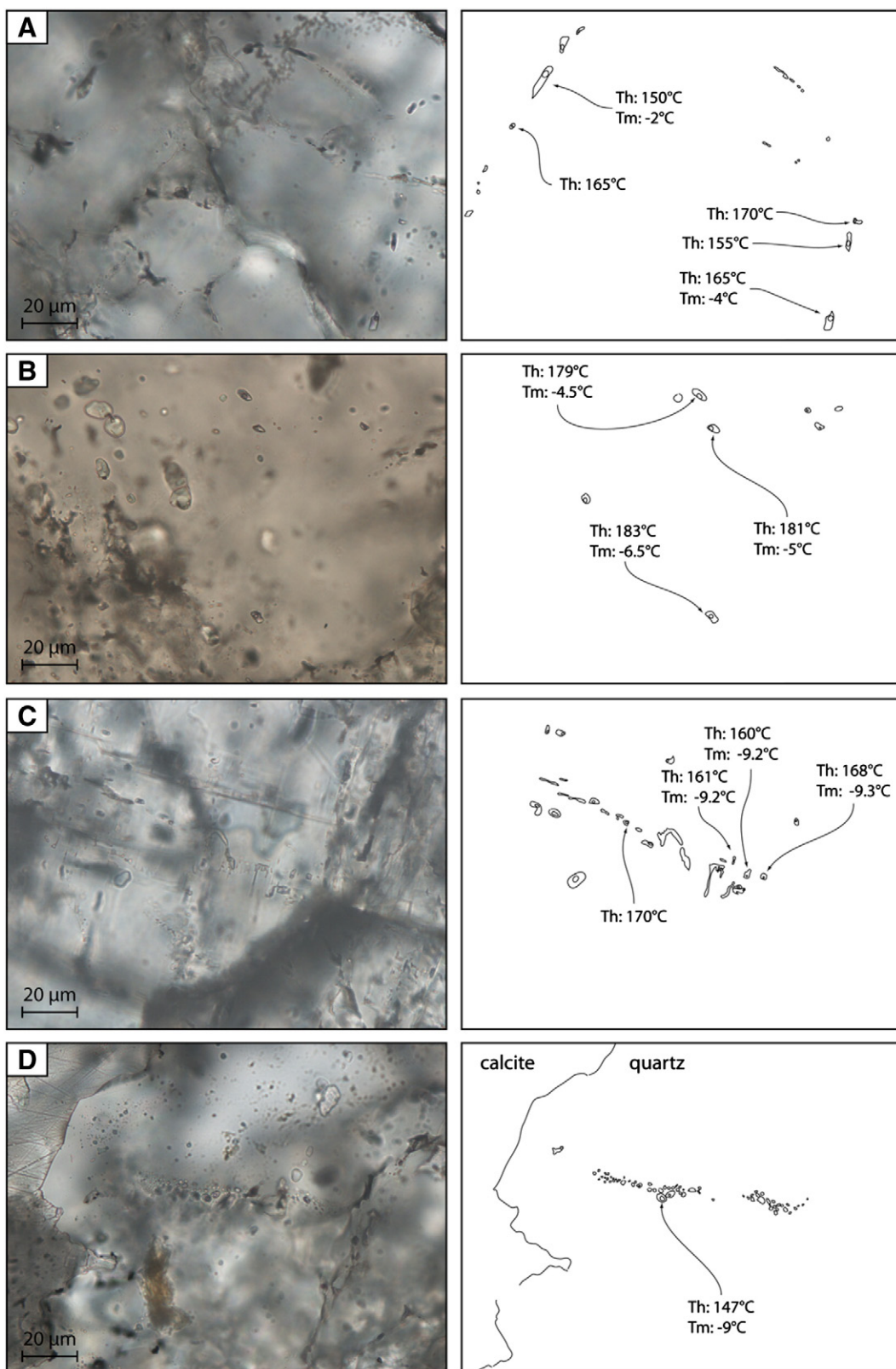


**Fig. 8.** Microphotographs of thin sections and corresponding sketch of fluid inclusions analyzed by microthermometry. A. Primary fluid inclusions distributed along growth surfaces in a quartz crystal. B. Cluster of primary fluid inclusions in a quartz crystal. C. Pseudo-secondary fluid inclusions in a calcite crystal, aligned along a trail parallel to the vein wall, supposed to develop in response to incremental crystal growth, when the vein-opening rate is lower than the crystal growth rate. D. Trail of pseudo-secondary fluid inclusions in a quartz crystal, parallel to the vein wall.

However, it is noteworthy that although the samples from a specific lithological layer have highly variable calcite–phyllosilicate relative proportions (e.g., Bourg d'Oisans samples in Table 1), their

isotopic signatures are very close (Fig. 11), meaning that the rock isotopic composition was equilibrated at the scale of the lithological layer.

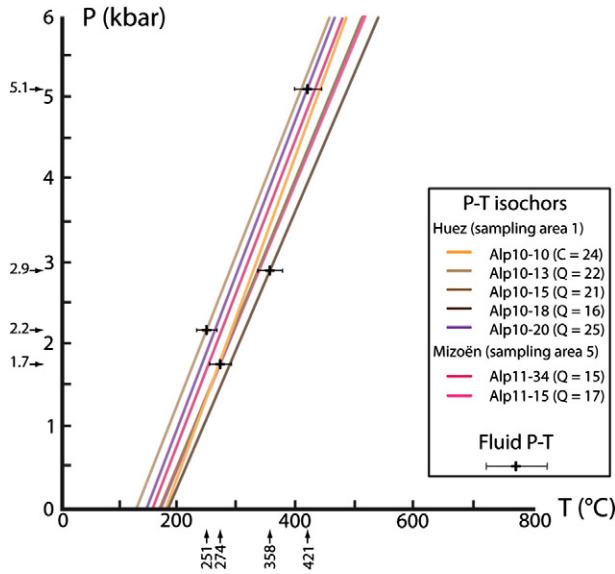


**Fig. 9.** Isochoric P-T relationships calculated from microthermometric measurements on quartz and calcite crystals from cover veins above the Huez and Mizoën basement shear zones. Host mineral phase and number of measurements are noted for each sample (Q for quartz and C for calcite). The isochors were computed from the homogenization (Th) and melting (Tm) temperatures, using equations from Bodnar (1993) for salinity and from Bodnar and Vityk (1994) for isochor calculations. Fluid temperatures were calculated from  $\delta^{18}\text{O}$  values of equilibrium quartz and calcite in veins. The error bars are thermometer uncertainties (see Table 2). Fluid pressures are inferred from the intersection of the equilibrium temperatures and the relative isochors.

#### 7.1.2. Fluid flow within the metasedimentary cover: evidence for a nearly-closed fluid system

In both the Bourg d'Oisans and Mizoën basins, calcite isotopic compositions are very similar in veins and associated host-rocks, whatever the vein generation, suggesting local fluid–rock equilibrium in cover rocks all along the successive vein formation. This vein–host-rock isotopic equilibrium precludes massive external fluid influx during deformation (e.g., Burkhard and Kerrich, 1988; Marquer and Burkhard, 1992). Indeed, basement-derived fluids may have very different isotopic signatures, as suggested by the calcite vein analyzed in the Huez basement shear zone (Figs. 7A and 11), and in agreement with the isotopic signature estimated for basement fluids by Henry et al. (1996) (Fig. 11). Therefore, the percolation of important amounts of basement-derived fluids into the overlying cover veins would have modified their isotopic signatures, as observed in the northern ECM basal thrusts of the sedimentary nappes (e.g., Burkhard and Kerrich, 1988; Kirschner et al., 1999) or Glarus thrust (e.g., Burkhard et al., 1992) reported in Fig. 11.

In our rocks, the absence of oxygen isotopic fractionation between host-rock and vein calcite suggests that vein formation occurred at P-T conditions high enough to allow the host-rock mineral isotopic reequilibration mentioned above (i.e., probably close to the peak P-T conditions). Therefore, as indicated by the scale of isotopic reequilibration mentioned above, fluid circulation in the cover rocks was restricted to the scale of the sedimentary formation, i.e., tens to a hundred meter scale. This is supported by observations under cathodoluminescence where calcite from veins and host-rocks exhibits very similar color, whatever the vein generation (Fig. 6G–H), suggesting no evidence of massive external fluid influx in those rocks. Henry et al. (1996) have drawn the same conclusion of a closed-system fluid circulation at the unit-scale for similar cover rocks from the La Grave basin.

Both isotopic and cathodoluminescence homogeneity of calcite in veins and host-rocks thus suggest a local origin for the vein calcite. Dissolution patterns of calcite crystals in the host-rock close to vein walls (Fig. 6A) confirm that calcite was partly dissolved by pressure-solution processes and locally transferred to the successively opening fluid-filled veins where it crystallized. Quartz and calcite pressure-

solution and recrystallization in adjacent veins are common deformation mechanisms observed during burial (Bons, 2000; Fisher et al., 1995; Ramsay, 1980; Yardley and Bottrell, 1992) and which have already been described in this area (Gratier and Vialon, 1980; Gratier et al., 1973) and in the northern ECM (Burkhard and Kerrich, 1988; Kirschner et al., 1995). As there is no evidence for infiltration of an important amount of external fluid, diffusive mass transfer likely occurred through the pervasive fluid produced locally by the metamorphic dehydration reactions undergone by clay minerals (i.e., phyllosilicate fraction of the marls) during burial (Cartwright and Buick, 2000; Fisher et al., 1995; Marquer and Burkhard, 1992; Oliver and Bons, 2001; Verlaguet et al., 2011). Making simplified assumptions on the clay mineralogy of the marls protolith (i.e., kaolinite, smectite, illite; see Verlaguet et al., 2011 for further details), modal composition calculations suggest that about 0.1–2 vol.% of fluid may have been produced by metamorphic reactions during the Alpine burial.

However, several authors state that the salinity increase in fluid inclusions from cover veins with the proximity to the Triassic dolomites (Bernard, 1978; Gratier and Vialon, 1980; Gratier et al., 1973; Nziengui, 1993; Poty, 1967) supports the idea of small-scale percolation of Triassic-derived NaCl-rich fluids in the overlying Liassic cover. This is consistent with our salinity data obtained from fluid inclusions in veins from Huez (i.e., just above the Triassic layer, location 1 in Figs. 2, 3A), which correspond to the highest salinity values measured by these authors for the whole Bourg d'Oisans sedimentary cover. Moreover, the isochors calculated from our fluid inclusion microthermometric data (Fig. 9) are in good agreement with those calculated from previous data and reported in Fig. 12 (Bernard, 1978; Gratier et al., 1973; Nziengui, 1993).

On the contrary, the isotopic signature of calcite from Triassic layer veins is clearly different (i.e., lower  $\delta^{18}\text{O}$  and  $\delta^{13}\text{C}$ ) from that of the host-rock calcite (Fig. 7A). This isotopic disequilibrium between Triassic vein and host-rock (Fig. 7B–C) suggests external fluid infiltration through the vein during calcite precipitation. In addition, the Triassic vein isotopic ratio is intermediate between Triassic host-rock and basement isotopic ratios (Figs. 7A, 11), suggesting that the thin Triassic layer underwent basement-derived fluid infiltrations.

#### 7.1.3. Local infiltration of basement-derived fluid in the cover above shear zones

From isotopic data, it can be concluded that there was no massive influx of external fluids in Liassic layers. However, trace element analysis gives complementary insights on the source and scale of fluid circulation. Above the Huez shear zone, veins from Villard-Reculas, situated a few hundred meters above the basement (location 2 in Figs. 2, 3A, 10D), have very similar composition patterns than their host-rocks (Fig. 10C), which is consistent with a local origin of both vein filling elements and fluid (Fig. 10D). On the contrary, in the Huez samples situated just above the sheared basement-cover interface (location 1 in Figs. 2, 3A, 10D), veins present strong relative enrichments in Cr, Co, Ni, Zr, and Hf compared to their host-rock (Fig. 10C). Interestingly, the underlying mafic basement rocks (location 3 in Figs. 2, 3A, 10D) present similar trace element patterns in both sheared and unsheared zones for all elements but Cr, Co, and Ni, suggesting that their concentration may have been modified during shearing: these elements are specifically enriched in the talc-rich zone of the sheared basement (Fig. 10A). Moreover, SEM analysis revealed that, in this talc-rich zone, Ni- and Cr-bearing minerals are Variscan pyrite cores and chromite crystals, respectively (Fig. 5). Both minerals were partially dissolved and replaced by Alpine hydrated phases, as described in detail below, suggesting a release of both Ni and Cr in the infiltrating fluid phase during the Alpine basement shearing.

Therefore, there are clues that small amounts of basement-derived fluids percolated into the cover just above the Huez shear zone (Fig. 10D). However, these fluid amounts must have been very limited: the isotopic signature of this basement-derived fluid, which was

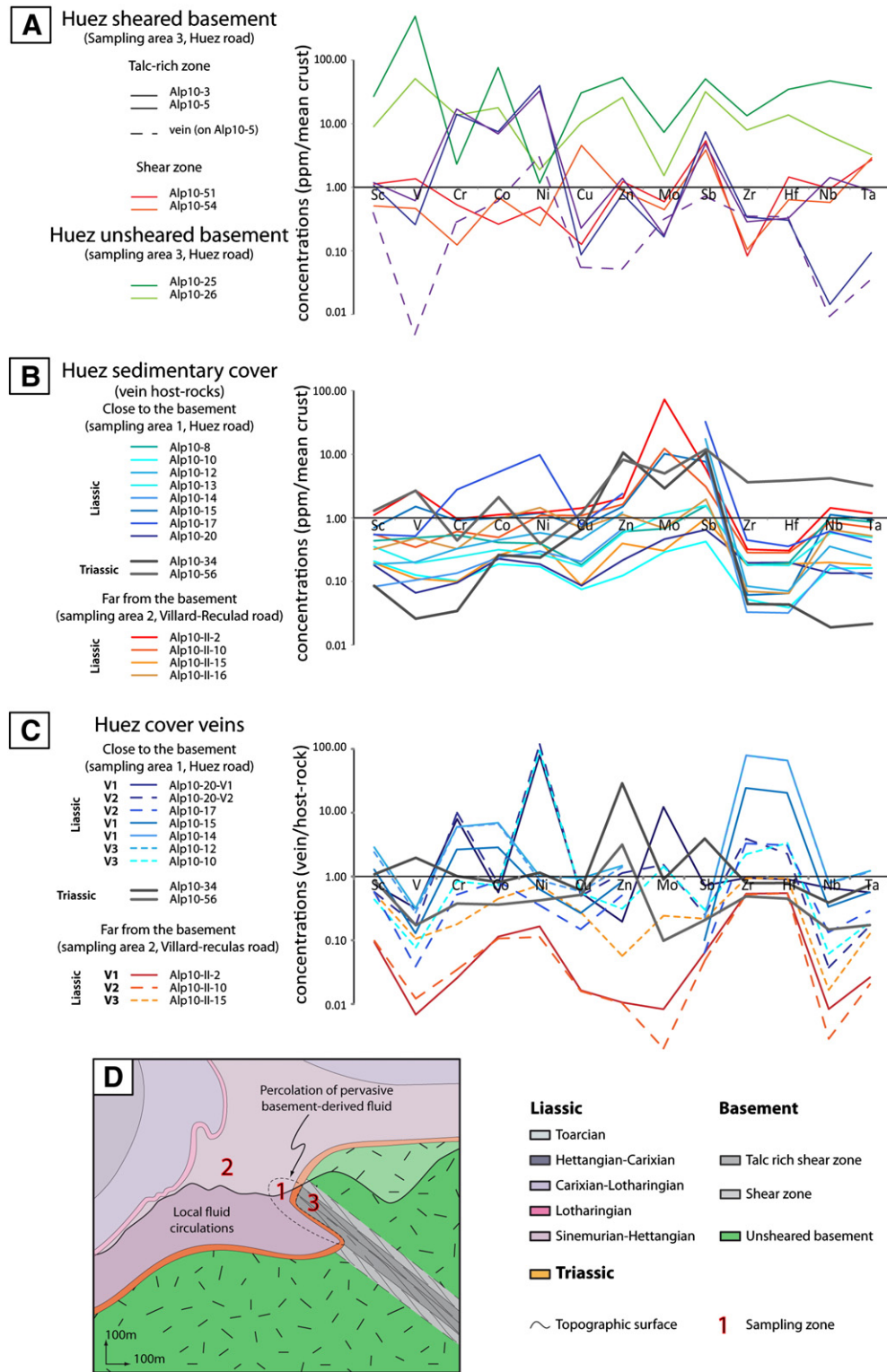


**Fig. 10.** Trace element patterns for Huez basement shear zone and its sedimentary cover. A. Trace element compositions for Huez basement shear zone and its inner talc-rich zone, and outside the shear zone, normalized to the mean crust (Taylor and McLennan, 1985). B. Trace element compositions for cover host-rocks above the Huez basement shear zone normalized to the mean crust. C. Trace element compositions of cover veins normalized to their host-rock composition, above the Huez basement shear zone. D. Cross-section of the Huez shear zone with sampling area locations, and schematic representation of fluid circulation in the cover above the Huez shear zone. All over the cover, fluid circulations are limited to the sedimentary scale, except a few meters above the shear zone, where trace element data provide evidence of spatially-limited basement-derived fluid percolations.

obviously very different from that of cover rocks (i.e., calcite basement vein, Fig. 7A), affected only the Triassic layer (still attached to basement rocks), and was buffered by the isotopic signature of Liassic cover rocks. Moreover, the scale of infiltration of these basement-derived fluids was spatially limited to a few tens of meters in the cover (Fig. 10D). Indeed,

in Villard-Reculad (location 2 in Figs. 2, 3A, 10D), the trace element signal of basement-derived fluids is not detected anymore. The very limited flux of percolating fluids through the cover rocks is in agreement with the structural observation that veins are mostly isolated structures and do not constitute a connected network in the metasedimentary

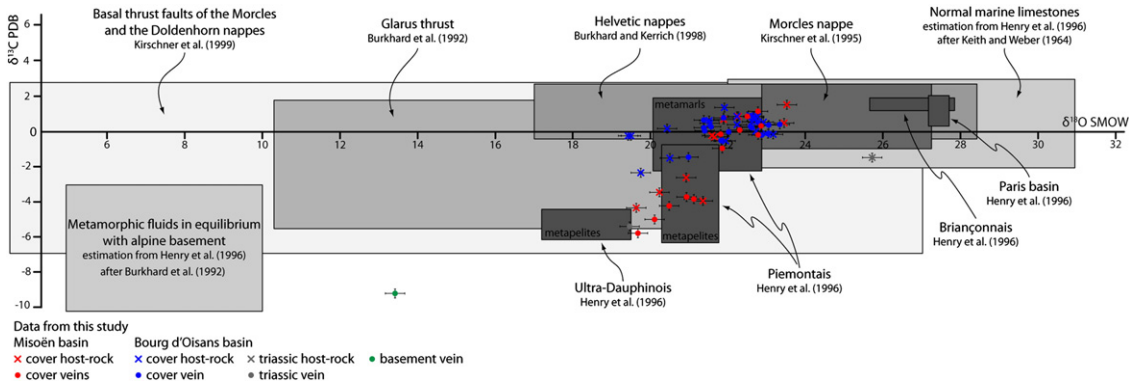


**Fig. 11.** Isotopic ratios ( $\delta^{18}\text{O}$  and  $\delta^{13}\text{C}$ ) of cover veins and their host-rocks, compared to typical isotopic signatures of different Alpine areas: Ultra-Dauphinois, Briançonnais, Piemontais (Henry et al., 1996), Mörclès nappe (Kirschner et al., 1995), all the Helvetic nappes (Burkhard and Kerrich, 1988), and across major tectonic contacts in the ECM cover: the Glarus thrust (Burkhard et al., 1992) and the basal thrust of the Mörclès and the Doldenhorn nappes (Kirschner et al., 1999). Typical isotopic signature of marine limestone and calculated isotopic composition of Alpine basement fluids (estimations in Henry et al. (1996), from Burkhard et al. (1992) and Keith and Weber (1964) are also reported.

cover. It is interesting to note that the three successive vein generations of Huez samples present a similar basement-derived trace element signal. Therefore, there is no evidence for significant change in the scale of the fluid system during progressive deformation.

Moreover, in the Triassic dolomites still attached to the sheared basement, sphalerite, pyrite, and galena were observed to have crystallized in calcite fractures. Accordingly, compared to their host-rocks, veins in these Triassic layers show enrichments in some trace elements ( $\text{Zn} \pm \text{Sb}$ ; Fig. 10B) that are locally concentrated in the underlying talc-rich Huez basement shear zone (Fig. 10A), which supports the hypothesis of local basement-derived fluid percolations into the cover, through the basement-cover interface, above basement shear zones. Interestingly, in La Gardette ancient gold mine (situated in the Bourg d'Oisans basin), similar basement-derived fluid percolation across the unconformity was observed, although this zone is not situated above a basement

shear zone: a 500 meter long quartz dyke enriched in sulfur minerals is rooted in the Pelvoux granite (source of the sulfur minerals; Poty, 1967), affects the overlying gneiss and ends in the first 30 m of the Triassic dolomite (Cathelineau et al., 1990; Poty, 1967). However, the source of this local basement fluid circulation remains unclear (Feybesse et al., 2004; Marignac et al., 1997).

Therefore, this study shows that fluid circulations in the Oisans sedimentary cover were restricted to the lithological unit scale, i.e., the fluid system was almost closed. However, when shortening started, small amounts of basement-derived fluids percolated above the basement shear zones into the cover on a few tens of meter scale. These conclusions are in agreement with those of Garofalo (2012) who showed that Alpine marine sediments were generally metamorphosed under closed-system conditions whatever the locality and the metamorphic grade, i.e., element mobility from the sediments is negligible except locally, in narrow shear zones where some specific elements (including Ni and Cr) can be strongly mobilized by the circulation of ascendant fluids.

## 7.2. Implications for basement fluids

The mobilization of specific elements (Cr, Co, Ni) from basement rocks provides insights into the basement fluid properties during shearing. Samples from the talc-rich area of the Huez basement shear zone (Table 1) show enrichments in Cr, Co, Ni ( $\pm \text{Zn}$  and  $\text{Sb}$ ; Fig. 10A) relative to the mean crust, similarly to talc and chlorite schists observed in other settings (e.g., Spandler et al., 2008). The retrogression of the amphibole + plagioclase Variscan paragenesis to Alpine phyllosilicates (chlorite + talc; Fig. 5A) required fluid influx during shearing. Moreover, the partial replacement of the Variscan pyrite crystals by Fe-oxide or hydroxide (i.e., rims around pyrite cores, Fig. 5B) during Alpine fluid infiltration (i.e., linked to talc formation in amphibole cracks) and the partial dissolution of Variscan chromite crystals in Alpine shear zones (Fig. 5C–D–E) suggest a progressive evolution towards more oxidizing conditions in basement rocks with their shearing. Indeed, the internal fluid in equilibrium with the Variscan paragenesis was likely reduced, as shown by the presence of both pyrite and chromite, whereas the external fluid responsible for Alpine phyllosilicate formation had to be more oxidizing.

Interestingly, the pyrite cores are Ni-rich whereas Ni is absent from the Fe-oxide or hydroxide rims, which means that Ni may have been released into the fluid phase during pyrite Alpine oxidation. Similarly, Cr-rich chromite crystals are partially dissolved and surrounded by Cr-rich Alpine chlorite, suggesting Cr release during the Alpine shearing (Fig. 5C–D–E). Therefore, the oxidizing fluid circulating in the basement shear zone may have become enriched in  $\text{SO}_4^{2-}$  while dissolving sulfur minerals such as pyrite, which was obviously a good complexing anion for metallic elements such as Cr and Ni that were released coevally by

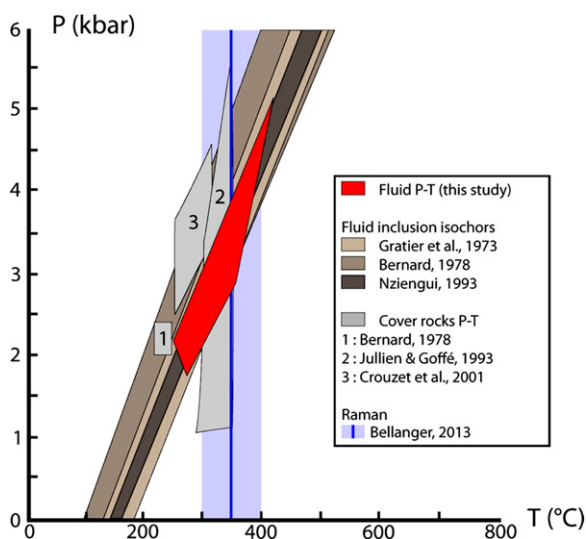


**Fig. 12.** Fluid P-T range for cover rocks above the Huez shear zone. Fluid temperatures are estimated on the basis of equilibrium temperature between quartz and calcite in veins. Fluid pressures are estimated from fluid temperatures and isochors (PT relationship) computed from microthermometric analysis. Gray zones are P-T conditions determined from (1) fluid inclusion studies in quartz and previous K/Na temperature estimation in albite (Bernard, 1978; Poty et al., 1974); (2) stability of pyrophyllite + margarite + cookeite + quartz + Mg-rich-chlorite (Jullien and Goffé, 1993); (3) previous fluid inclusion studies and Cuire pyrrhotite temperature (Crouzet et al., 2001 and references therein). T max reached by cover rocks ( $350\text{ }^{\circ}\text{C} \pm 50\text{ }^{\circ}\text{C}$ ) was estimated by RAMAN spectroscopy of the carbonaceous matter (Bellanger, 2013). Brown zones are isochor domains calculated from the microthermometric data (homogenization and melting temperatures) of Bernard (1978), Gratier et al. (1973) and Nziengui (1993), using the equation of Bodnar and Vityk (1994).

pyrite and chromite partial dissolution. Similar mobilization of metallic low-mobility elements (e.g., Ni, Cr, Zn) by S-rich fluids was observed by Li et al. (2013) and Spandler et al. (2011) in subduction zone settings. This  $\text{SO}_4^{2-}$  fluid enrichment is supported by the presence of small barytine crystals (identified by SEM) in both the calcite vein in the basement talc-rich zone (Alp10-5, Fig. 10A) and in a Cr-Ni-rich V1 vein in Huez cover rocks, as well as the precipitation of various sulfur minerals (such as sphalerite, galena, pyrite) in Triassic veins above the shear zone. Element mobility was thus clearly controlled by both basement rock mineralogy (enriched in transition metals) and fluid composition, i.e., pH,  $\text{FO}_2$  and ligands (e.g., Cathelineau et al., 1990), as was observed for REE complexing and mobility in the Mont Blanc basement shear zones (Rolland et al., 2003).

Small amounts of this basement-derived fluid enriched in transition metals (Cr, Ni) percolated into the overlying metasedimentary cover. Its mixing with the  $\text{CO}_2$ -rich internally-produced cover fluid, locally at equilibrium with the cover carbonates, may have induced Ni and Cr release in veins within the Lias sediments, and similar sulfur mineral precipitation when percolating through the Triassic layer; the metallic element precipitation may have been caused by sudden changes in fluid pH conditions and  $X_{\text{CO}_2}$  (e.g., Gao et al., 2007).

### 7.3. Fluid pressure and temperature in the metasedimentary cover

Here, we combine the analysis of quartz and calcite isotopic signatures in veins to microthermometric measurements of fluid inclusions from the same veins to estimate both the temperature and pressure of the cover vein fluids above basement shear zones. Indeed, quartz and calcite present evidences of textural equilibrium in most veins (Fig. 6F), which implies their co-precipitation under similar P-T conditions. Oxygen isotopic fractionation being essentially dependent on temperature, the temperature of quartz + calcite co-precipitation in veins was estimated from the independent analysis of their  $\delta^{18}\text{O}$  signature (equation in Sharp and Kirschner, 1994; Table 2).

As most late veins only contain calcite and no quartz, all the veins analyzed in terms of P-T conditions are V1 or early veins (except Alp10-18, Table 2; Fig. 9). Above the Huez shear zone (locations 1 and 2 in Figs. 2–3A), the quartz–calcite equilibrium temperatures range from 144 to 421 °C ( $\pm 30$  °C, Table 2), but most samples plot in the 250–360 °C range (locations 1 and 2 in Table 2). Most of these calculated vein temperatures are consistent with the previous peak temperature estimates for the Bourg d’Oisans and the Mizoën basin cover rocks (300–350 °C, Fig. 12; Bellanger, 2013; Crouzet et al., 2001; Jullien and Goffé, 1993). For a few veins from Huez, combining quartz–calcite equilibrium temperatures to the isochors determined from microthermometric analysis of fluid inclusions in the same quartz or calcite crystals (Fig. 9) provides estimates of the vein fluid pressures (Fig. 12). The fluid pressures range from 1.7 to 5.1 kbar (Fig. 9), which is quite similar to the lithostatic pressure range estimated for the metamorphic peak conditions in these rocks (2–5 kbar, Jullien and Goffé, 1993; Poty et al., 1974; Fig. 12). Gratier and Vialon (1980) estimated fluid pressures of 2 kbar from microthermometric data coupled to temperature data estimated by Poty et al. (1974) for basement vein fluid inclusions (Na/K ratios), which corresponds to the low pressure bound estimated here. However, recalculating the isochors from the microthermometric data of Gratier and Vialon (1980) using the now widely used equation of Bodnar and Vityk (1994) results in steeper isochors (Fig. 12), coherent with ours (Fig. 9), and therefore would undoubtedly tend to higher pressure estimates.

Moreover, as stated before, the  $\delta^{18}\text{O}$  values for vein calcite are very close to that of the host-rock calcite (Fig. 7A), suggesting that most veins formed close to the peak temperature conditions. However, some V1 veins may have formed during the end of prograde path because (1) the veins are filled by local infiltration of fluid released by prograde metamorphic dehydration reactions into the host-rock and (2) their fluid temperature can be as low as 144 °C.

For the Mizoën basin (locations 4 and 5 in Table 2), the calculated vein temperatures range from 306 to 436 °C, but most temperatures are above 400 °C, which exceeds the estimated peak temperature in the Oisans cover rocks. As discussed in Appendix A.1, these higher values could be the result of an incomplete quartz powder decarbonation for some samples, due to the particularly fine micro-indentation of quartz and calcite in veins.

### 7.4. Structural implications

In the talc-rich area of basement shear zones, the abundant crystallization of phyllosilicate minerals (talc and chlorite) required the influx of important amounts of external fluids. This talc-rich zone is only a few meters wide inside the shear zone, suggesting that fluid circulation in the basement may have been channelized in the core of the shear zone. Therefore, basement shear zones served as preferential pathways for crustal fluid circulation, as observed in the Mont Blanc (Guermani and Pennacchioni, 1998; Rolland et al., 2003; Rossi et al., 2005) and Aar (Goncalves et al., 2012; Marquer and Burkhard, 1992; Oliot et al., 2010, 2014) basement rocks, as well as in other collisional or subduction-related settings (e.g., Badertscher et al., 2002; Burkhard et al., 1992; John et al., 2008; Kirschner et al., 1999; McCaig et al., 2000a,b). In turn, the crystallization of talc and chlorite may have enhanced deformation localization by progressive softening of these shear zones (Carpenter et al., 2009; Collettini et al., 2009; Moore and Rymer, 2007; Niemeijer et al., 2010) similarly to the weakening effect of the feldspar phengitization (e.g., Bos and Spiers, 2000, 2002; Gueydan et al., 2004; Oliot et al., 2010, 2014).

In northern ECM (e.g., Mont Blanc massif, Rolland et al., 2003), the largest basement shear zones may have propagated as thrusts into the overlying sedimentary cover with ongoing deformation, and became pathways for important amounts of basement-derived fluids, causing meter-scale opening of the fluid system, as recorded by isotopic data in the Aar–Gothard massifs (Burkhard et al., 1992; Kirschner et al., 1999; Marquer and Burkhard, 1992; Fig. 11). In contrast, in the Oisans massif, which underwent less shortening than northern ECM, the basement shear zones did not propagate into the sedimentary cover, preventing important circulation of basement-derived fluids in cover rocks, as shown by isotopic and cathodoluminescence data. Nevertheless, the trace element pattern of cover veins situated just above the basement-cover interface (Huez, location 1 in Figs. 2, 3A) recorded the infiltration of small amounts of basement-derived fluids, whereas in eastern Oisans (La Grave), where the basement is not sheared and the cover decoupled from the basement above a décollement, both isotopic and trace element patterns showed that cover rocks were isolated from basement fluid infiltration (i.e., closed system, Henry et al., 1996).

Even if only small amounts of basement-derived fluids percolated through the interface in western Oisans, they give key insights into the timing of shear zone development and basement shortening. Indeed, the percolation of basement-derived fluids into Huez cover rocks was recorded in the three successive vein generations (V1 to V3), which are all related to the E–W collisional shortening and subsequent basin inversion (Bellahsen et al., 2012; Boutoux et al., 2014; Gratier and Vialon, 1980). Moreover, the basement shear zones are also kinematically consistent with the East–West shortening. Therefore, the percolation of basement-derived fluids into cover veins, which occurred during the entire basin deformation history, unambiguously witnesses that the shortening of the Oisans massif basement began very early during the inversion of the pre-orogenic extensional basins, and lasted during the whole shortening phase. This is supported by geochronology data: the basement shear zone activation was dated to 30–34 Ma in the Pelvoux massif (Simon-Labréte et al., 2009), and mineralizations into basement veins give a date of 36–39 Ma (Cathelineau et al., 1990; Marignac et al., 1997; La Gardette gold mine) for basement fluid circulations. The simultaneous deformation of basement and cover basins

during collisional shortening, hence the absence of decoupling between cover and basement, supports an overall thick-skinned structural style.

If most of our cover veins are related to the ductile deformation event (V1, V2 and most V3), it cannot be excluded that part of the V3 veins could be associated to late brittle exhumation phase. Late fluid circulation, from 17 Ma to less than 10 Ma, was evidenced from late vertical veins in basement shear zones from the northern Belledonne and the Aar massifs (Berger et al., 2013; Gasquet et al., 2010), showing that fluid circulation lasted until the brittle exhumation of the ECM.

## 8. A model for fluid flow in the External Crystalline Massifs

Our results, combined with results of other fluid system studies in the ECM (Abarb et al., 2002; Badertscher et al., 2002; Burkhardt and Kerrich, 1988; Burkhardt et al., 1992; Kirschner et al., 1995, 1999; Marquer and Burkhardt, 1992; Rolland et al., 2003) allow proposing a general fluid flow model for the Alpine external zone. This fluid flow model is illustrated together with a schematic kinematic model of the ECM shortening in Fig. 13.

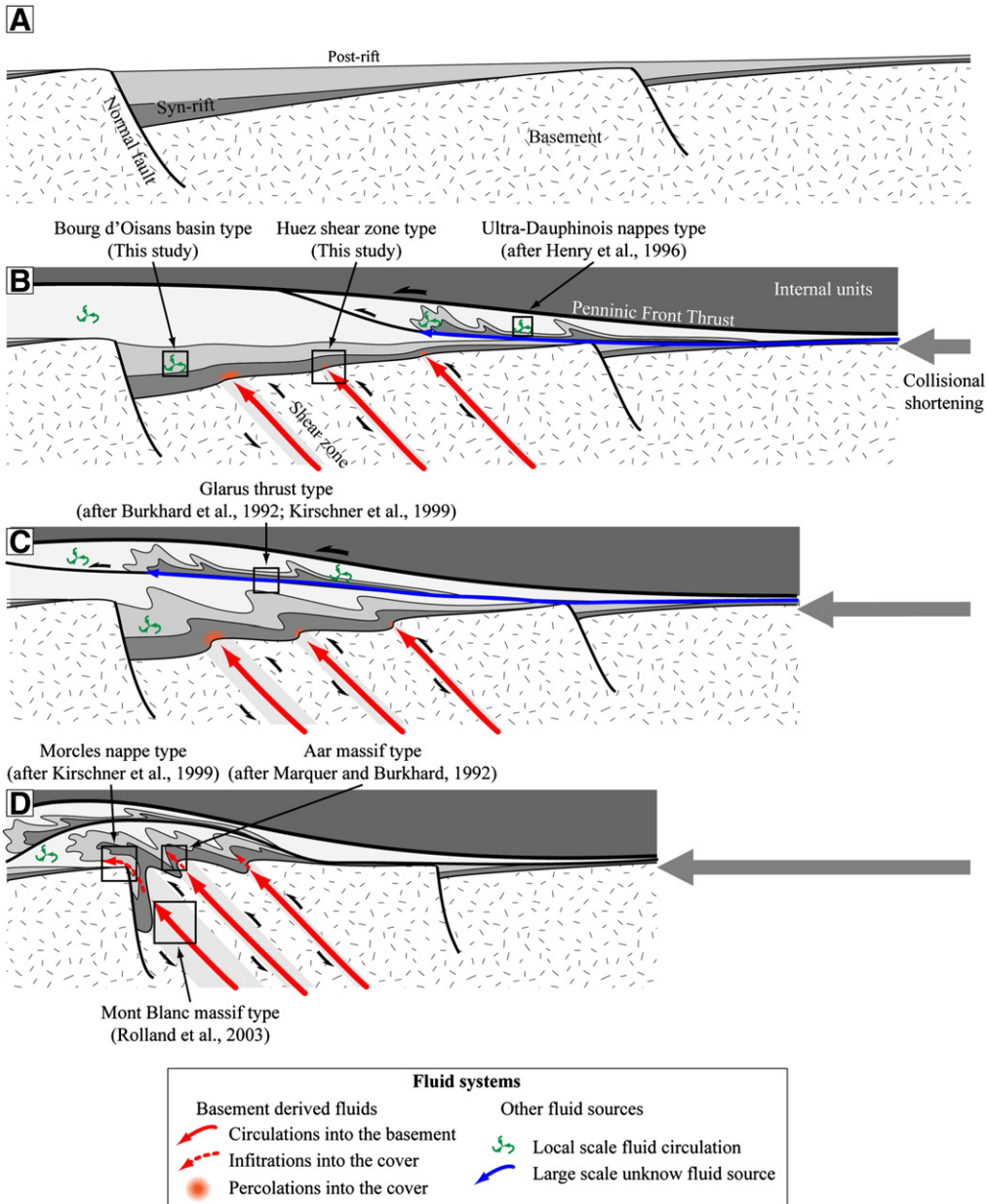


**Fig. 13.** Fluid system evolution through time and across the strike of the external Alpine Arc, proposed from the compilation of several studies of the fluid system in the ECM and projected on a schematic ECM inherited basin cross-section. A. Initial stage: proximal margin with tilted blocks. B. Initiation of Alpine collisional shortening. The crust is progressively buried to mid-crustal depth under the internal units. In the easternmost part (just below the Penninic Frontal Thrust), the cover is detached from the basement and fluid circulations are restricted to lithologic unit scale above and under the thrusts. In the inherited basins, basement shear zones channelized large-scale fluid circulations, while the cover was disharmonically folded with local-scale fluid circulations and limited basement-derived fluid percolation just above shear zones. C. Higher amount of Alpine collisional shortening. Large sedimentary nappes overthrust the inverted basins, allowing the channelization of large-scale fluid flow into the thrusts. In inverted basins, fluid channelization into basement shear zones gave rise to important fluid–rock interactions. D. Late Alpine collisional shortening. Fluid circulations in the sedimentary nappes were local at this time and flew across presently inactive thrusts. Inverted basins were progressively pinched and their cover formed recumbent anticlines with overhanging limbs strongly sheared by the basement shear zone propagation, in which basement-derived fluids probably circulated. Within cover nappes, basement-derived fluid flowed up to hundreds of meters above propagated basement shear zones.

The overall tectonic framework is the Alpine burial and collisional shortening of the European crust (see simplified section in Fig. 13A). Probably during the end of the crust burial beneath the internal units, i.e., the end of prograde path (Fig. 13B) or at the metamorphic peak, first ductile deformations initiate (S1 cleavage and associated veins, see Boutoux et al., 2014 for more details). At this stage, for example in the present-day eastern part of the Oisans massif (Ultra-Dauphinois, Fig. 13B), the cover has been locally detached from its basement and progressively overthrust the western inherited basins. In both the allochthonous and autochthonous units, the fluid system is overall closed (Henry et al., 1996) with isotopic reequilibration restricted to each lithologic unit. However, it is possible that large-scale fluid circulations occurred in the cover thrusts-décollement (thick blue arrow in Fig. 13B), as such zones were not sampled by Henry et al. (1996). Meanwhile, in the western part, the inherited basins (e.g., Oisans massif, Fig. 13B) were progressively shortened and inverted. Shear zones developed within the basement while the overlying cover was disharmonically folded (e.g., Bourg d'Oisans basin, Fig. 13B). Basement-derived fluids were channelized into basement shear zones, and locally infiltrated the overlying cover over a few tens of meters (e.g., the Huez shear zone described in this study, Fig. 13B). In the rest of the cover, i.e., far from basement shear zones, the fluid system remained closed, restricted to the sedimentary unit scale, and involved mainly formation and metamorphic fluids. To sum up, in the Oisans area (Bourg d'Oisans basin, Huez shear zone, Ultra-Dauphinois nappes, Fig. 13B), collisional shortening remained moderate, about 11.5 km (16.1%, Bellahsen et al., 2012, 2014) and thus we face an “immature” fluid system in the cover of the inherited basins.

With increasing shortening, coupled to increasing P-T conditions, basement shear zones developed through the increasing connection of anastomosed shear bands (Marquer and Burkhard, 1992) and were most likely the location of channelized basement-derived fluids (e.g., Aar, Goncalves et al., 2012; Mont Blanc, Rolland et al., 2003) with important fluid-rock interactions, highlighted by REE fractionation (Rolland et al., 2003). In areas where the cover was detached from the basement (e.g., Glarus thrust, Fig. 13C), fluid flow was channelized in the main thrust (Abart et al., 2002; Badertscher et al., 2002; Burkhard and Kerrich, 1988; Burkhard et al., 1992; Kirschner et al., 1999). The related presently one meter-thick calc-mylonite (Schmid et al., 1981) was the locus of  $\delta^{18}\text{O}$ -depleted fluid circulation, as attested by isotopic fronts (e.g., Badertscher et al., 2002), where metamorphic fluids derived from deeper (southern) parts of the thrust mixed with formation fluids northward. The extreme localization of the deformation (1 meter-thick thrust zone) may have permitted a very localized and fast fluid flow that explains the isotopic anomalies. Similar fluid flow probably occurred in the Moine Thrust that is also a very thin and localized thrust accommodating tens of km of shortening (McClay and Coward, 1981). To sum up, in and around the northern ECM (Mont Blanc, Glarus thrust above the Aar massif) where the amount of shortening was higher than in Oisans (10.6 km, 38.3% in the Mont Blanc massif and 12 km, 40% in the Aar massif vs. 11.5 km, 16.1% in the Oisans massif; Bellahsen et al., 2014), the structural style is still a mixed thin- and thick-skinned style. Large-scale fluid flow may occur both in basement shear zones and in large sedimentary nappe thrusts, and may have initiated during the previous step (Fig. 13B) although poorly documented.

In the last step of our model, the structural style switched to a pure thick-skinned style (Fig. 13D), i.e., the shortening was almost exclusively accommodated in basement shear zones. The fluid flow was still active in basement shear zones (Fig. 13D) both in the Mont Blanc (Rolland et al., 2003) and the Aar massifs (Marquer and Burkhard, 1992). The cover of these massifs, the Morcles nappe (Escher et al., 1993) and the Doldenhorn nappe (Burkhard and Kerrich, 1988), respectively, were disharmonically folded as recumbent anticlines with strongly sheared overhanging limbs. Although Burkhard and Kerrich (1988) and Marquer and Burkhard (1992) showed that basement-derived fluids circulated in the major cover thrusts of the Aar massif,

the reverse limbs of the above-cited nappes do not systematically bear evidence of large-scale fluid flow (Kirschner et al., 1999; red dashed line in Fig. 13D). These reverse limbs are interpreted as large shear zones (Ramsay et al., 1983). Thus, it appears that the shearing geometry distribution made them less prone to large-scale circulation of important amounts of basement-derived fluids, in contrast to localized structures such as few meter-thick thrust zones, which were efficient drains for localized, large-scale, fluids.

## 9. Conclusions

In this contribution, we analyzed the fluid system(s) in the inner part of the Alpine External zone, the External Crystalline Massifs (ECM). In this domain, pre-orogenic Liassic extensional basins were buried at mid-crustal depth and inverted during the collisional phase of the Alpine orogeny. During the basin shortening, the sedimentary cover was disharmonically folded over localized basement shear zones. Fluid circulations are associated to this deformation. Isotopic analyses and cathodoluminescence observations show that, as for the ultra-Dauphinois cover nappes, fluid circulations were restricted to local scale in the metasedimentary cover. In the basement shear zones, fluids were channelized as for the other ECM. On the basis of trace element analyses, we highlight the small amount of basement-derived fluid percolation in the metasedimentary cover above such shear zones. Stable  $^{18}\text{O}$  isotopic signature coupled to microthermometric analyses of fluid inclusions from cover veins above the Huez basement shear zone provides estimates of fluid temperature and pressure: around 250–400 °C and 2–5 kbar for veins that thus formed close to peak P-T conditions. These veins formed contemporaneously with the onset of and during the basin inversion and basement collisional shortening.

Our study documents the evolution of the fluid system in an area undergoing limited crustal collisional shortening. It therefore nicely complements earlier studies of fluid systems further North in the Western Alps (Mont Blanc and Aar massifs) where the crust suffered more shortening, and allow one to build a consistent conceptual model of fluid flow at the scale of the whole external Alpine collision zone.

Supplementary data to this article can be found online at <http://dx.doi.org/10.1016/j.lithos.2014.07.005>.

## Acknowledgments

The authors thank L. Jolivet and M. Bellanger for discussions and X. and M.O. Gonord for their warm welcome during field trips. Thanks are due to O. Boudouma, M. de Rafelis, N. Labourdette, J. Thibéroux and E. Delairis for their help with SEM, cathodoluminescence, calcite isotopic analysis, microthermometry and thin section preparation, respectively. Y. Rolland and an anonymous reviewer are acknowledged for their constructive reviews that helped at improving the manuscript. Thanks are due to M. Scambelluri for editorial handling. This study was funded by the “Syster” INSU program, BRGM contract L10 U 044 and ISTE (UPMC) funds.

## References

- Abart, R., Badertscher, N., Burkhard, M., Povoden, E., 2002. Oxygen, carbon and strontium isotope systematics in two profiles across the Glarus thrust: implications for fluid flow. Contributions to Mineralogy and Petrology 143 (2), 192–208. <http://dx.doi.org/10.1007/s00410-001-0326-5>.
- Badertscher, N.P., Beaudoin, G., Therrien, R., Burkhard, M., 2002. Glarus overthrust: a major pathway for the escape of fluids out of the Alpine orogen. Geology 30 (10), 875–878. [http://dx.doi.org/10.1130/0091-7613\(2002\)030-0875:GOAMPF>2.0.CO;2](http://dx.doi.org/10.1130/0091-7613(2002)030-0875:GOAMPF>2.0.CO;2).
- Barbier, R., Barfety, J.C., Bocquet, A., Bordet, P., Le Fort, P., Meloux, J., Mouterde, R., Pêcher, A., Petiteville, M., 1973. Carte géologique de la France (1/50,000), feuille La Grave (798). Bureau de Recherches géologiques et minières, Orléans.
- Barfety, J.C., Bordet, P., Carme, F., Debelmas, J., Meloux, M., Montjuvent, G., Mouterde, R., Sarrot-Reynauld, J., 1972. Carte géologique de la France (1/50,000), feuille Vizille (797). Bureau de Recherches géologiques et minières, Orléans.

- Bellahsen, N., Jolivet, L., Lacombe, O., Bellanger, M., Boutoux, A., Garcia, S., Moutherau, F., LePourhiet, L., Gumiaux, C., 2012. Mechanisms of margin inversion in the external Western Alps: implications for crustal rheology. *Tectonophysics* 560–561, 62–83. <http://dx.doi.org/10.1016/j.tecto.2012.06.022>.
- Bellahsen, N., Moutherau, F., Boutoux, A., Bellanger, M., Lacombe, O., Jolivet, L., Rolland, Y., 2014. Collision kinematics in the western external Alps. *Tectonics* 33. <http://dx.doi.org/10.1002/2013TC003453>.
- Bellanger, M., Bellahsen, N., Jolivet, L., Baudin, T., Augier, R., Boutoux, A., 2014. Basement shear zones development and shortening kinematics in the Ecrins Massif, Western Alps. *Tectonics* 33 (2), 84–111.
- Bellanger, M., 2013. Recourcissement alpin du massif des Ecrins: Cinématique, calendrier tectonique & conditions pression-température, (Thesis 3e cycle) 2013. Univ Orléans.
- Berger, A., Gnos, E., Janots, E., Whitehouse, M., Soom, M., Frei, R., Waight, T.E., 2013. Dating brittle tectonic movements with cleft monazite: fluid–rock interaction and formation of REE-minerals. *Tectonics* 32 (5), 1176–1189. <http://dx.doi.org/10.1002/tect.20071>.
- Bernard, D., 1978. Microthermométric des inclusions fluides de cristaux syn-cinétiques. Application à la couverture sédimentaire du Nord Pelvoux. Unpublished PhD Thesis, Univ Grenoble, 133 pp.
- Bohdan, R.J., 1993. Revised equation and table for determining the freezing point depression of H<sub>2</sub>O–NaCl solutions. *Geochimica et Cosmochimica Acta* 57 (3) (United States).
- Bohdan, R.J., Vityk, M.O., 1994. Interpretation of Microthermometric Data for H<sub>2</sub>O–NaCl Fluid Inclusions. *Fluid Inclusions in Minerals: Methods and Applications*. pp. 117–130.
- Bons, P.D., 2000. The formation of veins and their microstructures. *Journal of the Virtual Explorer* 2, 12.
- Bos, B., Spiers, C.J., 2000. Effect of phyllosilicates on fluid-assisted healing of gouge-bearing faults. *Earth and Planetary Science Letters* 184 (1), 199–210. [http://dx.doi.org/10.1016/S0012-821X\(00\)00304-6](http://dx.doi.org/10.1016/S0012-821X(00)00304-6).
- Bos, B., Spiers, C.J., 2002. Frictional-viscous flow of phyllosilicate-bearing fault rock: microphysical model and implications for crustal strength profiles. *Journal of Geophysical Research* 107 (B2), 2028. <http://dx.doi.org/10.1029/2001JB000301>.
- Boutoux, A., Bellahsen, N., Lacombe, O., Verlaguet, A., Moutherau, F., 2014. Inversion of pre-orogenic extensional basins in the external Western Alps: structure, microstructures and restoration. *Journal of Structural Geology* 60, 13–29. <http://dx.doi.org/10.1016/j.jsg.2013.12.014>.
- Burkhard, M., Kerrich, R., 1988. Fluid regimes in the deformation of the Helvetic nappes, Switzerland, as inferred from stable isotope data. *Contributions to Mineralogy and Petrology* 99 (4), 416–429. <http://dx.doi.org/10.1007/BF00371934>.
- Burkhard, M., Kerrich, R., Maas, R., Fyfe, W.S., 1992. Stable and Sr-isotope evidence for fluid advection during thrusting of the Glarus nappe (Swiss Alps). *Contributions to Mineralogy and Petrology* 112 (2–3), 293–311. <http://dx.doi.org/10.1007/BF00310462>.
- Carpenter, B.M., Marone, C., Saffer, D.M., 2009. Frictional behavior of materials in the 3D SAFOD volume. *Geophysical Research Letters* 36 (5). <http://dx.doi.org/10.1029/2008GL036660>.
- Cartwright, I., Buick, I.S., 2000. Fluid generation, vein formation and the degree of fluid–rock interaction during decompression of high-pressure terranes: the Schistes Lustrés, Alpine Corsica, France. *Journal of Metamorphic Geology* 18 (6), 607–624. <http://dx.doi.org/10.1046/j.1525-1314.2000.00280.x>.
- Cathelineau, M., Boiron, M.-C., Holliger, P., Poty, B., 1990. Metallogenesis of the French part of the Variscan orogen. Part II: time–space relationships between U, Au and Sn/W ore deposition and geodynamic events – mineralogical and U/Pb data. *Tectonophysics* 177, 59–79.
- Challandes, N., Marquer, D., Villa, I.M., 2008. PTt modelling, fluid circulation, and 39Ar–40Ar and Rb–Sr mica ages in the Aar Massif shear zones (Swiss Alps). *Swiss Journal of Geosciences* 101 (2), 269–288. <http://dx.doi.org/10.1007/s0015-008-1260-6>.
- Collettini, C., Viti, C., Smith, S.A., Holdsworth, R.E., 2009. Development of interconnected talc networks and weakening of continental low-angle normal faults. *Geology* 37 (6), 567–570. <http://dx.doi.org/10.1130/G25645A.1>.
- Crouzet, C., Ménard, G., Rochette, P., 2001. Cooling history of the Dauphinoise Zone (Western Alps, France) deduced from the thermopaleomagnetic record: geodynamic implications. *Tectonophysics* 340 (1), 79–93. [http://dx.doi.org/10.1016/S0040-1951\(01\)00142-1](http://dx.doi.org/10.1016/S0040-1951(01)00142-1).
- Dumont, T., Champagnac, J.D., Crouzet, C., Rochat, P., 2008. Multistage shortening in the Dauphiné zone (French Alps): the record of Alpine collision and implications for pre-Alpine restoration. *Swiss Journal of Geosciences* 101 (1), 89–110. [http://dx.doi.org/10.1007/978-3-7643-9500-4\\_6](http://dx.doi.org/10.1007/978-3-7643-9500-4_6).
- Dumont, T., Schwartz, S., Guillot, S., Simon-Labric, T., Tricart, P., Jourdan, S., 2012. Structural and sedimentary records of the Oligocene revolution in the Western Alpine arc. *Journal of Geodynamics* 18–38. <http://dx.doi.org/10.1016/j.jog.2011.11.006>.
- Escher, A., Masson, H., Steck, A., 1993. Nappe geometry in the western Swiss Alps. *Journal of Structural Geology* 15 (3), 501–509. [http://dx.doi.org/10.1016/0191-8141\(93\)90144-Y](http://dx.doi.org/10.1016/0191-8141(93)90144-Y).
- Etheridge, M.A., 1983. Differential stress magnitudes during regional deformation and metamorphism: upper bound imposed by tensile fracturing. *Geology* 11 (4), 231–234. [http://dx.doi.org/10.1130/0091-7613\(1983\)11<231:DSMDR>2.0.CO;2](http://dx.doi.org/10.1130/0091-7613(1983)11<231:DSMDR>2.0.CO;2).
- Feybesse, J.L., Bally-Maître, M.C., Feraud, J., 2004. La mine médiévale d'argent du Pontet, une fente alpine contemporaine de la surrection des massifs cristallins? *Comptes Rendus Geoscience* 336 (14), 1255–1264. <http://dx.doi.org/10.1016/j.crte.2004.06.009>.
- Fisher, D.M., Brantley, S.L., Everett, M., Dzvonik, J., 1995. Cyclic fluid flow through a regionally extensive fracture network within the Kodiak accretionary prism. *Journal of Geophysical Research: Solid Earth* (1978–2012) 100 (B7), 12881–12894. <http://dx.doi.org/10.1029/94JB02816>.
- Gao, G.Y., Yao, K.L., Şaşioğlu, E., Sandratskii, L.M., Liu, Z.L., Jiang, J.L., 2007. Half-metallic ferromagnetism in zinc-blende Ca<sub>x</sub>Sr<sub>1-x</sub> and BaC from first principles. *Physical Review B* 75 (17), 174442. <http://dx.doi.org/10.1103/PhysRevB.75.174442>.
- Garfalo, P.S., 2012. The composition of Alpine marine sediments (Bündnerschiefer Formation, W Alps) and the mobility of their chemical components during orogenic metamorphism. *Lithos* 128, 55–72. <http://dx.doi.org/10.1016/j.lithos.2011.10.009>.
- Gasquet, D., Bertrand, J.-M., Paquette, J.-L., Lehmann, J., Ratov, G., Guedes, R.D.A., Tiepolo, M., Boullier, A.-M., Scaillet, S., Nomade, S., 2010. Miocene to Messinian deformation and hydrothermal activity in a pre-Alpine basement massif of the French western Alps: new U–Th–Pb and argon ages from the Lauzière massif. *Bulletin de la Société Géologique de France* 181, 227–241. <http://dx.doi.org/10.2113/gssgbull.181.3.227>.
- Goncalves, P., Oliot, E., Marquer, D., Connolly, J.A.D., 2012. Role of chemical processes on shear zone formation: an example from the Grimsel metagranodiorite (Aar massif, Central Alps). *Journal of Metamorphic Geology* 30 (7), 703–722. <http://dx.doi.org/10.1111/j.1525-1314.2012.00991.x>.
- Gratier, J.P., Vialon, P., 1980. Deformation pattern in a heterogeneous material: folded and cleaved sedimentary cover immediately overlying a crystalline basement (Oisans, French Alps). *Tectonophysics* 65 (1), 151–179. [http://dx.doi.org/10.1016/0040-1951\(80\)90228-0](http://dx.doi.org/10.1016/0040-1951(80)90228-0).
- Gratier, J.P., Lejeune, B., Vergne, J.L., 1973. Etude des déformations de la couverture et des bordures sédimentaires des massifs cristallins externes de Belledonne, des Grandes Rousses et du Pelvoux (Thesis 3e cycle) Univ. Grenoble.
- Guermani, A., Pennacchioni, G., 1998. Brittle precursors of plastic deformation in a granite: an example from the Mont Blanc massif (Helvetic, western Alps). *Journal of Structural Geology* 20 (2–3), 135–148. [http://dx.doi.org/10.1016/S0191-8141\(97\)00080-1](http://dx.doi.org/10.1016/S0191-8141(97)00080-1).
- Gueydan, F., Leroy, Y.M., Jolivet, L., 2004. Mechanics of low-angle extensional shear zones at the brittle–ductile transition. *Journal of Geophysical Research: Solid Earth* (1978–2012) 109 (B12). <http://dx.doi.org/10.1029/2003JB002806>.
- Guillot, S., Ménéot, R.P., 2009. Paleozoic evolution of the external crystalline massifs of the Western Alps. *Comptes Rendus Geoscience* 341 (2), 253–265. <http://dx.doi.org/10.1016/j.crte.2008.11.010>.
- Henry, C., Burkhard, M., Goffe, B., 1996. Evolution of synmetamorphic veins and their wallrocks through a Western Alps transect: no evidence for large-scale fluid flow. Stable isotope, major- and trace-element systematics. *Chemical Geology* 127 (1), 81–109. [http://dx.doi.org/10.1016/0099-2541\(95\)00106-9](http://dx.doi.org/10.1016/0099-2541(95)00106-9).
- John, T., Klemd, R., Gao, J., Garbe-Schönberg, C.D., 2008. Trace-element mobilization in slabs due to non steady-state fluid–rock interaction: constraints from an eclogite-facies transport vein in blueschist (Tianshan, China). *Lithos* 103 (1), 1–24. <http://dx.doi.org/10.1016/j.lithos.2007.09.005>.
- John, T., Gussoni, N., Podladchikov, Y.Y., Bebout, G.E., Dohmen, R., Halama, R., Klemd, R., Magna, T., Seitz, H.M., 2012. Volcanic arcs fed by rapid pulsed fluid flow through subducting slabs. *Nature Geoscience* 5 (7), 489–492. <http://dx.doi.org/10.1038/ngeo1482>.
- Jullien, M.B., Goffé, B., 1993. Occurrences de cookéite et de pyrophyllite dans les schistes du Dauphinois (Isère, France): conséquences sur la répartition du métamorphisme dans les zones externes alpines. *Schweizerische Mineralogische und Petrographische Mitteilungen* 73, 357–363.
- Kirschner, D.L., Sharp, Z.D., Masson, H., 1995. Oxygen isotope thermometry of quartz–calcite veins: unraveling the thermal-tectonic history of the subgreenschist facies Morcles nappe (Swiss Alps). *Geological Society of America Bulletin* 107 (10), 1145–1156. [http://dx.doi.org/10.1130/0016-7606\(1995\)107<1145:OMTOQC>2.3.CO;2](http://dx.doi.org/10.1130/0016-7606(1995)107<1145:OMTOQC>2.3.CO;2).
- Kirschner, D.L., Masson, H., Sharp, Z.D., 1999. Fluid migration through thrust faults in the Helvetic nappes (Western Swiss Alps). *Contributions to Mineralogy and Petrology* 136 (1–2), 169–183. <http://dx.doi.org/10.1007/s004100050530>.
- Keith, M.L., Weber, J.N., 1964. Carbon and oxygen isotopic composition of selected limestone and fossils. *Geochim. Cosmochim. Acta* 28, 1787–1816. [http://dx.doi.org/10.1016/0016-7037\(64\)90022-5](http://dx.doi.org/10.1016/0016-7037(64)90022-5).
- Kretz, R., 1983. Symbols for rock-forming minerals. *American Mineralogist* 68, 277–279.
- Leloup, P.H., Arnaud, N., Sobel, E.R., Lacassini, R., 2005. Alpine thermal and structural evolution of the highest external crystalline massif: the Mont Blanc. *Tectonics* 24 (4), TC 4002. <http://dx.doi.org/10.1029/2004TC001676>.
- Lemoine, M., Gidon, M., Barfety, J.C., 1981. Les massifs cristallins externes des Alpes occidentales: d'anciens blocs basculés nus à Lias lors du rifting téthysien. *Comptes Rendus de l'Académie des Sciences Paris* 292, 917–920.
- Lemoine, M., Dardeau, G., Delpech, P.Y., Dumont, T., De Graciansky, P.C., Graham, R., Jolivet, L., Roberts, D., Tricart, P., 1989. Extension synrift et failles transformantes jurassiques dans les Alpes occidentales. *Comptes Rendus de l'Académie des Sciences Série 2* 309 (17), 1711–1716.
- Li, J.L., Gao, J., John, T., Klemd, R., Su, W., 2013. Fluid-mediated metal transport in subduction zones and its link to arc-related giant ore deposits: constraints from a sulfide-bearing HP vein in lawsonite eclogite (Tianshan, China). *Geochimica et Cosmochimica Acta* 120, 326–362. <http://dx.doi.org/10.1016/j.gca.2013.06.023>.
- Machel, H.G., Burton, E.A., 1991. Factors governing cathodoluminescence in calcite and dolomite, and their implications for studies of carbonate diagenesis. In: Barker, C.E., Kopp, O.C. (Eds.), *Luminescence Microscopy and Spectroscopy: Qualitative and Quantitative Applications*. Soc. for Sediment. Geol., pp. 37–57.
- Marignac, C., Cathelineau, M., Bank, D., Boiron, M.-C., Ayt Ougougdal, M., Argouarc'h, Y., Poty, B., 1997. Alpine fault sealing at the contact between a crystalline basement and its sedimentary cover: La Gardette (French Alps). *European current research on fluid inclusions. Biennial symposium No 14*, Nancy, FRANCE (01/07/1997), pp. 194–195.
- Marquer, D., Burkhard, M., 1992. Fluid circulation, progressive deformation and mass-transfer processes in the upper crust: the example of basement-cover relationships in the External Crystalline Massifs, Switzerland. *Journal of Structural Geology* 14 (8), 1047–1057. [http://dx.doi.org/10.1016/0191-8141\(92\)90035-U](http://dx.doi.org/10.1016/0191-8141(92)90035-U).
- Marquer, D., Calcagno, P., Barfety, J.C., Baudin, T., 2006. 3D modeling and kinematics of the external zone of the French Western Alps (Belledonne and Grand Châtelard Massifs, Maurienne Valley, Savoie). *Eclogae Geologicae Helvetiae* 99 (2), 211–222. <http://dx.doi.org/10.1007/s00015-006-1183-z>.

- McCaig, A.M., Wayne, D.M., Marshall, J.D., Banks, D., Henderson, I., 1995. Isotopic and fluid inclusion studies of fluid movement along the Gavarnie Thrust, central Pyrenees; re-action fronts in carbonate mylonites. *American Journal of Science* 295 (3), 309–343. <http://dx.doi.org/10.2475/ajs.295.3.309>.
- McCaig, A.M., Tritila, J., Banks, D.A., 2000a. Fluid mixing and recycling during Pyrenean thrusting: evidence from fluid inclusion halogen ratios. *Geochimica et Cosmochimica Acta* 64 (19), 3395–3412. [http://dx.doi.org/10.1016/S0016-7037\(00\)00437-3](http://dx.doi.org/10.1016/S0016-7037(00)00437-3).
- McCaig, A.M., Wayne, D.M., Rosenbaum, J.M., 2000b. Fluid expulsion and dilatancy pumping during thrusting in the Pyrenees: Pb and Sr isotope evidence. *Geological Society of America Bulletin* 112 (8), 1199–1208. [http://dx.doi.org/10.1130/0016-7606\(2000\)112<1199:FEADPD>2.0.CO;2](http://dx.doi.org/10.1130/0016-7606(2000)112<1199:FEADPD>2.0.CO;2).
- McClay, K.R., Coward, M.P., 1981. The Moine thrust zone: an overview. *Geological Society, London, Special Publications* 9 (1), 241–260. <http://dx.doi.org/10.1144/GSLSP.1981.009.01.22>.
- Moore, D.E., Rymer, M.J., 2007. Talc-bearing serpentinite and the creeping section of the San Andreas fault. *Nature* 448 (7155), 795–797. <http://dx.doi.org/10.1038/nature06064>.
- Niemeier, A., Marone, C., Elsworth, D., 2010. Fabric induced weakness of tectonic faults. *Geophysical Research Letters* 37 (3). <http://dx.doi.org/10.1029/2009GL041689>.
- Nziengui, J.J., 1993. *Excès d'argon radiogénique dans les quartz des fissures tectoniques: implications pour la datation des séries métamorphiques (Thesis 3e cycle) L'exemple de la coupe de la Romanche-Alpes occidentales françaises*. Univ. Grenoble (209 pp.).
- Oliot, E., Goncalves, P., Marquer, D., 2010. Role of plagioclase and reaction softening in a metagranite shear zone at mid-crustal conditions (Gotthard Massif, Swiss Central Alps). *Journal of Metamorphic Geology* 28 (8), 849–871. <http://dx.doi.org/10.1111/j.1525-1314.2010.00897.x>.
- Oliot, E., Goncalves, P., Schulmann, K., Marquer, D., Lexa, O., 2014. Mid-crustal shear zone formation in granitic rocks: constraints from quantitative textural and crystallographic preferred orientations analyses. *Tectonophysics* 612–613, 63–80. <http://dx.doi.org/10.1016/j.tecto.2013.11.032>.
- Oliver, N.H., Bons, P.D., 2001. Mechanisms of fluid flow and fluid–rock interaction in fossil metamorphic hydrothermal systems inferred from vein–wallrock patterns, geometry and microstructure. *Geofluids* 1 (2), 137–162. <http://dx.doi.org/10.1046/j.1468-8123.2001.00013.x>.
- Penniston-Dorland, S.C., Sorensen, S.S., Ash, R.D., Khadke, S.V., 2010. Lithium isotopes as a tracer of fluids in a subduction zone mélange: Franciscan Complex, CA. *Earth and Planetary Science Letters* 292 (1), 181–190. <http://dx.doi.org/10.1016/j.epsl.2010.01.034>.
- Poty, B., 1967. *La croissance des cristaux de quartz dans le filons sur l'exemple du filon de La Gardette (Bourg d'Oisans) et des filons du massif du Mont-Blanc (Thesis 3eme cycle)*. Univ. Nancy (164 pp.).
- Poty, B.P., Stalder, H.A., Weisbrod, A.M., 1974. Fluid inclusion studies in quartz from fissures of Western and Central Alps. *Schweizerische Mineralogische und Petrographische Mitteilungen* 54 (1974), 717–752.
- Ramsay, J.G., 1980. The crack-seal mechanism of rock deformation. *Nature* 284, 135–139.
- Ramsay, J.G., Casey, M., Kligfield, R., 1983. Role of shear in development of the Helvetic fold-thrust belt of Switzerland. *Geology* 11 (8), 439–442. [http://dx.doi.org/10.1130/0091-7613\(1983\)11<439:ROSIDO>2.0.CO;2](http://dx.doi.org/10.1130/0091-7613(1983)11<439:ROSIDO>2.0.CO;2).
- Roedder, E., 1984. Fluid inclusion, reviews in mineralogy. *Mineralogical Society of America* 12, 644.
- Rolland, Y., Cox, S., Boullier, A.M., Pennacchioni, G., Mancktelow, N., 2003. Rare earth and trace element mobility in mid-crustal shear zones: insights from the Mont Blanc Massif (Western Alps). *Earth and Planetary Science Letters* 214 (1), 203–219. [http://dx.doi.org/10.1016/S0012-821X\(03\)00372-8](http://dx.doi.org/10.1016/S0012-821X(03)00372-8).
- Rolland, Y., Rossi, M., Cox, S.F., Corsini, M., Mancktelow, N., Pennacchioni, G., Fornari, M., Boullier, A.M., 2008.  $^{40}\text{Ar}/^{39}\text{Ar}$  dating of synkinematic white mica: insights from fluid–rock reaction in low-grade shear zones (Mont Blanc Massif) and constraints on timing of deformation in the NW external Alps. *Geological Society, London, Special Publications* 299 (1), 293–315. <http://dx.doi.org/10.1144/SP299.18>.
- Rossi, M., Rolland, Y., Vidal, O., Cox, S.F., 2005. Geochemical variations and element transfer during shear-zone development and related épisyénites at middle crust depths: insights from the Mont Blanc granite (French–Italian Alps). In: Bruhn, D., Burlini, L. (Eds.), *High Strain Zones: Structure and Physical Properties*. Geological Society of London, Special Publications, 245, pp. 373–396.
- Salatün, A., Villemant, B., Semet, M.P., Staudacher, T., 2010. Cannibalism of olivine-rich cumulate xenoliths during the 1998 eruption of Piton de la Fournaise (La Réunion hotspot): implications for the generation of magma diversity. *Journal of Volcanology and Geothermal Research* 198 (1), 187–204. <http://dx.doi.org/10.1016/j.jvolgeores.2010.08.022>.
- Schmid, S.M., Casey, M., Starkey, J., 1981. The microfabrics of calcite tectonites from the Helvetic nappes (Swiss Alps). *Geological Society, London, Special Publications* 9 (1), 151–158. <http://dx.doi.org/10.1144/GSLSP.1981.009.01.13>.
- Sharp, Z.D., Kirschner, D.L., 1994. Quartz–calcite oxygen isotope thermometry: a calibration based on natural isotopic variations. *Geochimica et Cosmochimica Acta* 58 (20), 4491–4501. [http://dx.doi.org/10.1016/0016-7037\(94\)90350-6](http://dx.doi.org/10.1016/0016-7037(94)90350-6).
- Simon-Labré, T., Rolland, Y., Dumont, T., Heymes, T., Authemayou, C., Corsini, M., Fornari, M., 2009.  $^{40}\text{Ar}/^{39}\text{Ar}$  dating of Penninic Front tectonic displacement (W Alps) during the lower oligocene (31–34 Ma). *Terra Nova* 21 (2), 127–136. <http://dx.doi.org/10.1111/j.1365-3121.2009.00865.x>.
- Spandler, C., Hermann, J., Faure, K., Mavrogenes, J.A., Arculus, R.J., 2008. The importance of talc and chlorite “hybrid” rocks for volatile recycling through subduction zones; evidence from the high-pressure subduction mélange of New Caledonia. *Contributions to Mineralogy and Petrology* 155 (2), 181–198. <http://dx.doi.org/10.1007/s00410-007-0236-2>.
- Spandler, C., Pettke, T., Rubatto, D., 2011. Internal and external fluid sources for eclogite-facies veins in the Monviso meta-ophiolite, Western Alps: implications for fluid flow in subduction zones. *Journal of Petrology* 52 (6), 1207–1236. <http://dx.doi.org/10.1093/petrology/egr025>.
- Stünitz, H., 1998. Syndeformational recrystallization—dynamic or compositionally induced? *Contributions to Mineralogy and Petrology* 131 (2–3), 219–236. <http://dx.doi.org/10.1007/s004100050390>.
- Taylor, S.R., McLennan, S.M., 1985. *The Continental Crust: Its Composition and Evolution*. Blackwell, Oxford.
- Touret, J.L., Frezzotti, M.L., 2003. *Fluid inclusion in high pressure and ultrahigh pressure metamorphic rocks*. In: Carswell, D.A., Compagnoni, R. (Eds.), *Ultrahigh Pressure Metamorphism*. Eötvös University Press, Budapest, pp. 467–487.
- Tricart, P., Lemoine, M., 1986. From faulted blocks to megamullions and megaboudins: Thethyan heritage in the structure of the Western Alps. *Tectonics* 5 (1), 95–118. <http://dx.doi.org/10.1029/TC0051001p00095>.
- Verlaguet, A., Goffé, B., Brunet, F., Poinsot, C., Vidal, O., Findling, N., Menut, D., 2011. Metamorphic veining and mass transfer in a chemically closed system: a case study in Alpine metabauxites (western Vanoise). *Journal of Metamorphic Geology* 29 (3), 275–300. <http://dx.doi.org/10.1111/j.1525-1314.2010.00918.x>.
- Walther, J.V., Orville, P.M., 1982. Volatile production and transport in regional metamorphism. *Contributions to Mineralogy and Petrology* 79 (3), 252–257. <http://dx.doi.org/10.1007/BF00371516>.
- Wilkin, R.T., Barnes, H.L., Brantley, S.L., 1996. The size distribution of frambooidal pyrite in modern sediments: an indicator of redox conditions. *Geochimica et Cosmochimica Acta* 60 (20), 3897–3912. [http://dx.doi.org/10.1016/0016-7037\(96\)00209-8](http://dx.doi.org/10.1016/0016-7037(96)00209-8).
- Yardley, B.W.D., Bottrell, S.H., 1992. Silica mobility and fluid movement during metamorphism of the Connemara schists, Ireland. *Journal of Metamorphic Geology* 10 (3), 453–464. <http://dx.doi.org/10.1111/j.1525-1314.1992.tb00096.x>.

### V.3. Bilan : l'ouverture des systèmes géochimiques avec la déformation progressive.

Le signal géochimique (signature isotopique, cathodoluminescence) de la calcite des veines et de leur roche encaissante sont similaires, ce qui indique le remplissage de ces veines par des mécanismes de pression-dissolution et diffusion locale de matière sur de faibles distances. Cette étude nous a donc permis de montrer que l'hypothèse de transferts de matière restreints à petite échelle (unité lithologique) au sein de la couverture des bassins de l'Oisans est bien valable.

Un autre résultat important de cette étude est qu'on observe tout de même des indices (éléments traces) de percolation de fluides dérivés du socle dans des veines de la couverture situées juste à l'aplomb des cisaillements de socle (sur quelques dizaines de mètres). Il semble donc que les fluides profonds circulant à grande échelle dans les bandes de cisaillement du socle arrivent à percoler au travers du contact socle-couverture, malgré l'absence de propagation de ces bandes de cisaillement dans la couverture. On note cependant que ces indices de circulations de fluides profonds sont ténus et seules de faibles quantités de fluides dérivés du socle (trop peu pour modifier le signal isotopique) ont pu percoler dans la couverture, sur quelques dizaines de mètres seulement. Cette interprétation a cependant des implications structurales importantes puisqu'elle nous permet de montrer par des arguments géochimiques que les déformations du socle et de la couverture des bassins de l'Oisans sont synchrones.

L'intégration de ces résultats à un scénario de l'évolution des systèmes de circulation des fluides avec la déformation progressive nous permet d'avancer plusieurs résultats. Ainsi il apparaît que les circulations de fluides à grande échelle sont effectives dans le socle des MCE dès l'initiation de la déformation, datée approximativement au pic de métamorphisme (e.g. [Challandes et al., 2008](#) ; [Cenki-Tok et al., 2013](#) ; [Bellanger et al., 2015](#)). Dans la couverture des bassins hérités, les premières étapes du raccourcissement sont marquées par des circulations uniquement locales. Ce n'est que dans les dernières étapes de l'inversion des bassins, lorsque le raccourcissement devient suffisamment important pour permettre la propagation des cisaillements dans la couverture, que l'on voit les systèmes de circulation de fluides s'ouvrir localement dans la couverture des MCE septentrionaux (e.g. la nappe de Morcles).

Enfin, on a pu mesurer la pression et la température des fluides contemporains du pic de métamorphisme et à l'équilibre avec les roches de la couverture. Ces résultats, en accord avec

les études précédentes (e.g. Jullien et Goff, 1993), ne permettent pas de préciser la pression enregistrée par la couverture.

#### **VI.4. Question soulevées.**

On peut s'interroger ensuite sur les distances de propagation des signatures en éléments traces du socle dans la couverture. Ainsi, dans le cas où des fluides de socle sont chenalés dans la couverture, la signature du socle en éléments traces est-elle conservée dans le cisaillement ? Dans les veines à proximité du cisaillement ? La réponse à cette question pourrait alors nous permettre mieux caractériser l'enracinement de certaines structures. Ainsi le flanc inverse de la nappe de Morcles est fortement cisaillé, ce qui permet l'ouverture locale du système isotopique. L'analyse de la signature en éléments trace du flanc inverse de la nappe de Morcles et celle de la Mont Blanc Shear zone pourrait nous permettre d'appuyer ou non l'extension du cisaillement de socle dans la nappe de Morcles.

## **VI : Étude thermo-mécanique de l'inversion collisionnelle des bassins hérités de la marge européenne.**

**Inherited basin inversion style: thermo-mechanical modelling and comparison with the western External Alps.**

Manfred Lafosse, Alexandre Boutoux, Nicolas Bellahsen, Laetitia Le Pourhiet.

Article à soumettre à la revue *Tectonophysics* :

### **VI.1. Cadre et intérêt de l'étude.**

Dans les chapitres précédents, on a contraint la cinématique de raccourcissement de la croûte lors de l'inversion collisionnelle d'une marge depuis l'échelle du prisme jusqu'à celle d'un bassin. Ces études se basent notamment sur les interprétation de non réactivation des failles normales bordières des bassins hérités dans les massifs cristallins externes des Alpes de l'Ouest (e.g. faille du col d'Ornon, [Bellahsen et al., 2012](#) et de Chamonix, [Boutoux et al., 2014a](#)).

L'inversion de bassins extensifs a été étudiée depuis de nombreuses années dans la littérature à partir d'études de terrain (e.g., Butler) mais aussi de modélisation analogique (e.g. [Bonnet et al., 2007](#) ; [Bonini et al., 2012](#)) et numériques (e.g. [Buiter and Pfiffner 2003, 2009](#)). Ces auteurs ont pu déterminer (voire quantifier) certains des paramètres influant sur la géométrie de l'inversion des bassins tels que la friction internes des failles, leur orientation ou encore l'état thermique du socle et de la couverture du bassin. Dans les Alpes de l'Ouest, comme on l'a vu, certaines failles profondément enfouies ne sont pas réactivées lors de la collision (e.g. faille du Col d'Ornon, de Mizoën, [Boutoux et al., 2014a](#)). D'autres, enfouies moins profondément, sont réactivées, au moins partiellement réactivée (e.g. faille de Saint Laurent, [Fig. 2](#) dans [Lafosse et al., in prep](#)). Ces failles ont approximativement la même orientation pré-collisionnelle (e.g. [Bellahsen et al., 2014](#)). On peut ainsi s'interroger sur l'impact de leur profondeur d'enfouissement sur leur structure thermique et donc sur la réactivation des accidents hérités.

Le but de cette étude est donc de tester l'impact de l'enfouissement sur la réactivation des failles normales des bassins. On cherche ainsi à mieux comprendre l'évolution du style d'inversion collisionnel des bassins hérités de la marge européenne.

Ainsi, on construit un modèle thermo-mécanique constitué d'un bassin large de 13 km et profond de 5 km, aux dimensions cohérentes avec celles des bassins hérités alpins. Ce bassin est constitué de sédiments syn-rift moins résistants que le socle. L'ensemble du modèle est recouvert d'une couche peu résistante dite post-rift et de couches allochtones, elles aussi peu résistantes.

## **VI.2. Article.**

# Inherited basin inversion style: thermo-mechanical modelling and comparison with the western External Alps.

Lafosse, Manfred<sup>1,2</sup>; Boutoux, Alexandre<sup>1,2</sup>; Bellahsen Nicolas<sup>1,2</sup>, Le Pourhiet, Laetitia<sup>1,2</sup>

<sup>1</sup> Sorbonne Université, Univ. Paris 06, UMR 7193, ISTeP, F-75005 Paris, France.

<sup>2</sup> CNRS, UMR 7193, ISTeP, F-75005 Paris, France.

## Abstract

Inversion style of inherited extensive basins in the Western Alps is investigated with the help of thermo-mechanical modeling. 2D models consist on a half-graben embedded in a strong crust (basement) and filled with weak syn-rift sediments (cover). We investigate the relative influence of the basin normal fault internal friction versus basin burial depth under a 0 km to 8 km thick overlying nappe and 2 km of post rift deposits. We use a simple visco-plastic model with a symmetrical shortening. The inherited normal fault is implemented as a curved layer with a variable friction coefficient ( $\mu$ ) ranging between 0.1 and 0.6. We find that under a small burial the basin act as a mechanical defect in the crust structure. The symmetrical shortening of the crust leads to formation of a pop-down fold beneath the basin. Fault reactivation is inhibited with increasing basin burial resulting in basin pinching and cover extrusion. Basin pinching is accompanied by diffuse basement shearing while cover extrusion reflects the existence of a rheological contrast at basement/cover interface. Results are consistent with the evolution of the structures of external Western Alps inherited half-grabens, inverted after their burial underneath the Alpine internal units during the orogen collisional phase.

## I. Introduction

Restoration of several orogen external units show that continental collision involves most of the time previously stretched lithosphere structured by inherited extensive basins (e.g. the Alps, [Lemoine et al., 1989](#); the Pyrenees, [Beaumont et al., 2000](#); Taiwan, [Lacombe and Mouthereau, 2002](#)). Depending on the thermal state of the margin involved in the collision, crustal behavior in the orogen external zones can be describe through two deformation pattern end-members ([Mouthereau et al., 2013](#)): an “old” and “cold” lithosphere, structured several hundreds Ma before the collision, is deformed with “thin-skinned” style and the décollement

of the cover (syn- and post-rift sediments) from its basement. Margin deformations are then localized into cover and shortening is essentially accommodated by the cover thrusts while the basement is underplated under the orogen inner parts (e.g., Himalayan thrust belt, [Bollinger et al. 2004](#)). On the contrary, a “young” and “hot” lithosphere, structured few tens to hundreds Ma before its inversion, is deformed with “thick-skinned” style (e.g., Taiwan, [Mouthereau and Petit, 2003](#)). This is characterized by the shortening of (at least) the entire upper crust with the common reactivation of well oriented tectonic accidents (e.g., the inherited normal faults).

Compressional inversion of former extensional sedimentary basins is a particularly common phenomenon. Thus, numerous authors investigated the different parameters effects on the basin deformation style during its inversion. [Bonini et al. \(2012\)](#) synthesized the analogue modeling literature to define three main factors governing inherited normal fault reactivation: the steepness of the fault, its angle with compression, and the fault frictional resistance. Depending on the variation of those three parameters, several reactivation geometries can be defined as the development of low angle overthrusting, the extension in reverse of reactivated normal fault, development of basement short-cut ([Bonini et al., 2012 and reference therein](#)). Inherited basin inversion styles were also investigated using numerical modeling (e.g. [Buiter and Pfiffner, 2003](#), [Buiter et al., 2009](#)) and authors highlighted several parameters (as post-rift sediment thickness, internal normal fault strain, basin filling thermal conductivity, crustal geometry) facilitating the basin inversion as the thermal state of the crust. Moreover, they highlighted the localization of compressional deformation at the basin level during crustal shortening due to the rheological interface between weak basin filling and strong surrounding crust .

The western Alps are interpreted as shortened with a “thick-skinned” style with inverted inherited basin. Yet, the inversion deformation style is not consistent across strike. In the inner most part of the external zone, the External Cystalline Massifs, the inherited basins are inverted but the normal fault bordering them are not reactivated fore some ([Fig. 1; Bellahsen et al., 2012](#), [Boutoux et al., 2014a](#)). For author ones those fault can be reactivated during basin inversion ([Burkhard, 1988](#) ; [Burkhard et Sommaruga, 1998](#) ; [Bonnet et al., 2007](#)) while, the well oriented inherited normal faults are reactivated western of the ECM ([Fig. 1](#); e.g., [Roure and Colletta 1996](#); [Deville et al., 1994](#); [Deville and Chauviere, 2000](#); in [Bellahsen et al. 2014](#)). In this contribution we investigate conditions that control the style of inversion of normal fault during collision.

To date, the influence of burial on the basin deformation style during its inversion has never been investigated with thermo-mechanical models. Yet, burial influences the strength of basins, basement and faults by modifying the thermal profile of the crust. We use here a visco-plastic thermo-mechanical code to perform a parametric study of the relative effect of variable coefficient friction and variable burial of pre-shortening structures. In order to avoid mechanical interferences resulting from complicated geometry of structures insides the model, we limited the model to a single half-graben bordered by a listric normal fault covered with a constant thin layer of post-rift sediments and a variable thickness layer representing the allochthonous nappe. The model geometry is consistent with dimensions estimated from Western Alps half-graben cross-section restorations (Dumont et al., 2008; Bellahsen et al., 2012; Boutoux et al., 2014a) and non-inverted rift and half-graben geometry (Colletta et al., 1988). We use passive markers to compute the total strain evolution and the direction of lineations to highlight the deformation pattern (Le Pourhiet et al., 2012). Our model is two-dimensional and therefore does not take into account of oblique deformations.

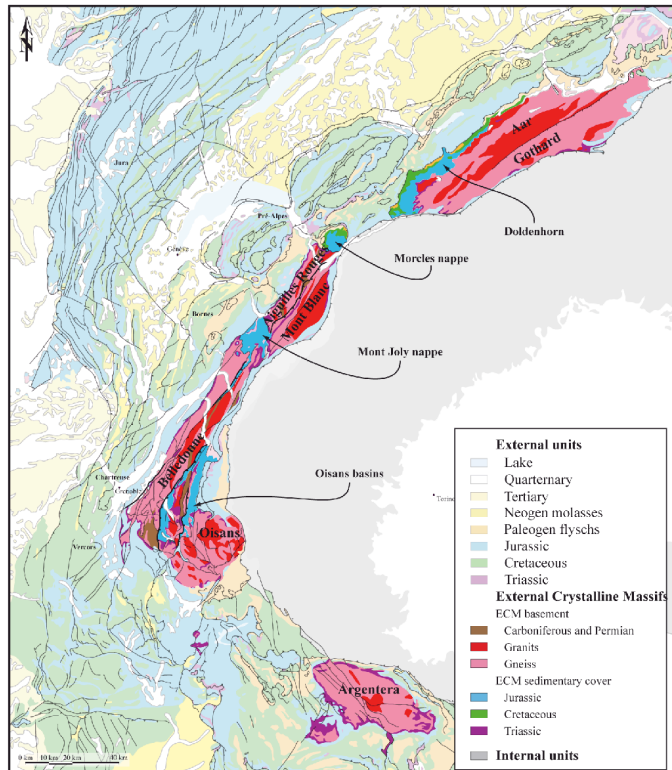


**Figure 1** Geological map of the Western Alps. Location of the External Crystallin Massifs and their sedimentary covers. ECM are inverted extensive inherited basins with no evidence of major normal faults bordering them inverse reactivation.

## II. Geological setting

### II.1. The external Western alps

The Western Alpine arc results from the Ligurian ocean closure followed by the continental subduction of European margin distal parts (now the internal alpine units) and finally the continental collision with Adria. The European margin was previously stretched during Liassic to Dogger times, and structured by extensive basins and crustal-scale normal faults (Barfety et al., 1979; Lemoine et al., 1986; Lemoine and Tricart, 1986; de Graciansky et al., 1989). The external part of the Western Alps (the Dauphinois zone) results from the European margin inversion during the Alpine collision phase. During this phase, starting at 30-35 Ma, the proximal part of European margin was inverted and partially buried under the internal units due to the activation of the Penninic Frontal Thrust (Rolland et al., 2008; Simon-Labbrick et al., 2009; Sanchez et al., 2011; Dumont et al., 2012; Bellahsen et al., 2012, 2014; Bellanger et al., 2014). The external zone consist of the External Crystalline Massifs (ECM: Oisans, Belledone, Aiguilles Rouges, Mont-Blanc, Aar-Gothard massifs; Fig. 1) that have been buried during collision and the fold-and-thrust-belt that experienced much less burial, (Vercors, Chartreuse, Aravis, Bornes massifs; Fig. 1). The ECM were buried to mid crustal depth with increasing depth from about 10 km in the Oisans massif to about 15 km in the Mont Blanc massif: they reached greenschist facies conditions, from 280 to 400°C and 3 kbar to 6 kbar (Jullien and Goffé, 1993; Kirshner et al., 1999; Crouzet et al., 2001; Bellanger et al., 2015; Boutoux et al., 2014b), from South to North.

The ECM and the fold-and-thrust-belts can be distinguish by the shortening style. It is thick-skinned in the ECM, where the inherited extensive basins are inverted but with no evidence of normal fault inverse reactivation (Fig. 2; Tricart and Lemoine, 1986, Bellahsen et al., 2012, 2014; Boutoux et al., 2014a). The basement is deformed by distributed shear zones producing kilometer-scale “basement folds”. Inherited basin cover is not significantly detached from the basement and is dysharmonically folded above basement shear zones.

In the fold-and-thrust-belt, the cover is shortened above a décollement in the Liassic or Triassic series, which was activated by crustal ramps beneath the frontal ECMs (Fig. 2; e.g. Burkhard and Sommaruga, 1998; Bellahsen et al., 2014, Deville et al., 1994; Deville and Chauvière, 2000). In these belts, inherited normal fault are reactivated as for the Saint-Laurent fault (Fig. 2).

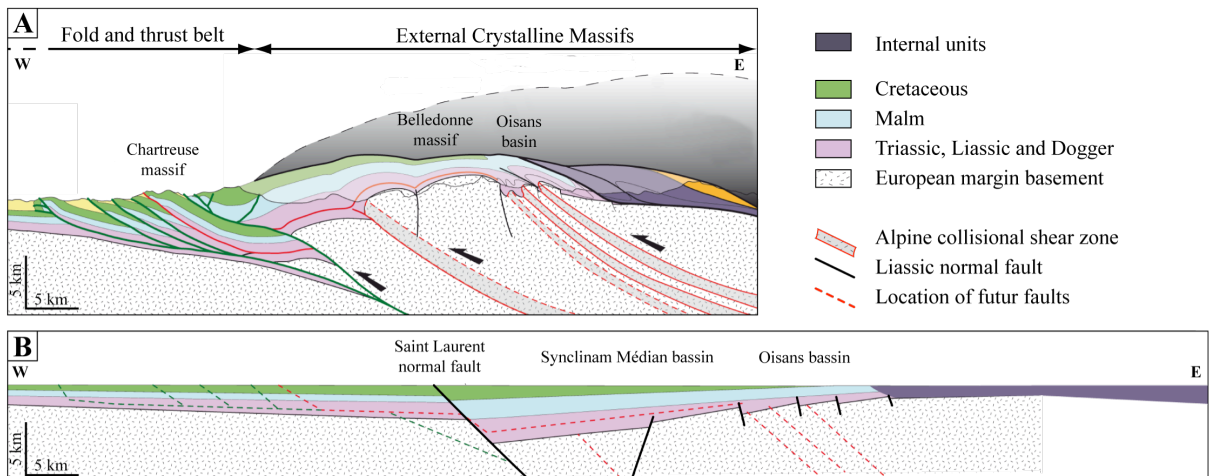


**Figure 2** Geological balanced cross section (A) of the External Western Alps and restoration (B), at the Oisans latitude. In Collisional shortening in the Alpine External zones is accommodated by “thin-skinned” style deformation in the fold and thrust belt and by “thick-skinned” style in the ECM. Shortening is localized under the inherited basins as crustal scale basement shearing. Note the reactivation and cross-cutting of the Saint-Laurent normal fault whereas the Oisans basins are inverted without reactivation of their bordering normal faults. Modified after Bellahsen et al., 2014.

The basins located between the Belledonne, Grandes Rousses, and Oisans massifs (names “Oisans basins” hereafter) are two inherited Liassic to Dogger half-grabens (e.g., Lemoine et al., 1989) (Fig. 1 and 2). They are filled with marls and limestones sediments and bordered by two crustal-scale normal faults: the Ornon and the Mizoën normal faults, from West to East respectively (Fig. 3; Barbier et al., 1972; Barfety et al., 1973). During the alpine collision, due to the activation of the Penninic Frontal Thrust (PFT), the inherited basins were buried at mid-crustal depth, reaching greenschist facies conditions around 3 kbar and 350°C (Bernard, 1978; Jullien and Goffé, 1993; Boutoux et al., 2014; Bellanger et al., 2015). After tectonic burial, those faults were not reactivated and the basin cover was not significantly detached from its cover (Fig. 3; Dumont et al., 2008; Bellahsen et al., 2012; Boutoux et al., 2014).

## II.2. Oisans basin inversion

In the ECM, collisional shortening was localized in the inherited basin due to their weakening effect (Bellahsen et al., 2012). In the Oisans basins, shortening in the basement is accommodated by five shear zones, which did not significantly propagate in the cover where the deformation is diffuse and characterized by synfolding cleavage (Fig. 3). The main outcropping shear zones in the Bourg d’Oisans basin are the Huez, the Col de Cluy and the Croix de Cassini shear zones (Bellahsen et al., 2012; Bellanger et al., 2014; Boutoux et al.,

2014a). The shear zones, cutting across the Variscan foliation, are characterized by mylonites and phyllonites (Bellahsen et al., 2012; Bellanger et al., 2014). Two main basement shear zones do not outcrop but are strongly suspected.

In the cover, five main kilometer-scale N-S folds are mapped in the field (Fig. 3; Barfety et al.; 1972). They are disharmonic folds, with East-dipping axial surfaces, associated with internal layer deformation (Fig. 3; Gratier and Vialon, 1980; Boutoux et al., 2014a).

In the Mizoën basin, two main “basement folds” (Dumont et al., 2008) were mapped and are interpreted as the result of intense and localized alpine shearing (Bellahsen et al., 2012).

The cover deformation is similar to the one in the Bourg d’Oisans basin. However, the cover is detached above the Emparis plateau (Fig. 3). In the field, two different cleavages associated to the E-W shortening can be observed (Fig. 3). S1 cleavage, mainly West-dipping, can be identified only close to the basement (Fig. 3). It is interpreted as the consequence of an early top-to-the-West basement-cover interface shearing (Bellashen et al., 2012; Boutoux et al., 2014a). This S1 cleavage is overprinted by a late East-dipping S2 cleavage (Fig. 3) that can be observed in the whole basin above a décollement and is associated to the main cover folds (Fig. 3; Dumont et al., 2008; Bellahsen et al., 2012; Boutoux et al., 2014a).

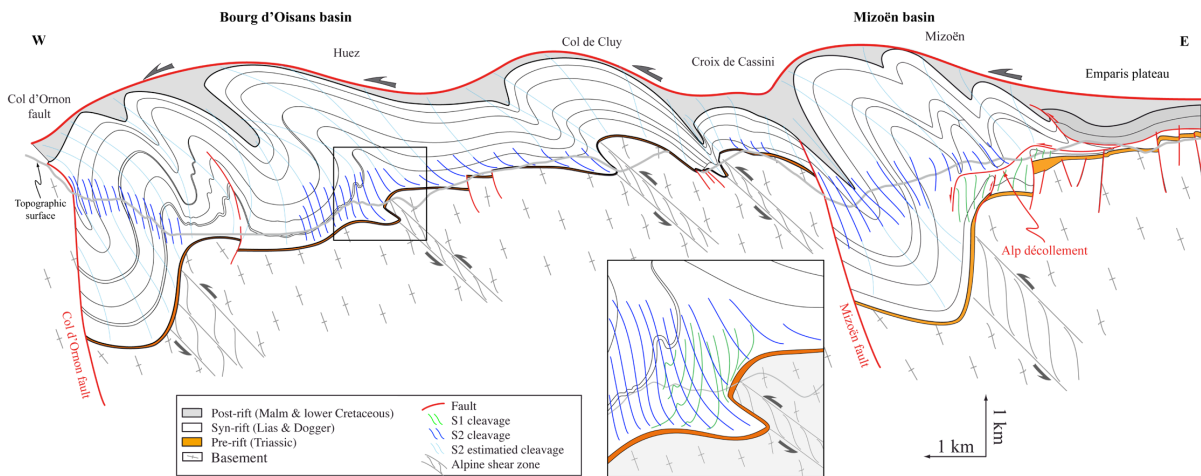


**Figure 3** Geological cross-section of the Oisans inherited basins. Basement shortening is accommodated by four shear zones in the Bourg d’Oisans basin: Bourg d’Oisans, Huez, Col de Cluy and Croix de Cassini; and by one in the Mizoën basin: the Mizoën shear zone. The two basin covers are dysharmonically folded and two main cleavages can be deciphered. S1 cleavage, generally dipping to the West, can only be seen close to the basement-cover interface. S2 cleavage, dipping to the East, is present in the entire cover. Note that in the Mizoën basin, S1 and S2 cleavages are segregated respectively below and above the Alp décollement. Modified after Boutoux et al., 2014.

## IV. Thermomechanical modeling of half-graben inversion

### IV.1. Numerical method

In this study, all the numerical experiments were obtained using GALE code (v1.6.1), a finite element code based on Arbitrary Lagrangian Eulerian particle in cell method ([Moresi et al 2003](#)). The code solves the incompressible Stokes flow for the velocity,  $\mathbf{v}$ , the pressure,  $P$ , with variable effective viscosity coefficients,  $\eta_{eff}$ , and variable density,  $\rho$ , following :

$$\nabla \eta_{eff} (\mathbf{J} + \mathbf{J}^T) - \nabla P = -\rho(T)$$

$$\mathbf{J} = \nabla \mathbf{v}$$

$$\nabla \cdot \mathbf{v} = 0,$$

and the Stokes flow solver is coupled with conservation of energy

$$\kappa \Delta T - \mathbf{v} \nabla T = \partial T$$

That only takes into account the heat (T) conduction and advection through the constant diffusivity  $\kappa$ . The computational mesh consisted of 256\*64 Q1 (bilinear) elements. Evolution in time is obtained through advection of particles (tracking lithology) and the thermal energy equation, with time steps limited to 10% of Courant criterion. Passive markers were added to compute the finite strain field at the level of the basin with adapting the script released along with [Le Pourhiet et al. \(2012\)](#) for 2D.

We use a first order approximation of rock rheology and approximate the ductile behaviour of rocks by a Newtonian flow rule in which dependence on temperature follows Frank-Kamenetskii, for which limits the number of parameters to a reference viscosity  $\eta_o$ , and a characteristic temperature  $\Theta$  in order to compute the effective viscosity,

$$\eta_{eff} = \eta_o e^{-\gamma \theta}$$

The Mohr-Coulomb yield criterial is simulated by a simplified Drucker-Prager viscoplastic flow rule ([Lemiale et al., 2008](#))

$$\eta_{eff} = \min \left( \frac{\tau^y}{2e^{II}}, \eta_0 \exp^{-\theta T} \right)$$

Where  $e^{II}$  is the second invariant of strain-rate and  $\tau^y$  is the yield stress computed from dynamic pressure  $P$  and material parameter including strain-dependent rock friction  $\phi(\epsilon^p)$  and cohesion  $C_0$

Following

$$\tau^y = \sin \phi(\epsilon^p) P + 2C_0 \cos \phi(\epsilon^p)$$

In the models presented here, we apply plastic softening to simulate wear inside the fault. The friction coefficient  $\mu = \tan(\Phi)$  in the upper and lower crust varies from 0.6 to 0.1 with plastic strain ( $\epsilon_p$ ) varying from 0 to  $10^3$  MPa.

## IV.2. Initial and boundary conditions

The initial geometry of the model is based on published restored cross sections (Bellahsen et al., 2012; Boutoux et al., 2014). We use a 300\*32-40 km box to avoid perturbations due to side effects at the edges of the model. We implement two mechanical layers and a basin (Fig. 4): (a) the sedimentary cover consists of 2 km-thick post-rift sediments and the nappe. The total thickness of the model (32-40 km) varies with the thickness of the nappe, i.e. from 0 km to 8 km. (b) The basement is 30 km-thick, except in the basin where it is thinner. (c) We consider a 25 km-long and 3.5 km-deep half-graben. The basin border normal fault in the model is 1 km thick, and dips  $70^\circ$  toward the East (Fig. 4). The box is submitted to a symmetrical shortening of 2 mm/y. We impose free slip condition at the lower surface and the edges of the box.

We choose an initial linear thermal gradient of  $22^\circ\text{C}/\text{km}$  across the model as indicated by thermobarometric data (Crouzet et al., 2001; Bellanger et al., 2015). Moreover, we consider for simplification that the system is thermally equilibrated, there is no heat provided by the base of the nappe.

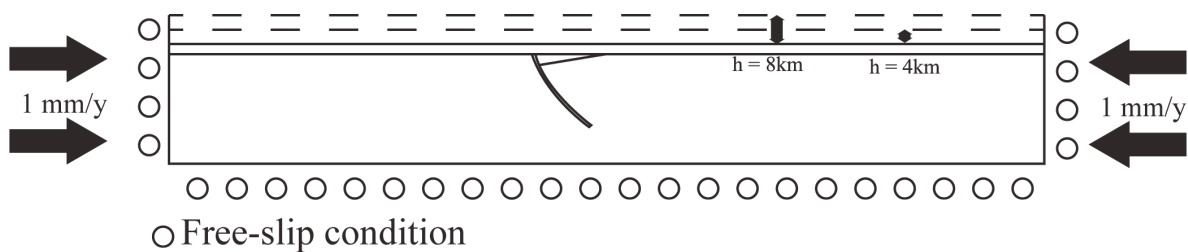


**Figure 4** Setup of the model : tick black arrow: shortening direction on either sides of the model. The picture keep the scale of the model.

As field observations show differences of mechanical behavior between the sedimentary layers and the basement in the MCE, we have tried to select creep parameters that reflect these observations within the physics of the numerical code and the geothermal gradient deduced from metamorphic facies of rocks. We pre-computed yield strength envelopes that account for the geometry of our models to ensure that with no burial: (1) the brittle-ductile

transition of the basement/nappe occurs at 12 km depth and (2) the brittle-ductile transition of the syn/postrift sediments occurs at 10 km depth.

The fault zone is modeled with the same creep parameters than in the basement, only friction coefficient (brittle strength) differs by varying from 0.1 to 0.6, the strongest fault having the same friction as basement rocks and sediments. **Table 1** summarizes the mechanical and thermal parameters of each of the three lithologies.

		Sediment	Crust	Fault
Density	$\rho$ (kg.m <sup>-3</sup> )	2400	2800	2800
Friction coefficient	$\mu$	0.85	6.6	0.6-0.1
Cohesive force	$C_0$ (MPa)	10	10	10
Thermal diffusivity	$\kappa$ (m <sup>2</sup> .s <sup>-1</sup> )	$1*10^{-6}$	$1*10^{-6}$	$1*10^{-6}$
Reference viscosity	$\eta_0$ (Pa.s <sup>-1</sup> )	$2.6*10^{24}$	$1*10^{27}$	$1*10^{-4}$
Temperature	$\theta$ (°K)	0.0460	0.2222	0.2222

**Table 1.** Material parameters.

## V. Results

### V.1. Role of burial and fault friction

We focus here on models at 1 Ma (**Fig. 5**) in order to present a compromise between early steps, presenting insufficient deformations to provide clear observations, and overly deformed later ones.

For low basin burial ( $h_{\text{burial}} = 2$  km) and  $\mu=0.4$  to  $\mu=0.1$  basement-cover interface is “folded” in the basin and normal fault is reactivated which leads to slightly pinching of the basin (**Fig. 5a, d**). Normal fault footwall is sheared top-to-the East and the shear zone is rooted into the normal fault. Thus, normal fault is reactivated as reverse faults at depth and extend as a shortcut at the surface. Cover is folded above basement folds with the same wavelength suggesting no décollement between basement and cover. For higher normal fault internal friction coefficient ( $\mu=0.6$ ), normal fault is as resistant as surrounding crust and are not reactivated (**Fig. 5g**). For lower  $\mu$ , basin is slightly pinched but no localized shortening structure develops.

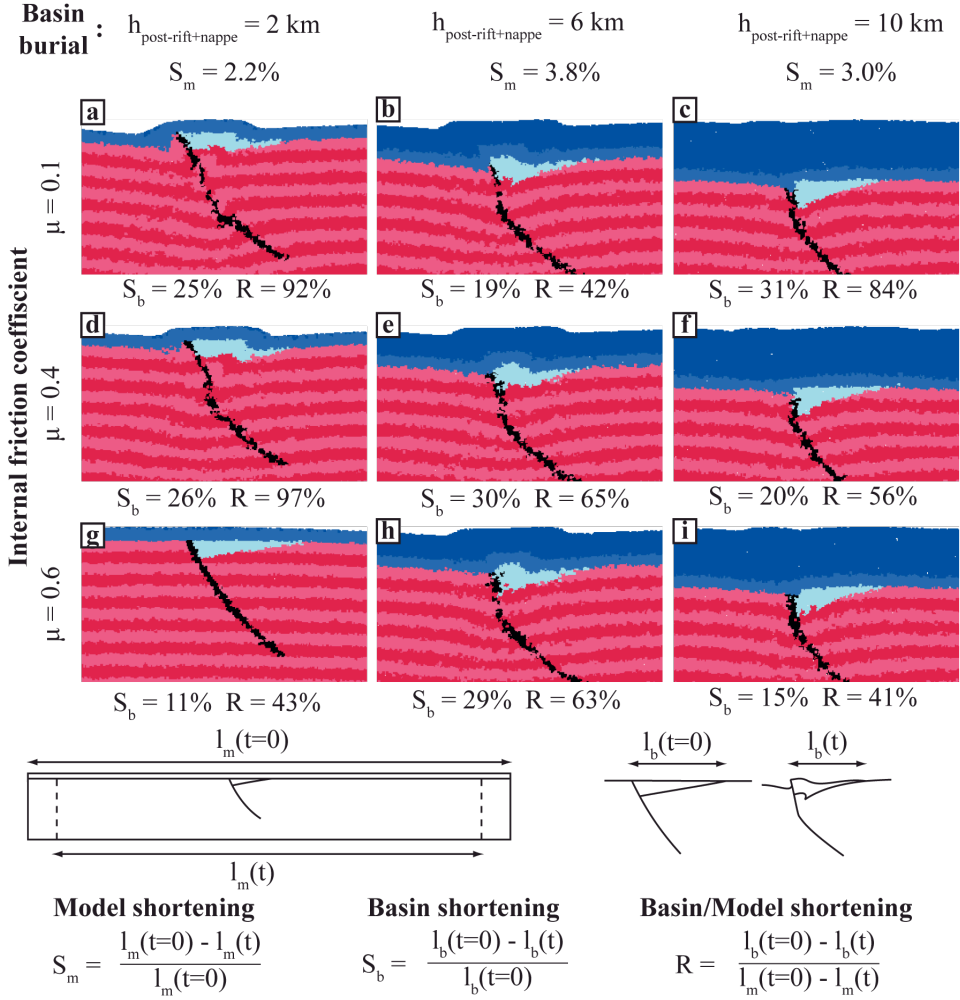


**Figure 5** Results at 1Ma. From A to I : zoom on the central part of the model, in the vicinity of the Half graben. From the graphic output, we compute for each model  $S_m$ ,  $S_b$ , and  $R$ . Striped red colors : crust, pale blue : half graben, medium dark bblue : post rift sediment, very dark blue : allochthonous material. Small cartoons represent the methodology used to compute the shortening characteristic.

For medium basin burial ( $h_{\text{burial}} = 6 \text{ km}$ ), the fault is slightly reactivated only for minor value of  $\mu$  ( $\mu = 0.1$ ) (Fig. 5b) and its upper part systematically clockwise rotated (Fig. 5b, e, h). As for low burial, basement is folded on the entire model thickness. Note that for medium burial, folding wavelength is lower than for than for low burial. While normal fault reactivation is inhibited, top to the East reverse shear zones develop into fault footwall. The inherited basin is pinched in response to basin folding, normal fault footwall rotation and hanging wall shearing. Pinching is systematically higher than for low burial. Above the basin, the cover is detached from the basement and display disharmonic folding (Fig. 5b, e, h).

For high basin burial ( $h_{\text{burial}} = 10 \text{ km}$ ), border normal fault is never reactivated whatever its internal fiction (from  $\mu=0.1$  to  $\mu=0.6$ ) (Fig. 5c, f, i). Basement deforms within a model width antiform fold, with higher amplitude than for medium burial. Normal fault footwall is

straighten up in its upper part. Top-to-the East basement shearing in the hanging wall develops only for higher value of  $\mu$  ( $\mu = 0.6$ ) (Fig. 5i). Thus, as for the medium burial case, the basin is pinched and disharmonic folds form in the cover above the basement fold that affects the hanging wall. Note that cover folds are systematically disharmonic even when the basement remains undeformed ( $\mu = 0.1$  and  $\mu = 0.4$ ) (Fig 5 c, f, i).

## V.2. Shortening localization

To quantify the localization of shortening at the scale of the model, we introduce some geologically relevant measures (Fig. 5);  $S_m$  is defined as the total model shortening (%) and  $S_b$  is defined as the shortening (%) cumulated within the basin.

After 1 Ma of shortening, in our model,  $S_m$  remains constant whatever the normal fault internal friction variation (from  $\mu=0.1$  to  $\mu=0.6$ ) depending only on basin burial (Fig. 5). Yet, with the increasing of the overlying nappe thickness,  $S_m$  does not vary importantly, from 2.2 % for low basin burial (4 km) to 3.8 % to intermediate basin burial (6 km) (Fig. 5).

For low basin burial ( $h_{\text{burial}} = 2$  km) and low to medium value of  $\mu$  ( $\mu = 0.1$  and  $\mu = 0.4$ ),  $S_b$  remains constant around 25% (Fig. 5a, c). For high value of  $\mu$  ( $\mu = 0.6$ )  $S_b$  is less than twice smaller ( $S_b = 11\%$ ) (Fig. 5g). For high value of  $\mu$ , the basin basement is indeed not sheared and therefore is less shortened. Thus for low basin burial, basin shortening is more likely accommodated by basin basement shearing than by basin pinching.

This kind of relationship, progressive decreasing of  $S_b$  with the increasing of  $\mu$ , can also be observed for important basin burial ( $h_{\text{burial}} = 10$  km). Here,  $S_b$  slowly decreases with  $\mu$ , about 30% for low value, 20% for intermediate values and 15 % for high values (Fig. 5b, e, h). Yet in those conditions of burial, basement shortening increases with  $\mu$ . Therefore basin shortening is accommodated by basin pinching rather than basement shearing.

For intermediate burial the relationship between the two parameters is in the opposite way, going from about 20 % shortening for low value of  $\mu$  ( $\mu = 0.1$ ) to about 30% for medium and high value of  $\mu$  ( $\mu = 0.4$  to  $0.6$ ) (Fig. 5c, f, i). Thus for intermediate basin burial, basin shortening is accommodated as much by basin pinching than basin shearing. With the increasing of  $\mu$ , basin shearing decreases while basin pinching remains constant. As a result, basin shortening decreases.

### V.3. Basin deformation, basement and cover.

The record of total strain on the marker grid allows us to compute finite deformation and plunges of synthetic lineations in the basin (Fig. 6). We choose to display results at 1 Ma for three values of burial with a fixed value of friction coefficient of the fault.

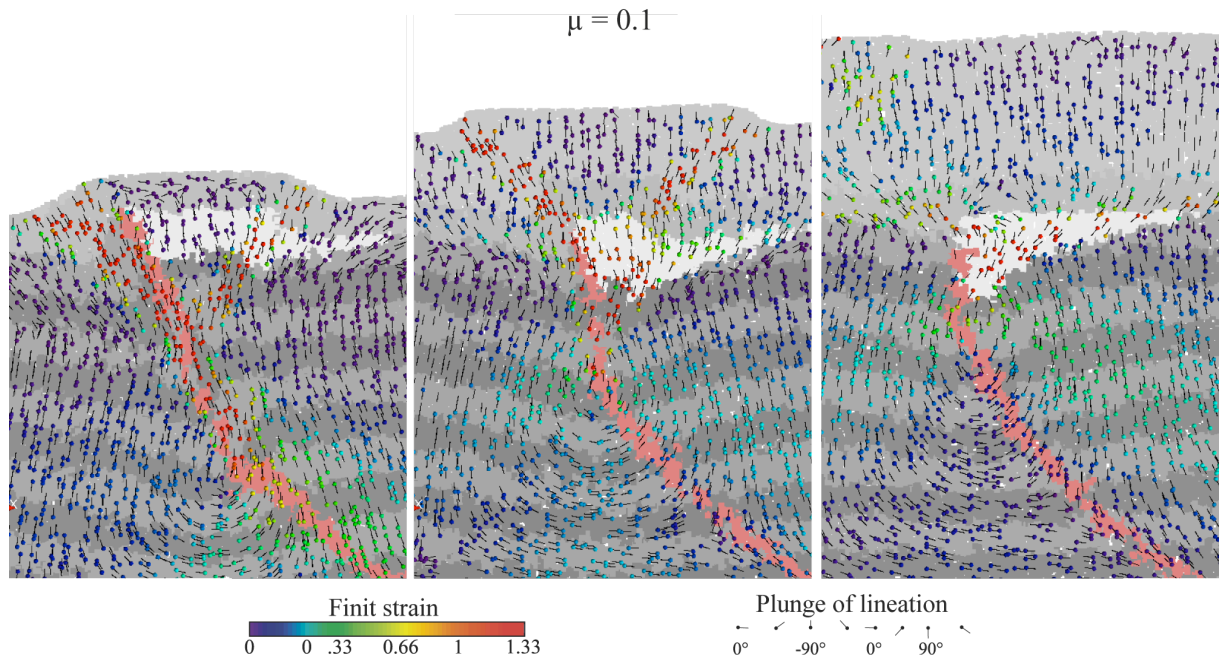


**Figure 6** Zoom on the basin at 1Ma. Colored balls represent the finit strain recorded on each marker. At the back, strips mark the finit deformation in the crust : offsets along the folt plane and a crustal scale pop-down fold in the vicinity of the basin

When burial is low, finite strain is maximum in two shear zones (Fig. 7): (i) the west-verging thrust, located at the inherited normal fault position at depth, has offsets higher than 2 km. (ii) the east-verging back thrust accommodates lower amount of shortening. Outside these shear-zones no important deformation is recorded. The effective viscosity ( $\eta_{\text{eff}}$ ) remains high in the basin (Fig. 7A), and drop drastically in the shear zones. At 1 Ma, the west-verging shear zone is displaced to the west of the inherited normal fault zone, however this inherited structure has recorded high finite strain. Consequently, this fault zone is reactivated in the early stage of the model and then is abandoned to be finally cross-cut in latest stages. This sequence is consistent with the brittle behaviour of the basin at low burial value.

$\mu = 0.1$   
Results at 1My

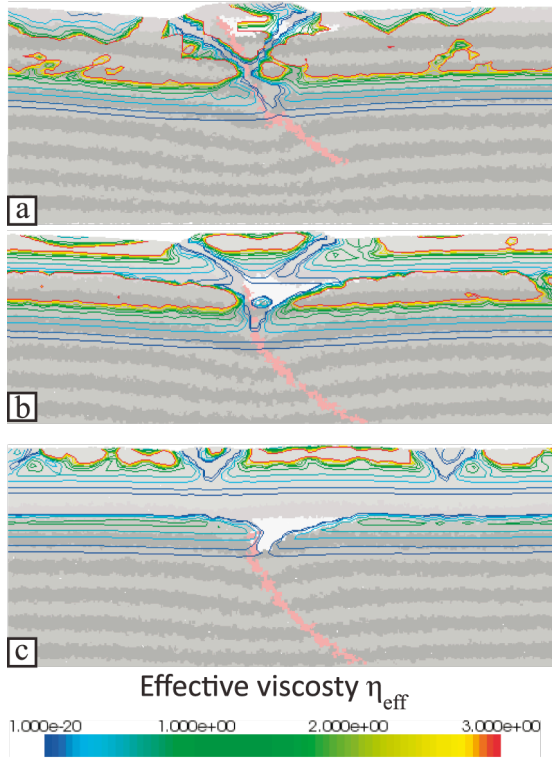


**Figure 8** Isocontour of effective viscosity  $\eta_{\text{eff}}$  at 1Ma and with a constant fault strength  $\mu=0.1$  A: No burial ( $h=2$ ), B: intermediate burial ( $h=6$ ), C: Important burial ( $h=10$ ). As  $\eta_{\text{eff}}$  depends to the deviatoric stress and to the speed of deformation, isocontours draw at each time step the resistance of materials. Note the importante decrease of  $\eta_{\text{eff}}$  in conjugated corridors. They are rooted in the basin on the B and C models. On B, note the drop of  $\eta_{\text{eff}}$  at the crust/sediment interface.

For an intermediate burial value, deformation is distributed in the basin with finite strain values between 50% and 100% (Fig. 7B). Both thrusts are still active, and lineation plunges are around 45° recording the east-verging shearing at the basement/cover interface. This shearing comes with the folding of the base of the basin.  $\eta_{\text{eff}}$  remains high in the crust (Fig 7B) but decreases in the basin indicating its ductile behavior. Isolines of  $\eta_{\text{eff}}$  (Fig. 7B) also show a viscosity drop at the basement/cover interface for these burial conditions. It marks the growth of a detachment level on this interface, decoupling cover from the basement without the need of an initially very weak layer at the cover base.

The shearing of basement/cover interface is also well represented on the Fig. 6C (maximal value of burial): while cover record lineations parallel to the interface and high strain values (1-1.33), crust record low finite strain values (0-0.2). The inherited normal fault is not reactivated with finite strain values at the footwall around 0-0.1. On the contrary, in the basin, the deformation is distributed and markers records high finite strain values (0.33-1.33) with lineation plunges around 45° toward the east.

The variability of effective viscosity between these three models is due to the thermal structure and is the direct consequence of our choice of rheological parameters. As we do not simulate the effect of the erosion, the thickness of stacked sediments (syn, post and allochthonous nappe) increases as the model shortens. Indeed Above the basin, compressive structures in the nappe tend to increase the burial of the basin. Moreover, flexure of the crust and the “pop-down” fold tend to increase the burial as well. Consequently our models show that the thickening of overlying structures favor the ductile behavior of the basin, the flexure of the basin also intensify this effect.

## VI. Discussion

In the models, we have made the assumption of a constant (laterally and through time) overlying nappe thickness. This is an oversimplification as ECM burial depth increases from East to West. Moreover, the burial depth increased through time and this was not modeled. However, most of the deformations in the ECM are estimated to have occurred at or close to the metamorphic peak (e.g. in the Oisans massif, [Bellanger et al., 2014](#)); in the Mont-Blanc massif, [Rolland et al., 2003](#); [Cenki-Tok et al., 2013](#)). This justifies our modeling strategy to simulate shortening under overriding nappes after their emplacement.

Based on these results, as well as results on the ECM structure from the literature, we propose a relationship between the basin inversion and the depth of burial (Fig. 8). In the ECM, collisional shortening is localized at the inherited basins that weakened the crust during its burial ([Bellahsen et al., 2012](#)). ECM basins were pinched and their basement presents antiforms (Fig. 8). Indeed, with the overlying nappe thickness increasing, border normal fault is straightened up while, at the base of the basin, the basement cover interface is folded. Good examples for this are the Oisans massif inherited basins (Fig. 8b) and other Alpine ECM (e.g., the Chamonix basin, [Boutoux et al., 2014a](#)). In the ECM inherited basin, basement folds are interpreted as due to the deformation localization and the development of basement shear bands (Fig. 8). Note that in numerical modeling, basement shear bands have dips opposite to

the inherited fault one. In the inherited ECM basin basement, shear zones dips parallel to the normal fault (Fig. 8). This difference could be linked to the boundary conditions: in the models, these are symmetrical while in nature the ECM are shortened while a strong west-verging shearing is imposed at the underthrusted crust top, i.e., the PFT.

In numerical modeling, the pinched shape of the basin is due to the inhibition of the normal fault reverse reactivation (Fig. 8d and e). This is in agreement with observations on most of the inherited Liassic normal faults in the ECM (Tricart and Lemoine, 1986; Boutoux et al., 2014a; Bellahsen et al., 2014; Fig. 1).

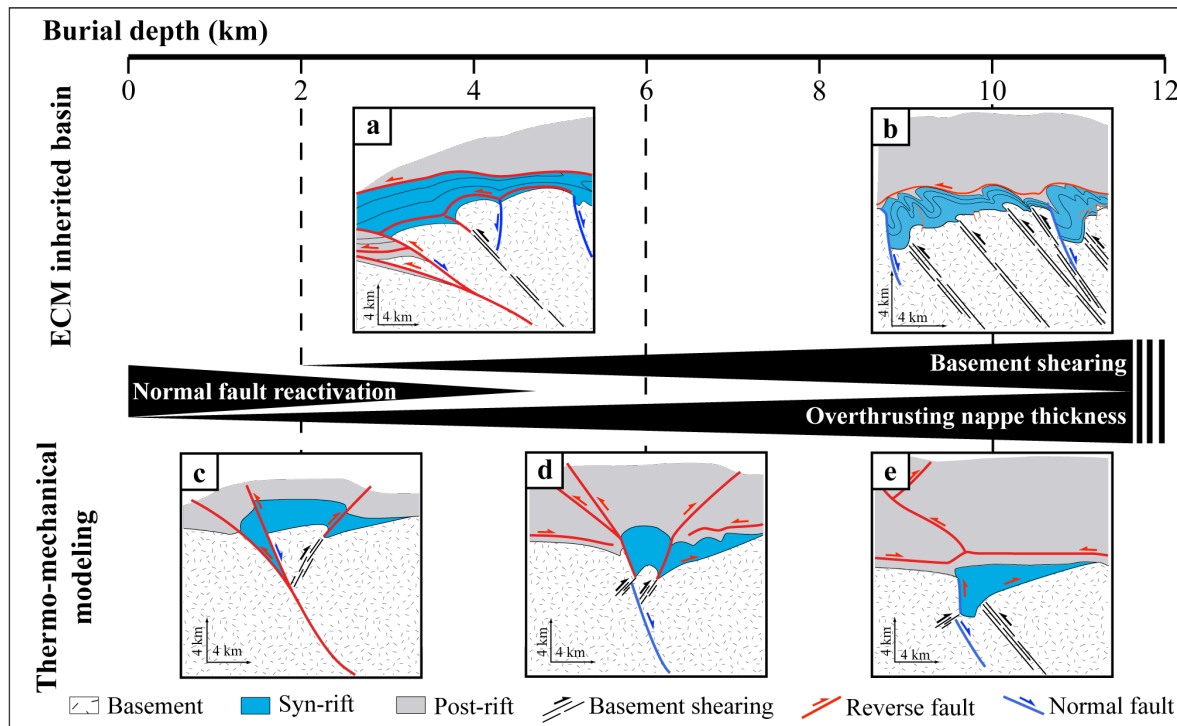


**Figure 9** Conceptual model of inherited basin inversion linked to their tectonically burial based on the comparison between Western Alps inherited basin and thermo-mechanical modeling. (a) and (b): natural examples taken from balanced cross-section in the external zones of Western Alps. (a) Cross section of the Saint-Laurent basin buried from 0 km to 5 km. Main normal fault controlling the basin extension is reactivated and short-cut the basement. Inner and smaller normal fault are straighten up and not reactivated. One basement shearing is suspected at the bottom of Belledone massif (Modified after Bellahsen et al., 2014). (b) Cross-section of the Oisans basins buried at around 10 km. Normal faults are straighten up and not reactivated. Crustal shortening is exclusively accommodated by basement shearing which are not extended to cover. Modified after Boutoux et al., (2014). (c), (d) and (e): thermo-mechanical modeling results. (c) Basin is buried only under 2 km post-rift sediments. Normal fault is reactivated and short-cut the basement. Basin basement is back-thrust sheared. (d) Basin is buried under 2 km post-rift sediments and 2 km of overlying nappe. Normal fault is lightly reactivated but crustal shortening is essentially accommodated by back-thrust, extended in the cover. (e) Basin is buried under 2 km post-rift sediments and 6 km of overlying nappe. Normal fault is not reactivated and total crustal shortening is accommodated by normal basement shearing. Shear zone is not extended in the cover. Basement/cover interface is sheared.

Interestingly, the Saint-Laurent basin, linked to the Synclinal-Médian basin, is restored as the cover of the Belledonne massif (Bellahsen et al., 2014, Fig. 2). This basin most likely marked the approximate western limit of the internal units overthrusting and therefore was buried below a very thin nappe (0 to 2 km; Deville and Chauviere, 2000; Bellahsen et al., 2014). The inherited normal fault was reactivated as thrust fault and shortcut the basement (Fig. 9a). The inverted basin geometry can be interpreted as intermediate between numerical modeling with complete (Fig. 8c) and partial (Fig. 8d) normal fault reactivation.

Further East in the Alpine External zone, there is no evidence of normal fault reverse reactivation during the basin inversion in several ECM basin (e.g. the Oisans massif, Tricard and Lemoine, 1986; the Chamonix basin, Boutoux et al., 2014a). According to numerical modeling, the normal fault reactivation inhibition in the ECM basins has to be linked to the basin burial depth increasing from West to East (Fig. 8).

At first order, in the ECM inherited basins, there is no décollement between cover and basement. However, ECM basement present kilometre-scale folds due to local shearing while in the cover there are hundreds meters-scale dysharmonically folded above the basement shear zones (e.g., the Morcle nappe, Escher et al., 1993). The disharmonic deformation of the cover above basement folds suggests short local décollements of the cover, or at least local shearing of the basement/cover interface (e.g., Escher et al., 1993; Burkhard, 1988; Bellahsen et al., 2012; Boutoux et al., 2014a). As suggested by our numerical models and other ones (e.g. Buiter and Pfiffner, 2003), rheological contrast can localize deformations in the cover bottom during shortening (Fig. 5 and 6). In our models, with basin pinching, cover is progressively extruded from the basin (Fig. 8e) and the basement-cover interface is sheared (Fig. 8e).

This shearing could be linked to S1 cleavage observed in the Oisans basin bottom covers (Bellahsen et al., 2012; Boutoux et al., 2014a). This S1 cleavage can be only deciphered close to the basement/cover interfaces and is generally west-dipping. Moreover, small basement back-thrust shear bands are observed close to the basement-cover interface in numerical models (Fig. 5i) like in the Mizoën basin (Fig. 3).

## VII. Conclusions

In this contribution, we investigated the inversion style of inherited basins using 2D thermo-mechanical modeling. We show that normal fault reactivation is inhibited with tectonic burial increase (from 2 to 8 km) whatever the inherited fault internal friction. Under high tectonic burial (8 km), crustal deformation is characterized by basin pinching, no inherited fault reactivation, and basement folding. The cover is extruded out of the basin and localized shear zones localized at the basement-cover interface.

Those results are consistent with the inversion style of inherited basins in the Western Alps. In the fold-and-thrust belt (Vercors-Chartreuse), there was no tectonic burial (or it was very low) and the inherited normal fault were reactivated. Further East, in the Grandes Rousses and Oisans massif, burial of the inherited basin reached about 10 km and their border inherited normal faults were not reactivated. In those basins, the basement was deformed by distributed shear zones (responsible for basement antiforms) while the cover is dysharmonically folded.

## Acknowledgments

GALE is software hosted by the Computational Infrastructure for Geodynamics (CIG) and developed by CIG, Monash University and the Victorian Partnership for Advanced Computing (VPAC). M. Bellanger, O. Lacombe, L. Jolivet, F. Moutherau, A. Verlaguet are thanked for fruitful discussions.

## References

- Barbier, R., Barféty, J.C., Bocquet, A., Bordet, P., Le Fort, P., Meloux, J., Mouterde, R., Pécher, A., Petiteville, M., 1973. Carte géologique de la France (1/50.000), feuille de La Grave (798). Bureau de Recherches géologiques et minière, Orléans.
- Barféty, J.C., Bordet, P., Carme, F., Debèlmas, J., Meloux, M., Montjuvent, G., Mouterde, R., Sarrot-Reynauld, J., 1972. Carte géologique de la France (1/50.000), feuille de Vizille (797). Bureau de Recherches géologiques et minières, Orléans.
- Barféty, J.C., Bordet, P., Carme, F., Debèlmas, J., Meloux, M., Montjuvent, G., Mouterde, R., Sarrot-Reynauld, J., 1972. Carte géologique de la France (1/50,000), feuille Vizille (797). Bureau de Recherches géologiques et minières, Orléans.

- Barf  ty, J.C., Gidon, M., Lemoine, M., Mouterde, R., 1979. Tectonique syns  dimentaire liasique dans les massifs cristallins de la zone externe des Alpes occidentales fran  aises: la faille du col d'Ornon. C.R. Acad. Sci. Paris 289, 1207e1210.
- Beaumont, C., Mufioz, J.A., Hamilton, J., Fullsack, P., 2000. Factors controlling the Alpine evolution of the central Pyrenees inferred from a comparison of observations and geodynamical models. J. Geophys. Res. 105, 8121–8145. doi:10.1029/1999JB900390; doi:10.1029/1999JB900390
- Bellahsen, N., Jolivet, L., Lacombe, O., Bellanger, M., Boutoux, A., Garcia, S., Mouthereau, F., Le Pourhiet, L., Gumiaux, C., 2012. Mechanisms of margin inversion in the external Western Alps: Implications for crustal rheology. Tectonophysics 560-561, 62–83. doi:10.1016/j.tecto.2012.06.022
- Bellahsen, N., Mouthereau, F., Boutoux, A., Bellanger, M., Lacombe, O., Jolivet, L., Rolland, Y., 2014. Collision kinematics in the western external Alps. Tectonics 33, 1–34. doi:10.1002/2013TC003453
- Bellanger, M., Bellahsen, N., Jolivet, L., Baudin, T., Augier, R., Boutoux, A., 2014. Basement shear zones development and shortening kinematics in the Ecrins Massif, Western Alps. Tectonics. doi:10.1002/2013TC003294.Received
- Bellanger, M., Augier, R., Bellahsen, N., Jolivet, L., Moni  , P., Baudin, T., Beyssac, O., 2015. Shortening of the European Dauphinois margin (Oisans Massif, Western Alps): New insights from RSCM maximum temperature estimates and 40Ar/39Ar in situ dating. J. Geodyn. 83, 37–64. doi:10.1016/j.jog.2014.09.004
- Bernard, D., 1978. Microthermom  trie des inclusions fluides de cristaux syn- cin  matiques. Application    la couverture s  dimentaire du Nord Pelvoux. Unpublished PhD Thesis, Univ Grenoble, 133 pp. Bodnar,
- Bollinger, L., Avouac, J.P., Beyssac, O., Catlos, E.J., Harrison, T.M., Grove, M., Goff  , B., Sapkota, S., 2004. Thermal structure and exhumation history of the Lesser Himalaya in central Nepal. Tectonics 23, n/a–n/a. doi:10.1029/2003TC001564
- Bonini, M., Sani, F., Antonielli, B., 2012. Basin inversion and contractional reactivation of inherited normal faults: A review based on previous and new experimental models. Tectonophysics 522-523, 55–88. doi:10.1016/j.tecto.2011.11.014
- Bonnet, C., Malavieille, J., Mosar, J., Bonini, M., Sani, F., Antonielli, B., 2007. Basin inversion and contractional reactivation of inherited normal faults: A review based on previous and new experimental models. Tectonophysics 26, n/a–n/a. doi:10.1016/j.tecto.2011.11.014
- Boutoux, A., Bellahsen, N., Lacombe, O., Verlaguet, A., Mouthereau, F., 2014. Inversion of pre-orogenic extensional basins in the external Western Alps: Structure, microstructures and restoration. J. Struct. Geol. 60, 13–29. doi:10.1016/j.jsg.2013.12.014
- Boutoux, A., Verlaguet, A., Bellahsen, N., Lacombe, O., Villemant, B., Caron, B., Martin, E., Assayag, N., Cartigny, P., 2014. Fluid systems above basement shear zones during inversion of pre-orogenic sedimentary basins (External Crystalline Massifs, Western Alps). Lithos. doi:10.1016/j.lithos.2014.07.005

Buiter, S.J.H., Pfiffner, O.A., 2003. Numerical models of the inversion of half-graben basins. *Tectonics* 22, 1–16. doi:10.1029/2002TC001417

Buiter, S.J.H., Pfiffner, O.A., Beaumont, C., 2009. Inversion of extensional sedimentary basins: A numerical evaluation of the localisation of shortening. *Earth Planet. Sci. Lett.* 288, 492–504. doi:10.1016/j.epsl.2009.10.011

Burkhard, M., Sommaruga, A., 1998. Evolution of the western Swiss Molasse basin: structural relations with the Alps and the Jura belt. *Geol. Soc. London, Spec. Publ.* 134, 279–298. doi:10.1144/GSL.SP.1998.134.01.13

Burkhard, M. 1988: L'Héloïte de la bordure occidentale du massif de l'Aar (évolution tectonique et métamorphique) *Eclogae Geologicae Helvetiae* 81, 63–114. Cenki-Tok et al., 2013

Colletta, B., Le Quellec, P., Letouzey, J., Moretti, I., 1988. Longitudinal evolution of the Suez rift structure (Egypt). *Tectonophysics* 153, 221–233. doi:10.1016/0040-1951(88)90017-0

Crouzet, C., Ménard, G., Rochette, P., 2001. Cooling history of the Dauphinoise Zone (Western Alps, France) deduced from the thermopaleomagnetic record: geodynamic implications. *Tectonophysics* 340, 79–93. doi:10.1016/S0040-1951(01)00142-1

Graciansky, P. De, Dardeau, G., Lemoine, M., Tricart, P., 1989. The inverted margin of the French Alps and foreland basin inversion. *Geol. Soc. London, Spec. Publ.* 44, 87–104. doi:10.1144/GSL.SP.1989.044.01.06

Deville, É., A. Mascle, C. Lamiraux, and A. Le Bras (1994), Tectonic styles, reevaluation of plays in southeastern France, *Oil Gas J.*, 31, 53–58.

Deville, É., Chauvière, A., 2000. Thrust tectonics at the front of the western Alps: constraints provided by the processing of seismic reflection data along the Chambéry transect. *Comptes Rendus l'Académie des Sci. - Ser. IIA - Earth Planet. Sci.* 331, 725–732. doi:10.1016/S1251-8050(00)01463-4

Dumont, T., Champagnac, J.-D., Crouzet, C., Rochat, P., 2008. Multistage shortening in the Dauphiné zone (French Alps): the record of Alpine collision and implications for pre-Alpine restoration. *Swiss J. Geosci.* 101, 89–110. doi:10.1007/s00015-008-1280-2

Dumont, T., Schwartz, S., Guillot, S., 2012. Structural and sedimentary records of the Oligocene revolution in the Western Alpine arc. *J. Geodyn.* 56–57, 18–38. doi:10.1016/j.jog.2011.11.006

Escher, A., Masson, H., Steck, A., 1993. Nappe geometry in the western Swiss Alps. *J. Struct. Geol.* 15, 501–509.

Gratier, J.-P., Vialon, P., 1980. Deformation pattern in a heterogeneous material: folded and cleaved sedimentary cover immediately overlying a crystalline basement (Oisans, French Alps). *Tectonophysics* 65, 151–179. doi:10.1016/0040-1951(80)90228-0

- Jullien, M., Goffé, B., 1993. Occurrences de cookéite et de pyrophyllite dans les schistes du Dauphinois (Isère, France): Conséquences sur la répartition du métamorphisme dans les zones externes alpines. Schweirsche Mineral. und Petrogr. Mitteilungen 73, 357–363.
- Kirschner, D.L., Masson, H., Sharp, Z.D., 1999. Fluid migration through thrust faults in the Helvetic nappes (Western Swiss Alps). Contrib. to Mineral. Petrol. 136, 169–183. doi:10.1007/s004100050530
- Lacombe, O., Mouthereau, F., 2002. Basement-involved shortening and deep detachment tectonics in forelands of orogens: Insights from recent collision belts (Taiwan, Western Alps, Pyrenees). Tectonics 21, 12–1–12–22. doi:10.1029/2001TC901018
- Le Pourhet, L., Huet, B., Agard, P., Labrousse, L., Jolivet, L., Yao, K., 2012. Strain localisation in mechanically Layered Rocks, insights from numerical modelling. Solid Earth Discuss. 4, 1165–1204. doi:10.5194/sed-4-1165-2012
- Lemiale, V., Mühlhaus, H.-B., Moresi, L., Stafford, J., 2008. Shear banding analysis of plastic models formulated for incompressible viscous flows. Phys. Earth Planet. Inter. 171, 177–186. doi:10.1016/j.pepi.2008.07.038
- Lemoine, M., Bas, T., Arnaud-Vanneau, A., Arnaud, H., Dumont, T., Gidon, M., Bourbon, M., Graciansky, P. De, Rudkiewicz, J., Megard-Galli, J., Tricart, P., 1986. The continental margin of the Mesozoic Tethys in the Western Alps. Mar. Pet. Geol. 3, 179–199. doi:10.1016/0264-8172(86)90044-9
- Lemoine, M., Dardeau, G., Delpech, P. Y., Dumont, T., De Graciansky, P. C., Graham, R., Jolivet, L., Roberts, D., Tricart, P., 1989. Extension synrift et failles transformantes jurassiques dans les Alpes occidentales. Comptes rendus de l'Académie des sciences. Série 2, Mécanique, Physique, Chimie, Sciences de l'univers, Sciences de la Terre, 309(17), 1711-1716.
- Moresi, L., Dufour, F., Mühlhaus, H.-B., 2003. A Lagrangian integration point finite element method for large deformation modeling of viscoelastic geomaterials. J. Comput. Phys. 184, 476–497. doi:10.1016/S0021-9991(02)00031-1
- Mouthereau, F., Petit, C., 2003. Rheology and strength of the Eurasian continental lithosphere in the foreland of the Taiwan collision belt: Constraints from seismicity, flexure, and structural styles. J. Geophys. Res. 108, 2512. doi:10.1029/2002JB002098
- Mouthereau, F., Watts, A.B., Burov, E., 2013. Structure of orogenic belts controlled by lithosphere age. Nat. Geosci. 6, 785–789. doi:10.1038/ngeo1902
- Rolland, Y., Rossi, M., Cox, S.F., Corsini, M., Mancktelow, N.S., Pennacchioni, G., Fornari, M., Boullier, A., 2008.  $^{40}\text{Ar}/^{39}\text{Ar}$  dating of synkinematic white mica: insights from fluid-rock reaction in low-grade shear zones (Mont Blanc Massif) and constraints on timing of deformation in the NW external Alps. Geol. Soc. London, Spec. Publ. 299, 293–315. doi:10.1144/SP299.18

Roure, F., & Colletta, B. (1996). Cenozoic inversion structures in the foreland of the Pyrenees and Alps. Mémoires du Muséum national d'histoire naturelle, 170, 173-209.

Simon-Labréteau, T., Rolland, Y., Dumont, T., Heymes, T., Authemayou, C., Corsini, M., Fornari, M., 2009. 40 Ar/39 Ar dating of Penninic Front tectonic displacement (W Alps) during the Lower Oligocene (31-34 Ma). *Terra Nov.* 21, 127–136. doi:10.1111/j.1365-3121.2009.00865.x

Sanchez, G., Rolland, Y., Schneider, J., Corsini, M., Oliot, E., Goncalves, P., Verati, C., Lardeaux, J.-M., Marquer, D., 2011. Dating low-temperature deformation by 40Ar/39Ar on white mica, insights from the Argentera-Mercantour Massif (SW Alps). *Lithos* 125, 521–536. doi:10.1016/j.lithos.2011.03.009

Tricart, P., Lemoine, M., 1986. From faulted blocks to megamullions and megaboudins: Tethyan héritage in the structure of the Western Alps. *Tectonics* 5, 95–118. doi:10.1029/TC005i001p00095

### **VI.3. Influence de l'enfouissement tectonique.**

Au cours de cette étude, on a démontré le fort contrôle de la profondeur d'enfouissement sur la réactivation ou non des accidents hérités et donc sur la géométrie des bassins inversés. Ce paramètre semble même prendre le pas sur la friction interne des failles normales. Ainsi, une faille normale, même parfaitement orientée par rapport aux contraintes et dotée d'une très faible friction interne, n'est pas réactivée si elle est enfouie sous une nappe suffisamment épaisse. De plus, on montre que de même que pour une marge très faiblement enfouie, le raccourcissement est localisé au niveau des bassins extensifs du fait de l'effet affaiblissant des bassins. Le raccourcissement s'exprime par le pincement de plus en plus prononcé du bassin dû au redressement de la faille bordière et au plissement distribué du socle. Lorsque la résistance de la faille augmente, on observe le développement d'un cisaillement localisé du socle. Enfin, on observe une dysharmonie entre des plissements de la couverture sur le socle, de plus en plus importante avec l'augmentation de la profondeur d'enfouissement du bassin. Ces résultats semblent parfaitement cohérents avec nos observations des bassins de l'Oisans et de l'ensemble des Massifs Cristallins Externes alpins. Ainsi, on explique la réactivation partielle des accidents hérités au front des MCE, telle que la faille normale de Saint-Laurent, alors que celles situées dans les MCE ne montrent pas d'indice de réactivation, ayant été enfouies entre 10 et 15 km de profondeur sous les nappes internes. De plus, on a montré que dans les bassins de l'Oisans, peu raccourcis, l'ensemble des structures et notamment le cisaillement de l'interface socle/couverture, malgré sa vergence opposée à celle du chevauchement des unités internes, s'explique avec la même cinématique de raccourcissement Est-Ouest.

### **VI.4. Limites du modèle : raccourcissement symétrique, complexité de la marge et vitesse d'enfouissement.**

Une des limites majeures de cette étude est le raccourcissement horizontal appliqué dans le modèle thermo-mécanique. Dans les Alpes de l'Ouest, les déformations sont à vergence Ouest du fait du charriage vers l'Ouest des unités internes au dessus des MCE. Au contraire, le modèle présenté ne permet qu'un cisaillement pur de la marge. Ainsi, le cisaillement du socle du bassin pend systématiquement vers la faille normale dans les modèles alors que les

cisaillements sont à vergence Ouest dans les MCE du fait du charriage d'Est en Ouest des unités internes.

Une limite importante à cette étude provient des conditions d'enfouissement des modèles. Ainsi, dans le cas de cette étude, le raccourcissement imposé au modèle est initié alors que la nappe le recouvrant est déjà en place. L'enfouissement est donc constant tout au long de la modélisation. Or, bien évidemment c'est loin d'être le cas pour les analogues de terrain que sont les bassins hérités des MCE. Les vitesses d'enfouissement estimées pour les MCE restent méconnus. Il semble cependant que leur vitesse de réchauffement soit rapide ( $100^{\circ}\text{C.Ma}^{-1}$ ). Ainsi, l'enfouissement du massif du Mont Blanc et de sa couverture est initié entre aux alentours de 32 Ma et les deux unités atteignent leur température maximale (respectivement à 400 et  $350^{\circ}\text{C}$ ). Il semble de plus que la couverture des bassins des MCE n'ait enregistré que peu de déformation lors de son enfouissement. Ainsi, les veines les plus précoces, formées dans la couverture des bassins de l'Oisans et de la nappe de Morcles ont enregistré des températures proches de celle du pic thermique des bassins ([Kirschner et al ;, 1999](#) ; [Boutoux et al., 2014b](#)). De même, les déformation du socle des bassins des MCE semblent être synchrone su pic de métamorphisme (e.g. [Rolland et al., 2008](#) ;[Challandes et al., 2008](#) ; [Bellanger et al., 2015](#)). Ainsi dans le cas des modèles présentés, si l'enfouissement instantané des bassins n'est pas réaliste, le raccourcissement initié au pic de pression semble cohérent avec les données.

## VII. Discussion.

Dans ce chapitre, on discute des évolutions, conjointes ou diachrones, de la pression et de la température enregistrés par les MCE lors de leur enfouissement, du pic de métamorphisme et de leur exhumation mais aussi au timing des déformations

### VII.1. Évolution P-T lors de l'enfouissement.

#### VII.1.1. Augmentation prograde de la température.

Plusieurs scenarios peuvent être avancés quant au timing et à la vitesse de l'enfouissement des futurs MCE et de leur couverture sous les unités internes alpines.

Dans le massif du Mont Blanc, le pic de métamorphisme est contraint en température à 400°C +/- 25°C (Rolland et al., 2003 ; Rossi et al., 2005) et daté à 29,5 Ma par datation U-Pb d'allanites syn-tectoniques (Cenki-Tok et al., 2013). L'âge de l'initiation de l'enfouissement du massif est estimé à partir de la fin de la sédimentation du bassin de flysch vers 32,5 Ma (Berger, 1992, 1995). On obtient une vitesse de réchauffement pour le massif de l'ordre de 100°C.Ma<sup>-1</sup>. Dans le couvert du massif du Mont Blanc, la nappe de Morcles, le pic de température est estimé à 350°C (équilibre <sup>18</sup>O isotopiques entre quartz et calcite) et est daté à 27 Ma (<sup>39</sup>Ar/<sup>40</sup>Ar, Kirschner et al., 1995). La vitesse de réchauffement de la nappe est donc du même ordre que celle du massif du Mont Blanc, aux alentours de 100°C/Ma<sup>-1</sup>.

Les massifs des Aiguilles Rouges et du Mont Blanc sont restaurés approximativement dans la même position structurale dans la marge européenne (Burkhard et Sommaruga, 1998 ; Leloup et al., 2005). De plus, les derniers sédiments recouvrant les deux massifs et marquant le début de l'enfouissement sont datés approximativement du même âge (respectivement à 32,5 Ma et 30 Ma, Berger, 1992, 1995, Sinclair et Allen, 1992). De ce fait, on propose approximativement la même vitesse de réchauffement pour le massif des Aiguilles Rouges (Boutoux et al., in prep). Enfin, dans l'Oisans, le pic de température est estimé à 330°C +/- 15°C (analyses RSCM de la couverture) et initié vers 33 Ma (<sup>39</sup>Ar/<sup>40</sup>Ar sur phengites syn-tectoniques) (Bellanger et al., 2015). L'enfouissement du massif est aussi contraint par le dépôt des flyschs priaboniens à l'Oligocène basal (Sinclair, 1997, Ford et Lickorisch, 2004). La vitesse de réchauffement du massif proposé par Bellanger et al. (2015) est du même ordre que pour le massif du Mont Blanc et sa couverture, aux alentours de 100°C Ma<sup>-1</sup>.

Dans le massif de l'Aar le pic de température est estimé à 450°C (+/- 25°C) déterminée par les équilibres isotopiques entre Quartz et Biotite au sein des bandes de cisaillement structurant le massif (Fourcade et al., 1989 ; Goncalves et al., 2012). L'initiation de l'enfouissement du massif est contraint par les derniers dépôts enregistrés au-dessus du massif, les flyschs de Taveyannaz, datés à entre 36 et 32,5 Ma (Lateltin et Muller, 1987). Les données géochronologiques datent l'initiation de la déformation dans le massif à partir 23 Ma (Chalandes et al., 2008, Rolland et al., 2009). Ainsi on peut estimer la vitesse de réchauffement aux alentours de 50°C.Ma<sup>-1</sup>. Challandes et al. (2008) proposent à partir de la modélisation thermique du massif une vitesse de réchauffement similaire (Fig. 22). Le modèle est contraint par le pic de température à 450°C et par l'enfouissement instantané du massif à 33 Ma. Ils observent ainsi une première étape de relaxation rapide de la température entre 33 et 23 Ma marqué par un réchauffement à 40 °C.Ma<sup>-1</sup> jusqu'à 400°C. (Fig. 22) Puis entre 23 et 17 Ma, la température atteint bien plus lentement son maximum. Ainsi, le massif de l'Aar semble se réchauffer bien moins rapidement que le massif du Mont Blanc.

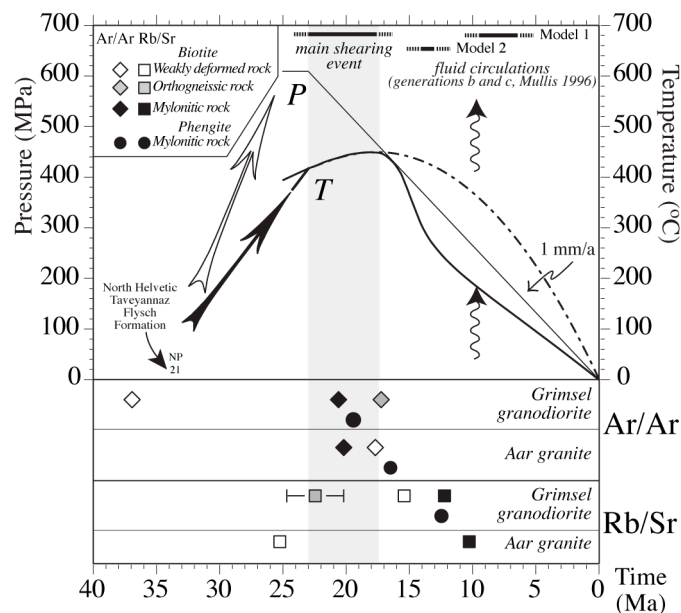


Figure 22. Modélisation 1D de l'évolution thermique du massif de l'Aar. Les ages 39Ar/40Ar et Rb-Sr montrent l'activation des dans de cisaillement autour du pic de température. (Chalandes et al., 2008).

Pourtant, si les datations réalisées par la méthode  $^{39}\text{Ar}/^{40}\text{Ar}$  datent l'activité des bandes de cisaillement dans les deux massifs à partir de 23 Ma (Aar : Fig. 22, Challandes et al., 2008 ; Mont Blanc : Rolland et al., 2008), la datation des allanites syn-tectoniques du massif du Mont Blanc indique une initiation de la déformation du massif bien plus précoce, à 29,5

Ma ([Cenki-Tok et al., 2013](#)). De ce fait, si le réchauffement du massif du Mont Blanc semble plus rapide, il faudrait réaliser le même type de datation U-Th-Pb dans les bandes de cisaillement du massif de l'Aar pour pouvoir les comparer. Enfin, on note que les erreurs sur les datations, particulièrement de l'enfouissement, peuvent être non négligeables ce qui engendre des variations des vitesses de réchauffement estimées pour les massifs. Ainsi, par exemple, compte tenu des barres d'erreurs, la vitesse de réchauffement du massif du Mont Blanc pourrait être de l'ordre de  $60^{\circ}\text{C}.\text{Ma}^{-1}$ . Enfin, il est possible que la relaxation thermique calculée pour le massif de l'Aar soit un peu lente car calculée en 1D. Il est en effet très probable que la relaxation soit plus rapide en 2D ou 3D. Des modèles restent donc à tester pour discuter plus avant ces vitesses de réchauffement.

#### *VII.1.2. Augmentation prograde de la pression.*

Si les conditions du pic de température dans les MCE commencent à être bien contraintes, ce n'est pas le cas de la pression (massif de l'Oisans 1-5kbar, [Jullien et Goffé, 1993](#) ; [Boutoux et al., 2014b](#) ; massif de l'Aar 6,5 kbar +/-1kbar, [Masson et Schreyer, 1987](#), [Goncalves et al., 2012](#)). Celle-ci n'est bien contrainte temporellement à son pic que dans le massif du Mont Blanc où il est estimé à 5kbar +/-0,05kbar et est synchrone du pic de température ([Cenki-Tok et al., 2013](#)). Ainsi le massif atteint sa pression maximale très rapidement, en 2 à 6 Ma. Le choix d'augmentation instantané de la pression dans les modèles d'enfouissement du massif de l'Aar proposé par [Challandes et al. \(2008\)](#), même s'il est évidemment exagéré, ne semble pas totalement inapproprié.

### **VII.2. Pic de métamorphisme.**

#### *VII.2.1. Un long pic de température.*

Une fois atteint, le pic thermique semble durer plusieurs Ma dans les massifs de l'Oisans, du Mont Blanc et de la nappe de Morcles. Dans la partie centrale du massif du Mont Blanc, les conditions P-T du pic de métamorphisme ( $400^{\circ}\text{C} +/-25^{\circ}\text{C}$  ; 5kbar +/-0,05kbar ; [Rolland et al., 2003](#)) sont datées de 29,5 Ma jusqu'à 16 Ma ([Rolland et al., 2008](#), [Cenki-Tok et al., 2013](#)). Ainsi, le pic thermique du massif s'étale sur presque 14 Ma. Dans la couverture du massif, les températures du flanc inverse de la nappe de Morcles varient entre 350 et

300°C entre 27 et 16 Ma (Kirschner et al., 1995). Dans ce cas, on note que le thermomètre utilisé, basé sur les  $\delta^{18}\text{O}$  de grains de quartz et de calcite ayant co-cristallisé, comporte une erreur minimale de 30°C (Kischner et al., 1994, 1995). Toujours est-il que la nappe de Morcles atteint plus ou moins un plateau thermique entre 27 et 16 Ma, légèrement plus court que celui du Mont Blanc. Dans le massif de l’Oisans, la température maximale enregistrée par les analyses RCSM est de 330°C +/-15°C et reste constante pendant quelques 8 Ma entre 33 et 25 Ma (Bellanger et al., 2015).

Dans le massif de l’Aar, Challandes et al., (2008) décrivent une légère augmentation de la température de 50°C entre la fin de l’enfouissement, à 23 Ma, et le pic de température daté à 17 Ma et estimé à 450 +/-25°C (Goncalves et al., 2012). Ainsi, de même que pour la nappe de Morcles, en prenant en compte l’erreur du thermo-baromètre, on peut estimer que le massif conserve plus ou moins sa température maximale pendant 5-6 Ma.

#### VII.2.2. Pic de pression.

Peu de données nous permettent d’établir si, de la même façon que le pic de température, le pic de pression s’étale sur plusieurs Ma dans l’ensemble des MCE. Dans le massif de l’Oisans par exemple, les estimations des pressions enregistrées par les bandes de cisaillement sont comprises entre 1 et 5 kbar (Bellanger et al., 2014). Des estimations plus précises ont pu être faites dans la couverture non décollée du massif (e.g. Bernard, 1978 : 2 à 2,4 kbar) mais ne sont pas datées sinon relativement. Il est donc difficile de savoir si ce massif a pu connaître un palier de pression à son pic. En revanche, dans le massif du Mont Blanc, la pression reste stable entre 29,5 et 16 Ma à 5kbar +/-0,05kbar (Cenki-Tok et al., 2013 ; Rolland et al., 2008). De la même façon, dans le massif de l’Aar, les modèles numériques proposés par Challandes et al. (2008) font l’hypothèse que la pression est constante depuis l’enfouissement instantané du massif à 33 Ma jusqu’à l’initiation de son exhumation, à 23 Ma. Rolland et al. (2009) proposent que la pression maximale soit conservée jusqu’entre 12 et 14 Ma. Ainsi, les phengites datées à 12-14 Ma comportent les mêmes rapports Si que celles mesurées par Massonne et Schrayer (1987) et datées par Challandes et al. (2008) entre 23 et 17 Ma. Dans ce cas, le pic de pression serait d’au moins 10 Ma si la pression maximale est contemporaine de l’initiation des bandes de cisaillement. On note cependant que Goncalves et al. (2012) relient les variations du rapport Si aux circulations de fluides. Ainsi, le maintien du pic de pression du massif jusqu’à 12 Ma reste incertaine.

Cependant au vu de l'ensemble des données, l'étalement dans le temps du pic de température semble s'appliquer sur une large portion des zones externes de l'arc alpin, depuis l'Oisans jusqu'à l'Aar et ainsi être caractéristique de la déformation des MCE (Bellahsen, 2014) et dû aux déformations distribués en profondeur qui n'impliquent que très peu d'exhumation des unités. En fin de compte, bien qu'il n'existe que très peu de données précises sur la pression au pic de métamorphisme, il semble très probable que celui soit long, avec une durée de 5 à 15 Ma.

### VII.3. Exhumation vs. Refroidissement.

L'initiation de l'exhumation du massif du Mont Blanc est estimée à 23 Ma (Boutoux et al., *in prep*) du fait de l'initiation de la Mont Blanc Shear Zone (Rolland et al., 2003) et l'exhumation majeure commence vers 16-18 Ma. Certaines bandes de cisaillement de la partie centrale du massif, datées à 16 Ma, sont formées dans les conditions P-T du pic de métamorphisme (Rolland et al., 2003). Ainsi entre 23 et 16 Ma, le refroidissement devrait rester faible, inférieur à 50°C. Entre 16 et 18 Ma, le massif subit une accélération de son refroidissement puisque les données ZFT du massif sont réparties entre 11 et 16 Ma (Goltzbach et al., 2008). De même, la donnée ZFT disponible pour le massif des Aiguilles Rouges est à 17 Ma (Soom, 1990), indiquant l'initiation du refroidissement et la fin du pic thermique (Boutoux et al., *in prep*). Enfin Burkhard et Sommaruga, (1998) datent l'activation du chevauchement subalpin connecté aux accidents structurant le massif des Aiguilles Rouges et enraciné sous le massif du Mont Blanc entre 16 et 18 Ma. Puisque la pression reste constante tout au long du pic de métamorphisme du Mont Blanc, on interprète ce refroidissement comme l'initiation de l'exhumation des deux massifs (AR et MB) par le jeu de cette rampe crustale.

Il semble pourtant exagéré d'attribuer l'ensemble de l'exhumation des MCE qu'au seul jeu de ces rampes crustales. En effet, dans le massif du Mont Blanc, la Mont Blanc Shear Zone est active au moins jusqu'à 6 Ma (Leloup et al., 2005) et le Mont Blanc Back Thrust est initié à 16 Ma (Rolland et al., 2008). Or, sur les coupes, ces deux structures semblent accommoder une partie de l'exhumation du massif (e.g. Escher et al., 1993 ; Leloup et al., 2005 ; Boutoux et al., *in prep*). Puisque le taux de refroidissement du massif du Mont Blanc est bien supérieur à celui du massif des Aiguilles Rouges (Fig.), la Mont Blanc Shear Zone et le Mont Blanc Back Thrust doivent accommoder une partie de l'exhumation (Boutoux et al., *in prep*). De même, dans le massif de l'Oisans, la fin du pic de température et l'initiation de

l'exhumation est datée à 25 Ma (Crouzet et al., 2001 ; Bellanger et al., 2015), avant l'initiation du raccourcissement dans la chaîne subalpine du Vercors datée vers 18-20 Ma (Philippe et al., 1998). A partir de cette date, le massif de l'Oisans est sans doute exhumé du fait de l'activité des rampes crustales et entre 25 et 18 Ma, l'initiation de l'exhumation du massif de l'Oisans est alors accommodée totalement par les bandes de cisaillement structurant le socle (Bellahsen et al., 2012, 2014). Enfin, Challandes et al. (2008), dans leur modèle du chemin P-T-t du massif de l'Aar, proposent que l'exhumation soit plus précoce que le refroidissement du massif. Ainsi, la pression suit un plateau à 6 kbar pendant 10 Ma, depuis l'enfouissement à 33 Ma jusqu'à l'initiation de l'exhumation à partir de 23 Ma. La phase de raccourcissement majeur du massif étant datée de cette période (Challandes et al., 2008, Rolland et al., 2009), l'exhumation du massif est associée au fonctionnement des bandes de cisaillement structurant le massif.

Il semble donc que tout le long de l'arc alpin, l'exhumation soit en partie accommodée par les cisaillements de socle structurant les MCE et par des rampes d'échelle crustale connectées aux chaînes subalpines.

## VII.4. Scénario d'inversion de la marge alpine.

Dans cette partie nous allons tenter d'intégrer à la fois les résultats des chapitres précédents et les questions soulevées et les quelques éléments de réponse apportés lors de la discussion dans un modèle conceptuel de l'inversion alpine.

La phase de collision, dans les Alpes de l'Ouest, fait suite à la subduction continentale de la partie distale de la marge européenne (la zone Briançonnaise notamment). Elle se caractérise par l'enfouissement et le raccourcissement « thick-skinned » de la partie proximale de la marge (la zone Dauphinoise) sous les unités d'affinité plus distale (unités internes). Les unités non enfouies (chaînes subalpines) sont décollées de leur socle et raccourcies en un style thin-skinned pour former la chaîne d'avant-pays.

### VII.4.1. Etat pré-collisionnel

On représente ici la marge européenne par un bloc 3D orienté Est-Ouest et épais d'une trentaine de kilomètres, en accord avec les restaurations proposées (Burkhard et Sommaruga, 1998 ; Bellahsen et al., 2014) et les données sismiques (e.g. profil ECORS-CROP, Roure et

al., 1990 Mugnier et al., Nicolas et al., 1990). La transition de comportement cassant/ductile séparant les croûtes inférieure et supérieure est située entre les isothermes 300 et 400 °C et est située aux alentours de 15 km de profondeur avant la collision (Fig. 22A). La marge est structurée par deux demi-grabens extensifs hérités de la phase de rifting liasique (Lemoine et al., 1989, Barféty et al., 1970a, b). Ces bassins, nommés « bassin 1 » et « bassin 2 » (Fig. 22A) sont respectivement profonds de 3 et 5 km et larges d'une quinzaine de kilomètres, en accord avec les restaurations (e.g. Burkhard et Sommaruga, 1998 ; Boutoux et al., 2014a). Les bassins sont chacun limités à l'Ouest par une faille normale orientée Nord/Sud à pendage 70° vers l'Est. L'accident d'échelle crustale représenté par un plan rouge à pendage Est symbolise le Front Pennique (Fig. 22A). Celui-ci permet le charriage des unités distales de la marge sur la marge proximale et est actif dès le début de la collision. La couverture sédimentaire mésozoïque de la marge (aussi bien le remplissage des bassins extensifs que la couverture des zones moins amincies) est symbolisée par une couche bleu clair (Fig. 22A). Les enveloppes rhéologiques de la croûte sont tracées à partir de la droite de friction de Byerlee (avec un coefficient de friction de 0,6) pour la partie cassante et de deux courbes de fluage pour la partie ductile. Pour le socle (/la croûte), la courbe de fluage est construite à partir des lois de glissement/dislocation du quartz. La courbe de fluage des sédiments de la couverture est tracée en appliquant un coefficient pré-exponentiel 1000 fois inférieur à celui du socle (Bellahsen et al., 2012).

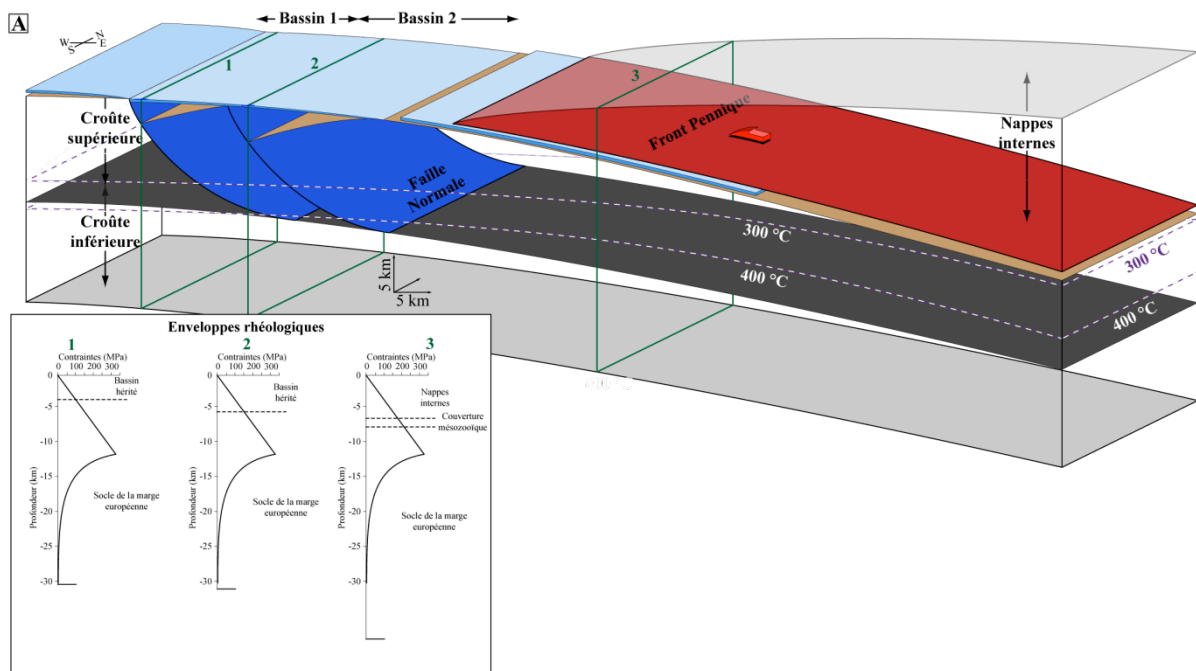


Figure 22A. Structure de la marge avant la collision.

#### *VII.4.2. Enfouissement de la marge*

L’initiation de la collision est datée aux environs de 35 Ma. Elle suit la phase de subduction continentale et est marquée par la progression vers l’Ouest des dépôts du flysch priabonien sur l’ensemble de l’arc alpin (Sinclair, 1997 ; Ford et Lickorisch, 2004). Ces derniers dépôts marquent l’initiation de l’enfouissement des futurs MCE de façon relativement synchrone sur l’ensemble de l’arc alpin. Ainsi, cet enfouissement est daté dans l’Oisans entre 34 et 28 Ma (Sinclair, 1997, Ford et Lickorisch, 2004, Mulder et al., 2010), entre 36 et 29 Ma au niveau de la nappe de Morcles et entre 34 et 33 Ma au niveau du massif de l’Aar (Lateltin, 1987 ; Fischer et Villa, 1990 ; Berggren et al., 1995 ; Ruffini et al., 1997). Le massif des Aiguilles Rouges, situé à l’Ouest du massif du Mont Blanc est enfoui quelques Ma après celui-ci, entre 32 et 29 Ma (Burkhard et Sommaruga, 1998 ; Boutoux et al., in prep.). L’enfouissement des bassins semble se faire rapidement et sans raccourcissement important ni de la couverture ni du socle des bassins hérités. Ainsi, le réchauffement des MCE et de leur couverture s’est fait avec une vitesse comprise entre 40 et 100°C.Ma<sup>-1</sup>, entre 36 et 23 Ma. (Kirschner et al., 1995 ; Challandes et al., 2008 ; Bellanger et al., 2015, Boutoux et al., in prep.). Pendant l’enfouissement, le raccourcissement de la couverture des bassins hérités est faible, comme dans la nappe de Morcles (Kischner et al., 1995) ou dans la couverture des bassins de l’Oisans (Bellahsen et al., 2012 ; Boutoux et al., 2014a et b). Il en est de même dans le socle des bassins hérités où le raccourcissement ne commence qu’au pic de métamorphisme dans l’Oisans (Bellanger et al., 2015), dans le Mont Blanc (Cenki-Tok et al., 2013) ou dans l’Aar (Challandes et al., 2008).

Pendant cette période d’enfouissement des MCE, les nappes Ultra-Helvétiques (nappes des Diablerets et du Wildhorn) enfouie autour de 36 Ma sont décollées de leur socle entre 36 et 32 Ma (Kirschner et al., 2003) et empilées au dessus de la couverture du Mont Blanc (Burkhard et Sommaruga, 1998).

Les chevauchements permettant le charriage de ces unités de couverture sur des distances plurikilométriques sont extrêmement localisés. Ainsi le Glarus Thrust qui permet le charriage des nappes Ultra-Helvétiques au-dessus du massif de l’Aar sur plus de 60 km n’est épais que de quelques mètres. Ces accidents très localisés permettent la chenalisation de quantités importantes de fluides profonds tout au long de leur fonctionnement, ce qui explique la modification des signatures isotopiques de la couverture à leur niveau (e.g. Badertscher et al., 2002 ; Burkhard et al., 1992 ; Abart et al., 2002). Dans notre modèle, le charriage vers

l’Ouest des unités internes permet l’enfouissement passif des bassins 1 et 2 sous le Front Pennique (Fig. 22B). La couverture mésozoïque de la marge située sur les hauts de socle est décollée et plissée au cours de l’enfouissement (Fig. 22B). Avec l’augmentation de la profondeur, le contraste rhéologique entre socle et couvercle est de plus en plus marqué (Fig. 22B).

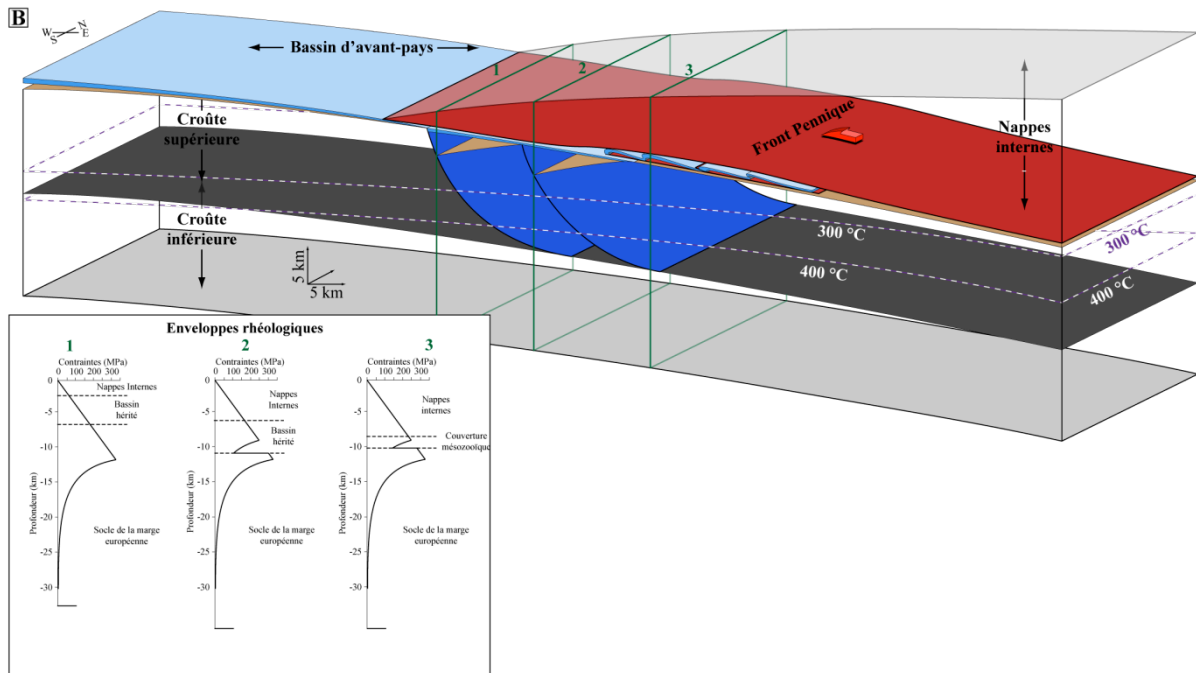


Figure 22B. Enfouissement des bassins de la marge proximale

#### VII.4.3. Pic de température, pic de pression et raccourcissement du socle des MCE.

Le pic de métamorphisme est atteint par les MCE et leur couverture entre 29,5 et 27 Ma dans les massifs de l’Oisans (Bellanger et al., 2015), du Mont Blanc (Cenki-Tok et al., 2013), de sa couverture (Kirschner et al., 1995). Le massif des Aiguilles Rouges étant situé plus à l’Ouest, celui-ci est enfoui avec un décalage léger par rapport au Mont Blanc et atteint son pic de métamorphisme probablement vers 26 Ma (Boutoux et al., *in prep*).

Dans le massif du Mont Blanc, le pic thermique est synchrone du pic de pression (Rolland et al., 2008, Cenki-Tok et al., 2013, Boutoux et al., *in prep*) et il est de ce fait probable que cela soit le cas aussi de sa couverture, la nappe de Morcles. Dans le massif de l’Aar les deux pics pourraient être diachrones et séparés de 5 Ma au maximum (Challandes et al., 2008). Les pics thermiques s’étalent sur plusieurs Ma sur l’ensemble des MCE. Dans l’Oisans il est daté entre 31 et 25 Ma (Bellanger et al., 2015) entre 29,5 et 16 Ma dans le Mont

Blanc (Rolland et al., 2008 ; Cenki-Tok et al., 2013), entre 27 et 16 Ma dans sa couverture la nappe de Morcles (Kirschner et al., 1995), entre 27 et 18 Ma dans les Aiguilles Rouges (Boutoux et al., in prep) et entre 23 et 17 Ma dans le massif de l'Aar (Challandes et al., 2008).

Le fonctionnement des bandes de cisaillement qui structurent le socle des MCE au niveau des anciens bassins hérités de la marge est contemporain du pic de métamorphisme. Ainsi, dans le massif du Pelvoux, à l'Est du massif de l'Oisans, les bandes de cisaillement sont datées entre 34 et 31 Ma (Simon-Labréteau et al., 2009). Dans l'Oisans, le pic de déformation a lieu entre 33 et 25 Ma (Bellanger et al., 2015). Enfin, dans le massif du Mont Blanc, ces bandes se forment entre 29,5 et 16 Ma (Rolland et al., 2008 ; Cenki-Tok et al., 2013) et entre 23 et 17 Ma dans le massif de l'Aar (Challandes et al., 2008).

Ces bandes sont caractérisées dans tous les MCE par le cisaillement très pénétratif du socle des bassins hérités (Rolland et al., 2003, Simon-Labréteau et al., 2009 ; Rolland et al., 2009 ; Bellahsen et al., 2012 ; Bellanger et al., 2015). Leur épaisseur varie de quelques cm à quelques dizaines de mètres dans la partie centrale du Mont Blanc (Rolland et al., 2003) à plusieurs centaines de mètres dans l'Oisans (Bellahsen et al., 2012 ; Bellanger et al., 2015) voire plusieurs kilomètres pour la Mont Blanc Shear Zone (Leloup et al., 2005). Ces bandes phyllonitiques et mylonitiques sont composées d'un assemblage minéral dont la composition varie en fonction des protolites. On note cependant la présence systématique de phengites et de chlorites syn-tectoniques caractéristiques du faciès métamorphique schiste vert ainsi que la réduction de la taille des grains du protolite et leur recristallisation dynamique (e.g. Rolland et al., 2003 ; Bellanger et al., 2014).

Malgré le raccourcissement des bassins hérités, leurs failles normales bordières ne sont pas réactivées, que ce soit dans l'Oisans (Bellahsen et al., 2012 ; Boutoux et al., 2014a) ou dans le bassin de Chamonix, au niveau du massif du Mont Blanc (Boutoux et al., 2014). Cela semble être le cas d'une grande partie des bassins hérités de l'arc alpin (Bellanger, 2013 ; Lafosse et al., in prep). On note cependant que plus au Nord, dans le massif de l'Aar en plus des cisaillements alpins néoformés, les accidents hérités (les failles normales) sont interprétés comme réactivés en inverses et étendus dans la couverture du massif (Burkhard, 1988).

Dans le modèle d'inversion de la marge, une fois atteint le pic de métamorphisme entre 300 et 400°C, le socle des bassins hérités commence à être cisaillé et raccourci sans être notablement exhumé (Fig. 22C). Le socle atteint la profondeur de fluage et dès lors prend un comportement ductile ce qui marque un très net affaiblissement de la résistance de la croûte au niveau des bassins hérités (Fig. 22C, Bellahsen et al., 2012, 2014). L'affaiblissement du socle au niveau des bassins provoque alors le plissement, du fait des cisaillements, et le

pincement des bassins ce qui entraîne le redressement et la non réactivation des failles normales héritées. On note que l'affaiblissement du socle en profondeur est sans doute renforcé par la formation de phyllosilicates (phengites, talc) dans les bandes de cisaillement des MCE (e.g. Challandes et al., 2008 ; Rolland et al., 2009 ; Bellanger et al., 2014 ; Boutoux et al., 2014b). Enfin, à ce stade, les cisaillements du socle ne sont pas propagés dans la couverture. (Fig. 22C, Lafosse et al., in prep).

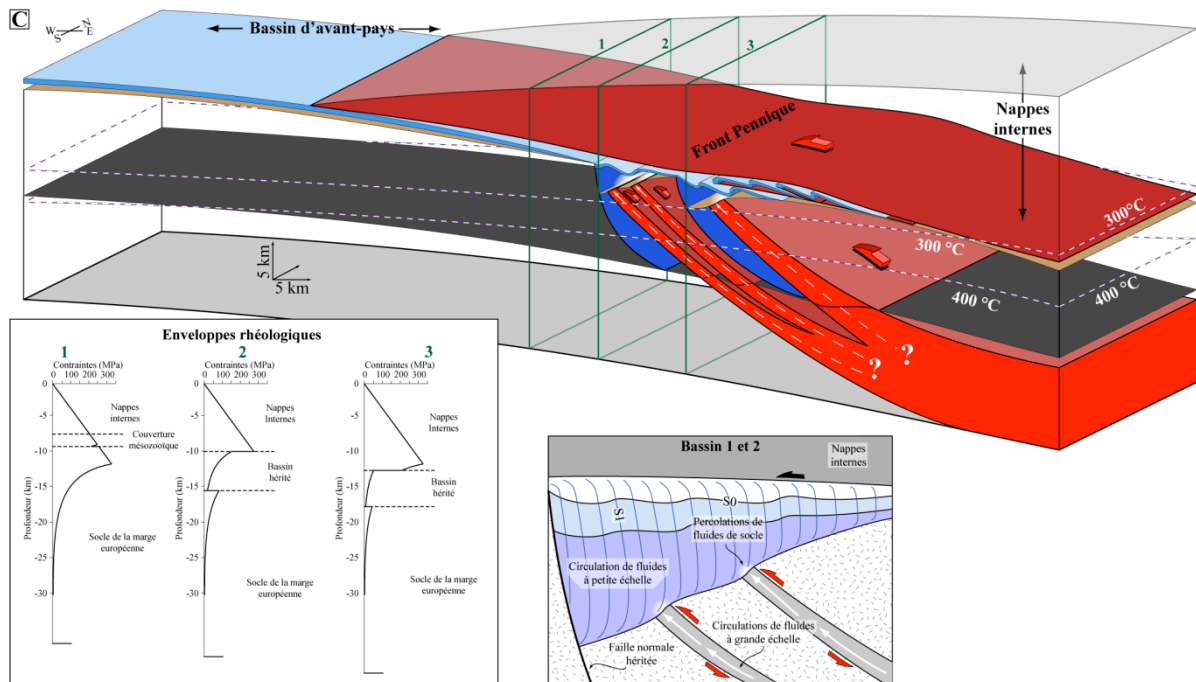


Figure 22C. Initiation de l'inversion de la marge au pic de métamorphisme.

#### VII.4.4. Raccourcissement de la couverture des bassins des MCE.

Si les déformations progrades de la couverture des bassins ne sont que peu contraintes, il semble que celle-ci ne soit que peu raccourcie au cours de l'enfouissement. Dans la couverture des bassins de l'Oisans et dans la nappe de Morcles la première génération de veine semble s'être développée à proximité du pic de métamorphisme (Boutoux et al., 2014b, Kirschner et al., 1995). Sur l'ensemble de l'arc alpin, on constate un même style des déformations de la couverture des bassins hérités, plissée disharmoniquement au-dessus des plis de socle, au niveau de l'Oisans (e.g. Gratier et al., 1973, Gratier et Vialon, 1980, Bellahsen et al., 2012), au niveau de la couverture du massif du Mont Blanc, les nappes du mont Joly et de Morcles, et du bassin de Chamonix (e.g. Epard, 1990 ; Escher et al., 1993 ;

Boutoux et al., 2014a) ou encore dans le Synclinal Médian (massif de Belledonne, Bellahsen et al., 2014).

On résume ici les grandes étapes de la déformation de la couverture lors du pic de métamorphisme. Ainsi, avec le pincement des bassins dû au cisaillement du socle et du fait de la non réactivation des failles normales, l'interface socle/couverture est cisaillée. Une première phase de schistosité (S1 top-vers l'Est) se développe alors au sein de la couverture (Bellahsen et al., 2012), associée à une première génération de veines métamorphiques (Boutoux et al., 2014a). Le raccourcissement des bassins s'intensifie progressivement au pic de métamorphisme alors que le charriage vers l'Ouest des unités internes se poursuit jusqu'à 27 Ma (Simon-Labréteau et al., 2009). De ce fait le plissement de la couverture s'intensifie et est progressivement déversé vers l'Ouest et associé au développement d'une seconde phase de schistosité et de veines métamorphiques (Bellahsen et al., 2012 ; Boutoux et al., 2014a, b). La déformation de la couverture s'arrête à ce stade dans l'Oisans mais se poursuit plus au Nord, au niveau de la couverture du Mont Blanc (Boutoux et al., 2014a).

Les bandes de cisaillement sont reconnues comme chenaux efficaces des circulations de fluides dès leur initiation (e.g. Challandes et al., 2008 ; Oliot et al., 2010, 2012 ; Goncalves et al., 2012 ; Boutoux et al., 2014b). Puisque les structures cisaillantes sont restreintes au socle des bassins hérités, dans la couverture les circulations de fluides demeurent très locales, de l'ordre de quelques centimètres à quelques mètres (Boutoux et al., 2014b). Ainsi dans les unités de couverture où les déformations sont diffuses (type Oisans), les circulations de fluides sont restreintes à l'échelle des unités lithologiques (Henry et al., 1996 ; Boutoux et al., 2014b). Ces circulations à petite échelle permettent la redistribution de la matière et l'accommodation de la déformation par pression-dissolution des sédiments de la couverture des bassins et des hauts de socle (Boutoux et al., 2014a). A l'aplomb des cisaillements de socle, il existe des indices de percolation de fluides de socle au sein de la couverture suggérant le caractère synchrone des déformations du socle et de la couverture des bassins hérités (Boutoux et al., 2014b).

Dans le modèle d'inversion de la marge, une fois atteint le pic de métamorphisme entre 300 et 400°C, le socle des bassins hérités 1 et 2 commence à être cisaillé et raccourci sans être notablement exhumé (Fig. 22C). Au niveau des anciens hauts de socle, en l'absence d'une couverture épaisse pour localiser la déformation, la croûte reste plus résistante (Fig. 22C). Dans les Bassins 1 et 2, la couverture épaisse commence à être plissée et une première phase de schistosité se développe (S1, Fig. 22C, Bassin 1 et 2). Cette schistosité pend vers l'Est au sommet de la couverture du fait du charriage des unités internes et pend vers l'Ouest

à l'interface socle/couverture du fait du pincement des bassins 1 et 2 (S1, [Fig. 22C, bassin 1 et 2](#)). Avec la poursuite du raccourcissement au pic de métamorphisme dans les bassins 1 et 2, une deuxième schistosité (S2) se développe. Cette schistosité (S2) se surimpose à S1 à l'interface socle/couverture (S1, [Fig. 22C, Bassin 1 et 2](#)). Les fluides chenalés dans les bandes de cisaillement de socle et percolant faiblement dans la couverture sont indiqués par les flèches blanches en pointillés ([Fig. 22C](#)).

#### *VII.4.5. Exhumation des MCE.*

L'exhumation des MCE est initiée de façon relativement uniforme entre 16 et 18 Ma le long de l'arc alpin ([Boutoux et al., in prep](#)). Elle est caractérisée par l'activation des chaînes subalpines (i.e. Vercors, Chartreuse, Bornes) dont les détachements basaux sont connectés à des rampes crustales enracinées sous les MCE ([Bellahsen et al., 2014](#)). Au niveau de l'Oisans le début de l'exhumation, initiée plus tôt, à 25 Ma ([Crouzet et al., 2001](#) ; [Bellanger et al., 2015](#)) semble être en partie accommodée par le fonctionnement des bandes de cisaillement de socle formées au pic de métamorphisme. Sur la partie Nord de l'Arc, au niveau du massif de l'Aar, l'activité des cisaillements de socle semble assurer une partie de l'exhumation du massif en trois principales étapes : 23-17 Ma, 14-12 Ma et 9-3 Ma ([Burkhard, 1988](#) ; [Challandes et al., 2008](#) ; [Rolland et al., 2009](#)).

Dans le modèle d'inversion de la marge, l'exhumation des bassins 1 et 2 est assurée principalement par l'activité d'une rampe crustale enracinée sous les massifs et connectée aux chevauchements de la chaîne d'avant-pays ([Fig. 22C](#)). Les deux bassins, et particulièrement le bassin 2, sont aussi exhumés du fait de l'activité des bandes de cisaillement du socle formées au pic de métamorphisme ([Fig. 22C Bassin 2](#)).

Après le pic de métamorphisme, si les bandes de cisaillements structurant le socle des bassins sont actives lors de l'exhumation, la couverture continue d'être raccourcie. Ainsi, dans le massif de l'Oisans, si les bandes de cisaillement sont actives entre 25 et 18 Ma, le plissement de la couverture continue alors de s'intensifier pendant l'exhumation. Puisque ces bandes ne se propagent pas dans la couverture, le style de déformation de cette dernière reste inchangé. Au niveau du massif du Mont Blanc, par contre, la déformation du bassin semble s'intensifier à partir de 16 Ma ([Rolland et al., 2008](#) ; [Boutoux et al., in prep](#)). Ainsi, la Mont Blanc Shear Zone est active jusqu'à 6 Ma ([Leloup et al., 2005](#)) et on note l'initiation du Mont Blanc Back Thrust à 16 Ma ([Rolland et al., 2008](#)). Le bassin de Chamonix est alors de plus en plus pincé et structuré en pop-up. Allant de pair avec cette structuration, la couverture du

massif est progressivement extrudée au-dessus du massif des Aiguilles Rouges et structurée en nappes (i.e. les nappes du Mont Joly et de Morcles, Epard, 1990 ; Escher et al., 1993). L’extrusion des nappes peut être datée par les dernières déformations enregistrées dans la nappe de Morcles, entre 16 et 10 Ma (Kirschner et al., 2003) et par le cisaillement de la partie sommitale du massif des Aiguilles Rouges (Egli, 2013).

Lors de son extrusion, le flanc inverse de la nappe de Morcles est très fortement étiré et cisaillé (Ramsay et Hubert, 1989) ce qui permet alors la chenalisation de fluides de socle (Kirschner et al., 1999). Les quantités de fluide de socle chenalés au sein de cette couverture sont alors suffisamment importantes pour perturber le signal isotopique des nappes. Si ces fluides dérivent du socle du Mont Blanc, il devrait alors exister une continuité entre la Mont Blanc Shear Zone et le flanc inverse de la nappe de Morcles (Boutoux et al., 2014b). Si les fluides de socle dérivent des petites bandes de cisaillement sommitales situées au sommet des Aiguilles Rouges (Egli, 2013), il existerait une continuité entre ces cisaillements et le flanc inverse de la nappe de Morcles. Néanmoins, ces bandes étant de faible ampleur, il semble peu probable qu’elles permettent la chenalisation de quantités de fluides suffisantes pour modifier la signature isotopique du flanc inverse de la nappe de Morcles. Enfin dans le massif de l’Aar, la propagation des bandes de cisaillement dans la couverture est là-aussi montrée par la variation du signal isotopique des veines de la couverture à proximité des cisaillements (Marqueur et Burkhard, 1992).

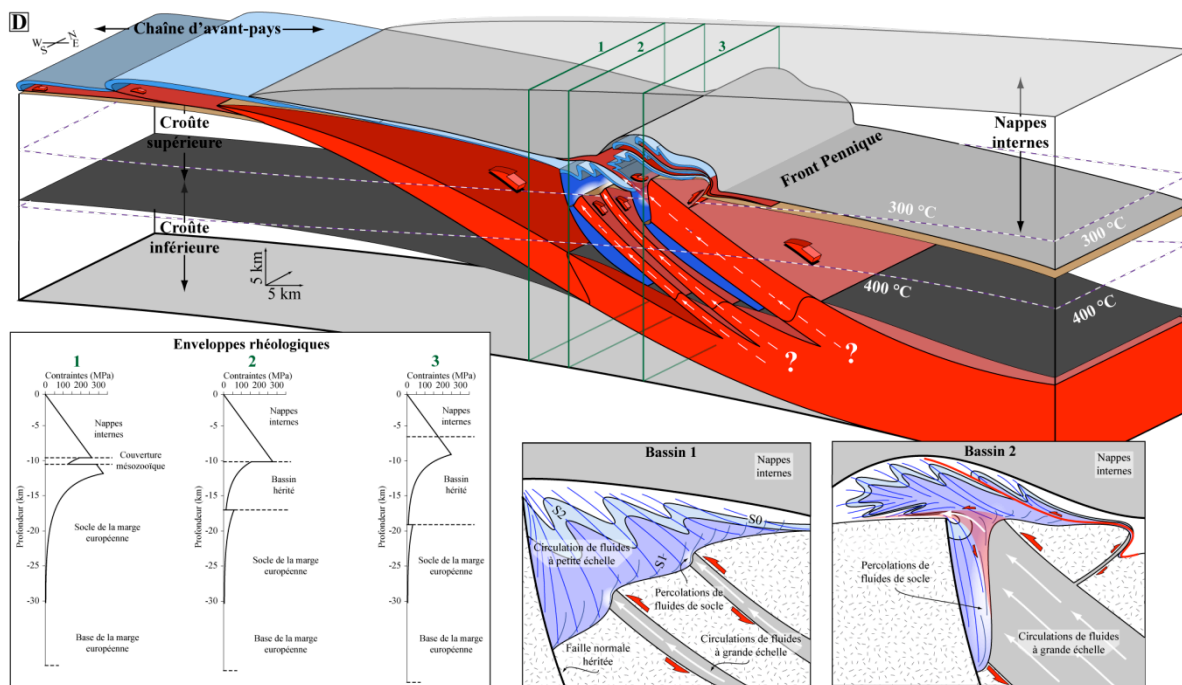


Figure 22D. Exhumation du prisme collisionnel.

## **VIII. Conclusions**

### **\* Nouvelles données thermochronométriques et thermiques pour le massif des Aiguilles Rouges**

Les nouvelles données thermochronologiques de basse température U-Th-Sm (ZHe) permettent de préciser la séquence de refroidissement du massif des Aiguilles Rouges qui semble s'initier avec l'activation des rampes crustales frontales. Les nouvelles données RSCM (Raman) de la couverture sédimentaire du massif des Aiguilles Rouges indiquent une température maximale de 315°C +/-25°C.

### **\* Chemins Temps-température des Aiguilles Rouges et du Mont Blanc.**

A partir des nouvelles données ZHe et Raman et de la compilation des données (thermochronologiques géochronologiques et sédimentaires) de la littérature, on propose des histoires thermiques pour les massifs des Aiguilles Rouge et du Mont Blanc. Les massifs sont enfouis entre 31 et 28 Ma et se réchauffent très rapidement, à des vitesses entre 60 et 100°C.Ma<sup>-1</sup>. Les pics de températures sont étalés dans le temps pour les deux massifs qui ne se refroidissent qu'à partir de 16 à 18 Ma. Jusqu'à 5 Ma, le massif du Mont Blanc se refroidit bien plus vite que celui des Aiguilles Rouges.

### **\* Evolution structurale**

La déformation des MCE des Aiguilles Rouges et du Mont Blanc n'a lieu qu'à partir du pic de métamorphisme initié entre 29,5 et 26 Ma. Les bandes de cisaillements développées au pic ne permettent pas d'exhumation notable avant 16 Ma. L'exhumation est assurée par des rampes crustales connectées aux chaînes subalpines et au jeu de la Mont Blanc Shear Zone. A partir de 16 Ma la nappe de Morcles est extrudée de son bassin et charriée sur le massif des Aiguilles Rouges.

### **\*Déformation de la couverture des bassins de l'Oisans**

On apporte de nouvelles données structurales et microstructurales sur la couverture des bassins hérités de Bourg d'Oisans et de Mizoën. L'ensemble des microstructures, schistosités et veines, de la couverture sont explicables dans un continuum de raccourcissement Est-Ouest. L'initiation de ce raccourcissement provoque le cisaillement de l'interface entre socle

et couverture du bassin. A la base de la couverture, on détermine trois générations de veines métamorphiques.

#### \* Remplissage des veines de la couverture des bassins de l’Oisans

On fournit de nouvelles données géochimiques du remplissage des veines métamorphiques et des roches de la couverture ainsi que du socle cisaillé pour les bassins de l’Oisans. Les veines métamorphiques de la couverture des bassins sont à l’équilibre géochimique avec leur roche encaissante (analyses isotopique, et observation en cathodoluminescence). Elles sont remplies par diffusion de matière depuis la matrice vers les veines (observations MEB). De petites quantités de fluides dérivés du socle ont percolé à la base de la couverture et à proximité du cisaillement de socle de Huez dès l’initiation du raccourcissement du bassin de Bourg d’Oisans (analyses des concentrations en éléments traces).

Le raccourcissement de la couverture et le fonctionnement des bandes de cisaillement du socle sont synchrones et réalisés dans des conditions P-T proches du pic de métamorphisme (250-400°C et 2-5kbar).

#### \* Circulations de fluides dans les MCE

Les bandes de cisaillements structurant les bassins hérités de la marge chenalise les circulations de fluides à l’échelle de la coûte dès leur initiation, au pic de métamorphisme. Les bandes de cisaillement étant restreintes au socle, les fluides chenalés percolent en faible quantité à la base de la couverture des bassins où ils se mélangent avec les fluides produits localement et à l’équilibre géochimique avec les roches de la couverture. Lors de la fin du pic de métamorphisme et du début de l’exhumation des MCE, la couverture de certains des bassins hérités, situés au Nord de l’Arc, est extrudée et structurée en nappe dont le flanc inverse est cisaillée. L’ouverture du système isotopique dans ces cisaillements s’explique par la propagation des cisaillements du socle dans le flanc inverse des nappes permettant l’extension des circulations de fluides de socle.

#### \* Nouvelle méthode de restauration contrôlée par la déformation finie des roches.

On développe une méthode de restauration des coupes déformées dans le domaine ductile. On propose la conservation de l’aire située entre les axes de plis et les limites stratigraphiques lors de la déformation. La restauration de la coupe est contrôlée localement par la restauration des ellipsoïdes de la déformation finie mesurée sur le terrain.

A partir de cette méthode, on restaure la nappe de Morcles au dessus du massif du Mont Blanc pour lequel on peut ainsi proposer des quantités et des taux de raccourcissement.

#### \* Style d'inversion des bassins des bassins hérités et enfouis

La modélisation thermomécanique de l'inversion des bassins hérités et enfouis montre que la réactivation en inverse des failles normales héritées est fortement dépendante de la profondeur. L'enfouissement tectonique favorise le plissement du socle ce qui entraîne le pincement des bassins hérités et l'extrusion de la couverture. Le style d'inversion mis en évidence par ces résultats est cohérent avec les observations menées dans les bassins de l'Oisans.

## IX. Perspectives de recherche.

### IX.1. Études structurale et microstructurale et datations géochronologiques des déformations du Mont-Blanc.

Il existe quelques données géochronologiques sur les bandes de cisaillement affectant les MCE ([Rolland et al., 2008](#) ; [Simon-Labbrick et al., 2009](#) ; [Cenki-Tok et al., 2013](#) ; [Bellanger et al., 2014](#)). Quelques études pétrologiques et thermo-barométriques ont permis de caractériser les conditions PT de formation de ces bandes de cisaillement ([Rolland et al., 2003](#) ; [Bellanger et al., 2015](#)). Ces études ont permis de dater précisément l'activation, lors du pic de métamorphisme, de ces bandes de cisaillement. Pourtant, elles ne nous permettent pas de comprendre précisément leur évolution au cours de la déformation progressive. On se propose donc, à partir d'une étude pétrologique et géochronologique précise de la Mont Blanc Shear Zone, de préciser l'évolution de cette bande de cisaillement au cours du temps et de caractériser le rôle de la foliation hercynienne sur son développement. Il s'agit alors de mieux définir les paramètres influant sur le développement d'une bande de cisaillement dans une roche comportant une forte anisotropie initiale et de préciser la cinématique de ce développement.

### IX.2. Étude de la structure thermique des nappes de Morcles, du Mont-Joly et des nappes de l'Ultra-Dauphinois.

Dans la nappe de Morcles, les isothermes calculés à partir de la cristallinité de l'illite sont moins plissés que les couches de celle-ci (Burkhard and Goy-Egenberger, 2003). Comme on l'a montré dans le modèle conceptuel de l'inversion de la marge proximale européenne, la couverture du Mont-Blanc a donc acquis sa structure thermique au cours de sa déformation. Le pic de température a été atteint pour la partie Nord de la couverture du bassin de Chamonix (la nappe de Morcles) pendant l'inversion du bassin. Puisque ces isothermes sont redressés et pentés vers l'Ouest, l'extrusion de la nappe a eu lieu après l'acquisition après le pic de température. La géométrie d'inversion des bassins hérités étant fortement dépendante de leur structure thermique (Buiter et al., 2009 ; Lafosse et al., *in prep*), il semble intéressant de mieux comprendre celle-ci dans le but de mieux caractériser leur inversion collisionnelle. Ainsi, l'apport de nouvelles données RSCM (Raman) nous permettrait de préciser la structure thermique de la nappe de Morcles de les confronter directement avec celles obtenues dans le bassin de Chamonix et ainsi de préciser le timing et la cinématique de l'inversion du bassin. Cette étude peut aussi être menée à partir de nouvelles données RSCM (Raman) réalisée sur la nappe du Mont Joly. Cette nappe est en effet interprétée comme l'équivalent Sud de la nappe de Morcles et est restaurée dans le bassin de Chamonix (Epard 1990). Enfin, il serait aussi intéressant de confronter la structure thermique de la nappe de Morcles (et du Mont-Joly) avec celles des nappes Ultra Dauphinoises. Ces nappes enfouies plus profondément que le bassin de Chamonix sont interprétées comme décollées précocement de leur socle situé au Sud-Est du massif du Mont-Blanc.

## X. Références.

- Affolter, T., Faure, J.-L., Gratier, J.-P., Colletta, B., 2008. Kinematic models of deformation at the front of the Alps: new data from map-view restoration. *Swiss J. Geosci.* 101, 289–303. doi:10.1007/s00015-008-1263-3
- Abart, R., Badertscher, N.P., Burkhard, M., Povoden, E., 2002. Oxygen, carbon and strontium isotope systematics in two profiles across the Glarus thrust: implications for fluid flow. *Mineral. Petrol.* 143, 192–208.
- Agard, P., Jolivet, L., Goffé, B., 2001. Tectonometamorphic evolution of the Schistes Lustres complex: implications for the exhumation of HP and UHP rocks in the western Alps. *Bull. la Société Géologique Fr.* 172, 617–636. doi:10.2113/172.5.617
- Badertscher, N.P., Beaudoin, G., 2002. Glarus overthrust: A major pathway for the escape of fluids out of the Alpine orogen. *Geology* 30, 875–878. doi:10.1130/0091-7613(2002)030<0875
- Badoux H (1971) Notice explicative, feuille 1305 Dt. de Morcles 1:25,000. *Atlas Geol Suisse*
- Barbier, R., Barfety, J.C., Bocquet, A., Bordet, P., Le Fort, P., Meloux, J., Mouterde, R., Pocher, A., Petiteville, M., 1973. Carte géologique de la France (1/50.000), feuille de La Grave (798). Bureau de Recherches géologiques et minière, Orléans.
- Barfety, J.-C., Gidon, M., Mouterde, R., 1970. Observations stratigraphiques et structurales sur le Mézozoïque des environs de Bourg-d'Oisans (Isère). *Géologie Alp.* 46, 23–28.
- Barfety, J.-C., Gidon, M., Haudour, J., Sarrot-Reynauld, J., 1970. Nouvelles observations sur les conditions de sédimentation du Trias et du Lias du Dôme de La Mure et de la Chaîne de Belledonne méridionale. *Géologie Alp.* 46, 5–16.
- Barfety, J.C., Bordet, P., Carme, F., Debemas, J., Meloux, M., Montjuvent, G., Mouterde, R., Sarrot-Reynauld, J., 1972. Carte géologique de la France (1/50.000), feuille de Vizille (797). Bureau de Recherches géologiques et minières, Orléans.
- Barfety, J. C., & Gidon, M. (1983). La stratigraphie et la structure de la couverture dauphinoise au Sud de Bourg d'Oisans. Leurs relations avec les déformations synsédimentaires jurassiques. *Géologie alpine*, 59, 5-32.
- Barfety, J. C., and A. Pêcher 1984, Geological map and explanatory text of the sheet n°822 "St Christophe en Oisans,"Bellahsen et al., 2012
- Beaumont, C., Mufioz, J.A., Hamilton, J., Fullsack, P., 2000. Factors controlling the Alpine evolution of the central Pyrenees inferred from a comparison of observations and geodynamical models. *J. Geophys. Res.* 105, 8121–8145. doi:10.1029/1999JB900390; doi:10.1029/1999JB900390
- Beaudoin, N., Bellahsen, N., Lacombe, O., Emmanuel, L., 2011. Fracture-controlled paleohydrogeology in a basement-cored, fault-related fold: Sheep Mountain Anticline, Wyoming, United States. *Geochemistry, Geophys. Geosystems* 12, n/a–n/a. doi:10.1029/2010GC003494
- Bellahsen, N., Jolivet, L., Lacombe, O., Bellanger, M., Boutoux, A., Garcia, S., Mouthereau, F., Le Pourhiet, L., Gumiaux, C., 2012. Mechanisms of margin inversion in the external Western Alps: Implications for crustal rheology. *Tectonophysics* 560-561, 62–83. doi:10.1016/j.tecto.2012.06.022
- Bellahsen, N., Mouthereau, F., Boutoux, A., Bellanger, M., Lacombe, O., Jolivet, L., Rolland, Y., 2014. Collision kinematics in the western external Alps. *Tectonics* 33, 1–34. doi:10.1002/2013TC003453
- Bellahsen, N. Les prismes commisionels : localisation de la deformation et evolution thermique. Habilitation à diriger des Recherches , Univ. UPMC. 117pp.
- Bellanger, M., Bellahsen, N., Jolivet, L., Baudin, T., Augier, R., Boutoux, A., 2014. Basement shear zones development and shortening kinematics in the Ecrins Massif, Western Alps. *Tectonics* 33, 84–111. doi:10.1002/2013TC003294.Received

- Bellanger, M., Augier, R., Bellahsen, N., Jolivet, L., Monié, P., Baudin, T., Beyssac, O., 2015. Shortening of the European Dauphinois margin (Oisans Massif, Western Alps): New insights from RSCM maximum temperature estimates and  $40\text{Ar}/39\text{Ar}$  in situ dating. *J. Geodyn.* 83, 37–64. doi:10.1016/j.jog.2014.09.004
- Berger, J. P. 1992. Correlative chart of the European Oligocene and Miocene: application to the Swiss Molasse Basin. *Eclogae Geologicae Helvetiae*, 85(3), 573-609.
- Berger, J. P. 1992. Updated version of Berger (1992) unpublished.
- Berggren, W.A., Kent, D.V., Swisher, C.C., & Aubry, M.P. 1995: A revised Cenozoic geochronology and chronostratigraphy. In: Berggren, W.A., Kent, D.V., Aubry, M.P. & Hardenbol, J. (Eds.): *Geochronology, time scales and global stratigraphic correlation*. Special Publication – SEPM (Society for Sedimentary Geology) 54, 129–212. Bernard, 1974
- Bernard, D., 1978. Microthermométrie des inclusions fluides de cristaux syn- cinématiques. Application à la couverture sédimentaire du Nord Pelvoux. Unpublished PhD Thesis, Univ Grenoble, 133 pp. Bodnar,
- Bonin, B., Brändlein, P., Bussy, F., Desmons, J., Eggenberger, U., Finger, F., ... & Vivier, G. (1993). Late Variscan magmatic evolution of the Alpine basement. In *Pre-Mesozoic geology in the Alps* (pp. 171-201). Springer Berlin Heidelberg.
- Bonini, M., Sani, F., Antonielli, B., 2012. Basin inversion and contractional reactivation of inherited normal faults: A review based on previous and new experimental models. *Tectonophysics* 522-523, 55–88. doi:10.1016/j.tecto.2011.11.014
- Bonnet, C., Malavieille, J., Mosar, J., Bonini, M., Sani, F., Antonielli, B., 2007. Basin inversion and contractional reactivation of inherited normal faults: A review based on previous and new experimental models. *Tectonophysics* 26, n/a–n/a. doi:10.1016/j.tecto.2011.11.014
- Braun, S., Ronzheimer, J. P., Schreiber, M., Hodgman, S. S., Rom, T., Bloch, I., & Schneider, U. 2013. Negative absolute temperature for motional degrees of freedom. *Science*, 339(6115), 52–55.
- Buiter, S.J.H., Pfiffner, O.A., 2003. Numerical models of the inversion of half-graben basins. *Tectonics* 22, 1–16. doi:10.1029/2002TC001417
- Buiter, S.J.H., Pfiffner, O.A., Beaumont, C., 2009. Inversion of extensional sedimentary basins: A numerical evaluation of the localisation of shortening. *Earth Planet. Sci. Lett.* 288, 492–504. doi:10.1016/j.epsl.2009.10.011
- Burkhard, M., Sommaruga, A., 1998. Evolution of the Western Swiss Molasse basin: structural relations with the Alps and the Jura belt. In: Mascle, A., Puigdefabregas, C., Luterbacher, H.P., Fernanfez, M. (Eds.), *Cenozoic Foreland Basins of Western Europe*, Geological Society, London Special Publication, vol. 134, pp. 279e298. <http://dx.doi.org/10.1144/GSL.SP.1998.134.01.13>.
- Burkhard, M. 1988. L'Helvétique de la bordure occidentale du massif de l'Aar (évolution tectonique et métamorphique). *Eclogae Geologicae Helvetiae*, 81(1), 63-114.
- Burkhard, M., Kerrich, R., Maas, R., Fyfe, W.S., 1992. Stable and Sr-isotope evidence for fluid advection during thrusting of the Glarus nappe (Swiss Alps). *Contrib. to Mineral. Petrol.* 112, 293–311. doi:10.1007/BF00310462
- Burkhard, M., Goy-Eggenberger, D., 2001. Near vertical iso-illite-crystallinity surfaces cross-cut the recumbent fold structure of the Morcles nappe, Swiss Alps. *Clay Miner.* 36, 159–170.
- Bussy, F., & von Raumer, J. F. 1994. U–Pb geochronology of Palaeozoic magmatic events in the Mont-Blanc Crystalline Massif, Western Alps. *Schweizerische Mineralogische und Petrographische Mitteilungen*, 74, 514–515.
- Bussy, F., Schaltegger, U., & Marro, C. 1989. The age of the Mont-Blanc granite (Western Alps): a heterogeneous isotopic system dated by Rb-Sr whole rock determinations on its microgranular enclaves. *Schweizerische Mineralogische und Petrographische Mitteilungen*, 69(1), 3-13.

- Bussy, F. (1990). Pétrogenèse des enclaves microgrenues associées aux granitoïdes calco-alcalins: exemple des massifs varisque du Mont Blanc (Alpes occidentales) et miocène du Monte Capanne (Ile d'Elbe, Italie) Thesis 3e cycle, Université de Lausanne).
- Bussy, F., Derron, M. H., Jacquod, J., Sartori, M., & Thelin, P. (1996). The 500 Ma-old Thyon metagranite; a new A-type granite occurrence in the western Penninic Alps (Wallis, Switzerland). European Journal of Mineralogy, 8(3), 565-575.
- Bussy, F., Hernandez, J., and Von Raumer, J., 2000. Bimodal magmatism as a consequence of the post-collisional readjustment of the thickened Variscan continental lithosphere (Aiguilles Rouges–Mont Blanc Massifs, Western Alps). Geological Society of America Special Papers, 350, p. 221-233. doi: 10.1130/0-8137-2350-7.221
- Butler, R.W.H., 1989. The influence of pre-existing basin structure on thrust system evolution in the Western Alps. Geol. Soc. London, Spec. Publ. 44, 105–122. doi:10.1144/GSL.SP.1989.044.01.07
- Butler, R.W.H., Tavarnelli, E., Grasso, M., 2006. Structural inheritance in mountain belts: An Alpine–Apennine perspective. J. Struct. Geol. 28, 1893–1908. doi:10.1016/j.jsg.2006.09.006
- Cartwright, J.A., Buick, I.S., 2000. Fluid generation, vein formation and the degree of fluid–rock interaction during decompression of high-pressure terranes: the Schistes Lustré, Alpine Corsica, France. J. Metamorph. Geol. 18, 607–624. doi:10.1046/j.1525-1314.2000.00280.x
- Ceriani, S., Fügenschuh, B., Schmid, S.M., 2001. Multi-stage thrusting at the “Penninic Front” in the Western Alps between Mont Blanc and Pelvoux massifs. Int. J. Earth Sci. 90, 685–702. doi:10.1007/s005310000188
- Challandes, N., Marquer, D., Villa, I.M., 2008. P-T-t modelling, fluid circulation, and 39Ar-40Ar and Rb-Sr mica ages in the Aar Massif shear zones (Swiss Alps). Swiss J. Geosci. 101, 269–288. doi:10.1007/s00015-008-1260-6
- Goffé, B., Chopin, C., 1986. High-pressure metamorphism in the Western Alps: zoneography of metapelites, chronology and consequences. Schweirsche Mineral. und Petrogr. Mitteilungen 66, 41–52.
- Choukroune, P., Ballèvre, M., Cobbold, P.R., Gautier, Y., Merle, O., 1986. Deformation and motion in the western alpine arc. Tectonics 5, 215–226.
- Corsini, M., Ruffet, G., Caby, R., 2004. Alpine and late-hercynian geochronological constraints in the Argentera Massif (Western Alps). Eclogae Geol. Helv. 97, 3–15. doi:10.1007/s00015-004-1107-8
- Crespo-Blanc, A., Masson, H., Sharp, Z.D., Cosca, M.A., Hunziker, J.C., 1995. A stable and 40Ar/39Ar isotope study of a major thrust in the Helvetic nappes (Swiss Alps): evidence for fluid flow and constraints on nappe kinematics. Geol. Soc. Am. Bull. 107, 1129–1144. doi:10.1130/0016-7606(1995)107<1129
- Croizé, D., Bjørlykke, K., Jahren, J., Renard, F., 2010. Experimental mechanical and chemical compaction of carbonate sand. J. Geophys. Res. 115, B11204. doi:10.1029/2010JB007697
- Crouzet, C., Ménard, G., Rochette, P., 2001. Cooling history of the Dauphinoise Zone (Western Alps, France) deduced from the thermopaleomagnetic record: geodynamic implications. Tectonophysics 340, 79–93. doi:10.1016/S0040-1951(01)00142-1
- Duchêne, S., Blichert-Toft, J., Luais, B., Télouk, P., Lardaix, J.-M., Aldarède, F., 1997. The Lu-Hf dating of garnets and the ages of the Alpine high-pressure metamorphism. Nat. Geosci. 387, 586–589.
- Dumont, T., Champagnac, J.-D., Crouzet, C., Rochat, P., 2008. Multistage shortening in the Dauphiné zone (French Alps): the record of Alpine collision and implications for pre-Alpine restoration. Swiss J. Geosci. 101, 89–110. doi:10.1007/s00015-008-1280-2
- Dumont, T., Simon-Labric, T., Authemayou, C., Heymes, T., 2011. Lateral termination of the north-directed Alpine orogeny and onset of westward escape in the Western Alpine arc: Structural and sedimentary evidence from the external zone. Tectonics 30. doi:10.1029/2010TC002836
- Dumont, T., Schwartz, S., Guillot, S., 2012. Structural and sedimentary records of the Oligocene revolution in the Western Alpine arc. J. Geodyn. 56-57, 18–38. doi:10.1016/j.jog.2011.11.006
- Egli, D., 2013. Kinematics and timing of alpine deformation in the Mont Blanc region (Western Alps). ETH Zurich.

- Ehlerss, T.A., Farley, K.A., 2003. Apatite ( U-Th )/He thermochronometry : methods and applications to problems in tectonic and surface processes. *Earth Planet. Sci. Lett.* 206, 1–14. doi:10.1016/S0012-821X(02)01069-5
- Epard, J.-L., 1990. La nappe de Morcles au sud-ouest du Mont-Blanc. (Thesis 3e cycle). Univ. Lausane.
- Epard, J. L., & Groshong Jr, R. H., 1993. Excess area and depth to detachment. *AAPG bulletin*, 77(8), 1291-1302.
- Escher, A., Masson, H., Steck, A., 1993. Nappe geometry in the western Swiss Alps. *J. Struct. Geol.* 15, 501–509.
- Escher A, Hunziker JC, Marthaler M, Masson H, Sartori M, Steck A (1997) Geologic framework and structural evolution of the western Swiss Italian Alps. In: Pfiffner AO et al. (eds) Deep structure of the Swiss Alps: results of the NRP20. Birkhäuser, Basel, pp 205–221
- Fabre, C., Boiron, M.-C., Dubessy, J., Cathelineau, M., Banks, D.A., 2002. Palaeofluid chemistry of a single fluid event: a bulk and in-situ multi-technique analysis (LIBS, Raman Spectroscopy) of an Alpine fluid (Mont-Blanc). *Chem. Geol.* 182, 249–264. doi:10.1016/S0009-2541(01)00293-5
- Fisher, D.M., Brantley, S.L., Everett, M., Dzvonik, J., 1995. Cyclic fluid flow through a regionally extensive fracture network within the Kodiak accretionary prism. *J. Geophys. Res.* 100, 12881–12894. doi:10.1029/94JB02816
- Fischer, H., & Villa, I. M. (1990). Erste K/Ar-und 40Ar/39Ar-Hornblende-Mineralalter des Taveyannaz-Sandsteins. *Schweizerische Mineralogische und Petrographische Mitteilungen*, 70(1), 73-75.
- Ford, M., Lickorish, W.H., 2004. Foreland basin evolution around the western Alpine Arc. *Geol. Soc. London, Spec. Publ.* 221, 39–63. doi:10.1144/GSL.SP.2004.221.01.04
- Ford, M., Duchêne, S., Gasquet, D., Vanderhaeghe, O., 2006. Two-phase orogenic convergence in the external and internal SW Alps. *J. Geol. Soc. London*. 163, 815–826. doi:10.1144/0016-76492005-034
- Garofalo, P.S., 2012. The composition of Alpine marine sediments (Bündnerschiefer Formation, W Alps) and the mobility of their chemical components during orogenic metamorphism. *Lithos* 128-131, 55–72. doi:10.1016/j.lithos.2011.10.009
- Gueydan, F., 2003. Analysis of continental midcrustal strain localization induced by microfracturing and reaction-softening. *J. Geophys. Res.* 108, 2064. doi:10.1029/2001JB000611
- Jourdan, S., Bernet, M., Schwartz, S., Guillot, S., Tricart, P., Chauvel, C., Dumont, T., Montagnac, G., Bureau, S., 2012. Tracing the Oligocene-Miocene Evolution of the Western Alps Drainage Divide with Pebble Petrology, Geochemistry, and Raman Spectroscopy of Foreland Basin Deposits. *J. Geol.* 120, 603–624. doi:10.1086/667813
- Lemoine, M., Dardeau, G., Delpech, P.Y., Dumont, T., De Graciansky, P.C., Graham, R., Jolivet, L., Roberts, D., Tricart, P., 1989. Extension synrift et failles transformantes jurassiques dans les Alpes occidentales. *C.R. Acad. Sci. Sér. II Méc. Phys. Chim. Sci. Univ. Sci. Terre* 309 (17), 1711e1716. Letouzey,
- Lemoine, M., Graciansky, P. De, 1988. Histoire d'une marge continentale passive: les Alpes occidentales au Mésozoïque. *Bull. la Société géologique Fr.* 8, 597–600.
- Lickorish, W. H., & Ford, M. (1998). Sequential restoration of the external Alpine Digne thrust system, SE France, constrained by kinematic data and synorogenic sediments. *Geol. Soc. London, Spec. Publ.* 134, 189-212.
- Fourcade, S., Marquer, D., Javoy, M., 1989. 180/160 variations and fluid circulation in a deep shear zone " The case of the Alpine ultramylonites from the Aar massif(Central Alps , Switzerland). *Chem. Geol.* 77, 119–131.
- Fügenschuh, B., Loprieno, A., Ceriani, S., Schmid, S.M., 1999. Structural analysis of the Subbriançonnais and Valais units in the area of Moûtiers (Savoy, Western Alps): paleogeographic and tectonic consequences. *Int. J. Earth Sci.* 88, 201–218.
- Glötzbach, C., Reinecker, J., Danišík, M., Rahn, M.K., Frisch, W., Spiegel, C., 2008. Neogene exhumation history of the Mont Blanc massif, western Alps. *Tectonics* 27, n/a–n/a. doi:10.1029/2008TC002257
- Goncalves, P., Oliot, E., Marquer, D., Connolly, J. a. D., 2012. Role of chemical processes on shear zone formation: an example from the Grimsel metagranodiorite (Aar massif, Central Alps). *J. Metamorph. Geol.* 30, 703–722. doi:10.1111/j.1525-1314.2012.00991.x

- Gratier, J.P., Lejeune, B., Vergne, J.L., 1973. Etude des déformations de la couverture et des bordures sédimentaires des massifs cristallins externes de Belledonne, des Grandes Rousses et du Pelvoux. Thesis 3e cycle Univ., Grenoble.
- Gratier, J.-P., Vialon, P., 1980. Deformation pattern in a heterogeneous material: folded and cleaved sedimentary cover immediately overlying a crystalline basement (Oisans, French Alps). *Tectonophysics* 65, 151–179. doi:10.1016/0040-1951(80)90228-0
- Groshong, R.H., Epard, J.-L., 1994. The role of strain in area-constant detachment folding. *J. Struct. Geol.* 16, 613–618. doi:10.1016/0191-8141(94)90113-9
- Guermani, A., Pennacchioni, G., 1998. Brittle precursors of plastic deformation in a granite: an example from the Mont Blanc massif (Helvetic, western Alps). *J. Struct. Geol.* 20, 135–148. doi:10.1016/S0191-8141(97)00080-1
- Gueydan, F., 2003. Analysis of continental midcrustal strain localization induced by microfracturing and reaction-softening. *J. Geophys. Res.* 108, 2064. doi:10.1029/2001JB000611
- Guillot, S., Ménot, R.-P., 1999. Nappe stacking and first evidence of late Variscan extension in the Belledonne Massif (External Crystalline Massifs, French Alps). *Geodin. Acta* 12, 97–111. doi:10.1016/S0985-3111(99)80026-6
- Handy, M.R., M. Schmid, S., Bousquet, R., Kissling, E., Bernoulli, D., 2010. Reconciling plate-tectonic reconstructions of Alpine Tethys with the geological-geophysical record of spreading and subduction in the Alps. *Earth-Science Rev.* 102, 121–158. doi:10.1016/j.earscirev.2010.06.002
- Henry, C., Burkhard, M., Goffé, B., 1996. synmetamorphic veins and their wallrocks through a Western Alps transect: no evidence for large-scale fluid flow. Stable isotope, major-and trace-element systematics. *Chem. Geol.* 127, 81–109. doi:10.1016/0009-2541(95)00106-9
- Hofmann, B.A., Helfer, M., Diamond, L.W., Villa, I.M., Frei, R., Eikenberg, J., 2004. Topography-driven hydrothermal breccia mineralization of Pliocene age at Grimsel Pass , Aar massif , Central Swiss Alps. *Schweirsche Mineral. und Petrogr. Mitteilungen* 84, 271–302.
- Jullien, M., Goffé, B., 1993. Occurrences de cookéite et de pyrophyllite dans les schistes du Dauphinois (Isère, France): Conséquences sur la répartition du métamorphisme dans les zones externes alpines. *Schweirsche Mineral. und Petrogr. Mitteilungen* 73, 357–363.
- Kirschner, D.L., Sharp, Z.D., Masson, H., 1995. Oxygen isotope thermometry of quartz-calcite veins: Unraveling the thermal-tectonic history of the subgreenschist facies Morcles nappe (Swiss Alps). *Geol. Soc. Am. Bull.* 107, 1145–1156. doi:10.1130/0016-7606(1995)107<1145
- Kirschner, D.L., Masson, H., Sharp, Z.D., 1999. Fluid migration through thrust faults in the Helvetic nappes (Western Swiss Alps). *Contrib. to Mineral. Petrol.* 136, 169–183. doi:10.1007/s004100050530
- Kirschner, D.L., Masson, H., Cosca, M.A., 2003. An 40 Ar/ 39 Ar, Rb/Sr, and stable isotope study of micas in low-grade fold-and-thrust belt: an example from the Swiss Helvetic Alps. *Contrib. to Mineral. Petrol.* 145, 460–480. doi:10.1007/s00410-003-0461-2
- Kralik, M., Clauer, N., Holnsteinner, R., Huemer, H., Kappel, K., 1992. Recurrent fault activity in the Grimsel Test Site ( GTS , Switzerland ): revealed by Rb-Sr , K-Ar and tritium isotope techniques. *J. Geol. Soc. London.* 149, 293–301. doi:10.1144/gsjgs.149.2.0293
- Labaume, P., Jolivet, M., Souquière, F., Chauvet, a., 2008. Tectonic control on diagenesis in a foreland basin: combined petrologic and thermochronologic approaches in the Grès d'Annot basin (Late Eocene-Early Oligocene, French-Italian external Alps). *Terra Nov.* 20, 95–101. doi:10.1111/j.1365-3121.2008.00793.x
- Lacombe, O., Moutherieu, F., 2002. Basement-involved shortening and deep detachment tectonics in forelands of orogens: Insights from recent collision belts (Taiwan, Western Alps, Pyrenees). *Tectonics* 21, 12–1–12–22. doi:10.1029/2001TC901018
- Lateltin, O. & Muller, D. 1987: Evolution paléogéographique du bassin des grès de Taveyannaz dans les Aravis (Haute-Savoie) à la fin du Paléogène. *Eclogae Geologicae Helveticae* 80, 127–140.

- Lemoine, M., Bas, T., Arnaud-Vanneau, A., Arnaud, H., Dumont, T., Gidon, M., Bourbon, M., De Graciansky, P.-C., Rudkiewicz, J.-L., Megard-Galli, J., Tricart, P., 1986. The continental margin of the Mesozoic Tethys in the Western Alps. *Mar. Petrol. Geol.* 3 (3), 179e199. [http://dx.doi.org/10.1016/0264-8172\(86\)90044-9](http://dx.doi.org/10.1016/0264-8172(86)90044-9).
- Lemoine, M., Graciansky, P. De, 1988. Histoire d'une marge continentale passive: les Alpes occidentales au Mésozoïque. *Bull. la Société géologique Fr.* 8, 597–600.
- Lemoine, M., Dardeau, G., Delpech, P. Y., Dumont, T., De Graciansky, P. C., Graham, R., Jolivet, L., Roberts, D., Tricart, P., 1989. Extension synrift et failles transformantes jurassiques dans les Alpes occidentales. *Comptes rendus de l'Académie des sciences. Série 2, Mécanique, Physique, Chimie, Sciences de l'univers, Sciences de la Terre*, 309(17), 1711-1716.
- Lickorish, W.H., Ford, M., 1998. Sequential restoration of the external Alpine Digne thrust system, SE France, constrained by kinematic data and synorogenic sediments. *Geol. Soc. London, Spec. Publ.* 134, 189–211. doi:10.1144/GSL.SP.1998.134.01.09
- Lickorish, W.H., Ford, M., Bürgisser, J., Cobbold, P.R., 2002. Arcuate thrust systems in sandbox experiments: A comparison to the external arcs of the Western Alps. *Geol. Soc. Am. Bull.* 114, 1089–1107. doi:10.1130/0016-7606(2002)114<1089:ATSISE>2.0.CO;2
- Marquer, D., Burkhard, M., 1992. Progressive deformation and mass-transfer processes in the upper crust: the example of basement-cover relationships in the External Crystalline Massifs, Switzerland. *J. Struct. Geol.* 14, 1047–1057.
- Massonne, H., Schreyer, W., 1987. Phengite geobarometry based on the limiting assemblage with K-feldspar , phlogopite , and quartz. *Contrib. to Mineral. Petrol.* 96, 212–224.
- McCaig, A.M., Tritlla, J., Banks, D.A., 2000. Fluid mixing and recycling during Pyrenean thrusting: evidence from fluid inclusion halogen ratios. *Geochim. Cosmochim. Acta* 64, 3395–3412.
- Moretti, I., Callot, J.P., 2012. Area, length and thickness conservation: Dogma or reality? *J. Struct. Geol.* 41, 64–75. doi:10.1016/j.jsg.2012.02.014
- Mohn, G., Manatschal, G., Müntener, O., Beltrando, M., Masini, E., 2010. Unravelling the interaction between tectonic and sedimentary processes during litho- spheric thinning in the Alpine Tethys margins. *International Journal of Earth Sciences* 99, S75eS101. Pfiffner,
- Moutherneau, F., Watts, A.B., Burov, E., 2013. Structure of orogenic belts controlled by lithosphere age. *Nat. Geosci.* 6, 785–789. doi:10.1038/ngeo1902
- Moutherneau, F., Lacombe, O., 2006. Inversion of the Paleogene Chinese continental margin and thick-skinned deformation in the Western Foreland of Taiwan. *J. Struct. Geol.* 28, 1977–1993. doi:10.1016/j.jsg.2006.08.007
- Mulder, T., Callec, Y., Parize, O., Joseph, P., Schneider, J.-L., Robin, C., Dujoncquoy, E., Salles, T., Allard, J., Bonnel, C., Ducassou, E., Etienne, S., Ferger, B., Gaudin, M., Hanquiez, V., Linares, F., Marchès, E., Toucanne, S., Zaragozi, S., 2010. High-resolution analysis of submarine lobes deposits: Seismic-scale outcrops of the Lauzanier area (SE Alps, France). *Sediment. Geol.* 229, 160–191. doi:10.1016/j.sedgeo.2009.11.005
- Mugnier, J. L., Guellec, S., Ms G., Roure, E, Tardy, M. & Vialon, E 1990. A crustal scale balanced cross-section through the external Alps deduced from the ECORS profile. In: Roure, E, Heitzmann, P. & Polino, R. (eds) Deep structure of the Alps. *Mémoires de la Société géologique Suisse*, 203-216. &
- Muñoz, J. A., 1992. Evolution of a continental collision belt: ECORS-Pyrenees crustal balanced cross-section. In *Thrust tectonics* (pp. 235-246). Springer Netherlands.
- Nicolas, A., Hirn, A., Nicolich, R., & Polino, R. (1990). Lithospheric wedging in the western Alps inferred from the ECORS-CROP traverse. *Geology*, 18(7), 587-590. doi: 10.1130/0091-7613(1990)018<0587:LWITWA>2.3.CO;2
- Mugnier, J. L., Guellec, G., Roure, F., Tardy, M., Vialon, P., 1990. Crustal balanced cross-sections through the external Alps deduced from the ECORS profil. In : F. Roure, P. Helzman and R. Polino, Editors, Deep structure of the Alps, Mem. Soc. Géol. France 156, Suisse 1, Italiana 1.

- Nziengui, J.J., 1993. Excès d'argon radiogénique dans les quartz des fissures tectoniques: implications pour la datation des séries métamorphiques(Thesis 3e cycle) L'exemple de la coupe de la Romanche-Alpes occidentales françaisesUniv. Grenoble (209 pp.).
- Oliot, E., Goncalves, P., Marquer, D., 2010. Role of plagioclase and reaction softening in a metagranite shear zone at mid-crustal conditions (Gotthard Massif, Swiss Central Alps). *J. Metamorph. Geol.* 28, 849–871. doi:10.1111/j.1525-1314.2010.00897.x
- Oliot, E., Goncalves, P., Schulmann, K., Marquer, D., Lexa, O., 2014. Mid-crustal shear zone formation in granitic rocks: Constraints from quantitative textural and crystallographic preferred orientations analyses. *Tectonophysics* 612-613, 63–80. doi:10.1016/j.tecto.2013.11.032
- Oliver, N.H.S., 1996. Review and classification of structural controls on fluid flow during regional metamorphism. *J. Metamorph. Geol.* 14, 477–492. doi:10.1046/j.1525-1314.1996.00347.x
- Oliver, N.H.S., Bons, P.D., 2001. Mechanisms of fluid flow and fluid-rock interaction in fossil metamorphic hydrothermal systems inferred from vein-wallrock patterns, geometry and microstructure. *Geofluids* 1, 137–162. doi:10.1046/j.1468-8123.2001.00013.x
- Philippe, Y., Deville, É., Mascle, A., 1998. Thin-skinned inversion tectonics at oblique basin margins: example of the western Vercors and Chartreuse Subalpine massifs (SE France). *Geol. Soc. London, Spec. Publ.* 134, 239–262. doi:10.1144/GSL.SP.1998.134.01.11
- Platt, J.P., Cunningham, P.C., Weston, P., Lister, G.S., Peel, F., Baudin, T., Dondey, H., 1989. Thrusting and backthrusting in the Briançonnais domain of the western Alps. *Geol. Soc. London, Spec. Publ.* 45, 135–152. doi:10.1144/GSL.SP.1989.045.01.07
- Poty, B., Stalder, H.A., Weisbrod, Alain, M., 1974. Fluid inclusions studies in quartz from fissures of Western and Central Alps. *Schweirsche Mineral. und Petrogr. Mitteilungen* 54, 717–752.
- Ramsay, J.G., 1981. Tectonics of the Helvetic Nappes. *Geol. Soc. London, Spec. Publ.* 9, 293–309. doi:10.1144/GSL.SP.1981.009.01.26
- Ramsay, J.G., Casey, M., Kligfield, R., 1983. Geology Role of shear in development of the Helvetic fold-thrust belt of Switzerland Role of shear in development of the Helvetic fold-thrust belt of Switzerland. *Geology* 11, 439–442. doi:10.1130/0091-7613(1983)11<439:ROSIDO>2.0.CO;2
- Ramsay, J.G., Huber, M.I., 1989. The Techniques of Modern Structural Geology, vol. 2. Folds and Fractures Academic Press, London. Rausenbaum et Lister, 2005
- Renard, F., Ortoleva, P., Gratier, J.P., 1997. Pressure solution in sandstones: influence of clays and dependence on temperature and stress. *Tectonophysics* 280, 257–266. doi:10.1016/S0040-1951(97)00039-5
- Rosenbaum, G., Lister, G.S., 2005. The Western Alps from the Jurassic to Oligocene: spatio-temporal constraints and evolutionary reconstructions. *Earth-Science Rev.* 69, 281–306. doi:10.1016/j.earscirev.2004.10.001
- Rolland, Y., Cox, S.F., Boullier, A.-M., Pennacchioni, G., Mancktelow, N.S., 2003. Rare earth and trace element mobility in mid-crustal shear zones: insights from the Mont Blanc Massif (Western Alps). *Earth Planet. Sci. Lett.* 214, 203–219. doi:10.1016/S0012-821X(03)00372-8
- Rolland, Y., Cox, S.F., Corsini, M., 2009. Constraining deformation stages in brittle–ductile shear zones from combined field mapping and 40Ar/39Ar dating: The structural evolution of the Grimsel Pass area (Aar Massif, Swiss Alps). *J. Struct. Geol.* 31, 1377–1394. doi:10.1016/j.jsg.2009.08.003
- Rossi, M., Rolland, Y., Vidal, O., Cox, S.F., 2005. Geochemical variations and element transfer during shear-zone development and related episyenites at middle crust depths : insights from the Mont Blanc granite (French-Italian Alps). *Geol. Soc. Am. Spec. Pap.* 245, 373–396. doi:10.1144/GSL.SP.2005.245.01.18
- Rossi, M., Rolland, Y., 2014. Stable isotope and Ar/Ar evidence of prolonged multi-scale fluid flow during exhumation of orogenic crust: example from the Mont Blanc and Aar massifs (NW Alps). *Tectonics*. doi:10.1002/2013TC003438
- Roure, F. (Ed.). 1996. The ECORS-CROP Alpine seismic traverse (No. 170). Société géologique de France.

- Roure, F., Colletta, B., 1996. Cenozoic inversion structures in the foreland of the Pyrenees and Alps. Mémoires du Muséum Natl. d'histoire Nat. 170, 173–209.
- Ruffini, R., Polino, R., Callegari, E., Hunziker, H. & Pfeiffer H. 1997: Volcanic clast-rich turbidites of the Tavayanne sandstones from the Thone syncline (Savoie France): records for a Tertiary post-collisional volcanism. Schweizerische Mineralogische und Petrographische Mitteilungen 77, 161–174. Sanchez et al., 2011
- Shea, W.T., Kronenberg, A.K., 1993. Strength and anisotropy of foliated rocks with varied mica contents. J. st 15, 1097–1121. doi:doi:10.1016/0191-8141(93)90158-7
- Sanchez, G., Rolland, Y., Schneider, J., Corsini, M., Oliot, E., Goncalves, P., Verati, C., Lardeaux, J.-M., Marquer, D., 2011. Dating low-temperature deformation by  $^{40}\text{Ar}/^{39}\text{Ar}$  on white mica, insights from the Argentera-Mercantour Massif (SW Alps). Lithos 125, 521–536. doi:10.1016/j.lithos.2011.03.009
- Simon-Labric, T., Rolland, Y., Dumont, T., Heymes, T., Authemayou, C., Corsini, M., Fornari, M., 2009.  $^{40}\text{Ar}/^{39}\text{Ar}$  dating of Penninic Front tectonic displacement (W Alps) during the Lower Oligocene (31-34 Ma). Terra Nov. 21, 127–136. doi:10.1111/j.1365-3121.2009.00865.x
- Sinclair, H.D., Allen, P., 1992. Vertical versus horizontal motions in the Alpine orogenic wedge: stratigraphic response in the foreland basin. Basin Res. 4, 215–232. doi:10.1111/j.1365-2117.1992.tb00046.x
- Sinclair, H.D., 1997. Tectonostratigraphic model for underfilled peripheral foreland basins: an Alpine perspective. Geol. Soc. Am. Bull. 109, 324–346.
- Soom, M. A., 1990. Abkühlungs- und Hebungsgeschichte der Extemmas- sive und der penninischen Decken beidseits der Simplon-Rhone-Linie seit dem Oligozän: Spaltspurdatierungen an Apatit/Zircon und K-Ar- Datierungen an Biotit/Muskowit (Westliche Zentralalpen) [Ph.D. the- sis]: Bern, Switzerland, University of Bern, 119 p. Sorby, H.C., 1863. On the Microscopical Structure of Meteorites. Proceeding R. Soc. London 13, 333–334.
- Spandler, C., Pettke, T., Rubatto, D., 2011. Internal and External Fluid Sources for Eclogite-facies Veins in the Monviso Meta-ophiolite, Western Alps: Implications for Fluid Flow in Subduction Zones. J. Petrol. 52, 1207–1236. doi:10.1093/petrology/egr025
- Stampfli, G.M., 1993. Le Briançonnais, terrain exotique dans les Alpes? Eclogae Geol. Helv. 86, 1–45.
- Tricart, P., Lemoine, M., 1986. From faulted blocks to megamullions and megaboudins: Tethyan héritage in the structure of the Western Alps. Tectonics 5, 95–118. doi:10.1029/TC005i001p00095
- Van der Beek, P.A., Valla, P.G., Herman, F., Braun, J., Persano, C., Dobson, K.J., Labrin, E., 2010. Inversion of thermochronological age-elevation profiles to extract independent estimates of denudation and relief history — II: Application to the French Western Alps. Earth Planet. Sci. Lett. 296, 9–22. doi:10.1016/j.epsl.2010.04.032
- Verlaguet, a., Goffé, B., Brunet, F., Poinsot, C., Vidal, O., Findling, N., Menut, D., 2011. Metamorphic veining and mass transfer in a chemically closed system: a case study in Alpine metabauxites (western Vanoise). J. Metamorph. Geol. 29, 275–300. doi:10.1111/j.1525-1314.2010.00918.x
- Von Raumer, J., Bussy, F., and Sharp, Z. D., 1996. Lac Cornu revisited: The evolution from lower to upper crust (Aiguilles-Rouges Massif, western Alps). Schweizerische Mineralogische und Petrographische Mitteilungen, 76, p. 120-121.
- De Wever, P., and J. Dercourt (1985), Les radiolaires triasico-jurassiques marqueurs stratigraphiques et paléogéographiques dans les chaînes alpines périméditerranéennes: une revue, Bull Soc géol France I (8), 5, 653– 662.
- De Wever, P., and R. Caby 1981, Datation de la base des schistes lustrés postophiolithiques par des radiolaires (Oxfordien supérieur? Kimmeridgien moyen) dans les Alpes Cottientes (Saint Véran, France), Comptes Rendus de l'Academie des Sciences, 292, 467– 472.
- Weyl, P. I., 1959. Pressure solution and the force of crystallization-a phenomenological theory. J. Geophys. Res. 64, 200-2025.

## **XI. Appendice.**

### Key Points:

- Five balanced cross sections of the western external Alps are presented
- Sequence of shortening and shortening and exhumation rates are determined
- The role of inherited Mesozoic margins on the collision kinematics is discussed

### Correspondence to:

N. Bellahsen,  
nicolas.bellahsen@upmc.fr

### Citation:

Bellahsen, N., F. Mouthereau, A. Boutoux, M. Bellanger, O. Lacombe, L. Jolivet, and Y. Rolland (2014), Collision kinematics in the western external Alps, *Tectonics*, 33, doi:10.1002/2013TC003453.

Received 29 SEP 2013

Accepted 28 MAR 2014

Accepted article online 3 APR 2014

## Collision kinematics in the western external Alps

**N. Bellahsen<sup>1,2</sup>, F. Mouthereau<sup>1,2</sup>, A. Boutoux<sup>1,2</sup>, M. Bellanger<sup>3,4</sup>, O. Lacombe<sup>1,2</sup>, L. Jolivet<sup>3</sup>, and Y. Rolland<sup>5</sup>**

<sup>1</sup>Sorbonne Universités, UPMC Université Paris 06, UMR 7193, ISTEPI, Paris, France, <sup>2</sup>CNRS, UMR 7193, ISTEPI, Paris, France, <sup>3</sup>Université Orléans, ISTO, CNRS, UMR 7327, Orléans, France, <sup>4</sup>BRGM, DGR/GSO, Orléans, France, <sup>5</sup>Geoazur, UMR 7329, CNRS-UNS-UPMC-IRD, Valbonne, France

**Abstract** The kinematics of the collision in Western Alps are investigated through five balanced cross sections of the whole external domain from the Oisans to the Mont Blanc massif. These cross sections were built using published data for the Jura and subalpine fold-and-thrust belts and new structural and field analysis for the External Crystalline Massifs. Five units are defined: the sedimentary nappes from innermost parts of the external zone (e.g., ultra-Dauphinois/Helvetic), the crystalline units with their dysharmonically folded cover (e.g., Morcles nappe), sedimentary nappes over the frontal parts of the crystalline massifs (the Aravis-Granier unit), the subalpine belts (e.g., Vercors, Chartreuse, Bauges, and Bornes), and the Jura. Except for the ultra-Dauphinois nappes, the shortening, including the cover shortening, always corresponds to basement shortening. The total amount of shortening increases from south (28 km, 20%) to north (66 km, 27%). Moreover, the shortening is slightly older in the south than in the north; deepwater turbidites (flysch) and shallow marine to freshwater clastics (molasse) basins are more developed in the north; pressure and temperature conditions are higher in the north; the average uplift rates are about 3 times higher in the north and more localized in space. We propose that these differences are due to along-strike variations in the structure of the European continental margin inherited from Mesozoic times. We then build five palinspastic maps: one at Cretaceous times showing the inherited European Mesozoic margin structure and four from Priabonian to upper Miocene times showing the collision kinematics and the related rotation of Adria.

### 1. Introduction

Mountain belts and related collisional structures are often noncylindrical features. At the Alpine-Himalayan orogenic belt scale, for example, along-strike variations are observed in the timing, kinematics, and structural evolution during the Tethys closure and subsequent collision. These differences are not only due to variations in convergence velocities and finite shortening but may also reflect the inherited geometry of oceanic and rifted continental domains, and age-dependent rheological properties of the lithosphere [Mouthereau *et al.*, 2013], which may imply different subduction-collision dynamics.

At a smaller scale, within each segment of the whole Alpine-Himalayan belt, the differential precollisional history of rifted continental margins can therefore control the kinematics of the subsequent collision. Toward the lateral termination of an ocean, the structure may evolve from a fully oceanized basin, through an area where extension stopped after mantle exhumation, to an aborted rift. This is presently the case in the northern Red Sea [Cochran and Martinez, 1988] or in the Woodlark basin [Taylor *et al.*, 1995], for example. The along-strike variations of collision kinematics when such oceanic domains are closing and the role of the preorogenic extensional structures in the style and amount of shortening are still open questions.

The aim of this paper is to unravel the variations of tectonic evolution along strike of a mountain belt, in terms of shortening and associated exhumation rates as well as rheology and structural styles and to discuss the role of the preorogenic continental margins and rift structure. The Western Alps (Figure 1) are taken as a case study as it is one of the best known mountain belts by means of timing and tectonic evolution from subduction to collision stages. The overall history of subduction of the Ligurian ocean beneath Adria is now well known and documented: the subduction started during mid-Cretaceous times and ended during Paleogene times. However, Handy *et al.* [2010] (following Stampfli *et al.* [2002] and Bousquet *et al.* [2002, and references therein]) suggested that a Cretaceous Valais ocean opened between the proximal European margin and the distal Briançonnais domain, from the Eastern to the Western Alps. On the contrary, Trumpy [1975] and Lemoine *et al.* [1986] argued that it aborted westward in the present-day Western Alps. In the latter model, the opening of the Valais domain may have taken place during the Jurassic [Manatschal *et al.*, 2006; Mohn *et al.*, 2010; Beltrando *et al.*, 2012] or the Cretaceous

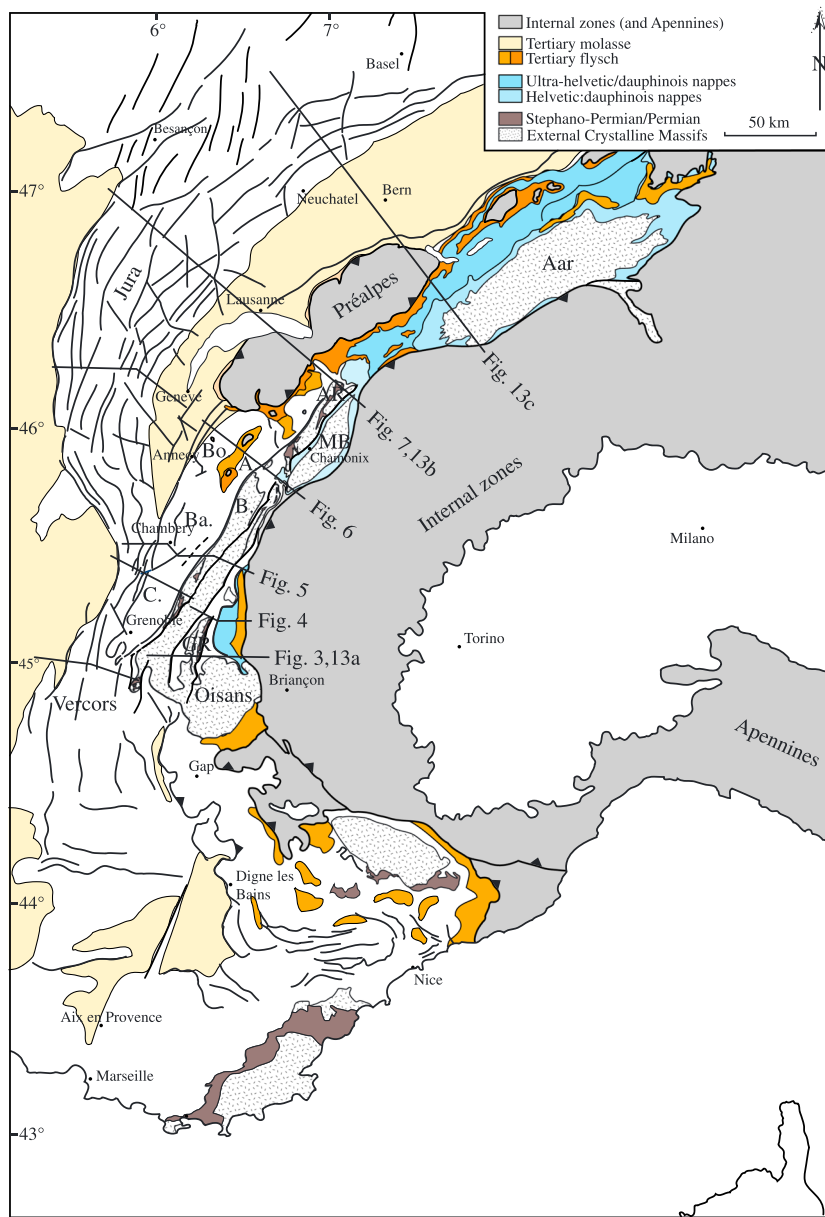


**Figure 1.** Structural map of the Western Alps. In gray are represented the internal units, including the Préalpes and the Sulens and Annes klippen (southwest of the Préalpes). Light blue areas are helvetic nappes (Morcles and Diablerets); darker blue areas represent the ultra-Helvetic and Ultra-Dauphinois nappes. Discontinuous straight lines give the locations of cross sections. Bo for Bornes, AR for Aiguilles Rouges, MB for Mont Blanc, B for Belledonne, Ba for Bauges, C for Chartreuse, and GR for Grandes Rousses.

[Loprieno *et al.*, 2010]. The opening and closure of this domain is thus still debated but is an important issue as the different models imply different (thermal) structures of the European distal margins.

Within this framework and beyond the problem of the Mesozoic structure, many questions on the inversion of the Alpine margin are still pending. What is the true effect of the inherited normal faults? In analogue models of the Alpine collision [e.g., Bonnet *et al.*, 2007], the shortening of the underthrusted European crust is strongly controlled by the presence of weak inherited faults. This suggests that the crust was weakened because of inherited faults. However, there are no clear evidences in the field of the reactivation of such inherited faults and the weakening effect is mainly due to the soft synrift sedimentary rocks filling the fault-bounded basins [Bellahsen *et al.*, 2012] and fluid-rock interactions leading to the formation of phyllosilicates in shear zones with distinct orientations to the normal faults [e.g., Wibberley, 1999; Bellanger *et al.*, 2014].

Is the size (width and thickness) of the foreland basin linked to the growth of the orogenic load or rather to a slab pull effect? As noticed in *Bonnet et al.* [2007], the orogenic foreland basin grows in width and thickness until the basement units start to exhume. *Ford and Lickorish* [2004] showed that the northward transgression rate of the northern foreland basin strongly decreased in early Aquitanian times (around 23 Ma). This decrease occurred coevally with the onset of the exhumation in the External Crystalline Massifs (ECM, Figure 1, 22–23 Ma, Aar and Mont Blanc massifs [*Challandes et al.*, 2008; *Rolland et al.*, 2009]). On the other hand, the along-strike variations of the molassic basin, i.e., the decrease in both width and thickness from Central to Western Alps [e.g., *Ford et al.*, 2006], may be due to the western end of the orogenic load according to *Ford and Lickorish* [2004]. However, there was an orogenic load in Western Alps during Oligocene times (in the western ECM [*Dumont et al.*, 2008; *Bellaehsen et al.*, 2012; *Bellanger et al.*, 2014]). Thus, the role of the orogenic load is still poorly understood.

To answer these questions, a prerequisite is a robust data set of finite shortening estimates over the whole Western Alps. Amounts of shortening seem to increase from the Western and Southwestern Alps toward the Central Alps [e.g., *Sinclair*, 1997; *Ford and Lickorish*, 2004; *Kempf and Pfiffner*, 2004], although there is to date no systematic and quantitative analysis of the rates all along the Western Alpine arc. Thus, we do not have clear quantification of the evolution of the Alpine wedge deformation toward its lateral western termination.

A reappraisal of shortening estimated over the whole Western Alps is proposed here and synthesized in the new data set. This data set is based on five balanced cross sections of the whole external zone from the Oisans to the Mont Blanc massifs. Structural style and sequence of shortening are documented and found to be consistent at the scale of the whole Western Alpine external arc. The amount of shortening for each deformation phase is discussed in the light of the timing and rate of cooling defined in the External Crystalline Massifs (ECMs) from a synthesis of published low-temperature thermochronology and pressure, temperature, time (P,T,t) constraints. Finally, palinspastic maps are presented for various Tertiary times and Middle Cretaceous times to discuss both the collision kinematics and the role of the inherited Mesozoic margin structure.

## 2. Geological Setting of Western Alps

The Alps are the result of the closure of the Ligurian ocean. In the Western Alps (Figure 1), Ligurian oceanic subduction started during Cretaceous times and lasted until late Paleocene to early Eocene times. Indeed, at that time, the first high pressure/low temperature (HP/LT) event is recorded in oceanic units before their exhumation [e.g., *Agard et al.*, 2002, and references therein]. Continental subduction is recorded as middle to upper Eocene, with the HP to Ultra-High Pressure (UHP) metamorphism of the alpine internal crystalline massifs (e.g., Dora Maira [*Duchene et al.*, 1997; *Rubatto and Hermann*, 2001; *Oberhänsli et al.*, 2004]) and the HP metamorphism of the Briançonnais unit (e.g., Vanoise [*Oberhänsli et al.*, 2004]). Collisional crustal thickening and orogenic development started during Oligocene times (Figure 2) with shortening of the external Alps and associated burial/exhumation (Dauphinois in France and Helvetic in Switzerland), especially the External Crystalline Massifs (ECM). In the following, we present a synthesis of the main studies on the external zone.

### 2.1. The External Crystalline Massifs and Their Sedimentary Nappes: Timing of Alpine Metamorphism, Shortening, and P,T Conditions

The Alpine ECM are composed from south to north of the following: the Argentera-Mercantour in the southwestern Alps; the Oisans, Grandes Rousses, Belledonne, Mont Blanc, and Aiguilles Rouges massifs in the Western Alps; and the Aar and Gothard massifs in the central Alps.

In the Argentera-Mercantour massif, two main NW-SE dextral transpressive shear zones were active between 34 and 20 Ma, according to  $^{40}\text{Ar}/^{39}\text{Ar}$  on synkinematic phengites, at about 375°C and 5–7 kb [*Sanchez et al.*, 2011]. E-W reverse shear zones were active around 22–23 Ma [*Corsini et al.*, 2004] or range between 20 and 26 Ma [*Sanchez et al.*, 2011], which witness a N-S shortening that has continued since then [*Bauve et al.*, 2014].

In the Oisans massif (Figure 3), the main shortening phase is E-W [*Dumont et al.*, 2008, 2011, 2012; *Bellaehsen et al.*, 2012; *Boutoux et al.*, 2014; *Bellanger et al.*, 2014], although there was oblique shortening at certain times and in certain places [*Dumont et al.*, 2008; *Bellanger et al.*, 2014]. *Simon-Labréte et al.* [2009] showed that the earliest E-W alpine shortening (witnessed by strike-slip shear zones) started around 34–31 Ma. In the southern part of the massif, an Eocene N-S shortening phase has been recognized, which is sealed by the deposition of late Eocene sediments. At the Eocene-Oligocene boundary, a N-S to NW-SE shortening phase is identified: while *Dumont et al.* [2008] proposed that it affected the entire western ECM, *Bellanger et al.* [2014] showed

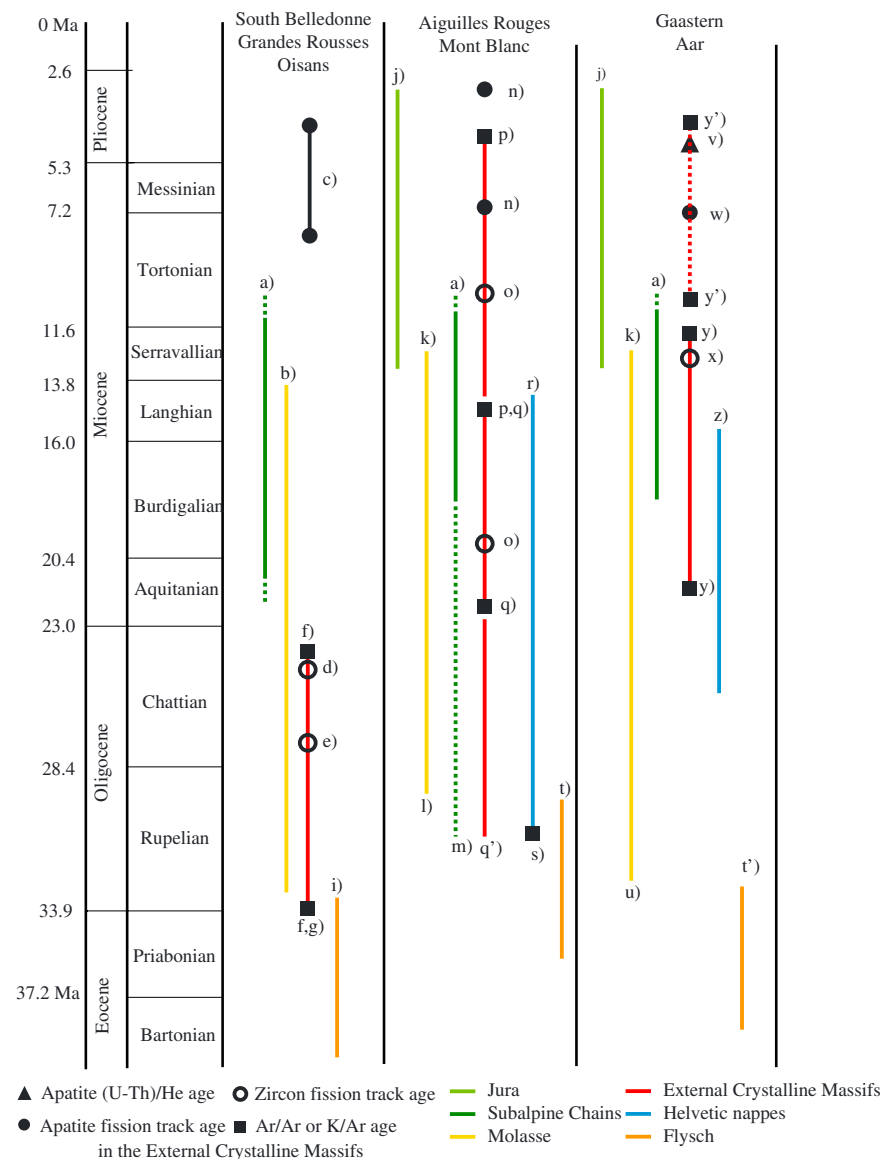


**Figure 2.** Synthesis of tectonic and sedimentary events in the western external Alps. Color bars are for the age of formation or deformation of the following units. For error bars and details on ages, see the cited references below. South Belledonne/Grandes Rousses/Oisans: (a) Main phase of folding in the subalpine chains (Vercors, Chartreuse, Bauges) after Arnaud [1975]. (b) Age of shallow marine to freshwater clastics deposit [see Ford and Lickorish, 2004; Ford et al., 2006]. (c) AFT age range in Grandes Rousses and Oisans [see Vernon et al., 2008]. (d) Minimal age of the Grandes Rousses exhumation from thermopalaeomagnetism [Crouzet et al., 2001]. (e) Minimal age of the Oisans massif (La Meije) exhumation onset from thermochronology in van der Beek et al. [2010]. (f) Age of the Oisans massif shortening from  $^{40}\text{Ar}/^{39}\text{Ar}$  data (M. Bellanger et al., The shortening of the European Dauphinois margin (Ecrins-Pelvoux Massif, Western Alps): New insights from T estimates and in-situ  $^{40}\text{Ar}/39\text{Ar}$  ages from basement reverse shear zones, submitted to *Journal of Geodynamics*, 2014). (g) Age of the eastern Oisans massif shortening [Simon-Labréte et al., 2009]. (i) End of the turbiditic sequence, "schistes à blocs" [Kerckhove, 1969; Fry, 1989; Mulder et al., 2010]. Aiguilles Rouges/Mont Blanc: (j) Main Jura folding phase [Bolliger et al., 1993; Steiniger et al., 1996; Kalin, 1997; Becker, 2000]. (k) End of overfilled basin [Ford et al., 2006]. (l) Onset of overfilled basin and (t) end of underfilled basin [Sinclair, 1997]. (m) Onset of subalpine chains shortening [Leloup et al., 2005]. (n) AFT ages [Carpentier, 1992; Seward and Mancktelow, 1994; Leloup et al., 2005]. (o) ZFT ages [Soom, 1990; Seward and Mancktelow, 1994; Leloup et al., 2005]. (p and q) Onset and end of Mont Blanc shear zones from  $^{40}\text{Ar}/^{39}\text{Ar}$  [Leloup et al., 2005; Rolland et al., 2008], respectively. (q') Onset of Mont Blanc deformation [Cenki-Tok et al., 2013]. (r) End of helvetic nappes deformation (Morcles) [Kirschner et al., 1996] and (s) their onset [Huon et al., 1994; Crespo-Blanc et al., 1995]. (t and t') End of underfilled basin [Sinclair, 1997]. Gaastern/Aar/Gothard: (u) Onset of overfilled basin [Sinclair, 1997]. (v) UTh/He age [Reinecker et al., 2008]. (w) AFT data [Reinecker et al., 2008]. (x) ZFT data [Michalski and Soom, 1990]. (y) Age of shortening from  $^{40}\text{Ar}/^{39}\text{Ar}$  in shear zones [Challandes et al., 2008; Rolland et al., 2009]. (y') Age of brittle faults in the Aar massif [Kralik et al., 1992; Hofmann et al., 2004].

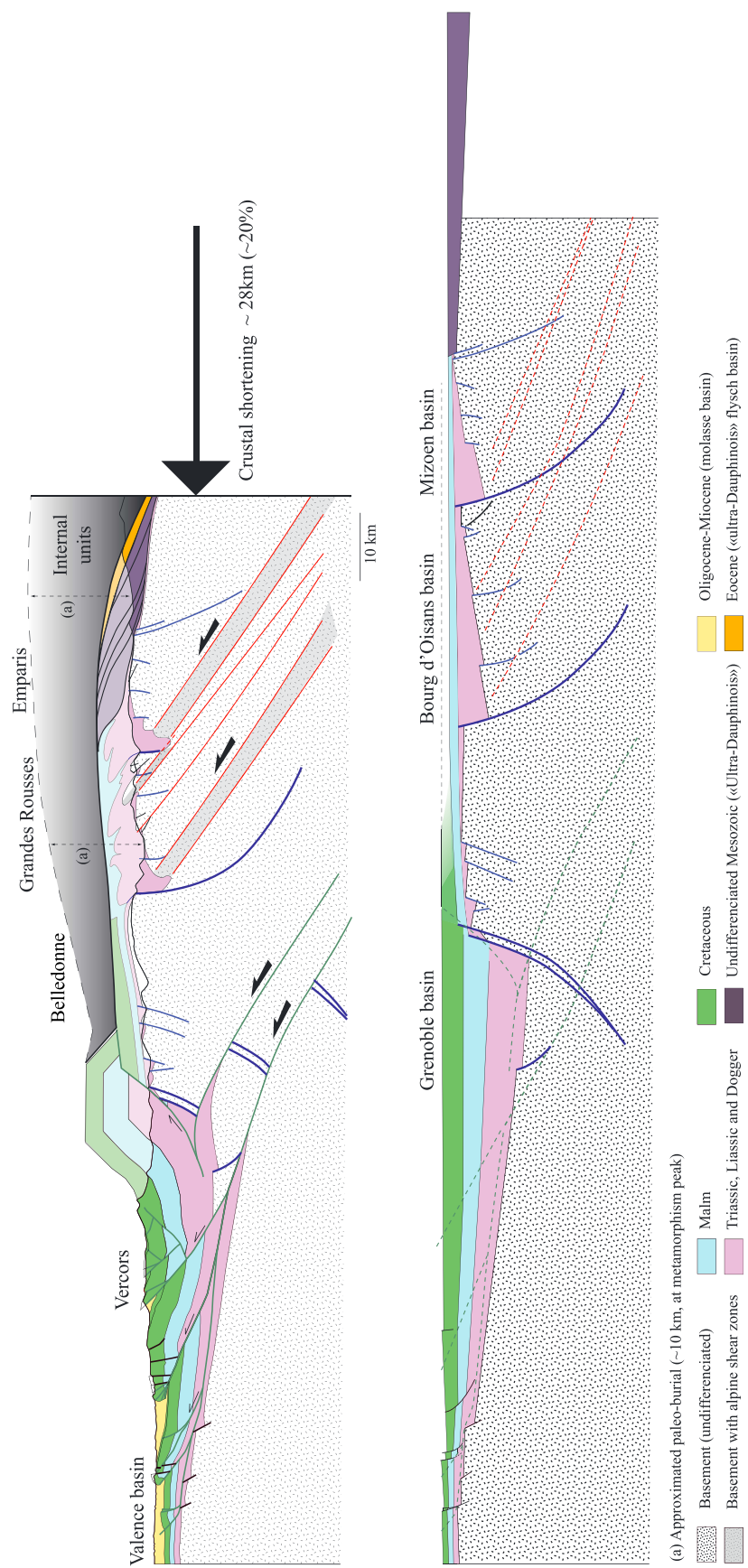


**Figure 3.** Balanced cross section through the Vercors-Oisans-Grande Rousses-south Belledonne massifs: the Vercors part (Vercors) being redrawn from Deville et al. [1994] and constrained by seismic data. An amount of shortening 28 km is recorded for the whole external zone: 11.5 km for the ECM during Oligocene-early Miocene times characterized by large basement Alpine shear zones above which the cover is disharmonically folded, 16.5 km for the subalpine chain whose thrusts root in a décollement within Liassic layers activated by fronta basement thrusts beneath the ECM. The inherited Liassic basins localized the Alpine shortening, although their bounding normal faults were not reactivated. In dark purple are represented detached Mesozoic (mainly Jurassic, ultra-Dauphinois) layers that were not taken into account in the crustal restoration of the Alpine shortening. They most probably witness a (early?) stage of thin-skinned tectonics. See text for explanation and discussion.

that it may be restricted to the cover in a narrow zone below the Penninic Frontal Thrust. This latter observation is consistent with field evidences further north [Ceriani and Schmid, 2004].

The ECM at the Oisans latitude can be divided into several units from west to east: the south Belledonne, Grandes Rousses, and Emparis units (Figure 3). Further southeast, two other units are present: the Meije and Combeynot units [Bellanger *et al.*, 2014, and references therein]. The total amount of shortening at this latitude is about 28 km, including 11.5 km accommodated within the ECM [Bellaïsen *et al.*, 2012], where the sedimentary cover is not significantly detached over the basement but is rather disharmonically deformed over it. Dysharmony or folds tightening in the cover is particularly well expressed above basement shear zones, displaying clear west verging kinematics. In the basement, the Alpine schistosity appears to be parallel to the inherited Variscan foliation, while the Alpine shear zones clearly deformed it. The shortening of these units occurred under green schist facies conditions (3–4 kb and 300–350°C) [Jullien and Goffé, 1993; Simon-Labréteau *et al.*, 2009]. The exhumation of these units started at least at 27 Ma from zircon fission track thermochronology (ZFT age) [van der Beek *et al.*, 2010] for the Meije massif (NE Oisans) and at least at 24 Ma from thermopaleomagnetism [Crouzet *et al.*, 2001] for the Grandes Rousses massif. Apatite fission track (AFT) showed that these massifs cooled through the 110°C isotherm at about 3–8 Ma (see a synthesis in Vernon *et al.* [2008]).

In the northern Belledonne massif, only few data are available. Marquer *et al.* [2006] described steep anastomosed brittle-ductile shear zones developed under green schist conditions. This Alpine kinematics is compatible with a NW-SE shortening along with a strong vertical stretching.

In the Mont Blanc massif (Figure 1), the development of anastomosed steep shear zones with a flower-type structure combining top-to-NW and SE sense of shear, along with right-lateral movements, mainly ranges from 22 to 15 Ma ( $^{40}\text{Ar}/^{39}\text{Ar}$  on phengites [Rolland *et al.*, 2008]) at around 400°C and 5 kb [Rolland *et al.*, 2003]. Recently, ages of  $29 \pm 1$  Ma were obtained from in situ allanite U-Pb dating in central Mont Blanc shear zones [Cenki-Tok *et al.*, 2013], which suggests that the onset of the shortening could be older (Figure 2).

In the Aiguilles Rouges massif, few ages of deformation are available in the literature. Leloup *et al.* [2005] considered that the uplift started around 20 Ma, which is consistent with the structural interpretation of Burkhard and Sommaruga [1998] where the upper Aiguilles Rouges basement thrusts were active during the OSM (Upper Freshwater Molasse) deposition, i.e., since 16 Ma. In both the Mont Blanc and the Aiguilles Rouges massifs, ZFT ages are about 8–15 Ma even though some data show older ages up to more than 20 Ma (Figure 2); AFT ages are about 3–8 Ma [Vernon *et al.*, 2008]. Similar ages are found for the Belledonne massif, although scarcer.

In the Aar massif, the main shearing event (along NE-SW shear zones) occurred between 17 and 21 Ma at 400–450°C and 6 kb [Challandes *et al.*, 2008] or 20–22 Ma [Rolland *et al.*, 2009] with west verging kinematics and was followed by reverse to dextral shear zones at 12–14 Ma [Rolland *et al.*, 2009]. Finally, brittle deformations have occurred since 9–5 Ma [Kralik *et al.*, 1992] and probably until 3 Ma [Hofmann *et al.*, 2004] (Figure 2). The kinematics of shortening during the first phase corresponds to a NW-SE contraction marked in the field by anastomosed shear zones, rather steep in the internal parts and/or even east verging (Gothard massif) [Marquer, 1990], while they are west verging in the more frontal parts [Burkhard, 1988]. The shortening is most likely younger in the Gaasterland massif and older in the Gothard massif [Burkhard, 1988].

In the external Alps, large units structurally above the ECM known as sedimentary nappes have been described: the Mörtsch, Diablerets, Wildhorn, and Doldenhorn nappes [e.g., Ramsay, 1981]. The Mörtsch and Doldenhorn nappes ("Helvetic nappes," Figure 1) are the cover of the Mont Blanc and the Aar massifs, respectively [Escher *et al.*, 1993; Burkhard, 1988; Ramsay, 1981], or less probably of subducted crust now buried below the internal units southeast of the Mont Blanc massif [Leloup *et al.*, 2005]. The Diablerets and the Wildhorn nappes ("ultra-Helvetic nappes," Figure 1) are associated to the innermost part of the external zone, in the east or southeast [e.g., Ramsay, 1981; Burkhard and Sommaruga, 1998]. They are made of Mesozoic and Cenozoic sedimentary rocks: Triassic, Jurassic, and Cretaceous layers are quite thick (especially in the Wildhorn nappe) and are overlain by ultra-helvetic deepwater turbidites (Eocene flysch). These units are structurally located below the penninic units and are the oldest units of the external zone. They were emplaced along a NW-SE direction [Ramsay, 1981] with a thin-skinned structural style [Burkhard and Sommaruga, 1998].

## 2.2. The External Fold-and-Thrust Belt and Foreland Basin Evolution

From south to north, the fold-and-thrust belts are named as follows: Vercors, Chartreuse, Bauges, Bornes-Aravis, and Chablais-Haut Giffre, as well as the Jura. Except for the latter, the age of shortening is usually

considered as being middle Miocene (Figure 2), the Burdigalian-Langhian shallow marine clastics being syntectonic in the Vercors massif [Arnaud, 1975] and the middle Miocene shallow marine clastics being syntectonic north of the Prealpes [see Burkhard and Sommaruga, 1998, and references therein]. The subalpine chains are composed of Mesozoic and Cenozoic sedimentary rocks. While the Mesozoic rocks are mainly carbonate, the Cenozoic ones are mainly siliciclastic: Oligocene and/or Miocene shallow marine to freshwater clastics (and carbonates) can be found, and these molassic series witness the uplift and erosion of more internal areas. In these massifs, the thrusts root in a décollement layer located within the (upper Triassic-) Liassic series [Deville et al., 1994; Philippe et al., 1998; Affolter et al., 2008].

The Jura fold-and-thrust belt shortening occurred from Serravallian times to Early Pliocene times (Figure 2) [Bolliger et al., 1993; Steiniger et al., 1996; Kalin, 1997; Becker, 2000]. Unlike the Vercors massif, the décollement level is located within the Triassic evaporites. Within these belts, the shortening directions are quite consistent, roughly perpendicular to the alpine arc: from WNW-ESE in the Vercors-Chartreuse [Philippe et al., 1998] to globally NW-SE in Jura (subperpendicular to the main folds and thrusts) even if two successive directions are observed in southern Jura and linked to the arc evolution [Homberg et al., 1999].

The position of the footwall cutoff is still a matter of debate. The décollement at the cover base may root in basement thrust ramps below the ECM or may be instead folded above the ECM, rooting eastward. There are evidences that the former occurred, especially based on seismic data [Pfiffner et al., 1997; Steck et al., 1997; Deville and Chauvière, 2000]. This is detailed further down.

In southern Oisans, Tertiary sedimentary rocks directly overlie the basement. They are Priabonian in age (and lowermost Oligocene for the formation top) and composed of three typical facies: shallow water limestones, pelagic marls, and deepwater turbidites. This trinity represents the sedimentation in the underfilled subsiding foreland basin [Sinclair, 1997] whose turbiditic succession is regionally referred to as the flysch facies. In northern Oisans, similar series ("Aiguilles d'Arves flysch") are overthrust over the Mesozoic cover, and their age is similar to the southern Oisans one. Their initial paleogeographical position is, however, more difficult to define. Around the Mont Blanc/Aiguilles Rouges massifs, the underfilled trinity is younger, the whole turbidites series being Oligocene (up to Rupelian, around 30 Ma), while it is slightly older in the Aar massif area (up to early Rupelian, around 34 Ma) [Sinclair, 1997]. The deepening upward stratigraphy of these Eocene-Oligocene series was mapped out all around the Alpine arc [Sinclair, 1997] and was modeled as a migrating flexural basin [Ford et al., 1999].

The molasse basin is an overfilled basin [Sinclair and Allen, 1992] with both shallow marine to freshwater clastics. In the Western Alps, the Oligocene freshwater clastic series are rather thin and restricted to small basins [Ford et al., 2006], the main depocenters being localized in the Devoluy (west of Gap, Figure 1) or in the Barrême syncline for example, while the Miocene shallow marine clastics are more widespread but also rather thin. In the North Alpine Foreland Basin (NAFB), in the western central Alps, the shallow marine to freshwater clastic series (molasse) are very thick (up to 4 km [Burkhard and Sommaruga, 1998] and possibly even more [Bonnet et al., 2007]). The zone of transition between these two subbasins (thin in the west and thick further northeast) is located around Chambéry in Savoie (Figure 1) [Ford and Lickorish, 2004]. Thus, there was no large molassic basin in SE France, while in the north the overfilled flexural basin migrated northward at the same rate as the underfilled one (around  $10 \text{ mm yr}^{-1}$  [Ford et al., 2006]) until Aquitanian times and then slowed down [Sinclair, 1997].

### 2.3. Open Questions on Structural Styles

There is a large consensus on the fact that the ECM are allochthonous: geophysical data show that the subalpine chains were deformed above a basal sedimentary décollement kinematically linked to frontal basement thrust ramps [Deville et al., 1994; Pfiffner et al., 1997; Burkhard and Sommaruga, 1998; Deville and Chauvière, 2000], connecting downdip to a middle lower crustal detachment. In such a perspective, the propagation of the deformation in the outermost part of the fold-and-thrust belt, i.e., the Jura, is necessarily also linked to the presence of basement thrusts below the ECM and not associated eastward to a décollement at the cover base above the ECMs: once the ECM started to be uplifted, it is likely that a décollement at the basement-cover interface of ECM would be unactivated. This is consistent with  $^{40}\text{Ar}/^{39}\text{Ar}$  ages in Rolland et al. [2008] and Cenki-Tok et al. [2013] that clearly indicate that the Mont Blanc massif started to shorten before the Jura shortening.

Less clear, however, is the structural style of the inner part of the fold-and-thrust belt. In the north, it appears that the Morcles nappe is the Mont Blanc cover [Escher *et al.*, 1993; Burkhard and Sommaruga, 1998]; in the northeastern Aiguilles Rouges massifs, the subalpine chain is very limited and most of the equivalent shortening is accommodated in the molassic series (shallow marine to freshwater clastics, NAFB) between the Préalpes and the Jura [Burkhard and Sommaruga, 1998]. Thus, the Mont Blanc cover is not strongly detached and transported toward the NW. Similarly, further south, the cover of the Oisans massif is not detached above its basement but is rather disharmonically folded above basement shear zones [Bellahsen *et al.*, 2012]. Thus, northeast of the Mont Blanc massif and in the Oisans Massif, the subalpine belts cannot be the former cover of the ECM as previously proposed by Doudoux *et al.* [1982].

According to these authors, the Bauges and the Bornes massifs are equivalent to the Morcles nappe. Thus, they would represent the cover of the internal Belledonne and the Mont Blanc massifs. Leloup *et al.* [2005] even assumed that the Bauges and Bornes massifs are the cover of units located southeast of the Mont Blanc massif. However, further south, it is clear that the Chartreuse and Vercors massifs are not the cover of the Belledonne basement, or at best it is the cover of its outermost part in some places [Deville *et al.*, 1994; Deville and Chauvière, 2000; Philippe *et al.*, 1998; Bellahsen *et al.*, 2012].

Alternatively, Epard [1990] proposed that the Mont Joly unit (SW Mont Blanc, Figure 1) is the equivalent of the Morcles nappe. Indeed, it represents the former cover of the southwestern termination of the Mont Blanc massif. This unit is only composed of the Triassic and Liassic layers. It remains unclear whether the upper part of the cover was detached from the lower part or not: northwest of the Mont Joly, the Mesozoic series of the Aravis massif may represent layers slightly detached from the Mont Joly unit.

To address these questions, we present regional cross sections assuming that all (or part) of both the subalpine chains and the Jura shortening are linked to basement thrusts beneath the ECMs [Burkhard and Sommaruga, 1998; Deville and Chauvière, 2000]. The cross sections aim at defining the structural styles for the whole external zone as well as the sequence of deformation and at providing rates of both shortening and exhumation. The along-strike structural variations are finally tentatively interpreted in terms of preorogenic geometry of the European passive margin.

### 3. Regional Balanced Cross Sections

In this part, we present five cross sections (Figures 3–7): two from the literature, the Vercors-Oisans section [Bellahsen *et al.*, 2012] and the Préalpes-Mont Blanc section [Burkhard and Sommaruga, 1998]; and three new ones, the Chartreuse-Grandes Rousses, Chartreuse-Belledonne, and Bornes-Mont Blanc cross sections. These three new cross sections have been balanced using assumptions detailed in Bellahsen *et al.* [2012]. These main assumptions are, for the ECM part of the section, constant surface for the sedimentary cover and constant length for the basement top (determined from the lower Triassic layers still attached to the basement and either mapped in the field or redrawn from geological maps). The outermost part of the sections (i.e., the fold-and-thrust belts) have been redrawn from the literature and constrained by seismic data; constant length and area were considered for the restoration [Deville *et al.*, 1994; Philippe *et al.*, 1998; Affolter *et al.*, 2008].

#### 3.1. The Vercors-Oisans Cross Section

This cross section (Figure 3) has been published in Bellahsen *et al.* [2012]. Thus, here we will only sum up the main insights. Several alpine shear zones deformed the basement in the Oisans, Grandes Rousses, and south Belledonne basement, most probably during Oligocene times, as the shortening later localized west of these shear zones on the frontal ramps during Miocene times. Such shear zones account for an amount of shortening of 11.5 km, while the frontal ramps below south Belledonne massif account for 16.5 km.

The ultra-Dauphinois flysch unit (deepwater turbidites) to the east is allochthonous. Bellanger *et al.* [2014] showed that it underwent NW-SE shortening. Thus, it must be restored somewhere east or southeast of the section (see further down). In any case, it shows that the alpine crustal shortening in the Oisans massif occurred west or northwest of the turbiditic basin.

In the ECM, the inherited Liassic normal faults were not reactivated [Bellahsen *et al.*, 2012]. Three main inherited normal faults were recognized: the faults controlling the Grenoble, Bourg d'Oisans, and Mizoen basins (Figure 3), the former being the deepest as attested by the very thick Mesozoic sedimentary

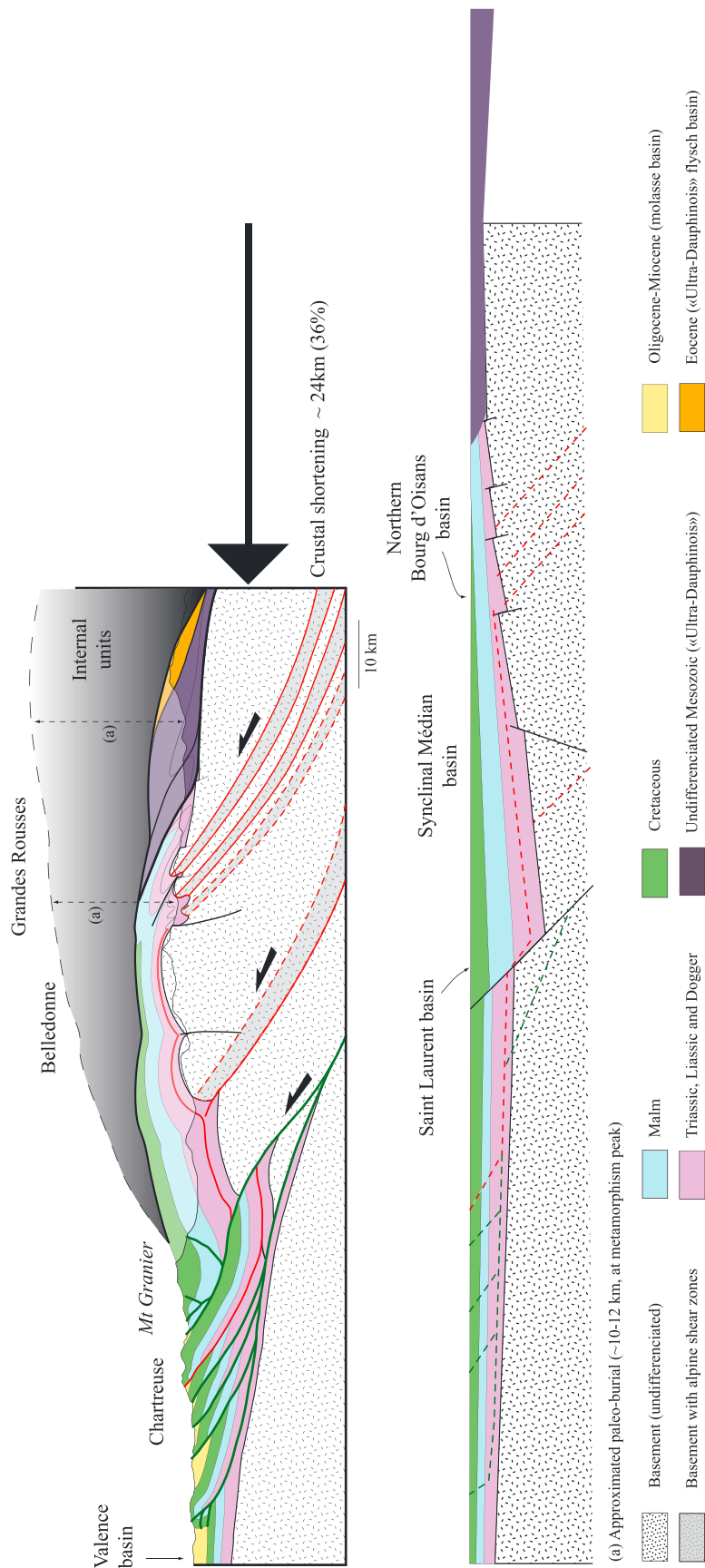
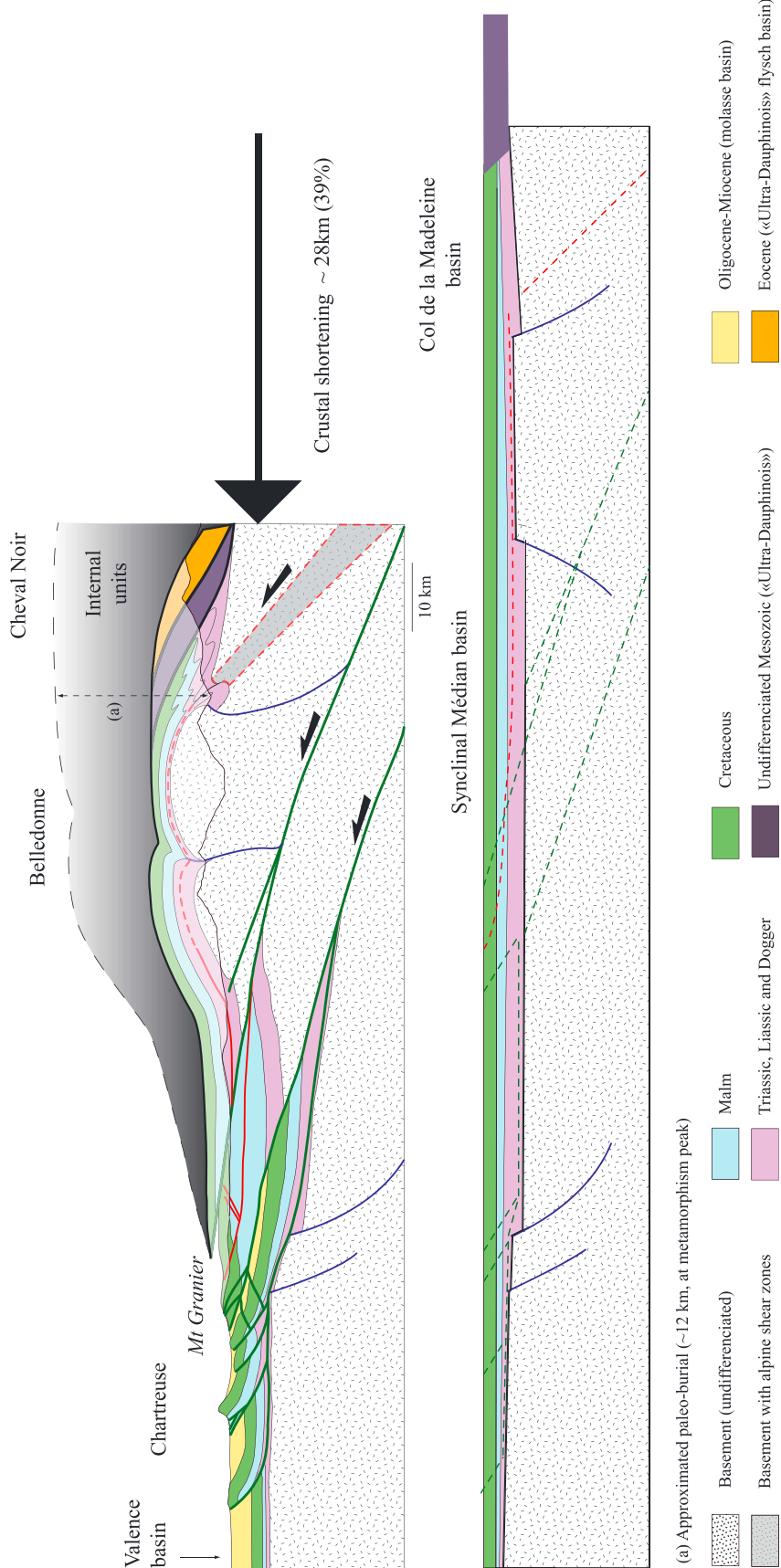


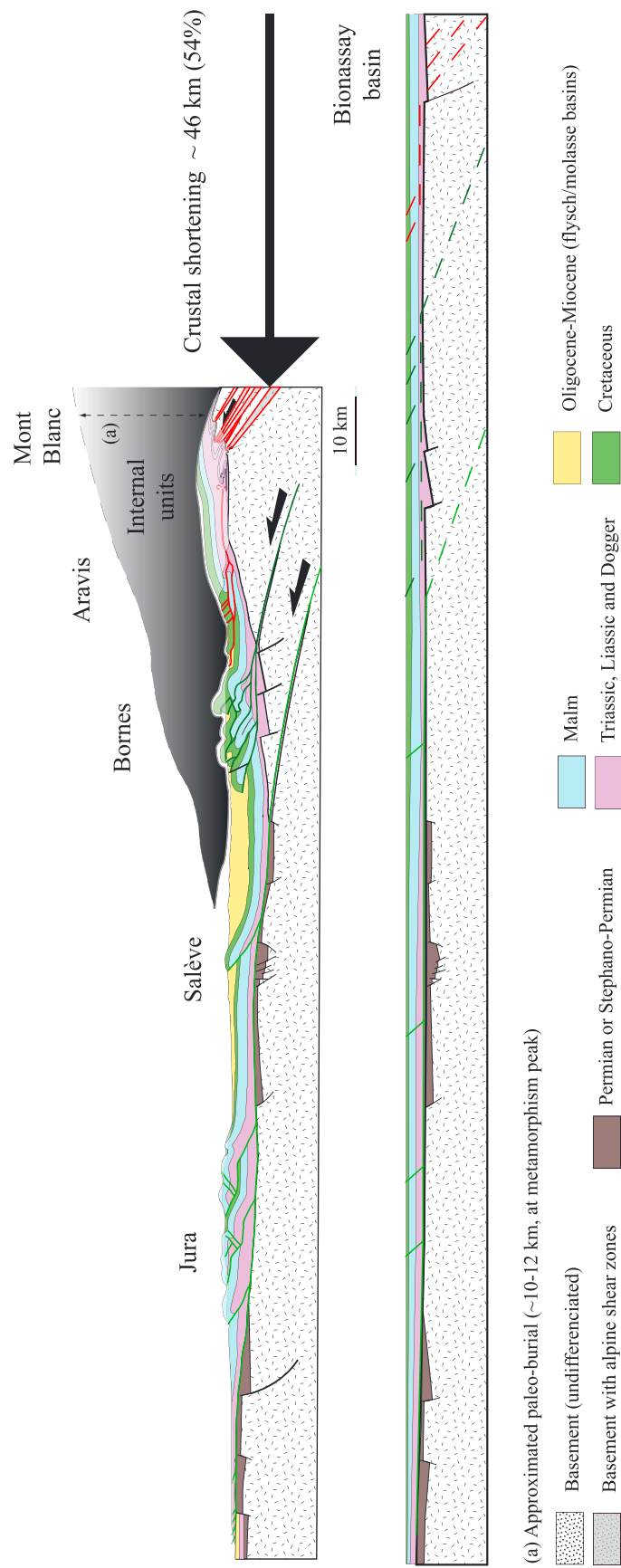
**Figure 4.** Balanced cross section through the Chartreuse-Belledonne-Grandes Rousses massifs: the Chartreuse part (Chartreuse) is redrawn from Deville et al. [1994] and constrained by seismic data. A total amount of shortening of 26.9 km for the whole external zone: 6.6 km for the ECM most likely during Oligocene-early Miocene times, 17.8 km for the subalpine chain whose thrusts root in a décollement within Liassic layers activated by frontal basement thrusts beneath the red thrust that root above the ECM. The outermost thrust is considered to belong to the Jura belt (2 km of shortening). A Mesozoic normal fault has been represented on the restored section based on thickness variations across the easternmost thrust in the subalpine chain. This implies a rather long-lived normal displacement during Mesozoic times. In dark purple are represented detached Mesozoic (mainly Jurassic, ultra-Dauphinois) layers that were not taken into account in the crustal restoration of the Alpine shortening. They most probably witness a (early?) stage of thin-skinned tectonics. See text for explanation and discussion.



(a) Approximated paleo-burial (~12 km, at metamorphism peak)

■ Basement (undifferentiated)  
■ Basement with alpine shear zones  
■ Malm  
■ Triassic, Liassic and Dogger  
■ Cretaceous  
■ Undifferentiated Mesozoic («Ultra-Dauphinois»)  
■ Oligocene-Miocene (molasse basin)  
■ Eocene («Ultra-Dauphinois») flysch basin

**Figure 5.** Balanced cross section through the north Chartreuse-Belledonne massifs: the Chartreuse-Belledonne cross section. The section is redrawn, for the subalpine chain part, from Deville and Chauvière [2000]. A total of 27.9 km of shortening is recorded for the whole external zone: 7.2 km for the subalpine chain during Oligocene-early Miocene times, 18.7 km for the subalpine chain whose thrusts root in a décollement within Liassic layers activated by frontal basement thrusts beneath the ECM, except for the red thrust that root above the ECM. The outermost thrust is considered to belong to the Jura belt. In dark purple are represented detached Mesozoic (mainly Jurassic, ultra-Dauphinois) layers that were not taken into account in the crustal restoration of the Alpine shortening. They most probably witness a (early?) stage of thin-skinned tectonics. See text for explanation and discussion.



(a) Approximated paleo-burial (~10–12 km, at metamorphism peak)

**Figure 6.** Balanced cross section through the Jura-Bornes-Mont Blanc massifs: the Bornes-Mont Blanc cross section. The subalpine (Bornes) and Jura parts are redrawn from Affolter et al. [2008] and partly constrained by seismic data. For the Bresse graben and Jura relationships, see also Bergerat et al. [1990] and Philippe et al. [1998]. A total of about 46 km of shortening is recorded for the whole external zone: 3.1 km for the ECM during Early Miocene times characterized by basement Alpine shear zones in the Mont Blanc massif above which the cover is disharmonically folded [Epard, 1990], 17 km for the subalpine chain whose thrusts root in a décollement within Liassic layers activated by basement thrusts beneath the northern Belledonne massif, 25.9 km for the Jura whose thrusts root in the Triassic evaporites activated by lower Belledonne basement thrusts. The Mont Blanc shear zones are located beneath an inherited Liassic basin. East of the Bornes massif, i.e., in the Aravis massif, the shortening observed in the field has been rooted in the lower Jurassic layers above the Mont Blanc units and their disharmonic basal sedimentary rocks (Triassic and lower Jurassic). See text for explanation and discussion.

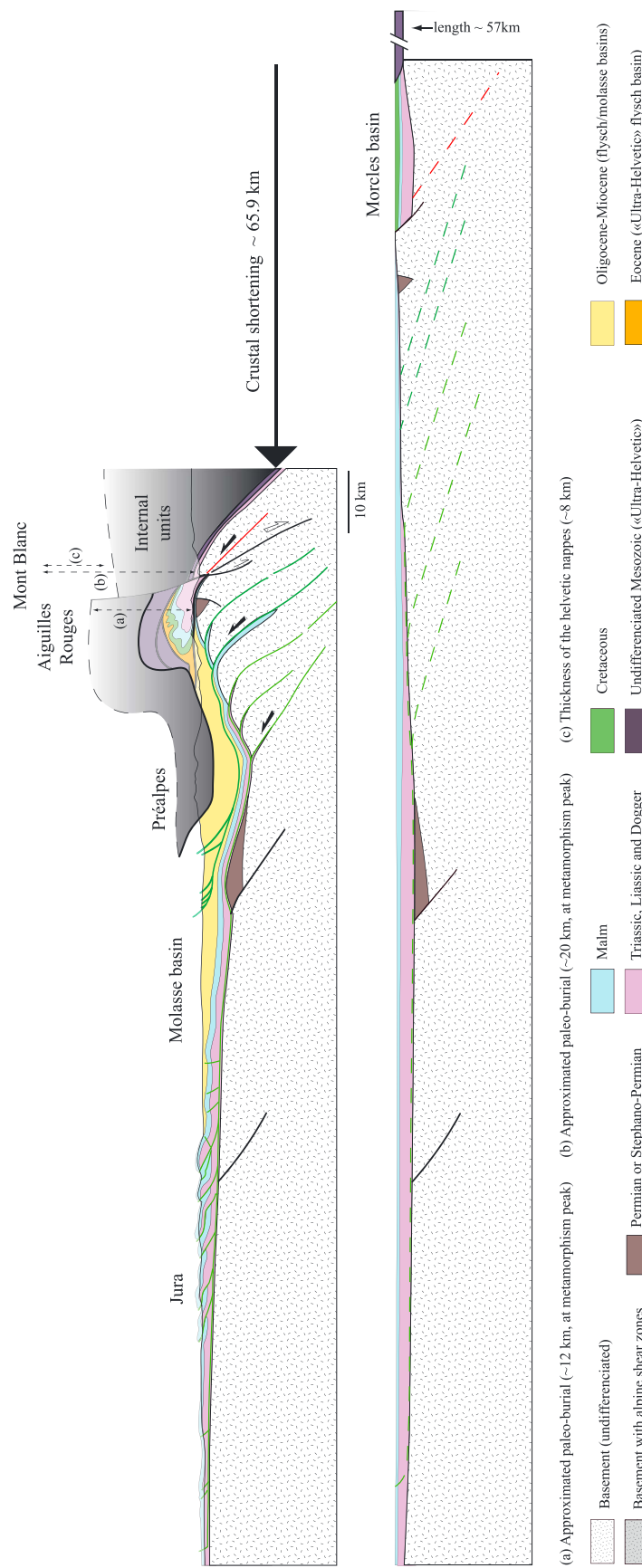


**Figure 7.** Balanced cross section through the Jura-Préalpes-Aiguilles Rouges-Mont Blanc massifs: the Prealpes-Mont Blanc cross section [Burkhard and Sommaruga, 1998]. The Jura and molasse basin parts were constrained by seismic data. A total amount of shortening of about 65.9 km is recorded for the whole external zone: 10.6 km for the ECM during Early Miocene times characterized by large basement Alpine shear zones in the Mont Blanc massif above which the cover (Mornes nappe) is disharmonically folded and sheared, 26 km for the subalpine chain that affect the tertiary shallow marine to freshwater clastics (NAFB) whose thrusts root in a décollement within tertiary layers activated by basement thrusts beneath the Aiguilles Rouges, 29.3 km for the Jura whose thrusts root in the Triassic evaporates activated by lower Aiguilles Rouges basement thrusts. The Mont Blanc shear zones are located beneath an inherited Liassic basin. The sedimentary nappes above the Mornes nappe (dark purple, ultra-Helvetic) witness a (early?) stage of thin-skinned tectonics. See text for explanation and discussion.

cover. It is noteworthy that the Grenoble normal fault is not only a Liassic fault but was also active during upper Jurassic (Figure 3).

Moreover, the cover deformed dysharmonically above “basement antiforms” that actually reflect cumulated continuous shortening accommodated by basement shear zones (Figure 8a). Thus, there is no need for major décollement between the cover and the basement. Below the Eocene turbidites unit, however, in the eastern part, small cover units are detached from their basement. In the ECM, the upper part of the cover cannot be unambiguously drawn as it has been strongly eroded (Figure 3). It is probable that the upper Mesozoic series have been eroded during the Pyrenean phase (Eocene in age) as the Cenozoic formations unconformably overlie the basement in southern Oisans [Ford, 1996].

Further west, in the Vercors fold-and-thrust belt, cover units are detached in Liassic series (or upper Triassic) at the front of basement thrust ramps [Deville et al., 1994]. There, the cover was affected by several normal faults (Figure 3) that may have initiated during Mesozoic times and were reactivated during the Oligocene before the fold-and-thrust-belt formation.

### 3.2. The Chartreuse-Grandes Rousses Cross Section

The subalpine part of the cross-section part (Figure 4) has been redrawn from Deville et al. [1994] in Philippe et al. [1998]. There, several thrusts deformed the sedimentary cover over a décollement in the Liassic series (or upper Triassic series) and the associated shortening corresponds to the displacement along two basement thrusts. It is noteworthy that the thrust spacing and the belt width are much smaller than in the previous cross section (Vercors, Figure 3) and mainly controlled by sedimentary rock thickness, much higher in the Vercors than in the Chartreuse massif, and by the rheological properties of the décollement level [Philippe et al., 1998]. The total amount of shortening on these thrusts is about 17.8 km and started during Burdigalian-Langhian times [Arnaud, 1975].

We propose that one of the thrusts (in red in Figure 4, Mt Granier) roots in the Liassic layers above the ECM basement, following Deville et al. [1994]. Thus, this thrust was activated before the ECM uplift and the frontal basement thrust activation. However, further east, no evidence of any significant décollement in the cover can be observed in the field. Indeed, in our section, the cover deformed dysharmonically over the basement shear zones that correspond to two basement highs of the Grandes Rousses redrawn from Bellahsen et al. [2012]. The flat surface at the cover base above the Belledonne high (décollement) was rooted above the basement shear zones located between the Grandes Rousses and Belledonne massifs (Figure 4). This means that the basement shear zone propagated into the cover, though it is poorly documented in the field because of the ductile behavior of the cover and exposure conditions. The amount of shortening along this early thrust observed at surface in the fold-and-thrust belt is quite important, around 3 km. Thus, it is likely that some of this amount (at least half of it) can be associated to the basement thrust that apparently offset the (red) flat (Figure 4).

As mentioned above, in the ECM, three basement shear zones (two cropping out and one hidden) most likely shortened the crust. The amount of shortening accommodated by these structures is about 6.6 km. Thus, the total amount over the external zone in this area is about 26.9 km: an amount of shortening of 2.5 km is attributed to the Jura phase, as the outermost thrusts are in the southern continuity of the Jura belt (Figure 1 and Table 1).

Several Mesozoic normal faults are attested by thickness variations (Figure 4): the main one is the Saint Laurent (du Pont) normal fault. This normal fault has been inferred from the section in Deville et al. [1994] redrawn here, where a significant Mesozoic thickness variation occurs across the easternmost fault within the subalpine belt (Figure 4). We consequently interpret this thrust as the propagation in the cover of a reactivated inherited Liassic normal fault. In the restored section, the normal fault controls thickness variations up to the Cretaceous layers. This implies a long-lived fault activity having continued after the end of the Ligurian rifting (Liassic to Dogger times) and which may correspond to the Cretaceous extension recorded further south [e.g., Homberg et al., 2013; Bertok et al., 2012] and north (Valais domain [Handy et al., 2010, and references therein]). Other normal faults are the “Synclinal Médian” and northern Bourg d’Oisans faults, as well as other minor faults in and around the Grandes Rousses massif (Figure 4). We found no evidence for their Alpine reverse reactivation.

As in the previous cross section (Figure 3), east of the section, detached units of Liassic rocks considered as ultra-Dauphinois are overthrust by the Eocene flysch unit.

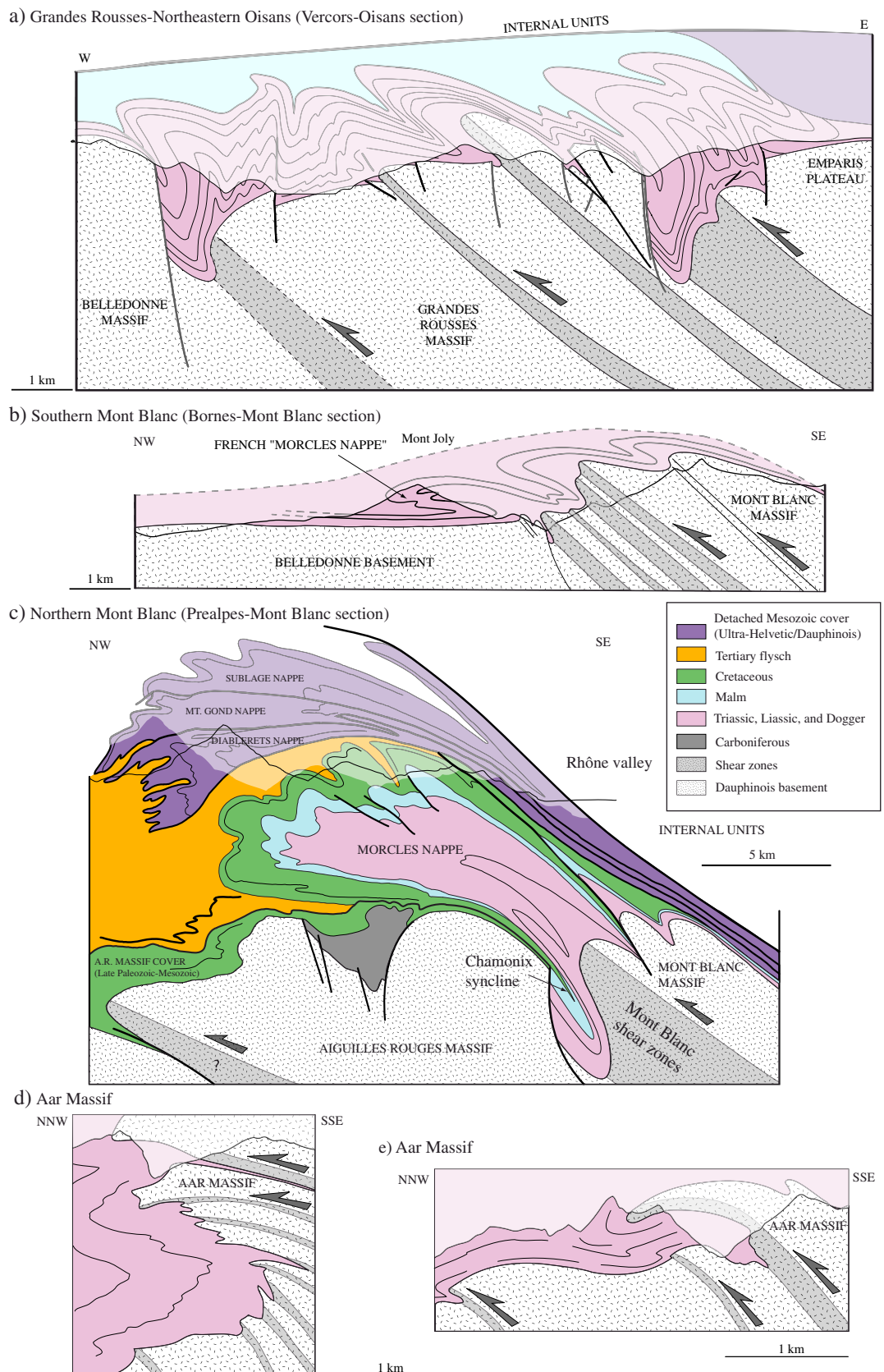


Figure 8

**Table 1.** Shortening and Amounts of Shortening for Each Section During Each Phase<sup>a</sup>

	Total Amount of Shortening (km)	Uncertainty (km)	ECM (km)	Subalpine (km)	Jura (km)	Shortening ECM (%)	Shortening Crust (%)	Shortening External Zone (%)
Vercors-Oisans	28	±2	11.5	16.5	0	16.1	27.5	20.6
Chartreuse-Grandes Rousses	26.9	±2	6.6	17.8	2.5	14.8	35.9	27.1
Bauges-Chatelard	27.9	±2	7.2	18.7	2	18.5	39.6	27.5
Bornes-Mont Blanc	46	±5	3.1	17	25.9	29.1	54.6	24.0
Préalpes-Mont Blanc	65.9	+10, -1	10.6	26	29.3	38.3	57.2	27.1
Préalpes-Aar	~69	?	12	31	26	40	67	29

<sup>a</sup>The uncertainty for the Préalpes-Mont Blanc section is from *Burkhard and Sommaruga* [1998]. The uncertainty for the Préalpes-Aar section is unknown, as it is not balanced in *Burkhard* [1988]. However, we consider the value as an order of magnitude. Uncertainty for the Vercors-Oisans section is from *Bellahsen et al.* [2012] and mainly due to uncertainty of Triassic length in ECM and at the transition subalpine chain/ECM. The same uncertainty is used for the Chartreuse-Grandes Rousses and Chartreuse-Belledonne section. For the Chartreuse-Grandes Rousses and Chartreuse-Belledonne sections, the frontal thrust has been considered as belonging to the Jura belt (see Figure 1). The shortening is calculated in three different ways (see Figure 12).

### 3.3. The Chartreuse-Belledonne Cross Section

In this cross section (Figure 5), the western part (Chartreuse and west Belledonne) was redrawn after *Deville and Chauvière* [2000]. There, several thrusts in the cover rooted in two basement thrusts. In this cross section built after seismic data, one may find the best evidence for the allochthonous nature of the ECM, the basement clearly overthrusting the sedimentary cover of the subalpine belt. The amount of shortening accommodated by these basement thrusts is about 18.7 km.

As in the previous section (Figure 4), a thrust in the eastern part of the folded belt (in red, Figure 5, Mt Granier) roots within the Liassic layers but above the Belledonne basement high. The flat is thus drawn until east of Belledonne where it roots in a basement shear zone. Within the Belledonne massif, a vertical fault (Figure 5) is mapped out in the field [e.g., *Marquer et al.*, 2006]: it is most probably an inherited Jurassic normal fault (bounding the Synclinal Median basin as in the previous cross section, Figure 4) that was dipping west and was not significantly reactivated but deformed and verticalized.

There are three main inherited normal faults: one hidden below the subalpine belt (observed on seismic lines [*Deville and Chauvière*, 2000]), the normal fault east of the Synclinal Médian basin (see above), and the normal fault that controls the Col de la Madeleine basin (Figure 5).

The amount of shortening associated to the deformation within the ECM is about 7.2 km. Thus, the total amount over the external zone in this area is about 27.9 km: an amount of shortening of 2 km is attributed to the Jura phase, as the most external thrusts are in the southern continuity of the Jura belt (Figure 1 and Table 1).

Here again, below the frontal penninic thrust, an allochthonous Eocene flysch unit overthrusted a unit made of Liassic series itself detached from its basement in the eastern part (ultra-Dauphinois).

### 3.4. The Bornes-Mont Blanc Cross Section

The fold-and-thrust belt part of this cross section (Figure 6) was redrawn after [*Affolter et al.*, 2008], from the western end of the section to the Aravis massif. It consists of two parts: the Jura and the subalpine chains. In the former, the amount of shortening is about 25.9 km and is accommodated by numerous thrusts that rooted in Triassic evaporites [*Affolter et al.*, 2008]. The décollement has been subsequently deformed below the internal Jura by later high-angle basement thrusts related to inversion of permo-carboniferous basins (e.g., *Lacombe and Mouthereau* [2002]; Figures 6 and 7). The décollement within the Triassic is connected to a basement thrust as in *Burkhard and Sommaruga* [1998]. In the latter (subalpine chains), an amount of shortening of 17 km is recorded

**Figure 8.** Detailed cross sections showing the basement-cover relationships in the different ECM. (a) Along the Vercors-Oisans section, the cover is disharmonically folded above basement shear zones [*Bellahsen et al.*, 2012]. (b) Along the Bornes-Mont Blanc section, the cover is disharmonically folded above basement shear zones: the Mont Joly (Figure 1) structure is from [*Epard*, 1990], who interpreted it as the "French" Morcles nappe. In the field, clear Alpine shear zones can be observed and correspond to the mapped basement top "folds". (c) Along the Préalpes-Mont Blanc section, the Morcles nappe is interpreted as the Mont Blanc cover [*Escher et al.*, 1993]. The Morcles nappe geometry and Aiguilles Rouges massif structure is from [*Escher et al.*, 1993]. We have modified the original figure to display the Mont Blanc shear zones and the probable Chamonix normal fault also drawn in *Burkhard and Sommaruga* [1998]. (d and e) Basement-cover relationships in the Aar massif from [*Ramsay et al.*, 1983] and [*Heim*, 1921], respectively. Note that each inverted basement "fold" limb corresponds to basement shear zones as observed in Figures 8a–8c.

and accommodated in a basement thrust. Such structural choice is made for along-strike structural consistency with the other cross sections. Indeed, it is clear that further south the subalpine chains are due to the activation of a décollement by basement thrusts beneath the ECM (Figures 4 and 5, for example).

However, in Figure 6, thrusts in the Aravis massif have not been rooted in any basement thrust for several reasons. Firstly, basement thrusts are not clearly exposed in the field. Secondly, in the western Belledonne massif, as in northwestern Aiguilles Rouges massif, sedimentary rocks display top-to-the-NW thrusts and NW verging folds. These thrusts probably root near basement shear zones further east such as in the previous cross sections. Such structures are then older than the ECM shortening and uplift, or coeval with their early deformation.

In the easternmost part of the section, the SW Mont Blanc structures consist of NW verging basement shear zones observed in the field and associated recumbent folds in the cover. There, the cover is not detached over the basement (Figure 8b) and displays similar geometries as in the Morcles nappe (Figure 8c) [Epard, 1990; Escher *et al.*, 1993], in northern Oisans (Figures 3 and 8a) [Bellahsen *et al.*, 2012], and in the Aar massif (Figures 8d and 8e) [Ramsay *et al.*, 1983, and references therein]. The associated amount of shortening is about 3.1 km. Thus, the total amount over the whole external zone is about 46 km (Table 1).

### 3.5. The Prealpes-Mont Blanc Cross Section

This cross section (Figure 7) has been redrawn from *Burkhard and Sommaruga* [1998]. Thus, we will only sum up the main implications. The total amount of shortening is about 65.9 km (Table 1), among which 29.3 km is linked to the three frontal basement thrusts of the lower part of the Aiguilles Rouges massif, attesting for the shortening in Jura fold-and-thrust belt that shortened above a décollement in the Triassic layers [*Burkhard and Sommaruga*, 1998; *Affolter et al.*, 2008]. The structures in the Aiguilles Rouges massif have been drawn as basement thrusts, although they might have been more distributed shear zones (e.g., *Steck et al.* [1997], see discussion part).

The amount of shortening within the Tertiary sedimentary rocks of the NAFB (NW of the Préalpes, structures equivalent to the subalpine chains further SW) is about 26 km above a décollement in the Tertiary series and rooted in two thrusts of the upper Aiguilles Rouges.

The Morcles unit is a recumbent anticline that represents the cover of the Mont Blanc massif, where an amount of shortening of 10.6 km is recorded. The Morcles nappe is thus not strongly detached from its basement, although it has been slightly translated toward the NW as attested by the intense shearing of its overhanging limb [*Escher et al.*, 1993]. In Figure 8c, adapted from *Escher et al.* [1993], we added the Mont Blanc shear zones [*Leloup et al.*, 2005; *Rolland et al.*, 2008] and the inherited Jurassic normal fault in the Chamonix syncline (see also [*Boutoux et al.*, 2014]), although it does not clearly crop out in the syncline. However, this normal fault is necessary to explain the cover thickness difference above the Aiguilles Rouges massif (thin series) and above the Mont Blanc massif (thick series).

The two upper sedimentary nappes, the Diablerets and the Wildhorn nappes, consist of detached units that represent the cover of more internal crustal domains (ultra-Helvetic).

## 4. Discussion

Here we present a synthesis of the structural style of the external zone of the Western Alps in order to provide a structural map consistent at the scale of the whole orogenic domain. Then, the sequence and amount of shortening can be determined, as well as average estimates of exhumation/uplift rates. The shortening sequence is also used to produce palinspastic maps from the SW to the central Alps at four key periods of the Tertiary evolution. Finally, a restoration of the Mesozoic proximal continental margins is proposed and discussed.

### 4.1. Structural Style

On the cross sections presented above, the shortening that is recorded in both the Jura and the subalpine chains is connected to displacement along basement thrusts below ECMs. Evidence for such a geometry can be found in the subalpine chains on seismic lines (see interpretation of *Deville and Chauvière* [2000] for the Western Alps and *Pfiffner et al.* [1997] and *Steck et al.* [1997] for the central Alps) where the basement clearly overthrusts the sedimentary cover of the fold-and-thrust belt. Alternatively, the subalpine chains could have been emplaced before the ECM uplift, and if so, their shortening would have to be rooted above them. This sequence of tectonic events was proposed by *Leloup et al.* [2005] or *Affolter et al.* [2008], for example, and requires the subalpine chain shortening to be older than the ECM uplift.

This model was supported by uplift ages in the Mont Blanc and Aiguilles Rouges massifs not older than 22 Ma. Moreover, the Morcles nappe is sometimes interpreted as equivalent of the subalpine chains [Doudoux *et al.*, 1982; Leloup *et al.*, 2005]. However, in the south, at the Oisans latitude, the subalpine chain emplaced about 15 Ma ago, i.e., significantly younger than the exhumation of the Oisans ECM that started before 27 Ma [van der Beek *et al.*, 2010]. North of the Mont Blanc massif, the lateral equivalent to the subalpine chains, i.e., the Subalpine Molasse thrust, is dated back to 15–20 Ma [Burkhard and Sommaruga, 1998], while the Mont Blanc shortening started around 30 Ma [Cenki-Tok *et al.*, 2013]. Thus, the timing of ECM and Subalpine shortening are well-constrained and likely express the sequential involvement of inner ECM basement units followed by the subalpine chain. As a consequence, the subalpine chain appears kinematically related with frontal basement thrusts. This interpretation is similar to that proposed by Burkhard and Sommaruga [1998], redrawn in Figure 4, but also by Ménard and Thouvenot [1987], Guellac *et al.* [1990], and Mugnier *et al.* [1990] around the ECORS profile location. The subalpine belts are represented in dark green in Figure 9.

If the subalpine chains are linked to ECM basement thrusts, then the same should be for Jura, as it is younger than the subalpine chains and the ECM uplift (compare ages in Arnaud [1975] and Philippe *et al.* [1998] and ages in Kalin [1997], Bolliger *et al.* [1993], Steiniger *et al.* [1996], Becker [2000], and Rolland *et al.* [2008]). This Jura unit is represented in light green in Figure 9.

The basement structures in the frontal ECM are named “basement thrusts” but may very well be localized shear zones [e.g., Steck *et al.*, 1997]; many of them unfortunately do not crop out. In the “internal” ECM (Mont Blanc, Oisans), the structures accommodating shortening are indeed shear zones. In the frontal ECM, the structures might be more localized as they activate upper décollements (at the base of the sedimentary cover): they are probably brittle-ductile thrusts/shear zones, more localized than the Mont Blanc shear zone but more distributed than a cataclastic thrust.

Few units in the subalpine chains cannot be explained by the activation of a décollement due to basement thrusts below the frontal ECM. Indeed, several thrusts branch on a décollement above the ECM (Figure 10) as shown in Deville *et al.* [1994] and redrawn in Figures 4 and 10d, in Deville and Chauvière [2000] and redrawn in Figures 5 and 10c, and in Affolter *et al.* [2008] and redrawn in Figures 6 and 10b. These (small) units suggest that the ECM cover was slightly detached from the basement, which justifies considering it as a unit distinct from the subalpine one in a strict sense. However, further north, around the northeastern Aiguilles Rouges massif, the cover is thin and not detached from its basement (Figures 7 and 10a) [Escher *et al.*, 1993]. Thus, this unit must terminate in this area and is restricted to the “French Alps.” Similarly, further south on the section south of Grenoble (Figures 3 and 10e) from Deville *et al.* [1994], this unit does not appear and probably also terminates around the southern Belledonne massif (south of the Rochail massif), as we find no evidences for such a unit in the field between Gap and Grenoble (Figure 1).

The geometry of the thrusts bearing this unit is compatible with the geometry proposed in Epard and Escher [1996], where sedimentary nappes are related to basement shortening along shear zones that are located several kilometers toward the internal zones. The faults belonging to this unit are represented in red in Figure 9. Since the subalpine chain has later deformed this unit, it could hardly be represented in map view at this scale.

Thus, our analysis proposes a new unit, named “Aravis-Granier” unit, corresponding to a part of the sedimentary cover whose shortening is attested by folds and thrusts that branch on a décollement within the Liassic series above the ECM (Figure 9). However, this unit is not observed either north of the Mont Blanc massif or southwest of the Belledonne massif. This along-strike variation in the structural style may be explained by the depth of underthrusting of the European crust and the extent of the internal units. In the north, the crust was buried down to about 20 km (in the Mont Blanc for example). We here propose that, at this depth and corresponding temperature (400°C [Rolland *et al.*, 2008]), the crust was very weak and detached in the middle lower crust (Figure 11d; see also further down). As a consequence, both the basement and its cover could be shortened in the same way without any significant décollement as there would be little rheological contrast between the basement and the cover (Figure 11d). Southwest of the Mont Blanc, the Belledonne massif was probably buried down to less than 10 km, as the Aiguilles Rouges massif [Leloup *et al.*, 2005], probably due to their frontal position. Such burial did not induce a strong weakening of the crust (Figure 11b). Then, the sedimentary layers were probably much weaker than the deforming basement, and as a consequence, part of the cover detached from the basement. In the

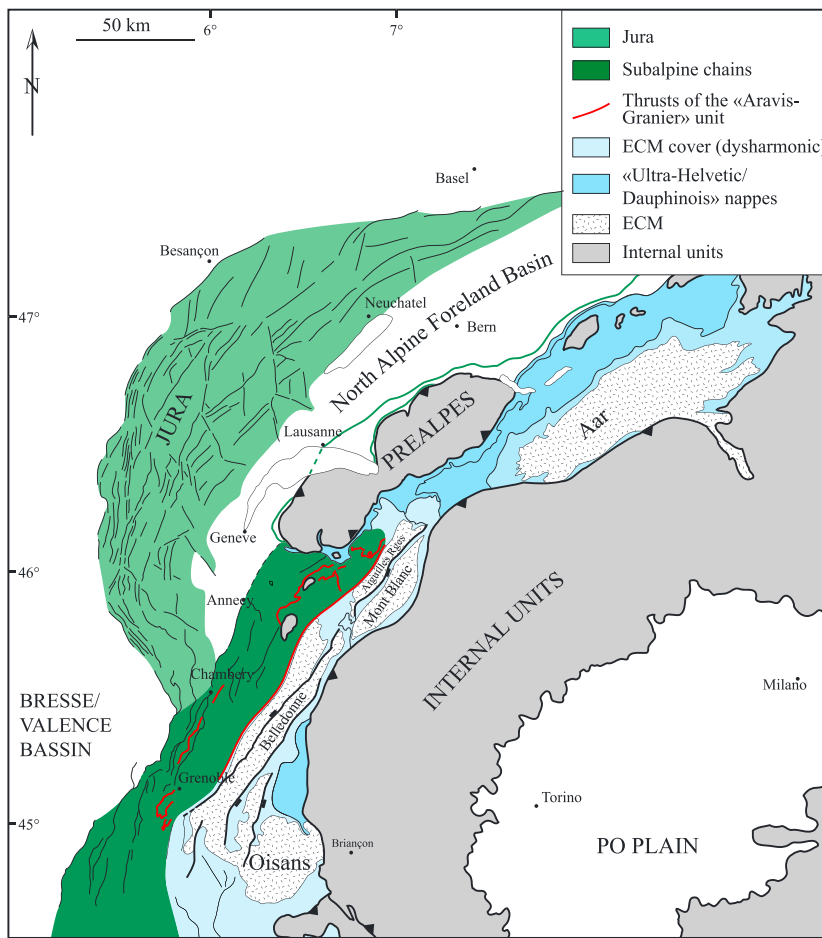


**Figure 9.** New structural map of Western Alps. Colored areas correspond to different units. Light green represents Jura, and dark green represents subalpine chains. By subalpine chains, we mean fold-and-thrust belts that are due to the activation of a basal décollement activated by basement frontal thrusts beneath ECM. Light blue areas represent the Helvetic-Dauphinois sedimentary nappes or cover of the ECM that are autochthonous (western limb in northeastern Aiguilles Rouges), disharmonically folded above basement shear zones (Oisans cover and Mont Joly), and/or slightly sheared above their basement (Morcles). In darker blue are the early detached sedimentary units that represent the cover of ultra-Dauphinois/helvetic basement. Finally, in red, we have represented the thrusts that correspond to the detached part of the ECM cover; i.e., upper part of the Mont Joly unit for example. In other words, along the Préalpes-Mont Blanc section (NE section), the whole Mesozoic cover of the Mont Blanc is represented by the Morcles nappe, while along the Bornes section (SW Mont Blanc), the Mont Joly (French Morcles) is only made of the lower Jurassic layers. The rest of the cover is displaced and composes the “Aravis-Granier” unit.

southwest Belledonne massif, the burial was lower than in the northeast Belledonne massif but the cover was not detached (see above). There, the amount of shortening is much lower than further north. As a consequence, the shortening east of Belledonne was not significant enough to imply a décollement above Belledonne as further north. The presence of a detached unit at the ECM front is thus ascribed to a combination of particular crustal rheology and significant amount of shortening, two parameters themselves probably not independent from each other.

In light blue in Figure 9, the ECM cover is not significantly detached over its basement as shown by [Bellahsen et al., 2012] (pink in Figures 3–7 and 10). This includes the Morcles nappe, NE of the Mont Blanc massif (Figure 8c) [Escher et al., 1993], and the Mont Joly, its French equivalent SW of the massif (Figure 8b) [Epard, 1990]. Recent ages of Mont Blanc deformation around 30 Ma [Cenki-Tok et al., 2013] confirm the structural interpretation invoking that the Morcles nappe is the Mont Blanc cover; these ages are synchronous with earliest deformation in the Morcles nappe at 30 Ma [Kirschner et al., 1996]. The Morcles recumbent anticline was then emplaced over the Aiguilles Rouges.

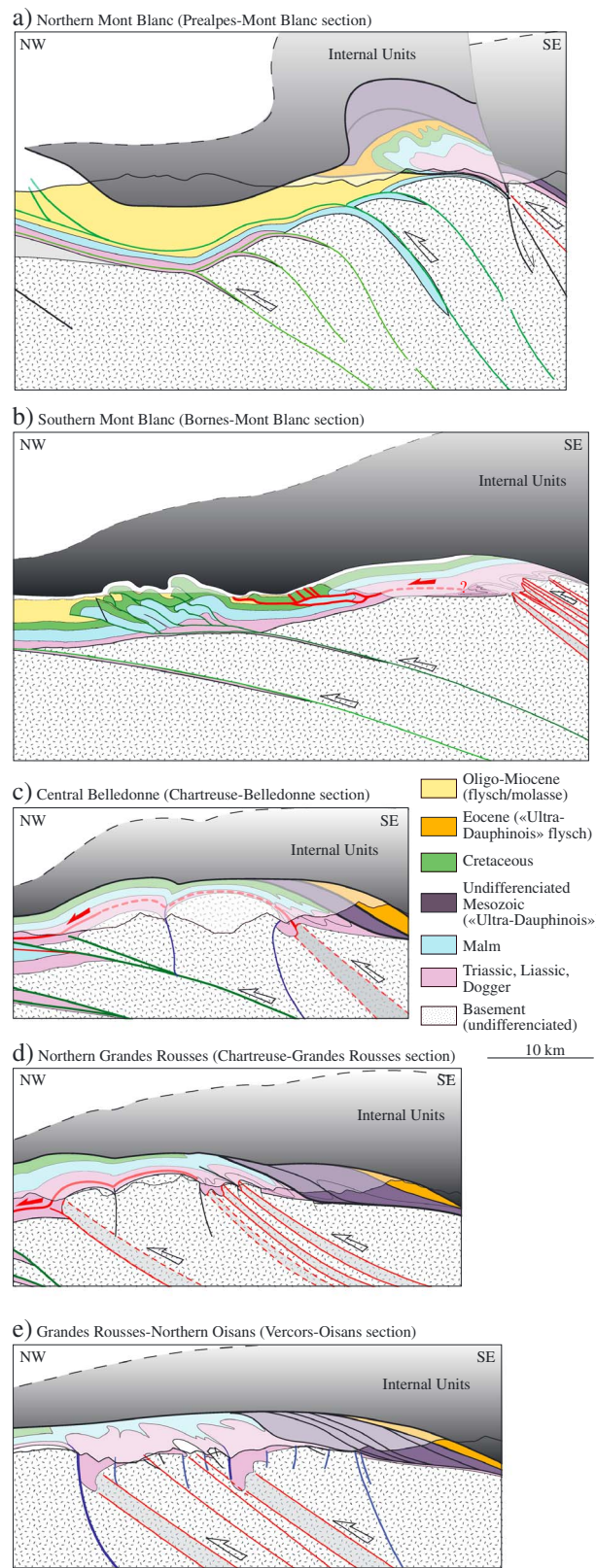


**Figure 10.** Zooms of the ECM-subalpine chain relationship from cross sections from Figures 5–9. Note the presence of the red thrust (Aravis–Granier unit): the upper part of the cover of the Belledonne massif is detached from the rest of the cover, except in the northernmost and the southernmost cross sections.

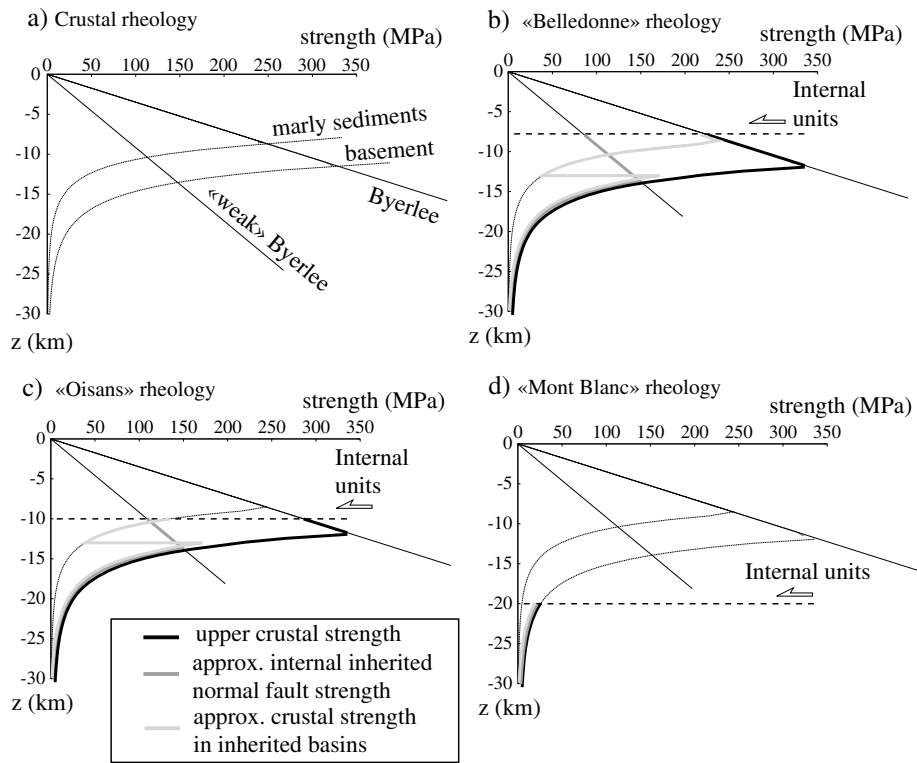


**Figure 11.** Rheology of the crust. (a) Before the collision (see *Bellaïsen et al.* [2012] for details). “Weak byerlee” is taken for the inherited Liassic normal fault internal strength. “Marly sediments” is for the Liassic sedimentary rocks in the inherited basins. (b) During the collision for the Belledonne part of the Chartreuse-Grandes Rousses and Chartreuse-Belledonne sections. (c) During collision for Oisans massif on the Vercors-Oisans section. The crustal strength with an inherited basin is lower than both the crust without basin and the inherited normal faults internal strength. (d) During collision for the Mont Blanc massif on the Bornes-Mont Blanc and the Préalpes-Mont Blanc sections. The crust is ductile and very weak.

Further south (around the Grandes Rousses and north of the Oisans massif), the structural style is similar but with less shortening (compare Figures 3–7). All these areas similarly show recumbent anticlines in the sedimentary cover and are associated with distributed shear zones within the basement (Figure 8).

Finally, the sedimentary nappes above the Mörles unit, i.e., the Diablerets and the Wildhorn nappes (Ultra-Helvetic) are most likely detached over their basement as in *Burkhard and Sommaruga* [1998]. Similar geometries can be found north of the Oisans massif. The detached Liassic units in Figures 3–5 may be equivalent to the ultra-Helvetic nappes mentioned above. These units have been represented in dark blue in Figure 9 (purple in Figure 10). These ultra-Dauphinois/Helvetic nappes probably emplaced during the early Alpine collision, most likely during early Oligocene [e.g., *Burkhard and Sommaruga*, 1998; *Ceriani et al.*, 2001; *Simon-Labréte et al.*, 2009; *Bellanger et al.*, 2014]. These cover units are the only ones that could possibly be unrelated to basement shortening. Beside these units, in the Alpine external zone, all the shortening observed in the cover (fold-and-thrust-belt and ECM cover) corresponds to basement shortening.

#### 4.2. Amounts of Shortening

According to the above results, the shortening recorded in the external zone is related to basement shortening and therefore reflects the presence of a deep crustal detachment. Here we present a summary of amount of shortening estimates (Figure 12 and Table 1).

Our estimates of the frontal basement thrust displacements mainly arise from balanced cross sections of fold-and-thrust belts in the literature, and their northward increase is consistent with previous works [*Ménard and Thouvenot*, 1987; *Sinclair*, 1997]. Our estimate of the total amount of shortening through the external zone along the ECORS profile is similar to those proposed by *Mugnier et al.* [1990] and by *Guellec et al.* [1990]. We

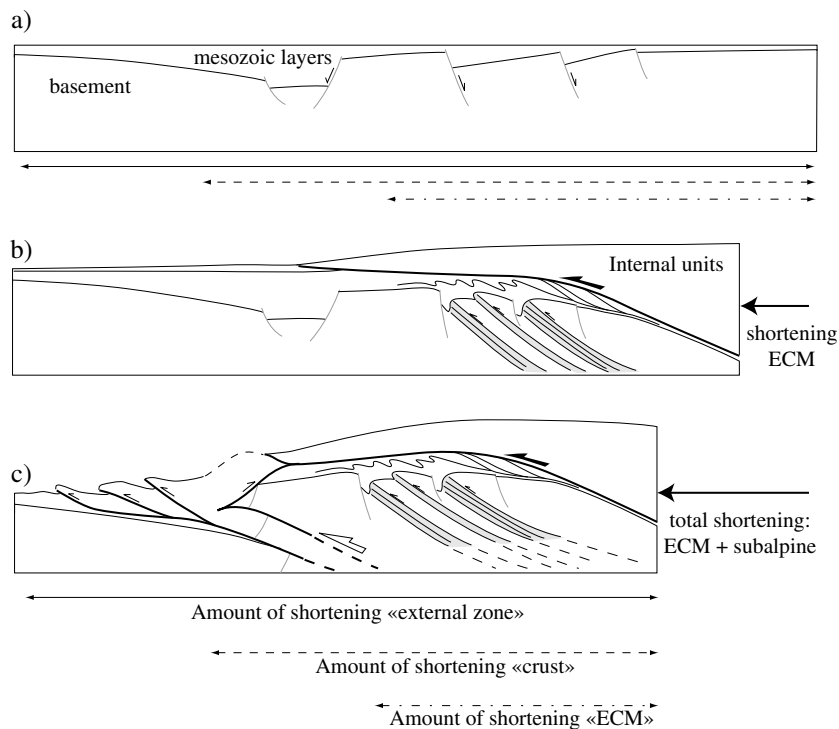


**Figure 12.** Amounts of shortening measurements. Schematic structures of the Oisans section during (a) preorogenic times, (b) early burial beneath internal units with ECM shortening, and (c) late subalpine chain shortening, from *Bellahsen et al. [2012]*. The amount of shortening “ECM” is calculated considering the initial and final width of deformed ECM, i.e., the extent of the main basement shear zones. The amount of shortening of the crust (ECM plus frontal thrusts) is calculated considering the initial and final width of the crust, i.e., from the Penninic Frontal Thrust (PFT) to the outermost buried basement thrust. The amount of shortening “external zone” is calculated considering the initial and final width of the whole external zone, i.e., from the PFT to the frontal cover thrust.

found that the amount of shortening over the entire external zone increases from 28 km in the south (Vercors-Oisans section) to 65.9 km in the north (Prealpes-Mont Blanc section) (Table 1). This is due to (1) variations in the amount of shortening in the ECM, (2) an increase in the amount of shortening in the subalpine chains, and (3) an increase due to the Jura northward.

The whole external zone shortening ranges between 20% in the south and around 30% in the north, consistent with the range of shortening values typically observed in the Alps and other young peri-Tethyan orogens [e.g., *Mouthereau et al.*, 2013]. However, it is noteworthy that this variation is not as large as the variation of the amount of shortening (Table 1). This is due to the contribution of locally more thin-skinned deformation featured in the Jura that increases the total amount of shortening as well as the original width of the restored external domain. The width enlarged because of the presence of both an efficient décollement in Triassic layers and the thick NAFB [e.g., *Fillon et al.*, 2013], allowing efficient stress transfer without much internal strain. This outlines a stronger basement relative to cover in the foreland.

The shortening considering the basement only (%; Figure 12) increases northward more than the shortening calculated over the whole external zone (Table 1). This is mainly due to the increase in amount of shortening along the frontal thrusts from south to north. This means that, northward, the amount of crustal shortening increases (most likely because of more convergence in the north) and is more localized in space. Note, however, that this does not mean that the deformation at smaller scale is more localized in terms of deformation mechanisms. This is actually the opposite: toward the north, in the Mont Blanc [*Rolland et al.*, 2008] and Aar massifs [*Marquer, 1990*], the deformation observed in the field is more distributed than in the south [*Bellahsen et al., 2012*]. In the north the deformation is clearly ductile, while it is only brittle-ductile in the south. This tendency is of course also clear from the P,T conditions: the deformation occurred at about 300–350°C and around 3 kb in the south (Oisans massif [*Jullien and Goffé, 1993*]) and at about 400 to 450°C and 5–6 kb in the north [e.g., *Challandes et al., 2008; Rossi et al., 2005*].

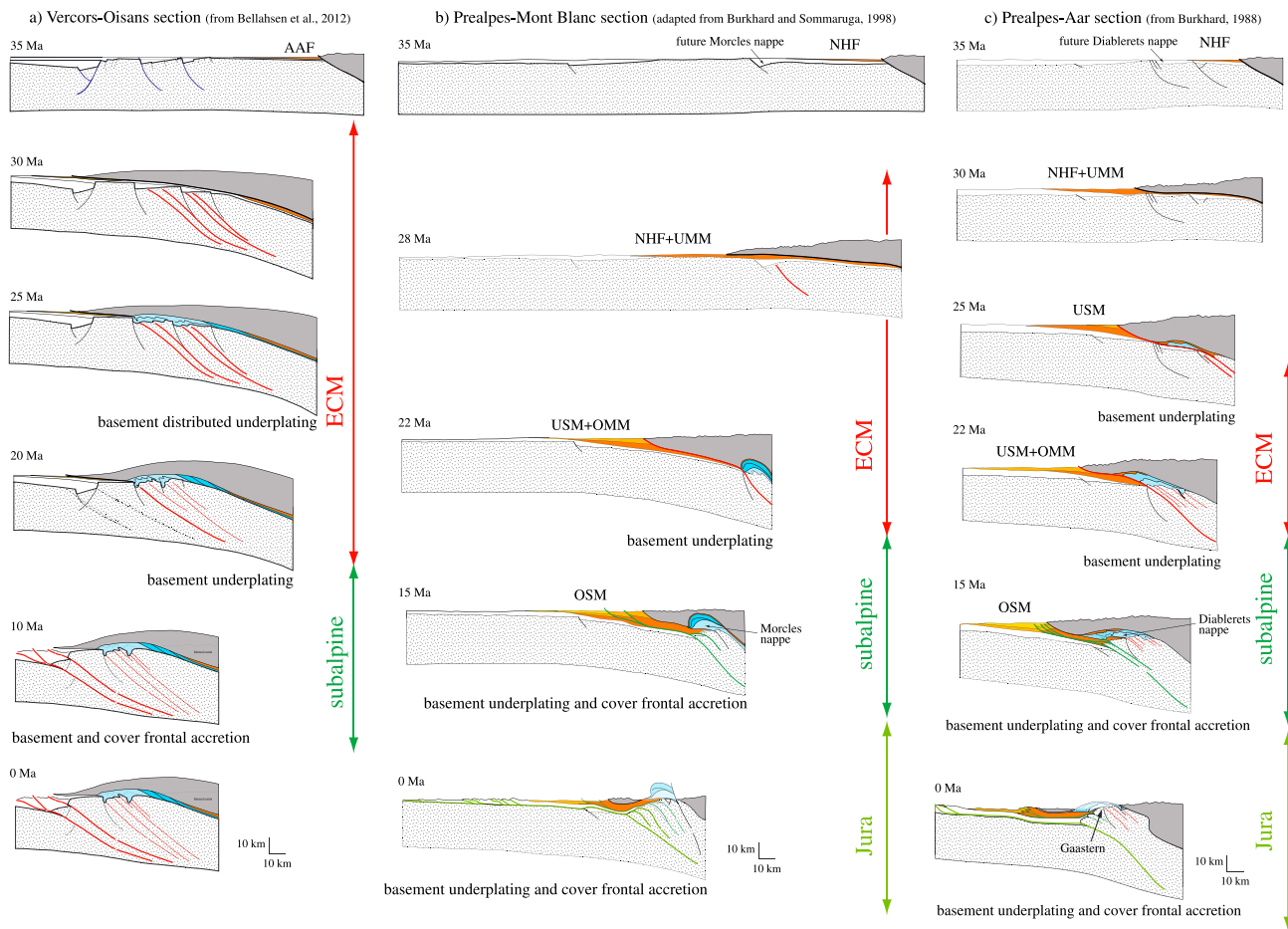


**Figure 13.** Sequence of shortening for the Vercors-Oisans, the Préalpes-Mont Blanc, and the Préalpes-Aar sections. (a) Shortening sequence for the Vercors-Oisans section from Bellahsen *et al.* [2012]. During the ECM phase (after the deepwater turbidites deposition and burial phase), the crust deformed by distributed underplating in the basement. During the subalpine phase, frontal accretion in the basement produces frontal accretion in the cover and a basal décollement activation. AAF is for Aiguilles d'Arves Flysch. (b) Shortening sequence for the Mont Blanc section deduced from the balanced cross section in Burkhard and Sommaruga [1998]. The sequence is quite similar to the one described for the Aar section (Figure 13c). NHF is for north Helvetic Flysch. UMM is for Lower Marine Molasse (German terminology), USM for Lower Freshwater Molasse, OMM for Upper Marine Molasse, and OSM for Upper Freshwater Molasse. (c) Shortening sequence for the Aar section [Burkhard, 1988] with age constraints from Challandes *et al.* [2008]. After the phase of deepwater turbidites deposition and subsequent burial beneath the internal units, the orogenic wedge deformed mainly by basement underplating (ECM phase). During the subalpine phase, basement underplating led to frontal accretion of cover units. During the Jura phase, the underplating of the lowest basement unit led to the fast basinward propagation of the orogenic front and the frontal accretion of cover units.

When P,T conditions increase, the deformation is more distributed at the field scale (i.e., rather small scale) but shortening is more localized at the orogen-scale due to change in crustal strength. In other words, under “high” P,T conditions the basement shortening did not “propagate” far toward the foreland, while basement deformation is distributed far toward the foreland under lower P,T conditions, which can be related to the rheology of the crust during collision (Figure 11): a weak crust induces more localized shortening at the orogen-scale.

The cause of these along-strike variation of P,T conditions is still an open question: it may either be due to efficient “subduction/underthrusting” of the crust in the north because of a higher crustal strength and/or more efficient slab pull in the north linked to the complete crustal breakup in the Valais domain (see last section).

#### 4.3. Sequence of Shortening

As described above, the timing of deformation within the different units is as follows: (1) emplacement of the ultra-Dauphinois/Helvetic sedimentary nappes during early Oligocene, (2) shortening of the ECM basement

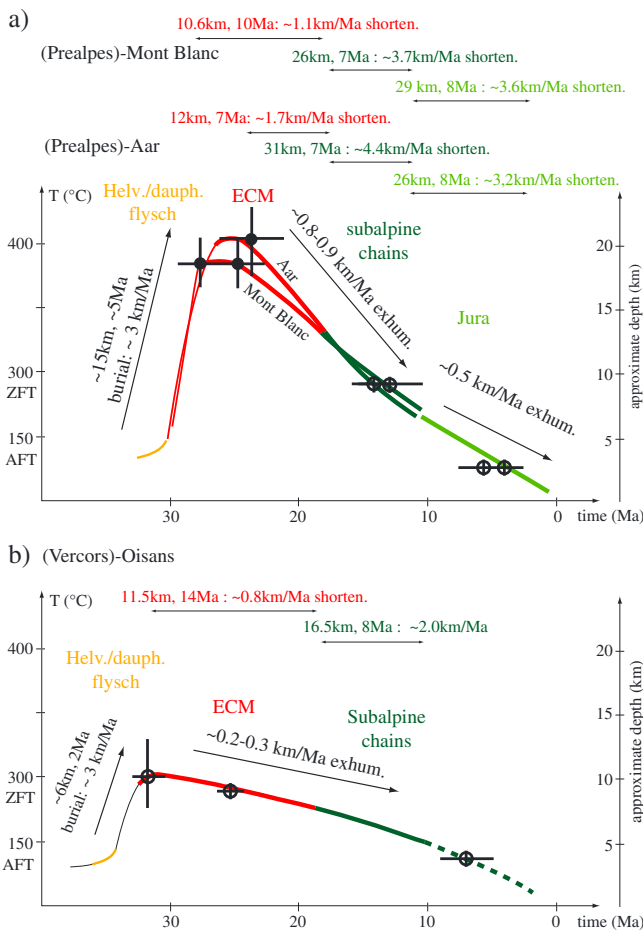


**Figure 14.** Amounts of exhumation and shortening through time and during the different shortening stage of the sequence: the ECM shortening, the subalpine, and the Jura phases from the data synthesized in Figures 2 and 13 and Table 1. (a) Mont Blanc and Aar data. Exhumation rates are calculated from estimation of depth at various times: metamorphic peak [e.g., Leloup et al., 2005; Rolland et al., 2008; Challandes et al., 2008] and thermochronology (AFT, ZFT) for the retrograde path [see Vernon et al., 2008]. (b) Oisans data. The maximum depth is poorly constrained and estimated from the maximum temperature, around 300°C, that provide a rough estimate of the pressure considering a 30°C/km geothermal gradient. ZFT and AFT data provide other constraints [e.g., van der Beek et al., 2010]. Black circles are pressure constraints; errors bars are thus given for depth. Open circles are constraints on pressure deduced from temperature constraints; errors bars are given for temperature.

Aiguilles Rouges), while small amounts of frontal accretion occurred within the cover. During the time of Jura formation in late Miocene to early Pliocene, basement units were also underplated (lower Aiguilles Rouges), while a very wide area was accreted in frontal parts within the cover (NAFB and Jura mountains).

In the Aar massif, a similar sequence was described [Burkhard, 1988] (Figure 13c): underplating of basement units during the ECM deformation in Late Oligocene to early Miocene times, underplating of basement units and accretion in the cover during the shortening of the upper Gaastern unit, and basement underplating with much larger amount of cover accretion (Jura) during the emplacement of the lower Gaastern unit.

To summarize, underplating is a long-lived process in the north and is characterized locally by high crustal shortening (up to around 60%, considering the basement only, Table 1 and Figures 11, 13b, and 13c). On the contrary, frontal accretion is an important process in the south along with lower crustal shortening (as low as

and their cover during Oligocene to early Miocene times, (3) activation of both the basement frontal ramps and the décollement below the subalpine chains during Miocene times, and (4) activation of both the lower frontal basement ramps and the décollement below the Jura chain in the north during late Miocene/early Pliocene. This forward sequence is consistent with results from earlier studies [e.g., Burkhard and Sommaruga, 1998; Bellahsen et al., 2012].

This forward sequence is, however, variable from north to south. In the south, the ECM shortened in a distributed way (see previous section) during Oligocene times before the deformation localized on the frontal ramp that activated the subalpine chain (Figure 13a). Thus, the deformation of the orogenic wedge is characterized by accretion and thrust stacking from below the wedge ("distributed underplating," Figure 13a) but without wedge widening (frontal accretion) during Oligocene times. This was followed during Miocene times by frontal accretion and wedge widening.

Further north, in the Mont Blanc massif, during Oligocene to early Miocene times, the basement shortened during its underplating below the internal units (Figure 13b). During middle Miocene times and the activation of a fold-and-thrust belt in the foreland basin, the dynamics still consisted of underplated basement units (upper

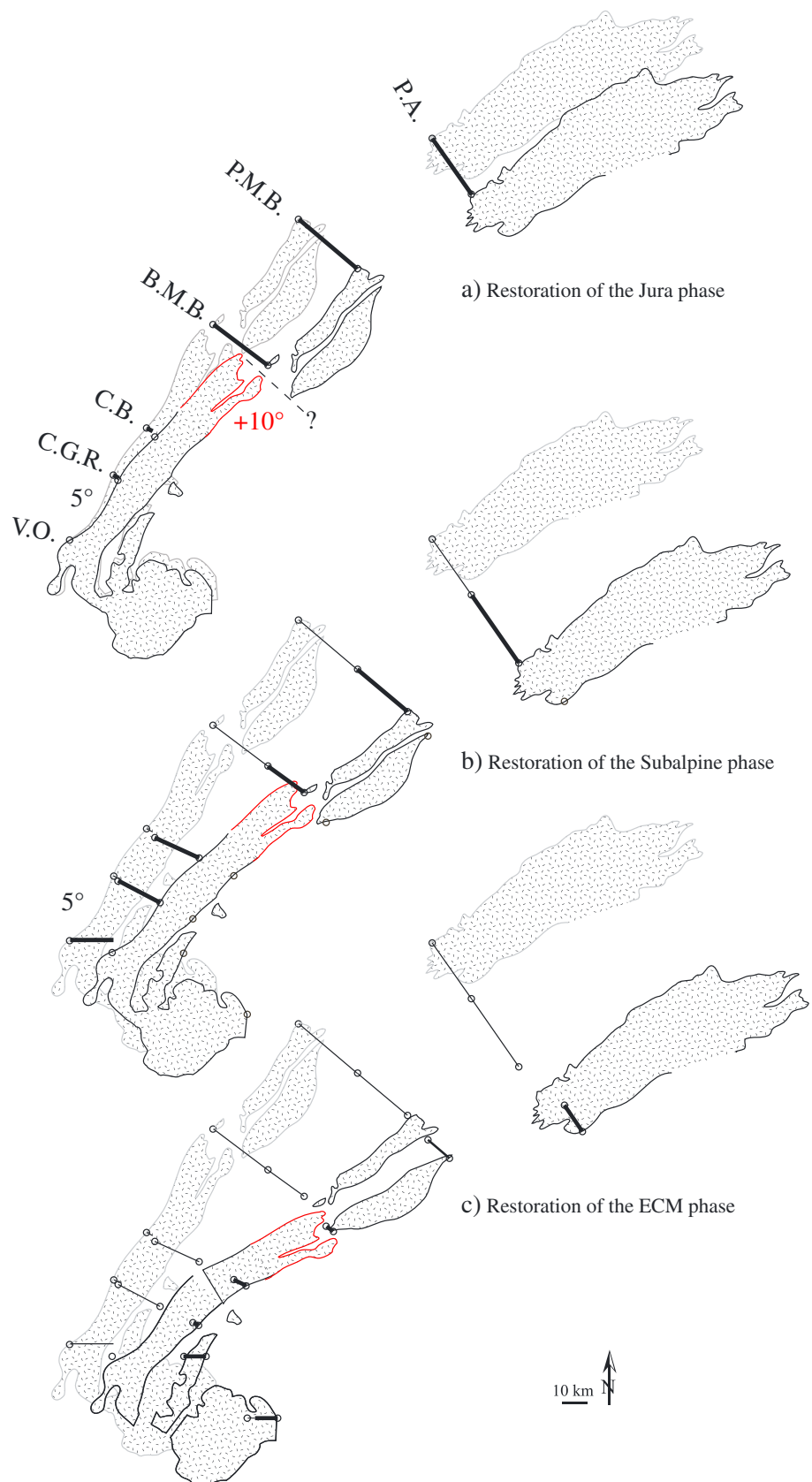


Figure 15

about 25%, Table 1). It is also noteworthy that underplating occurred in the south (ECM shortening), but it is quite different from that in the north, as it occurred in a distributed way (Figure 13a).

This shortening sequence being well defined, we present average long-term rates of shortening ( $\text{km Ma}^{-1}$ , Figure 14) and exhumation ( $\text{km Ma}^{-1}$ , Figure 14). We calculated the rate of crustal shortening for each of the defined periods of crustal shortening ("ECM," "Subalpine," and "Jura"). Rates of exhumation are derived from estimated pressure peak (assuming an average density of  $2.7 \text{ kg/m}^3$ ). Available thermochronological data (AFT, ZFT, and UTh/He) are used to derive complementary constraints on exhumation at intermediate depth assuming a steady geotherm of  $30^\circ\text{C}/\text{km}$ .

The burial rate is estimated using the age of the deepwater turbidites deposition (flysch basin, at the surface) and the age of the pressure peak. It is similar from north to south, about  $3 \text{ km Ma}^{-1}$  (Figure 14). During the ECM shortening phase, the shortening rate is about  $0.8 \text{ km Ma}^{-1}$  (11.5 km during 14 Ma, Oligocene times) in the Oisans (Figure 14b), about  $1.1 \text{ km Ma}^{-1}$  (10.6 km during 10 Ma, Oligocene to early Miocene times) in the Mont Blanc, and about  $1.7 \text{ km Ma}^{-1}$  (12 km during 7 Ma, early Miocene times) in the Aar.

During the subalpine phase, the shortening rate is about  $2.0 \text{ km Ma}^{-1}$  (16.5 km during 8 Ma, Miocene times) in the Oisans (Figure 14b), about  $3.7 \text{ km Ma}^{-1}$  (26 km during 7 Ma, Miocene times) in the Mont Blanc, and about  $4.4 \text{ km Ma}^{-1}$  (31 km during 7 Ma, early Miocene times) in the Aar (Figure 14a).

During the Jura phase, the shortening rate is about  $3.6 \text{ km Ma}^{-1}$  (29 km during 8 Ma, late Miocene early Pliocene times) in the Mont Blanc and about  $3.2 \text{ km Ma}^{-1}$  (26 km during 8 Ma, late Miocene early Pliocene times) in the Aar (Figure 14a).

The crustal shortening rates along the Prealpes-Aar and Prealpes-Mont Blanc sections are about 2 to 3 times higher than along the Vercors-Oisans section, during both the ECM and the subalpine phases.

The exhumation rates averaged over these two phases show a rather constant value through time, about  $0.2\text{--}0.3 \text{ km Ma}^{-1}$  for the Oisans massif (Figure 14b), which is consistent with the cooling rates of Crouzet *et al.* [2001]. For the Mont Blanc and the Aar massifs, it is of about  $0.8\text{--}0.9 \text{ km Ma}^{-1}$  (Figure 14a), which is consistent with rates given in Rolland *et al.* [2009] from  $^{40}\text{Ar}/^{39}\text{Ar}$  compared to K-Ar ages [Kralik *et al.*, 1992] for the Aar massif. This is also consistent with fission track dating [Vernon *et al.*, 2008, and references therein]. Similar rates are described for the Mont Blanc over the last 16 Ma [Seward and Mancktelow, 1994; Rolland *et al.*, 2008].

Thus, the exhumation rates are also about 3 times higher in the Aar massif than in the Oisans massif. An explanation has to be found for the northward along-strike increase of both the shortening and exhumation rates and will be discussed in the next sections. In any case, the link between the two rates can be explained as follows: (1) assuming shortening rates 3 times higher in the north than in the south and (2) given that the southern massifs are much wider than in the north, it is consistent to find higher exhumation

**Figure 15.** Displacement field for ECM through time and constraints for palinspastic reconstructions from the shortening sequence; see Table 1 and Figures 3–7. (a) Displacement field of ECM for the Jura phase. The Aar and the Mont Blanc massifs present large displacement, as well as the small basement outcrop between the Belledonne and the Aiguilles Rouges massifs. On the contrary, very few displacements are recorded along the other cross sections. Thus, the displacement field is highly discontinuous. Either there is a large transfer fault between the Belledonne massif and the Aiguilles Rouges-Mont Blanc massifs, or the northern Belledonne massif suffered clockwise rotation. We have arbitrarily rotated back the northern Belledonne massif (in red) of about  $10^\circ$  clockwise. However, this may be less or much more. In any case, a rotation ( $5^\circ$  clockwise) is recorded between the Vercors-Oisans and the Chartreuse-Belledonne sections, as the shortening corresponding to the Jura phase is about 2 km for the Chartreuse-Grandes Rousses and the Chartreuse-Belledonne sections. Note that along the Chartreuse-Belledonne section, a shortening slightly higher than 2 km has been taken into account, as a shortening of 2 km would have implied much internal deformation in the ECM. (b) Displacement field of ECM for the subalpine phase. The displacement increases from south to north and witnesses a clockwise rotation of the ECM at the Alpine arc scale. At the massif scale, the south Belledonne massif suffered a clockwise rotation of about  $5^\circ$ . (c) Displacement field during the ECM shortening phase. During this phase, the shortening consists of internal deformation of the ECM. Thus, we cannot simply rigidly move them. However, as their extent represented on the map is their present-day outcrop, we decided not to change their size. We rather decided to assign to the eastern border of each massif the shortening recorded in this massif. Thus, at this step, the "external circle" (west of the thick line) represents the position of a point along the internal border of the ECM, and the "internal circle" (east of the thick line) represents its position before the ECM shortening.

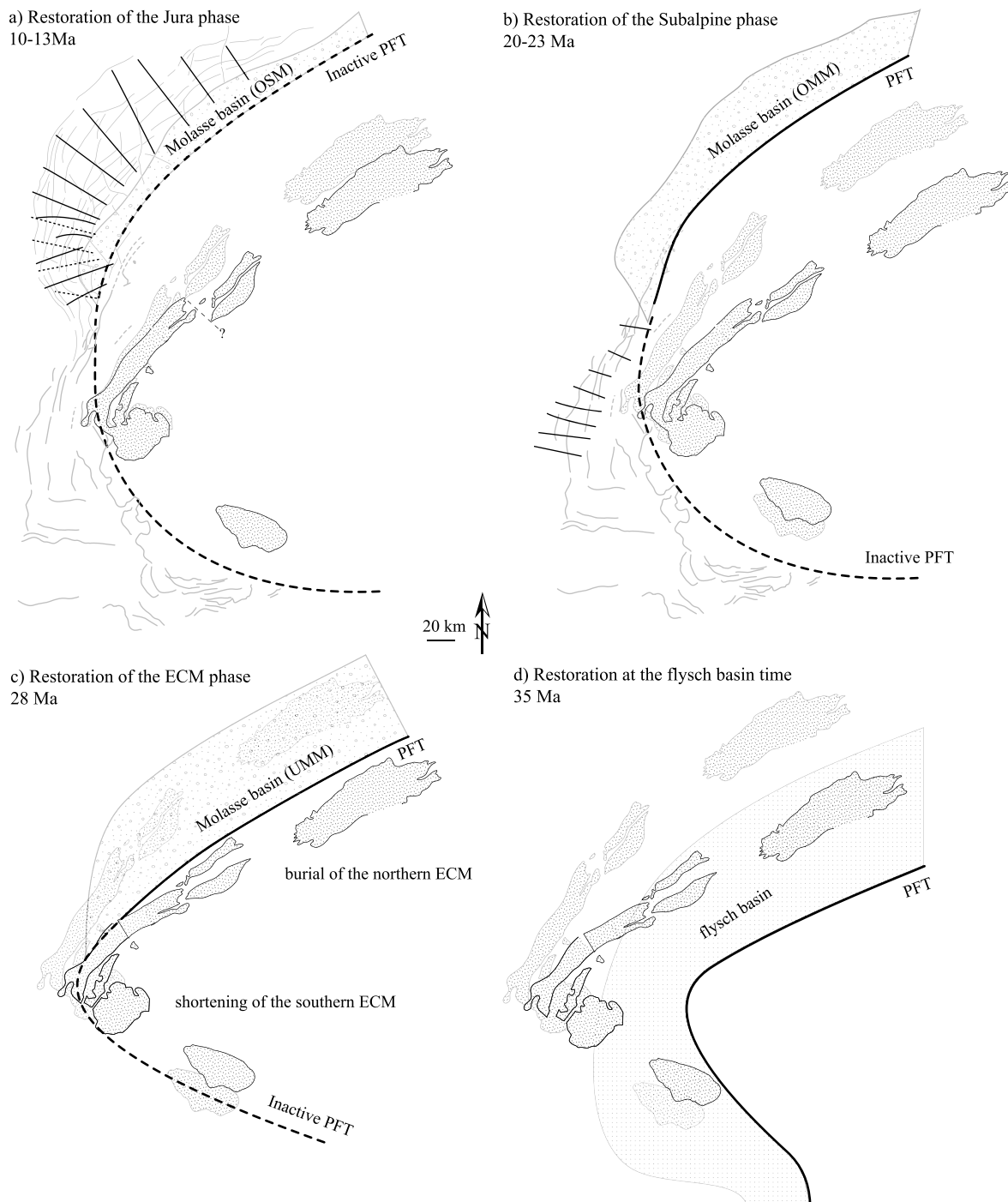


**Figure 16.** Palinspastic reconstructions at different times. The position of the ECMs derives from the restoration presented in Figure 15 based on the cross sections (Figures 3–7). The position of the basins is from Ford *et al.* [2006] and the cross sections presented in this contribution. (a) Restoration at 10–13 Ma, before the Jura phase. The PFT was inactive during this phase; freshwater clastics deposited (OSM). The straight lines represent the maximum compressive stress in the Jura belt and the dashed lines a late orientation [Homberg *et al.*, 1999]: where only straight lines are represented, the orientation did not change through time. (b) Restoration at around 20 Ma, before the subalpine phase. The northern PFT has been inactive since around 20–25 Ma (onset of the ECM shortening), while the southern part was inactive earlier. Shallow marine clastics deposited (OMM) in the NAFB. The straight lines indicate the maximum compressive stress [Philippe *et al.*, 1998]. (c) Restoration at around 28 Ma. The southern ECMs were already shortening; the southern part of the PFT was inactive. The area where the PFT switched from active to inactive is probably around the same area where the NAFB shallow marine to freshwater clastics laterally end. In the north, the PFT (and the southern limit of the shallow marine to freshwater clastic basin) was located north of the Aiguilles Rouges and Aar massifs as there are no clastics on their cover. (d) Restoration at around 35 Ma, before the shortening of the external zone and during the deepwater turbidites deposition. The northern limit of the turbiditic basin is located north of the Aiguilles Rouges and Aar massifs as their cover presents deepwater turbidite formation. On the contrary, the western limit of the turbiditic basin was probably located east of the Belledonne and Grandes Rousses massifs as no turbidites crops out.

rates in the north. In other words, the exhumation is much more localized in space in the north than in the south.

The Oligo-Miocene collisional kinematics thus varies from south to north along the Alpine arc. Does this along-strike variation of shortening kinematics explain the along-strike variation of the molassic foreland basin dynamics? This basin is well developed, large, and thick in the north (NAFB), while it is very restricted in the south (west of the Oisans) to localized basins [e.g., *Ford and Lickorish, 2004*]. This may be explained by the distributed shortening in the Oisans-Grandes Rousses-Belledonne massifs that almost doubled the orogen width. Such a large orogenic wedge may have prevented the formation of a thick molassic basin.

The localized exhumation of the ECM in the north also explains the preservation of the Préalpes klippen, while no traces of internal units are found in the south as a consequence of the distributed and rather uniform uplift of the ECM and associated erosion of the internal units.

#### 4.4. Palinspastic Tertiary Restorations

The sequence of shortening described above provides a unique opportunity to produce precise palinspastic maps of the Western Alps at different times. Figure 15 shows the way the amount of shortening has been restored for each phase: before the Jura shortening phase (middle to late Miocene, Figure 16a), before the subalpine phase (early Miocene, Figure 16b), before or during the ECM shortening phase (Oligocene, Figure 16c), and during the flysch deposition (Late Eocene, Figure 16d), which is the precollisional stage.

For each step, the position of the ECM is restored according to the sequence and amount of shortening calculated from the cross sections. The sections have been drawn parallel to the local Alpine shortening direction [*Malavieille et al., 1984*]: E-W for the Oisans massif [*Bellanger et al., 2014*], and NW-SE for the northern Belledonne massif [*Marquer et al., 2006*], the Mont Blanc massif [*Gourlay, 1986; Leloup et al., 2005*], and the Aar massif [*Ramsay and Huber, 1989*]. Thus, the restoration can be performed parallel to the section. For the southern section only, the shortening in the subalpine chain (WNW-ESE [*Philippe et al., 1998*]) is slightly oblique to the section (E-W). This has been taken into account for the palinspastic restoration (Figure 15b).

Figure 16a is the restoration before the Jura shortening phase, at about 10–15 Ma. On this map, one can observe displacement fields and the position of the ECM that vary quite strongly along strike. Indeed, the Jura shortening is strongly not cylindrical at the Alpine arc scale. This phase did not affect the crust at the Oisans latitude; it is responsible for several kilometers of amount of shortening along the Chartreuse-Grandes Rousses (CGR) and Chartreuse-Belledonne (CB) sections (Figure 15a, which implies a rotation of about 5° clockwise of the SW Belledonne massif) while there is a large shortening along the Préalpes-Mont Blanc (PMB) and the Préalpes-Aar (PA) sections. Similar variations were already noticed by *Affolter et al. [2008]*. On our map, it is noteworthy that a strong variation most likely occurs between the Bornes-Mont Blanc and the Chartreuse-Belledonne sections. Thus, we arbitrarily affected the northern Belledonne massif of a 10° clockwise rotation (Figure 15a) that adds to the rotation induced by the increase of Jura shortening from the Vercors-Oisans section to the Chartreuse-Belledonne one. If no large rotation occurred as suggested in *Heller et al. [1989]*, a transfer fault might have been active between the Belledonne and the Mont Blanc massifs (Figure 15a), which is not described in the literature. The (future) thrusts of the Jura belt are represented in Figure 16a, as well as the trend of the maximum compressive principal stress from *Homberg et al. [1999]*. One may observe that the early stress field strongly correlates with our displacement field: the along-strike change of the early compression orientation recorded in the Jura (from NW-SE in the central part to WSW-ENE in the southern part, straight lines, Figure 16a) fits well the shift in our displacement field. Thus, the Aiguilles Rouges and Mont Blanc massifs may have played the role of indenter for the Jura belt. At this time, the Penninic Frontal Thrust (PFT) is inactive as a thrust as all ECM have already started to exhume.

Figure 16b is the restoration before the subalpine phase, at about 20 Ma. The ECMs are restored taking into account the shortening accommodated by the frontal ramps and the subalpine belt. As this shortening increases northward less drastically than for the Jura phase, the displacement pattern shows a more regular rotation with a pole located SW of the Oisans massif (Figure 16b). As a result of this shortening phase, the subalpine belt is activated with the compression trend reported in Figure 16b from *Philippe et al. [1998]*. The PFT became inactive at about 20–25 Ma in the north due to the shortening and exhumation of the ECM [*Leloup et al., 2005; Rolland et al., 2008, 2009; Challandes et al., 2008*], while it was probably already inactive at

this time in the south as the ECM exhumation started at least at 27 Ma [*van der Beek et al.*, 2010]. It is noteworthy that this sequence of deformation correlates well with the fact that the molassic basin is much more developed in the north [e.g., *Sinclair*, 1997; *Ford et al.*, 2006, and references therein].

Figure 16c is the restoration at 28 Ma. In the south, only part of the shortening of the ECMs has been restored as some shortening has occurred earlier in the Oisans massif [*Simon-Labrec et al.*, 2009]. A clockwise rotation of the northern part of the Belledonne massif is implied by our data, especially the shortening along the Chartreuse-Belledonne section. The PFT is most likely active everywhere but gets inactive in the south at about this time (see above).

Figure 16d is the restoration at 35 Ma during the deepwater turbidites deposition. The position of the PFT is quite uncertain but might have been located south of the Aar massif and east of the Oisans massif. It controls the deposition of a large turbiditic flysch-type basin all around the Alpine arc.

During the whole period considered above (from late Eocene to Pliocene), the movement along the PFT also accommodated convergence: from about 110 km in the south to about 200 km in the north (Figure 16). These values added to the shortening estimates from the cross sections (Table 1) provide the following convergence values since 35 Ma for the external zone: around 270 km of convergence for the northern part of the studied area (Mont Bland and Aar massifs) and around 140 km for the southern part (Oisans massif). This variation in convergence along strike the Alpine arc witnesses the rotation of Adria relatively to Europe [*Ustaszewski et al.*, 2008; *Handy et al.*, 2010, and references therein], which is recorded in many ECMs [e.g., *Rolland et al.*, 2008, 2009, 2012]. This rotation may be due to the push of the African plate coupled to the slab rollbacks (especially in western Mediterranean [e.g., *Dewey et al.*, 1989; *Jolivet and Faccenna*, 2000; *Faccenna et al.*, 2004]). Now the questions are as follows: what is the structure of the European margins inherited from Mesozoic times and whether or not they might play a role in the Adria Tertiary rotation?

#### 4.5. Restored Mesozoic Margins

Our reconstruction at 35 Ma provides constraints on the geometry of the European margin in the external zone as no significant collisional deformation occurred before this age, at least north of the Oisans massif where no Pyrenean shortening is described. We assume that a complete crustal breakup occurred in the Valais domain in Western Alps at least around and northeast of the Petit Saint Bernard pass [*Loprieno et al.*, 2010; *Beltrando et al.*, 2012]. There, mantle exhumation occurred with no significant mafic magmatism [*Beltrando et al.*, 2007; *Masson et al.*, 2008]. Thus, there was probably no oceanic crust, although it is still proposed by many authors [see *Handy et al.*, 2010, and references therein].

Moreover, there is no evidence for oceanic spreading west of the Briançonnais domain from the Pyrenees to the Western Alps; there is no metamorphic unit attesting for oceanic subduction, except for the Ligurian one: there is no evidence of HP/LT metamorphism of the Dauphinois margin that would have been due to significant slab pull of an ocean between the Dauphinois and the Briançonnais.

In the Pyrenees, a rifting event is recorded during Albo-Cenomanian times. In southeast France [*Homberg et al.*, 2013, and references therein], a polyphase extensional event is recorded between upper Tithonian and Aptian times. This duration fits particularly well the timing of the Valaisan rifting, if it is Early Cretaceous in age [*Schwizer*, 1984; *Steinmann*, 1994; in *Handy et al.*, 2010; see also *Loprieno et al.*, 2010] but significantly postdates the middle Jurassic Valais rifting according to *Manatschal et al.* [2006], *Mohn et al.* [2010], and *Beltrando et al.* [2012].

Thus, the Pyrenees and southeast France basins may be considered as the rifted transition zone between the Bay of Biscay and the Valais domain. (1) During the Liassic and Dogger times, the Ligurian rifting occurred [*Lemoine et al.*, 1986] as well as possibly the Valais rifting [*Manatschal et al.*, 2006]. (2) The Ligurian ocean started to open during upper Jurassic times. Meanwhile, continental extension continued in southeast France basin [*Homberg et al.*, 2013], possibly in the future Bay of Biscay [*Jammes et al.*, 2009], in the internal Alps (e.g., in the Ligurian Briançonnais [*Bertok et al.*, 2011]), and in the future external Alps: indeed several normal faults active during the upper Jurassic (Figures 3 and 4). The direction of extension may have been similar to the one prevailing during the Ligurian rifting in a strict sense (NW-SE [e.g., *Homberg et al.*, 2013]). (3) During the early Cretaceous, rifting continued in southeast France [*Homberg et al.*, 2013, and references therein] and Pyrenees [*Jammes et al.*, 2009, and references therein] with a possibly N-S direction of extension. Spreading occurred in the Bay of Biscay [Aptian, e.g., *Sibuet et al.*, 2004] and possibly in the east (Aptian times [*Handy et al.*,

2010, and references therein]). The mantle was exhumed during hyperextension during Albo-Cenomanian times in the Pyrenees [e.g., *Jammes et al.*, 2009] and possibly during early Cretaceous in the Valais domain [*Loprieno et al.*, 2010]. In the internal Alps, active normal faults are also reported (external Briançonnais [*Bertok et al.*, 2012]), and in the external Alps, early Cretaceous faults are clearly observed and reported in cross sections (Figures 4 and 7): In the Chartreuse-Grandes Rousses section (Figure 4), *Deville et al.* [1994] showed a strong variation in Mesozoic layer thickness (especially Cretaceous). In the Mont Blanc section (Figure 7), the Chamonix inherited normal fault controlled both Jurassic and Cretaceous depocenters [*Burkhard and Sommaruga*, 1998]. In the Vercors-Oisans section (Figure 3), there might have been a Cretaceous basin in the Grenoble basin, although the complete Mesozoic section lacks above the Belledonne massif. Some of these faults, as well as all the other Mesozoic faults, have similar orientation (NE-SW) as other Mesozoic faults, such as the Cévennes fault system, and were most likely reactivated structures inherited from Variscan times.

In any case, and whatever the age of the Valais domain (middle to late Jurassic or/and early Cretaceous), there must be a transition between an eastern Valais domain with oceanic crust and/or only exhumed mantle and a western rifted domain in southeast France. In other words, one may find a place, between Western and Central Eastern Alps, where the margin evolved through space from hyperextended margin (with mantle exhumation) and/or oceanized domain to a rifted domain with thinned continental crust [e.g., *Mohn et al.*, 2010]. Such setting has been represented in Figure 17. In the following, we discuss the inversion of such margins and their possible effect on the collision kinematics.

First, it is most likely that the increase in amount of (collisional) shortening and total convergence from south to north is not counterbalanced by a northward decrease of (collisional) shortening in the internal units. Such shortening is very difficult to constrain due to the lack of clear passive markers. However, the examination of the geological maps does not suggest that the shortening in the southern internal units is 2 or 3 times greater than in the northern ones. This is consistent with the fact that in the north, the shortening started later than in the south (22 Ma in the Aar Massif [*Rolland et al.*, 2009], 30 Ma in the Mont Blanc massif [*Cenki-Tok et al.*, 2013], and 31–34 Ma in the Oisans massif [*Simon-Labréte et al.*, 2009]): the Mesozoic basins between the external Dauphinois and the Briançonnais may have been wider in the north than in the south.

The northward increase of the amount of convergence (including shortening) may thus have been controlled by the basin size and the plate kinematics. Indeed, it is suggested that the Adria motion relative to stable Europe turned from N-S to NW-SE [*Schmid et al.*, 1996] or from NW-SE to almost E-W [*Capitanio and Goes*, 2006] at around 35 Ma or slightly later [see also *Dumont et al.*, 2011, 2012, and references therein]. Given these uncertainties, it is uneasy to discuss the effect of convergence obliquity on along-strike shortening gradient, although it might have an effect. However, such control cannot explain the shortening style differences: indeed the distribution of shortening and exhumation strongly vary from north to south. We here propose that it is, at least in part, controlled by the inherited margin structure.

The southern (Oisans) part of the European margin collided during early Oligocene times. The crust was not buried to more than 10 km depth, and the shortening started along with a coeval or slightly later exhumation. The northern (Mont Blanc, Aar) part of the margin started to shorten (slightly) later but also after a burial twice as large as in the south. This had several consequences that we detail in the next paragraph. But first, we suggest that this may be a direct consequence of the margin structure: in the south, no mantle exhumation occurred between the buoyant Dauphinois and the Briançonnais. Thus, in the absence of negative buoyancy due to oceanic lithosphere or distal hyperextended margin (with no or little crust left), the Dauphinois margin did not subduct significantly and collisional shortening occurred fast after burial, which slowed down the convergence even more. In the north, where the transition between aborted rift and oceanic basin took place (maybe in Central Alps, western Switzerland), the slab pull may have been more important, driving the margin further down, at about 20 km depth. In agreement with increased subduction/underthrusting, a deeper burial in the north may also reflect initially higher crustal strength of the foreland basement, e.g., due to mineralic composition or variable thermotectonic preorogenic history (see *Moutheau et al.* [2013] for a general discussion).

Such different burial had several consequences. The pressure peak of collisional deformations in Central Alps is about 5 kb. At corresponding depth (20 km), the crust, which may have been originally stronger than southward becomes very weak and ductile during underthrusting (Figure 11d). As a consequence, the basement deformation did not propagate very “fast”/far toward the external area, but deformation in the cover did. A stack of underplated units emplaced leading to an antiformal stack geometry. The exhumation

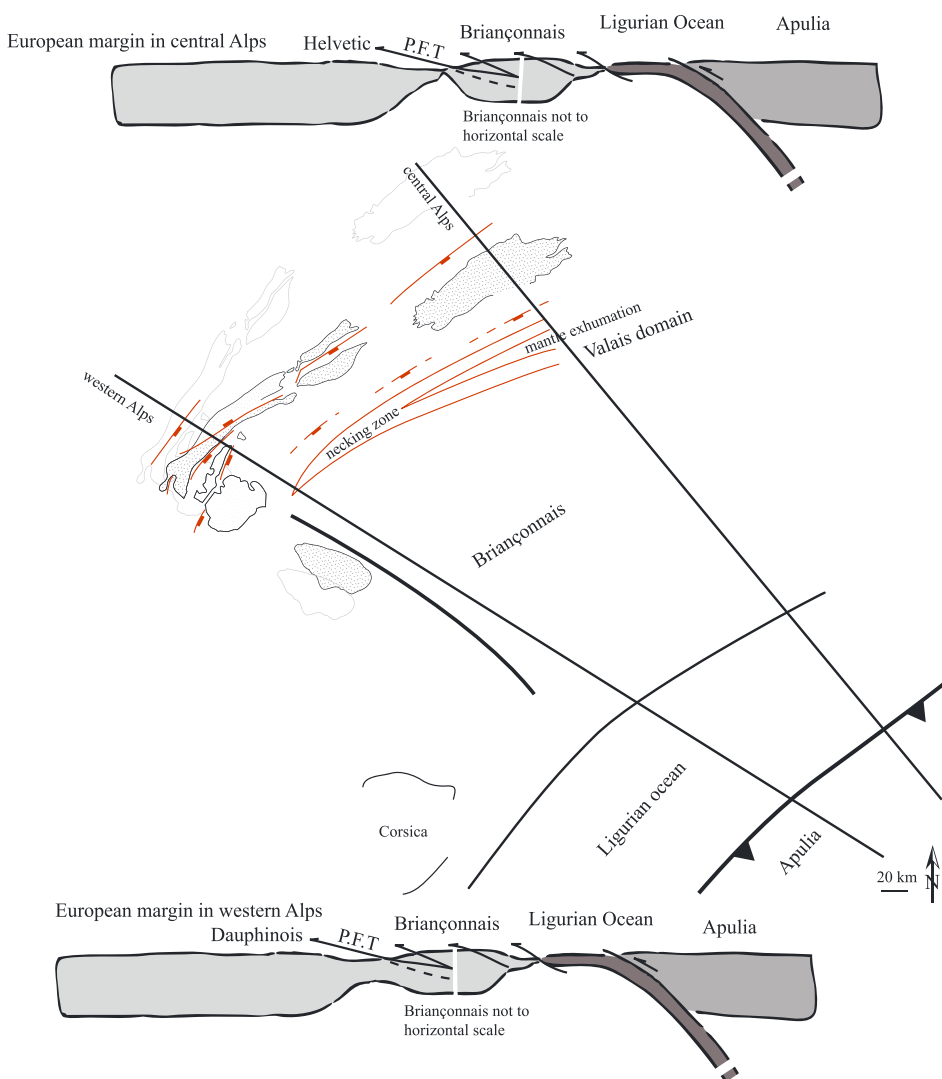


**Figure 17.** European margin geometry at Mesozoic times (upper Cretaceous). On the palinspastic map, the ECMs are represented in their present-day position (in gray) and in their Cretaceous position (in black). The Mesozoic normal faults have been drawn according to their restored position. The Valais domain terminated westward with a possible large domain in the east (with exhumed mantle?) and a smaller one in the west (rifted domain). Two simplified crustal cross sections of the future Central Alps and Western Alps are presented. The eastern Helvetic domain is much more thinned than the eastern Dauphinois domain.

occurred in a narrow zone, which explains the high exhumation rates. To the south, in Western Alps, the crust burial is about 10 km (Figure 11c), and therefore the crust remained at the brittle-ductile transition. With respect to the north, the basement hence appears relatively stronger. Overall, the thick-skinned deformation dominates and deformation propagates by frontal accretion of basement units; as a consequence, the exhumation is more distributed. We show that the tectonic burial played a key role in modifying the initial crustal rheology. This study complements earlier inferences from global analysis of shortening in thrust belts [Moullereau *et al.*, 2013] and from numerical modeling [e.g., Jamme and Huisman, 2012] showing that in the absence of any tectonic burial an inherently weak crust like the European crust rather implies a distribution of the deformation and a large orogenic wedge.

## 5. Conclusions

Five balanced cross sections of the whole external zone of the Western Alps provide constraints on the space and time variations of both the amount and the sequence of shortening. Three phases and five units are recognized and are consistent at the scale of the external Western Alps. (1) The “ECM phase” is characterized

by Oligo-Miocene distributed shortening of the ECMs (from Oisans to Aar massifs) and their disharmonically folded cover. Only two tectonic units are detached from their basement: the ultra-Helvetic/Dauphinois units that are present from NE Oisans to around the Aar massif and a unit, called "Aravis-Granier" unit, that corresponds to the upper western ECM cover (Belledonne and Aiguilles Rouges). The latter unit does not extend along strike northeast of the Aiguilles Rouges and SW of Belledonne. (2) The "subalpine phase" is characterized by displacement along basement thrust ramps below the ECMs that transfer deformation up section in a décollement in the Dauphinois cover base responsible for the shortening of the subalpine belts (Vercors, Chartreuse, Bauges, and Bornes massifs) during Middle Miocene times. (3) The "Jura phase" is characterized by basement thrusts below the ECMs that activated a décollement NW of the North Alpine Foreland Basin during upper Miocene to lower Pliocene times.

The amount of crustal shortening determined from the cross sections during each of these phases increases from south (Oisans, total amount of shortening: 28 km) to north (Mont Blanc and Aar, total amount of shortening: 65.9 km or more). The corresponding shortening rates are 2 or 3 times higher in the north than in the south. Similarly, the exhumation rates (from thermochronology and thermobarometry data from the literature) are 2 or 3 times higher in the north (Mont Blanc, Aar) than in the south (Oisans). This relationship is due to shortening by underplating and then localized exhumation in the northern ECM. This shortening distribution probably influenced the North Alpine Foreland Basin that laterally decreased in size southward (toward the Oisans area) where the shortening is more distributed.

The variable localization of the shortening in the Alpine external zone can be explained by the along-strike variations of the inherited margin structure. From the Central Alps to Western Alps, the possible westward decrease of the size of the Valais domain, along with a decrease of the amount of thinning of its margins, may have induced the following consequences: toward the north, where the Valais domain was highly thinned, both the large domain width and the negative buoyancy of its lithosphere ensured a deep burial of the Helvetic margin (down to at least 20 km, Aar and Mont Blanc massifs) strongly reducing the initial crustal strength. Toward the south, where the Valais domain ended and was replaced by the Dauphinois aborted rift, the small width of the basin and its buoyant crust inhibited deep burial (to about 10 km) along with less drastic decrease of the initial crustal strength. As a consequence, in the north the crust was underthrusted, promoting crustal weakening, then underplated with more pronounced shortening of the basement. To the south, the basement was less buried. Hence, the deformation follows characteristic structural style of thick-skinned belt characterized by basement frontal accretion, typical young margins.

#### Acknowledgments

This work was funded by the Syster program 2010–2011 (INSU-CNRS) and the BRGM contract L10 U 044. This work benefited from discussions with L. Labrousse, C. Rosenberg, A. Verlaguet, L. Bayet, and T. Baudin. We thank F. Roure and M. Beltrando for very constructive reviews.

#### References

- Affolter, T., J.-L. Faure, J.-P. Gratier, and B. Colletta (2008), Kinematic models of deformation at the front of the Alps: New data from map-view restoration, *Swiss J. Geosci.*, 101(2), 289–303, doi:10.1007/s00015-008-1263-3.
- Agard, P., P. Monié, L. Jolivet, and B. Goffé (2002), Exhumation of the Schistes Lustrés complex: In situ laser probe  $^{40}\text{Ar}/^{39}\text{Ar}$  constraints and implications for the Western Alps, *J. Metamorph. Geol.*, 20(6), 599–618, doi:10.1046/j.1525-1314.2002.00391.x.
- Arnaud, H. (1975), *Carte Géologique de la France à 1/50 000: Romand sur Isère (feuille 795)*, BRGM, Orléans.
- Bauve, V., R. Plateaux, Y. Rolland, G. Sanchez, N. Béthoux, B. Delouis, and R. Darnault (2014), Long-lasting transcurrent tectonics in SW Alps evidenced by Neogene to present-day stress fields, *Tectonophysics*, doi:10.1016/j.tecto.2014.02.006.
- Becker, A. (2000), The Jura Mountains—An active foreland fold-and-thrust belt?, *Tectonophysics*, 321, 381–406.
- Bellahsen, N., L. Jolivet, O. Lacombe, M. Bellanger, A. Boutoux, S. Garcia, F. Moutherau, L. Le Pourhet, and C. Gumiaux (2012), Mechanisms of margin inversion in the external Western Alps: Implications for crustal rheology, *Tectonophysics*, 560–561, 62–83, doi:10.1016/j.tecto.2012.06.022.
- Bellanger, M., N. Bellahsen, L. Jolivet, T. Baudin, R. Augier, and A. Boutoux (2014), Basement shear zones development and shortening kinematics in the Ecrins Massif, Western Alps: Shortening in the Ecrins Massif, *Tectonics*, 33, 84–111, doi:10.1002/2013TC003294.
- Beltrando, M., D. Rubatto, R. Compagnoni, and G. Lister (2007), Was the Valaisian basin floored by oceanic crust? Evidence of Permian magmatism in the Versoyen Unit (Valaisian domain, NW Alps), *Ophioliti*, 32(2), 85–99.
- Beltrando, M., G. Frasca, R. Compagnoni, and A. Vitale-Brovarone (2012), The Valaisian controversy revisited: Multi-stage folding of a Mesozoic hyper-extended margin in the Petit St. Bernard pass area (Western Alps), *Tectonophysics*, 579, 17–36, doi:10.1016/j.tecto.2012.02.010.
- Bergerat, F., J. L. Mugnier, S. Guellac, C. Truffert, M. Cazes, B. Damotte, and F. Roure (1990), Extensional tectonics and subsidence of the Bresse basin: An interpretation from ECORS data, *Mém. Soc. Géol. France*, 156, 145–156.
- Bertok, C., L. Martire, E. Perotti, A. d'Atri, and F. Piana (2011), Middle-Late Jurassic syndepositional tectonics recorded in the Ligurian Briançonnais succession (Marguareis–Mongoie area, Ligurian Alps, NW Italy), *Swiss J. Geosci.*, 104(2), 237–255, doi:10.1007/s00015-011-0058-0.
- Bertok, C., L. Martire, E. Perotti, A. d'Atri, and F. Piana (2012), Kilometre-scale palaeoescarpments as evidence for Cretaceous synsedimentary tectonics in the External Briançonnais omain (Ligurian Alps, Italy), *Sediment. Geol.*, 251–252, 58–75.
- Bolliger, T., B. Engesser, and M. Weidmann (1993), Première découverte de mammifères pliocènes dans le Jura neuchâtelois, *Elogae Geol. Helv.*, 86, 1031–1068.
- Bonnet, C., J. Malavieille, and J. Mosar (2007), Interactions between tectonics, erosion, and sedimentation during the recent evolution of the Alpine orogen: Analogue modeling insights, *Tectonics*, 26, TC6016, doi:10.1029/2006TC002048.

- Bousquet, R., B. Goffé, O. Vidal, R. Oberhänsli, and M. Patriat (2002), The tectono-metamorphic history of the Valaisan domain from the Western to the Central Alps: New constraints on the evolution of the Alps, *Geol. Soc. Am. Bull.*, 114(2), 207–225.
- Boutoux, A., N. Bellahsen, O. Lacombe, A. Verlaguet, and F. Mouthereau (2014), Inversion of pre-orogenic extensional basins in the external Western Alps: Structure, microstructures and restoration, *J. Struct. Geol.*, 60, 13–29, doi:10.1016/j.jsg.2013.12.014.
- Burkhard, M. (1988), L'Helvétique de la bordure occidentale du massif de l'Aar (évolution tectonique et métamorphique), *Eclogae Geol. Helv.*, 81, 63–114.
- Burkhard, M., and A. Sommaruga (1998), Evolution of the western Swiss Molasse basin: Structural relations with the Alps and the Jura belt, *Geol. Soc. London Spec. Publ.*, 134(1), 279–298, doi:10.1144/GSL.SP.1998.134.01.13.
- Capitanio, F. A., and S. Goes (2006), Mesozoic spreading kinematics: Consequences for Cenozoic Central and Western Mediterranean subduction, *Geophys. J. Int.*, 165(3), 804–816, doi:10.1111/j.1365-246X.2006.02892.x.
- Carpena, J. (1992), Fission track dating of zircon: Zircons from Mont Blanc granite (French-Italian Alps), *J. Geol.*, 100, 411–421.
- Cenki-Tok, B., J. R. Darling, Y. Rolland, B. Dhuime, and C. D. Storey (2013), Direct dating of mid-crustal shear zones with synkinematic allanite: New in situ U-Th-Pb geochronological approaches applied to the Mont Blanc massif, *Terra Nova*, 26, 29–37, doi:10.1111/ter.12066.
- Ceriani, S., and S. M. Schmid (2004), From N-S collision to WNW-directed post-collisional thrusting and folding: Structural study of the frontal Penninic units in Savoie (Western Alps, France), *Eclogae Geol. Helv.*, 97, 347–369.
- Ceriani, S., B. Fugenschuh, and S. M. Schmid (2001), Multi-stage thrusting at the "Penninic Front" in the Western Alps between Mont Blanc and Pelvoux massifs, *Int. J. Earth Sci.*, 90, 685–702.
- Challandes, N., D. Marquer, and I. M. Villa (2008), P-T-t modelling, fluid circulation, and  $^{39}\text{Ar}$ - $^{40}\text{Ar}$  and Rb-Sr mica ages in the Aar Massif shear zones (Swiss Alps), *Swiss J. Geosci.*, 101(2), 269–288, doi:10.1007/s00015-008-1260-6.
- Cochran, J. R., and F. Martinez (1988), Evidence from the northern Red Sea on the transition from continental to oceanic rifting, *Tectonophysics*, 153, 25–53.
- Corsini, M., G. Ruffet, and R. Caby (2004), Alpine and late-hercynian geochronological constraints in the Argentera Massif (Western Alps), *Eclogae Geol. Helv.*, 97(1), 3–15, doi:10.1007/s00015-004-1107-8.
- Crespo-Blanc, A., H. Masson, Z. Sharp, M. Cosca, and J. Hunziker (1995), A stable and  $^{40}\text{Ar}/^{39}\text{Ar}$  isotope study of a major thrust in the Helvetic nappes (Swiss Alps): Evidence for fluid flow and constraints on nappe kinematics, *Geol. Soc. Am. Bull.*, 107(10), 1129–1144.
- Crouzet, C., G. Ménard, and P. Rochette (2001), Cooling history of the Dauphinoise zone (Western Alps, France) deduced from the thermo-paleomagnetic record: Geodynamic implications, *Tectonophysics*, 340(1), 79–93.
- Deville, É., and A. Chauvière (2000), Thrust tectonics at the front of the Western Alps: Constraints provided by the processing of seismic reflection data along the Chambéry transect, *C.R. Acad. Sci.*, 331(11), 725–732.
- Deville, É., A. Mascle, C. Lamiriaux, and A. Le Bras (1994), Tectonic styles, reevaluation of plays in southeastern France, *Oil Gas J.*, 31, 53–58.
- Dewey, J. F., M. L. Helman, S. D. Knott, E. Turco, and D. H. W. Hutton (1989), Kinematics of the western Mediterranean, in *Alpine Tectonics*, *Geol. Soc. London Spec. Publ.*, vol. 45, edited by M. P. Coward, D. Dietrich, and R. G. Parker, pp. 265–283.
- Doudoux, B., B. M. de Lepinay, and M. Tardy (1982), Une interprétation nouvelle de la structure des massifs subalpins savoyards (Alpes Occidentales): Nappes de charriage Oligocènes et déformations superposées, *C.R. Acad. Sci.*, 295, 63–68.
- Duchene, S., J. Blachert-Toft, B. Luais, P. Télouk, J.-M. Lardeaux, and F. Albarede (1997), The Lu-Hf dating of garnets and the ages of the Alpine high-pressuremetamorphism, *Nature*, 387, 586–589.
- Dumont, T., J. D. Champagnac, C. Crouzet, and P. Rochat (2008), Multistage shortening in the Dauphine zone (French Alps): The record of Alpine collision and implications for pre-Alpine restoration, *Swiss J. Geosci.*, 101, 89–S110, doi:10.1007/s00015-008-1280-2.
- Dumont, T., T. Simon-Labric, C. Authemayou, and T. Heymes (2011), Lateral termination of the north-directed Alpine orogeny and onset of westward escape in the Western Alpine arc: Structural and sedimentary evidence from the external zone, *Tectonics*, 30, TC5006, doi:10.1029/2010TC002836.
- Dumont, T., S. Schwartz, S. Guillot, T. Simon-Labric, P. Tricart, and S. Jourdan (2012), Structural and sedimentary records of the Oligocene revolution in the Western Alpine arc, *J. Geodyn.*, 56, 18–38.
- Epard, J.-L. (1990), La nappe de Morcles au sud-ouest du Mont Blanc, *Mém. Géol. Lausanne* 3.
- Epard, J.-L., and A. Escher (1996), Transition from basement to cover: A geometric model, *J. Struct. Geol.*, 18(5), 533–548.
- Escher, A., H. Masson, and A. Steck (1993), Nappe geometry in the Western Swiss Alps, *J. Struct. Geol.*, 15(3–5), 501–509.
- Faccenna, C., C. Piromallo, A. Crespo-Blanc, L. Jolivet, and F. Rossetti (2004), Lateral slab deformation and the origin of the western Mediterranean arcs, *Tectonics*, 23, TC1012, doi:10.1029/2002TC001488.
- Fillon, C., R. Huismans, and P. van der Beek (2013), Syntectonic sedimentation effects on the growth of fold-and-thrust belts, *Geology*, 41, 83–86.
- Ford, M. (1996), Kinematics and geometry of early Alpine, basement-involved folds, SW Pelvoux massif, SE France, *Eclogae Geol. Helv.*, 89, 269–295.
- Ford, M., and W. H. Lickorish (2004), Foreland basin evolution around the western Alpine Arc, in *Deep-Water Sedimentation in the Alpine Basin of SE France: New Perspectives on the Gres d'Annot and Related Systems*, *Geol. Soc. London Spec. Publ.*, vol. 221, edited by P. Joseph and S. A. Lomas, pp. 39–63.
- Ford, M., W. H. Lickorish, and N. J. Kusznir (1999), Tertiary foreland sedimentation in the Southern Subalpine Chains, SE France: A geodynamic appraisal, *Basi Res.*, 11, 315–336.
- Ford, M., S. Duchene, D. Gasquet, and O. Vanderhaeghe (2006), Two-phase orogenic convergence in the external and internal SW Alps, *J. Geol. Soc. London*, 163, 815–826, doi:10.1144/0016-76492005-034.
- Fry, N. (1989), Southwestward thrusting and tectonics of the Western Alps, *Geol. Soc. London Spec. Publ.*, 45, 83–109.
- Gourlay, P. (1986), La déformation du socle et des couvertures delphino-helvétiques dans la région du Mont-Blanc (Alpes occidentales), *Bull. Soc. Géol. Fr.*, 2, 159–169.
- Guellec, S., J.-L. Mugnier, M. Tardy, and F. Roure (1990), Neogene evolution of the western Alpine foreland in the light of ECORS data and balanced cross-section, *Mém. Soc. Géol. Fr.*, 156, 165–184.
- Handy, M. R., S. M. Schmid, R. Bousquet, E. Kissling, and D. Bernoulli (2010), Reconciling plate-tectonic reconstructions of Alpine Tethys with the geological-geophysical record of spreading and subduction in the Alps, *Earth Sci. Rev.*, 102(3–4), 121–158, doi:10.1016/j.earscirev.2010.06.002.
- Heim, A. (1921), *Geologie der Schweiz*, vol. 2/1, pp. 259–476, Tauchnitz, Leipzig.
- Heller, F., W. Lowrie, and A. M. Hirt (1989), A review of palaeomagnetic and magnetic anisotropy results from the Alps, *Geol. Soc. London Spec. Publ.*, 45(1), 399–420, doi:10.1144/GSL.SP.1989.045.01.22.
- Hofmann, B. A., M. Helfer, L. W. Diamond, I. M. Villa, R. Frei, and J. Eikenberg (2004), Topography-driven hydrothermal breccia mineralization of Pliocene age at Grimsel Pass, Aar massif, Central Swiss Alps, *Schweiz. Mineral. Petrogr. Mitt.*, 84(3), 271–302.
- Homberg, C., O. Lacombe, J. Angelier, and F. Bergerat (1999), New constraints for indentation mechanisms in arcuate belts from the Jura Mountains, France, *Geology*, 27(9), 827–830.

- Homberg, C., Y. Schnyder, and M. Benzaggagh (2013), Late Jurassic-Early Cretaceous faulting in the Southeastern French basin: Does it reflect a tectonic reorganization?, *Bull. Soc. Geol. Fr.*, 184, 501–514.
- Huon, S., M. Burkhard, and J.-C. Hunziker (1994), Mineralogical, K-Ar, stable and Sr isotope systematics of K-white micas during very low-grade metamorphism of limestones (Helvetic nappes, western Switzerland), *Chem. Geol.*, 113(3), 347–376.
- Jammes, S., and R. S. Huismans (2012), Structural styles of mountain building: Controls of lithospheric rheologic stratification and extensional inheritance, *J. Geophys. Res.*, 117, B10403, doi:10.1029/2012JB009376.
- Jammes, S., G. Manatschal, L. Lavier, and E. Masini (2009), Tectonosedimentary evolution related to extreme crustal thinning ahead of a propagating ocean: Example of the western Pyrenees, *Tectonics*, 28, TC4012, doi:10.1029/2008TC002406.
- Jolivet, L., and C. Faccenna (2000), Mediterranean extension and the Africa-Eurasia collision, *Tectonics*, 19(6), 1095–1106, doi:10.1029/2000TC900018.
- Jullien, M., and B. Goffé (1993), Cookeite and pyrophyllite in the Dauphinois black shales (Isère, France): Implications for the conditions of metamorphism in the Alpine external zones, *Schweiz. Mineral. Petrogr. Mitt.*, 73, 257–363.
- Kalin, D. (1997), Litho-and biostratigraphy of the mid-to late Miocene Bois de Raube-formation (Northwestern Switzerland), *Eclogae Geol. Helv.*, 90, 97–114.
- Kempf, O., and O. A. Pfiffner (2004), Early Tertiary evolution of the North Alpine Foreland Basin of the Swiss Alps and adjoining areas, *Basin Res.*, 16(4), 549–567, doi:10.1111/j.1365-2117.2004.00246.x.
- Kerckhove, C. (1969), La “zone du Flysch” dans les nappes de l’Embrunais-Ubaye (Alpes occidentales), *Géol. Alp.*, 45, 5–204.
- Kirschner, D. L., M. A. Cosca, H. Masson, and J. C. Hunziker (1996), Staircase 40/Ar39Ar spectra of fine-grained white mica: Timing and duration of deformation and empirical constraints on argon diffusion, *Geology*, 24(8), 747–750.
- Kralik, M., N. Clauer, R. Holzsteiner, H. Huemer, and F. Kappel (1992), Recurrent fault activity in the Grimsel Test Site (GTS, Switzerland): Revealed by Rb-Sr, K-Ar and tritium isotope techniques, *J. Geol. Soc.*, 149(2), 293–301, doi:10.1144/gsjgs.149.2.0293.
- Lacombe, O., and F. Mouthereau (2002), Basement-involved shortening and deep detachment tectonics in forelands of orogens: Insights from recent collision belts (Taiwan, Western Alps, Pyrénées), *Tectonics*, 21(4), 1030, 10.1029/2001TC901018.
- Leloup, P., N. Arnaud, E. Sobel, and R. Lacassim (2005), Alpine thermal and structural evolution of the highest external crystalline massif: The Mont Blanc, *Tectonics*, 24, TC4002, doi:10.1029/2004TC001676.
- Lemoine, M., et al. (1986), The continental margin of the Mesozoic Tethys in the Western Alps, *Mar. Pet. Geol.*, 3, 179–199.
- Loprieno, A., R. Bousquet, S. Bucher, S. Ceriani, F. H. Dalla Torre, B. Fügenschuh, and S. M. Schmid (2010), The Valais units in Savoy (France): A key area for understanding the palaeogeography and the tectonic evolution of the Western Alps, *Int. J. Earth Sci.*, 100(5), 963–992, doi:10.1007/s00531-010-0595-1.
- Malavieille, J., R. Lacassim, and M. Mattauer (1984), Signification tectonique des linéations d’allongement dans les Alpes occidentales, *Bull. Soc. Géol. Fr.*, 26(5), 895–906.
- Manatschal, G., A. Engström, L. Desmurs, U. Schaltegger, M. Cosca, O. Müntener, and D. Bernoulli (2006), What is the tectono-metamorphic evolution of continental break-up: The example of the Tasna Ocean–Continent Transition, *J. Struct. Geol.*, 28(10), 1849–1869, doi:10.1016/j.jsg.2006.07.014.
- Marquer, D. (1990), Structure et déformation alpine dans les granites hercyniens du massif du Gothard (Alpes centrales suisses), *Eclogae Geol. Helv.*, 83, 77–97.
- Marquer, D., P. Calcagno, J. C. Barfety, and T. Baudin (2006), 3D modeling and kinematics of the external zone of the French Western Alps (Belleclonne and Grand Chatelard Massifs, Maurienne Valley, Savoie), *Eclogae Geol. Helv.*, 99, 211–222, doi:10.1007/s00015-006-1183-z.
- Masson, H., F. Bussy, M. Eichenberger, N. Giroud, C. Meilhac, and S. Presniakov (2008), Early Carboniferous age of the Versoyon ophiolites and consequences: Non-existence of a “Valais ocean” (Lower Penninic, Western Alps), *Bull. Soc. Géol. Fr.*, 179(4), 337–355.
- Ménard, G., and F. Thouvenot (1987), Coupes équilibrées crustales: Méthodologie et application aux Alpes occidentales, *Geodin. Acta*, 1, 35–45.
- Michalski, I., and M. Soom (1990), The Alpine thermo-tectonic evolution of the Aar and Gotthard massifs, central Switzerland: Fission track ages on zircon and apatite and K-Ar mica ages, *Schweiz. Mineral. Petrogr. Mitt.*, 70, 373–387.
- Mohn, G., G. Manatschal, O. Müntener, M. Beltrando, and E. Masini (2010), Unravelling the interaction between tectonic and sedimentary processes during lithospheric thinning in the Alpine Tethys margins, *Int. J. Earth Sci.*, 99(S1), 75–101, doi:10.1007/s00531-010-0566-6.
- Mouthereau, F., A. B. Watts, and E. Burov (2013), Structure of orogenic belts controlled by lithosphere age, *Nat. Geosci.*, 6(9), 785–789, doi:10.1038/ngeo1902.
- Mugnier, J.-L., S. Guellec, G. Ménard, F. Roure, M. Tardy, and P. Vialon (1990), A crustal scale balanced cross-section through the external Alps deduced from the ECORS profile, *Mém. Soc. Géol. Fr.*, 156, 203–216.
- Mulder, T., et al. (2010), High-resolution analysis of submarine lobes deposits: Seismic-scale outcrops of the Lauzanier area (SE Alps, France), *Sediment. Geol.*, 229(3), 160–191, doi:10.1016/j.sedgeo.2009.11.005.
- Oberhängli, R., et al. (2004), Map of the metamorphic structure of the Alps (1:1'000'000), Commission for the Geological Map of the World (UNESCO), Paris.
- Pfiffner, O. A., S. Sahli, and M. Stauble (1997), Structure and evolution of the external basement massifs (Aar, Aiguilles Rouges/Mt. Blanc), in *Deep Structure of the Swiss Alps: Results from NRP 20*, pp. 139–153, Springer, New York.
- Philippe, Y., E. Deville, and A. Mascle (1998), Thin-skinned inversion tectonics at oblique basin margins: Example of the western Vercors and Chartreuse Subalpine massifs (SE France), in *Cenozoic Foreland Basins of Western Europe*, *Geol. Soc. London Spec. Publ.*, vol. 134, edited by A. Mascle et al., pp. 239–262.
- Ramsay, J. (1981), Tectonics of the Helvetic nappes, in *Thrust and Nappe Tectonics*, Special Publications, vol. 9, pp. 293–309, Geological Society, London.
- Ramsay, J. G., and M. Huber (1989), *Strain Analysis, The Techniques of Modern Structural Geology*, vol. 1, Academic Press, London.
- Ramsay, J. G., M. Casey, and R. Kligfield (1983), Role of shear in the development of the Helvetic fold-thrust belt of Switzerland, *Geology*, 11, 439–442.
- Reinecker, J., M. Danišák, C. Schmid, C. Glotzbach, M. Rahn, W. Frisch, and C. Spiegel (2008), Tectonic control on the late stage exhumation of the Aar Massif (Switzerland): Constraints from apatite fission track and (U-Th)/He data, *Tectonics*, 27, TC6009, doi:10.1029/2007TC002247.
- Rolland, Y., S. Cox, A.-M. Boullier, G. Pennacchioni, and N. Mancktelow (2003), Rare earth and trace element mobility in mid-crustal shear zones: Insights from the Mont Blanc Massif (Western Alps), *Earth Planet. Sci. Lett.*, 214(1–2), 203–219, doi:10.1016/S0012-821X(03)00372-8.
- Rolland, Y., M. Rossi, S. F. Cox, M. Corsini, N. Mancktelow, G. Pennacchioni, M. Fornari, and A. M. Boullier (2008),  $^{40}\text{Ar}/^{39}\text{Ar}$  dating of synkinematic white mica: Insights from fluid-rock reaction in low-grade shear zones (Mont Blanc Massif) and constraints on timing of deformation in the NW external Alps, *Geol. Soc. London Spec. Publ.*, 299(1), 293–315, doi:10.1144/SP299.18.
- Rolland, Y., S. F. Cox, and M. Corsini (2009), Constraining deformation stages in brittle-ductile shear zones from combined field mapping and Ar-40/Ar-39 dating: The structural evolution of the Grimsel Pass area (Aar Massif, Swiss Alps), *J. Struct. Geol.*, 31, 1377–1394.
- Rolland, Y., J.-M. Lardeaux, and L. Jolivet (2012), Deciphering orogenic evolution, *J. Geodyn.*, 56–57, 1–6.

- Rossi, M., Y. Rolland, O. Vidal, and S. F. Cox (2005), Geochemical variations and element transfer during shear zone development and related episyenites at middle crust depths: Insights from the study of the Mont-Blanc Granite (French-Italian Alps), *Geol. Soc. London Spec. Publ.*, 245, 373–396.
- Rubatto, D., and J. Hermann (2001), Exhumation as fast as subduction?, *Geology*, 29(1), 3–6.
- Sanchez, G., Y. Rolland, J. Schneider, M. Corsini, E. Oliot, P. Goncalves, C. Verati, J.-M. Lardeaux, and D. Marquer (2011), Dating low-temperature deformation by  $^{40}\text{Ar}/^{39}\text{Ar}$  on white mica, insights from the Argentera-Mercantour Massif (SW Alps), *Lithos*, 125, 521–536.
- Schmid, S. M., O. A. Pfiffner, N. Froitzheim, G. Schönborn, and E. Kissling (1996), Geophysical-geological transect and tectonic evolution of the Swiss-Italian Alps, *Tectonics*, 15, 1036–1064, doi:10.1029/96TC00433.
- Schwizer, B. (1984), Die Tristel-Formation. Vergleichende Untersuchungen in Graubünden, Liechtenstein, Vorarlberg und Bayern, PhD Thesis, Univ. of Bern.
- Seward, D., and N. S. Mancktelow (1994), Neogene kinematics of the central and Western Alps: Evidence from fission-track dating, *Geology*, 22(9), 803–806.
- Sibuet, J. C., S. P. Srivastava, and W. Spakman (2004), Pyrenean orogeny and plate kinematics, *J. Geophys. Res.*, 109, doi:10.1029/2003JB002514.
- Simon-Labréte, T., Y. Rolland, T. Dumont, T. Heymes, C. Authemayou, M. Corsini, and M. Fornari (2009), Ar-40/Ar-39 dating of Penninic Front tectonic displacement (W Alps) during the Lower Oligocene (31–34 Ma), *Terra Nova*, 21, 127–136.
- Sinclair, H. D. (1997), Tectonostratigraphic model for underfilled peripheral foreland basins: An Alpine perspective, *Geol. Soc. Am. Bull.*, 109, 324–346.
- Sinclair, H. D., and P. A. Allen (1992), Vertical versus horizontal motions in the Alpine orogenic wedge: Stratigraphic response in the foreland basin, *Basin Res.*, 4, 215–232.
- Soom, M. A. (1990), Abkühlungs- und Hebungsgeschichte der Externmassive und der Penninischen decken beidseits der Simplon-Rhone-Linie seit dem Oligozän: Spaltpurdatierungen an apatit/zirkon und K/Ar-datierungen an biotit/muskowit (westliche zentralalpen), PhD, Univ. of Bern.
- Stampfli, G. M., G. D. Borel, R. Marchant, and J. Mosar (2002), Western Alps geological constraints on western Tethyan reconstructions, *J. Virtual Explor.*, 8, 77–106.
- Steck, A., J. L. Epard, A. Escher, P. Lehner, R. Marchant, and H. Masson (1997), Geological interpretation of the seismic profiles through western Switzerland: Rawil (W1), Val d'Anniviers (W2), Mattertal (W3), Zmutt-Zermatt-Findelen (W4) and Val de Bagnes (W5), in *Deep Structure of the Swiss Alps: Results from NRP 20*, edited by O. A. Pfiffner et al., pp. 123–138, Birkhäuser Verlag, Basel: Boston.
- Steiniger, F. F., W. A. Berggren, D. V. Kent, R. L. Bernor, S. Sen, and J. Agusti (1996), Circum-Mediterranean Neogene (Miocene and Pliocene) marine-continental chronologic correlations of European Mammal Units, in *The Evolution of Western Eurasian Neogene Mammal Faunas*, edited by R. L. Bernor, V. Fahrbusch, and H.-W. Mittmann, pp. 7–46, Columbia Univ. Press, New York.
- Steinmann, M. (1994), Ein Beckenmodell für das Nordpenninikum der Ostschweiz, *Jahrb. Geol. Bundesanst.*, 137, 675–721.
- Taylor, B., A. Goodliffe, F. Martinez, and R. Hey (1995), Continental rifting and initial sea-floor spreading in the Woodlark basin, *Nature*, 374, 534–537.
- Trumpy, R. (1975), Penninic-Austroalpine boundary in the Swiss Alps: A presumed former continental margin and its problem, *Am. J. Sci.*, 279, 209–238.
- Ustaszewski, K., S. M. Schmid, B. Fugenschuh, M. Tischler, E. Kissling, and W. Spakman (2008), A map-view restoration of the Alpine-Carpathian-Dinaridic system for the Early Miocene, *Swiss J. Geosci.*, 101, 273–294, doi:10.1007/s00015-008-1288-7.
- Van der Beek, P. A., P. G. Valla, F. Herman, J. Braun, C. Persano, K. J. Dobson, and E. Labrin (2010), Inversion of thermochronological age-elevation profiles to extract independent estimates of denudation and relief history—I: Application to the French Western Alps, *Earth Planet. Sci. Lett.*, 296, 9–22.
- Vernon, A. J., P. A. van der Beek, H. D. Sinclair, and M. K. Rahn (2008), Increase in late Neogene denudation of the European Alps confirmed by analysis of a fission-track thermochronology database, *Earth Planet. Sci. Lett.*, 270(3–4), 316–329, doi:10.1016/j.epsl.2008.03.053.
- Wibberley, C. (1999), Are feldspar-to-mica reactions necessarily reaction-softening processes in fault zones?, *J. Struct. Geol.*, 21, 1219–1227.